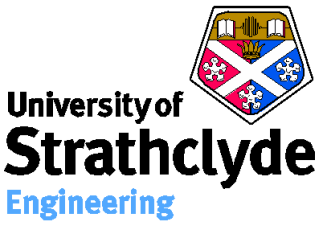

Theoretical and Experimental Investigations of Multiphase Flow in Safety Relief Valves

Wael Mohammed Ahmed Ibrahim Elmayyah

A thesis presented in fulfilment of the requirements for the degree of

Doctor of Philosophy

Department of Mechanical Engineering
University of Strathclyde
Glasgow, UK
2010

Dedicated to

To my Father, who always encourages me to learn

To my mother and my wife

Without your support, I could not make this.

Theoretical and Experimental Investigations of Multiphase Flow in Safety Relief Valves

Wael Elmayyah

Abstract

In general, two phase flow through safety relief valves (SRV) is a complex flow and dominated by heat, momentum and mass transfer between phases. It is even more complex for flows in a safety valve where turbulence, flow separation and shock waves associated with compressible flow occur. Unfortunately, the literature indicates that there is no generic model with sufficient accuracy to predict the two phase flow conditions in an SRV. However, existing CFD techniques do provide the potential for predicting the two phase flow in the valve with the possibility of improving the valve design. In this study, two phase flow through an SRV has been investigated experimentally and computationally using a two dimensional mixture model of the two phase flow. Investigations have been carried out on a conventional spring loaded relief valve using a two phase mixture of air and water. The mixture model has been used with the standard k- ε turbulence model to predict the two phase flow through the SRV. Quasi steady flow has been assumed to investigate the valve flow-lift and force-lift characteristics. Tests have been carried out for a range of pressures (7- 12 barg) and water mass fraction (0-0.71) and compared with the CFD predicted results. Comparisons have also been made with the ISO 4126-10 sizing model for safety valves. The CFD predictions compare well with the experimental data with an accuracy better than the ISO 4126-10 sizing model. Scaling parameters for force and flow have been presented to assist SRV design under single and two phase flow conditions.

Declaration

This thesis is the result of the author's original research. It has been composed by the author and has not been previously submitted for examination which has led to the award of a degree.

Signed:

Date:

Acknowledgements

This PhD study could not have been done without the help of a lot of other people. So, it is my pleasure to have the opportunity to express my thanks to those who have helped me. I'd like to thank Dr. Bill Dempster for his continuous help, guidance and support. Dr. Bill was always there to listen, advise, guide and give constructive feedback. I'd like to thank Gerry, the most helpful technician I have ever seen, for his great help during the experimental installations and the experimental work. Also, I'd like to say thank you for my colleague and friend Shehab for his advice and help during the research time especially in the computational issues. My colleagues, Alistair, Andrew, Muhammad, Sherief and Mark have made my research a very good time to enjoy. Special thanks to Alistair who gives us smiles all the time. Great thanks go to my wife, my kids (Ahmed and Ali) and my parents for being supportive and patient, especially my wife who always suffers to provide me with the best environment to study and learn. Final thanks go to Yahia (my youngest son) who gives me pleasure and smiles and wastes my time!

Contents

Abstract **iii**

Acknowledgements **v**

Table of Contents **vi**

List of Figures **x**

List of Tables **xv**

Nomenclature **xvi**

1 Introduction **1**

1.1 Safety Relief Valve 2

1.2 Objective 5

1.3 Thesis Layout 6

2 Safety Relief Valves Background **7**

2.1 Historical Background 8

2.2 Function and Definition 8

2.3 Construction and Operation 11

3 Literature Review **16**

3.1 Safety Relief Valve Design Requirement 17

3.2 Single Phase Applications 19

3.2.1 International Standards Requirements for Safety Relief Valves under Single Phase Flow . . . 19
3.2.2 Simplified Models for Safety Relief Valve . . . 21
3.2.3 Sizing of Safety Relief Valves for Single Phase Flow . . . 23
3.2.4 CFD in Modelling Safety Relief Valve . . . 24
3.2.5 Operational Problems of Safety Relief Valve . . . 26
3.2.6 Overview . . . 27
3.3 Safety Relief Valve under Two Phase Flow . . . 28
3.3.1 International Standards Requirements for SRV under Two Phase Flow . . . 30
3.3.2 Simplified Models and Sizing of SRV . . . 30
3.3.3 Experimental Measurements of SRV . . . 35
3.3.4 CFD Modelling for Two Phase Flow . . . 36
3.3.5 Overview . . . 38

4 Single Phase Flow Studies 40
4.1 Introduction . . . 41
4.2 Valve Construction . . . 41
4.3 Single Phase Testing . . . 42
4.3.1 Test Rig Construction . . . 43
4.3.2 Experimental Procedures . . . 45
4.4 Computational Model . . . 50
4.4.1 Model Equations . . . 50
4.4.2 Computational Grid . . . 52
4.4.3 Boundary Conditions and Solution . . . 53
4.5 Results and Discussion . . . 55
4.5.1 Experimental Results . . . 55
4.5.2 CFD Results . . . 57
4.5.3 Discussion . . . 62
4.5.3.1 Flow-Lift Characteristics under Single Phase Flow 62
4.5.3.2 Force-Lift Characteristics under Single Phase Flow 66

4.6 Valve Design Approach for Single Phase Flow: 74

5 Two Phase Flow Studies 81

5.1 Introduction 82

5.2 Experimental Studies 83

5.2.1 Experimental Setup 83

5.2.2 Experimental Procedures 85

5.3 Two Phase Flow Modelling 88

5.3.1 Mixture Model 89

5.3.1.1 Basic Equations 90

5.3.2 Computational Model 95

5.3.3 Boundary Conditions and Solution 96

5.4 Experimental Results 97

5.4.1 Flow-Lift Characteristics 97

5.4.2 Force- Lift Characteristics 100

5.5 Mixture Model CFD Results 104

5.6 Simplified Models 113

5.6.1 Homogeneous Equilibrium Model Equations 113

5.7 Discussion 115

5.7.1 Flow-Lift Characteristics under Two Phase Flow 115

5.7.2 Force-Lift Characteristics under Two Phase Flow 119

5.7.2.1 Effect of the gland on the flow 122

5.7.3 Effect of Water Dispersion on Flow Properties 130

5.8 Valve Design Approach for Two Phase Flow 136

5.8.1 Normalised Air Flow Rate 136

5.8.2 Normalised Force 139

6 Conclusions and Future Work 141

6.1 Summary 142

6.2 Single Phase Studies Conclusions 142

6.3 Two Phase Studies Conclusions 145

6.4 Future Work 148

Bibliography **149**

Appendix **156**

A **156**

A.1 CAD Drawings 157

A.1.1 Valve CAD Drawings 157

A.1.2 The Modified Gland 163

A.1.3 The Converging Section Dimensions 163

A.1.4 Dempster et al [20] Valve drawing 164

A.2 HNE-DS model equations 170

List of Figures

1.1 Safety Relief Valve Assembly 3

2.1 Counter weight safety relief valve 9
2.2 Typical Safety valves 12
2.3 Construction of Safety valve 12
2.4 Safety valve operation 14
2.5 Safety valve pressure and lift characteristics 14

3.1 General opening and closing characteristics for a SRV 17

4.1 Valve construction (Dim. in inches) 42
4.2 Construction of test rig for single phase flow measurement 44
4.3 Scheme drawing of the test rig for single phase flow 44
4.4 Air supply circuit diagram 45
4.5 The effect of the spring on the flow rate and piston force 48
4.6 The effect of the gland on the air flow rate at 11.7 barg (170 psi) . 49
4.7 The effect of the gland on the piston force at 11.7 barg (170 psi) . 49
4.8 Computational grid of the valve (Dim. in inches) 54
4.9 The effect of the gland on the air flow rate at 11.7 barg (170 psi) . 56
4.10 The effect of the gland on the piston force and back pressure at 11.7 barg (170 psi) 56
4.11 Contours of static temperature and pressure at 2.5 mm lift and 11.7 barg 58
4.12 Contours of Mach number and Air velocity at 2.5 mm lift and 11.7 barg. Area 1,2 and 3 are shown in Figure 4.13 59

4.13 Contours of Mach number at 2.5 mm lift and 11.7 barg at Area 1,2 and 3 shown in Figure 4.12 60
4.14 CFD and experimental flow-Lift characteristics at 11.7 barg . . . 61
4.15 CFD and experimental piston force-lift characteristics at 11.7 barg 61
4.16 Piston force-Lift characteristics at 12 barg with the modified gland 62
4.17 Flow-Lift characteristics at 11.7 barg 63
4.18 The critical plane at piston face at lower lifts 64
4.19 Critical plane at piston side at higher lifts (11.7 barg) 64
4.20 Static pressure at the inlet of the passageway around the piston (11.7 barg) 65
4.21 Pressure contours on piston front and back face 65
4.22 Experimental force-lift characteristics with gland at 11.7 barg . . 67
4.23 Force-lift and back pressure- lift characteristics at 11.7 barg with gland 68
4.24 Force-lift and back pressure- lift characteristics at 12 barg with the modified gland 69
4.25 Static pressure contours on the piston front face at 11.7 bar (170 psi) and 4 mm lift (Fluent 3D model) 70
4.26 Static pressure contours on the piston back face at 11.7 bar (170 psi) and 4 mm lift (Fluent 3D model) 71
4.27 Three [33] and two dimensional force-lift characteristics at 11.7 bar (170 psi) with gland 73
4.28 Static pressure contours on the piston front face at 11.7 bar (170 psi) (Fluent 3D model [20]) 74
4.29 Flow-lift characteristics at different pressures with gland 77
4.30 Piston force-lift characteristics at different pressures with gland . 77
4.31 Normalised force, flow and spring-lift characteristics 78
4.32 Normalised flow rate-lift characteristics 78
4.33 Normalised force-lift characteristics (no gland) 79
4.34 Normalised force-lift characteristics (with gland) 79

4.35 General opening and closing characteristics for a SRV 80

5.1 Test rig construction scheme 84
5.2 Test rig construction 85
5.3 Water Injection circuit diagram 86
5.4 Water Injection circuit 86
5.5 Computational grid for the valve and the converging section . . . 96
5.6 Air flow-Lift at 12.07 barg (175psi) 98
5.7 Mixture flow-Lift at 12.07 barg (175psi) 98
5.8 Flow-Lift at 8.62 barg (125psi) 99
5.9 Mixture Flow-Lift at 8.62 barg (125psi) 99
5.10 The effect of the modified gland on air flow rate 100
5.11 Effect of the modified gland on piston force at 2mm lift at 12.07 barg 101
5.12 Force-Lift at 12.07 barg (175psi) with modified gland 102
5.13 Force-Lift at 8.62 barg (125psi) with modified gland 102
5.14 Force-Lift at 12.07 barg (175psi) without gland 103
5.15 Force-Lift at 8.62 barg (125psi) without gland 103
5.16 Contours of Mach number at single phase air and 0.05 kg/s water flow rate, 3mm lift and 12.07 barg (with gland). Area 1 and 2 are shown in Figure 5.17 106
5.17 Contours of Mach number 0.05 kg/s water flow rate, 3mm lift and 12.07 barg (with gland) at Area 1 and 2(shown in Figure 5.16) . 106
5.18 Contours of Static Pressure and Water volume fraction at 4mm lift and 12.07 barg (no gland) 107
5.19 Contours of slip at 3mm lift and 12.07 barg at 0.01 and 0.05 kg/s (with gland) 108
5.20 Predicted Flow-lift characteristics with and without the slip at 0.01kg/s water flow rate and 12.07 barg pressure. 109
5.21 Predicted Force-lift characteristics with and without the slip at 0.01kg/s water flow rate and 12.07 barg pressure. 109

5.22 Air flow rate- Lift at 12.07 barg (175psi) 110
5.23 Mixture flow rate- Lift at 12.07 barg (175psi) 110
5.24 Force-Lift at 12.07 barg (175psi) with the modified gland 111
5.25 Force-Lift at 12.07 barg (175psi) with no gland 112
5.26 Back pressure-Lift at 12.07 barg (175psi) with the modified gland 112
5.27 HEM, ISO, HNE-DS and the Mixture model at 8.62 barg at valve fully open position (L=7 mm) compared by the experimental results 115
5.28 Effect of the water flow rate on air flow rate at 12.07 barg 116
5.29 Water volume fraction at lift 4mm and 12.07 bar 117
5.30 Effect of the water mass fraction on mixture flow rate at 4 mm lift 117
5.31 Effect of the water mass fraction on mixture flow rate at 1 mm lift 118
5.32 Deviation percent of the CFD results from the experimental results at 8.6 barg at 1 mm and 4 mm lift 118
5.34 Air flow-lift at 12.07 barg (175psi) 120
5.33 Force-lift Characteristics at 12.07 barg 120
5.35 Pressure distribution on piston face at 0.5 mm lift, 12.07 bar . . . 121
5.36 Pressure distribution on piston face at 2 mm lift, 12.07 bar 122
5.37 Force and back pressure at different water flow rate at 2 mm lift with no gland 124
5.38 Static pressure contours at 4 mm lift ,12.07 bar with the modified gland (case 1) 126
5.39 Static pressure contours at 4 mm lift ,12.07 bar without the gland (case 2) 126
5.40 Static pressure at the piston walls ,4 mm lift ,12.07 bar without the gland (case2) 127
5.41 Static pressure contours at 4 mm lift ,12.07 bar without the gland (Case 2) 127
5.42 Back pressure at single phase flow at different pressures 128
5.43 Static pressure contours single phase at 2.5 mm lift , 8.6 bar with no gland 129

5.44 Static pressure contours single phase at 2.5 mm lift ,12.07 bar with no gland 129
5.45 Static pressure contours at 2.5 mm lift ,13.8 bar with no gland . . 130
5.46 Effect of injection nozzle geometry on air flow rate 131
5.47 Effect of injection nozzle geometry on force 132
5.48 Injection Nozzle geometry 133
5.49 Air flow rate at 2 mm lift at different water flow rate, pressure 12.07 barg (175psi) 134
5.50 Air flow rate at 1 mm lift at different water flow rate, Pressure 12.07 barg (175psi) 134
5.51 Air flow rate at 2 mm lift at different water mass fraction, Pressure 12.07 barg (175psi) 135
5.52 Air flow rate at 1 mm lift at different water mass fraction, Pressure 12.07 barg (175psi) 135
5.53 Air flow rate - water mass fraction at all lifts and pressure 138
5.54 Normalised flow -lift characteristics 139
5.55 Normalised force- lift characteristics 140

List of Tables

3.1 Comparison of the required function values for safety valves at different standards 20

4.1 Experimental test matrix (Single phase flow) 46

4.2 Predicted force values at 0.5 and 4mm lift at 11.7 bar 73

5.1 Experimental test matrix for two phase flow 87

Nomenclature

a	Acceleration (m/s^2)
a_s	Sound speed (m/s)
A	Area (m^2)
C	Constant
C_D	Drag coefficient
E	Total specific energy (J/kg)
f_{drag}	Drag factor
F	Force (N)
g	Gravitational acceleration (m/s^2)
G	Mass flux $(kg/m^2.s)$
G_k	The generation of turbulence kinetic energy due to the mean velocity gradients (J/kg)
G_b	The generation of kinetic energy due to buoyancy (J/kg)
k	Turbulence kinetic energy (J/kg)
K	Thermal conductivity $(W/m.K)$
L	Piston lift (mm)
m	Mass (kg)
M	Mach number
M_w	Molecular weight (g/mol)
P	Pressure (Pa)

P_a	Atmospheric pressure (Pa)
Pr	Prandtl Number
R	Universal gas constant $(J/mol.K)$
Re_r	Relative Reynolds number
S	The modulus of the mean rate-of-strain tensor
t	Time (s)
T	Temperature (K)
u	Velocity component (m/s)
v	Specifice volume (m^3/kg)
x	Coordinate direction
x_a	Air mass fraction
x_w	Water mass fraction
Y_M	The contribution of the fluctuating dilatation in compressible turbulence to the overall dissipation rate (J/kg)

Greek Symbols

α	Air volume fraction
α_w	Water volume fraction
γ	Heat cpacity ratio
δ_{ij}	Kronecker delta
ε	Turbulent kinetic energy rate of dissipation (J/kg)
η_{crit}	Critical pressure ratio
μ	Viscosity $(kg/m.s)$
ρ	Density (kg/m^3)
σ	Turbulent Prandtl number
τ	Stress tensor
τ_v	Velocity time response (s)
ϕ	Slip factor
ω	Compressability factor

Subscript

a	Air
d	Discharge
dr	Drift
D	Drag
eff	Effective
G	Gas phase
i	Free index
j	Free index
l	Free index
L	Liquid phase
m	Mixture
N	Normalised
o	Stagnation condition
t	Turbulent
w	Water
k	Turbulent kinetic energy
ε	Turbulent kinetic energy rate of dissipation
μ	Viscous

Chapter 1

Introduction

1.1 Safety Relief Valve

Many industries including automotive, printing, aerospace and power plants use safety relief valves. These valves are designed and used to protect a pressurised system against excessive operating pressure. They are required to open at a predetermined system pressure and to discharge an amount of fluid to ensure a pressure reduction and then to close after the normal system pressure has been restored. The two terms "Safety valves" and "Safety relief valves" (SRV) are generally used to describe the valve responsible for protecting the system against excessive pressure rise. They are mainly used with compressible fluid conditions while the term "safety relief valve" could be extended to be used with incompressible fluid conditions. Safety relief valves could be classified using many categories according to the capacity, operating method, working fluids...etc. A discussion on safety relief valve classification is presented in Chapter 2.

The gas flow behaviour through safety relief valves is very complex and is characterised by viscous effects, turbulence, flow separation, critical flow conditions and shock waves. These may affect adversely on the system resulting in noise and vibration. More complications in flow occur when two phase flow occurs in safety relief valves. In most practical applications two phase flow can occur due to depressurisation, cavitation or steam condensation or through entrainment of liquids in the pressurised storage system. Two phase flow can be accompanied by mass, momentum and heat exchange between phases which makes it difficult to predict the flow behaviour. Two phase flow is more complicated and more difficult to predict when it occurs through small geometries with high velocity and high compressibility. In addition, safety relief valves performance significantly changes when exposed to two phase flow.

It is normal for the design of safety relief valves to depend on experimental measurements and a trial and error design process to achieve the required level of valve performance. Till now there is no such direct design method for safety relief valves under two phase flow, although there are several codes and methods for selecting and sizing safety relief valves. These methods and their accuracy

will be discussed in Chapter 3. Due to the complexity of two phase flow and lack of knowledge, safety relief valves are still oversized when selected for use, which reflects the uncertainty in design procedures. A good understanding of safety relief valves under two phase flow with good prediction techniques will lead to improved valve design, which will ensure the safe operation of the pressurised system and the proper opening and closing of the valve. Under sizing of a design will result in a deficient safety valve with a high risk of danger. On the other hand, oversizing may not be safe in all conditions because it results in overpressure in the downstream piping. Thus the downstream piping need to be designed for higher pressure and will result in more expensive piping cost. In addition, excess loss of fluids means higher costs and greater damage to the environment.

One of the most commonly used safety relief valves is the conventional spring loaded safety relief valve. It is cheap, easy to install , maintain and use. In this study a conventional spring loaded safety relief valve commonly found in the refrigeration industry has been used to investigate the influence of two phase flow on safety relief valve performance. Figure 1.1 shows a cross section in the assembled valve.

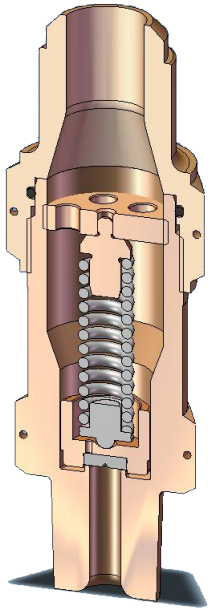

Figure 1.1: Safety Relief Valve Assembly

To improve the control and design of safety relief valves for opening, closing and mass flow rate, the valve characteristics should be well understood. These are steady state relationships for the flow through and force acting on the main moving elements of the valve. Since the opening and closing of the valve piston is dependent on the fluid forces and the spring resistance, obtaining the force-piston displacement (lift) characteristics for any safety valve is the essential step to design, develop or select the valve. On the other hand piston displacement controls the discharge flow rate and thus affects the forces exerted on the piston. Hence, obtaining the flow rate -lift curve in conjunction with the force-lift curve will capture the most important features responsible for the valve performance.

Since most safety relief valves components have very small geometrical dimensions, it is often very difficult and very expensive to perform detailed flow measurements of the internal flow structure. However, basic experimental work to validate the CFD predictions is essential to provide confidence in a predictive model. For this study a test rig has been constructed to create the two phase flow through the safety relief valve and facilitates the measurements of the pressure, temperature, force and flow rates. These basic measurements will not provide much details on the internal valve flow but good enough to validate the CFD model. Hence, the importance of computational fluid dynamics flow simulations becomes evident allowing detailed quantification and visualisation of the valve internal flow structure in order to study the impact of geometry variations in the design process.

While the operation of the valve is essentially a dynamic process the operation of the valve can be understood by assuming quasi static conditions whereby the dynamic force and mass flow acting on the valve piston are functions of the piston position (lift) alone. This assumes pressure wave effects are negligible which is more applicable to the closing than the opening phase of a safety relief valve operation. However, the initial design process is often based on the quasi steady approach and directly uses the force-lift and mass flow–lift characteristics of the valve.

A two dimensional axisymmetric model has been used to represent the valve geometry and flow path. Different models have been developed at different piston lift to model the valve at different piston position. Fluent 6.3.2 has been used to model and solve the mixture multiphase model. The mixture model is a simplified model of the full multiphase model and is considered a good alternative when simulating a dilute flow of droplets of liquid in a gas, suspensions of solid particles in a gas or small bubbles in a liquid. Experimentally, the measured properties were pressure, air and water mass flow rate, force and lift. The obtained experimental results in conjunction with the CFD predicted results give the necessary knowledge to develop a design approach to SRV under two phase flow.

1.2 Objective

The main objective of this study is to develop a fluid design approach to safety relief valves under two phase flow using computational fluid dynamics. To achieve this main objective the following have been undertaken:

1. Investigation of safety relief valves with single phase flow:
    - Application of CFD to investigate safety relief valve flow conditions.
    - Develop an experimental test rig for validation.
    - Data analysis to define an approach for design.
2. Investigation of safety relief valves with two phase flow:
    - Investigation of CFD models for two phase flow prediction of air- water flow through safety relief valve.
    - Application of a CFD models to predict two phase flow through the safety valve.
    - Develop an experimental test rig for results validation.
    - Data analysis to define an approach for the design of the safety valve under two phase flow.

1.3 Thesis Layout

After the thesis introduction and setting the objective in Chapter 1, Chapter 2 presents a background to safety relief valves. This background will provide a brief historical review and then introduce valve definitions according to the standard codes, valve function, usage, operation and classifications.

Chapter 3 presents a literature review of safety relief valve research under single and two phase flow conditions. This chapter provides an overview of the experimental work and models related to safety relief valves that are available in the literature.

Chapter 4 presents a study on safety relief valves under single phase flow and includes the mathematical model, computational model and experimental work. The results are presented and discussed. Scaling parameters for the flow and force have been introduced to assist in valve design under single phase flow conditions.

Chapter 5 is the main contribution of this PhD study and discusses the capability of the two phase mixture model to predict air-water flows through a safety relief valve. It includes the experimental work and mathematical model equations for the CFD mixture model with the computational model details. In addition three models used by the international standards and widely used in the literature are presented in Chapter 5. The results are discussed and scaling parameters for the flow and force have been introduced to assist in valve design under two phase flow.

Chapter 6 presents the conclusions and the future work.

Chapter 2

Safety Relief Valves Background

2.1 Historical Background

As soon as man succeeded in containing steam in a pressurised vessel, the need for a safety device became evident. As long as 2000 years ago, the Chinese were using vessels with hinged lids to allow (relatively) safer usage of steam. At the beginning of the 14^{th} century, chemists used conical plugs to act as safety devices. Around 1680 and after many explosions, the French physicist Denis Papin succeeded in making the first counter weight safety valve for his high pressure cooker. Figure 2.1 presents a simple but more developed design for a counter weight valve [56]. Papin moved the weight along the lever arm to adjust the vessel relief pressure. Later, compression springs replaced the counterweights. Two successive attempts of developing safety relief valves could be considered the start of the developed effective safety relief valves. The first was in 1848 by Charles Ritchie and the second in 1863 by William Naylor [62].

After several boiler explosions on ships and locomotives resulting from faulty safety devices, it was necessary to find a practical way of introducing safety codes. In 1911, the American Society of Mechanical Engineers (ASME) was asked to formulate a design code. This was due to 1700 boiler explosions, which led to 1300 deaths in the New England region of the USA, in only five years between 1905 and 1911 [44]. The boiler & pressure vessel committee was formed and hence the ASME Section 1 for fired vessels was formulated and became obligatory for designers to follow . Today, every pressurised system is equipped with one or more safety relief valve. The operation of pressurised systems is regulated by the law and controlled by safety procedures to ensure that dangerous conditions are prevented.

2.2 Function and Definition

The primary function of a safety valve is to gurantee the mechanical integrity of a pressurized system and therefore protect life and property. In addition it could be used in many industrial applications to protect a process against over

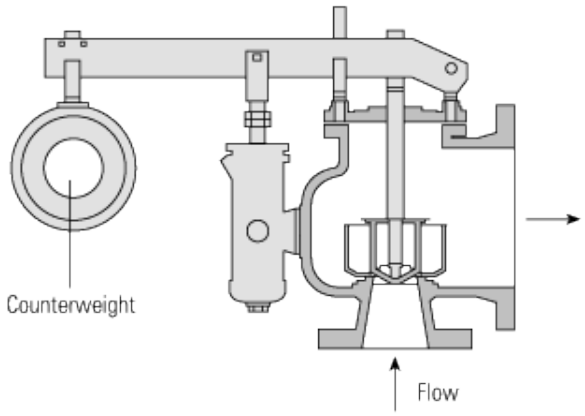

Figure 2.1: Counter weight safety relief valve

pressure. The safety valve is normally closed to seal the pressurised system. It operates by opening to release a volume of fluid from within the plant or the pressurised system when a preadjusted maximum pressure is reached, hence reduce the pressure and reclose to seal the system again. As the safety valve may be the only remaining device to prevent catastrophic failure under overpressure conditions, it is important that safety relief valve must be self actuated.

The terms "safety valve" and "safety relief valve" are generic terms to describe many varieties of pressure relief devices that are designed to prevent fluid pressure build-up. In most national standards, specific definitions are given for safety and safety relief valves. A wide range of different valves are available for many different applications and performance criteria.

According to the ASME /ANSI PTC25.3[1] code applicable in the USA, the general term ***pressure relief valve*** is defined as "A spring-loaded pressure relief valve which is designed to open to relieve excess pressure and to reclose and prevent the further flow of fluid after normal conditions have been restored. It is characterised by a rapid-opening 'pop' action or by opening in a manner generally proportional to the increase in pressure over the opening pressure. It may be used for either compressible or incompressible fluids, depending on design, adjustment, or application."

[1](ANSI) American National Standards Institute

This general definition includes the terms “safety valve” , “safety relief valves” and “relief valves”, as follows

Safety valve - A pressure relief valve actuated by inlet static pressure and characterised by rapid opening or pop action.

Safety relief valve - A pressure relief valve characterised by rapid opening or pop action, or by opening in proportion to the increase in pressure over the opening pressure, depending on the application, and which may be used either for liquid or compressible fluid.

Relief valve - A pressure relief device actuated by inlet static pressure having a gradual lift generally proportional to the increase in pressure over the opening pressure. Relief valves are commonly used in liquid systems, especially for lower capacities and thermal expansion duty. They can also be used on pumped systems as pressure overspill devices.

In Europe the BS 6759[2] and DIN 3320[3] define the safety valve as follows:

Safety valve - A valve which automatically, without the assistance of any energy other than that of the fluid concerned, discharges a certified amount of the fluid so as to prevent a predetermined safe pressure being exceeded, and which is designed to re-close and prevent the further flow of fluid after normal pressure conditions of service have been restored. From the above definitions it is noticeable that there are some differences in definition for safety valves between the USA and European standards, “safety valves” in Europe is nearly similar to the “safety relief valve” in USA codes. This information should be considered when dealing with safety valve research and studies from different countries.

According to the operation method, safety relief valves could be classified into direct (loaded) and pilot operated safety relief valves. Direct loaded safety relief valves are the most common employed valves. In this type, fluid pressure is directly operating on the valve moving element against a direct mechanical load such as a spring or weight. Direct-loaded safety relief valves may be provided

[2]British Standard

[3](DIN) Deutsches Institut für Normung; in English, the German Institute for Standardization

with an auxiliary actuator to help in opening or closing. Pilot operated safety relief valves which consists of a main valve and a pilot. The main valve is in charge of relieving the pressure while the pilot controls the valve moving element according to the system pressure.

Safety relief valves could be classified according to the lift as well. The BS 6759 classify safety relief valves according to the lift as follow:

Lift safety valve (ordinary class) - The valve member lifts automatically a distance of at least $\frac{1}{24}^{th}$of the bore of the seating member, with an overpressure not exceeding 10% of the set pressure. ***High lift safety valve*** - Valve member lifts automatically a distance of at least $\frac{1}{12}^{th}$ of the bore of the seating member, with an overpressure not exceeding 10% of the set pressure. ***Full lift safety valve*** - Valve member lifts automatically to give a discharge area between 100% and 80% of the minimum area, at an overpressure not exceeding 5% of the set pressure. The ASME define the ***Low lift safety valve*** for the condition when "The actual position of the disc determines the discharge area of the valve" and the ***Full lift safety valve*** for the situation where " The discharge area is not determined by the position of the disc". Figure 2.2 shows typical safety valves. Classification of safety valves designs with basic construction and operation was presented by Taras'ev and Kuzin [65]. This classification gave a clear view of the area of application of each safety valve to assist with the valve design.

2.3 Construction and Operation

The basic spring loaded safety valve, referred to as standard or conventional is a simple, reliable self-acting device that provides overpressure protection. The basic elements of the design is the valve body with the valve inlet connection, or nozzle, mounted on the pressure-containing system. The outlet connection may be screwed or flanged for connection to a piped discharge system, or the fluid could be vented directly to the atmosphere.

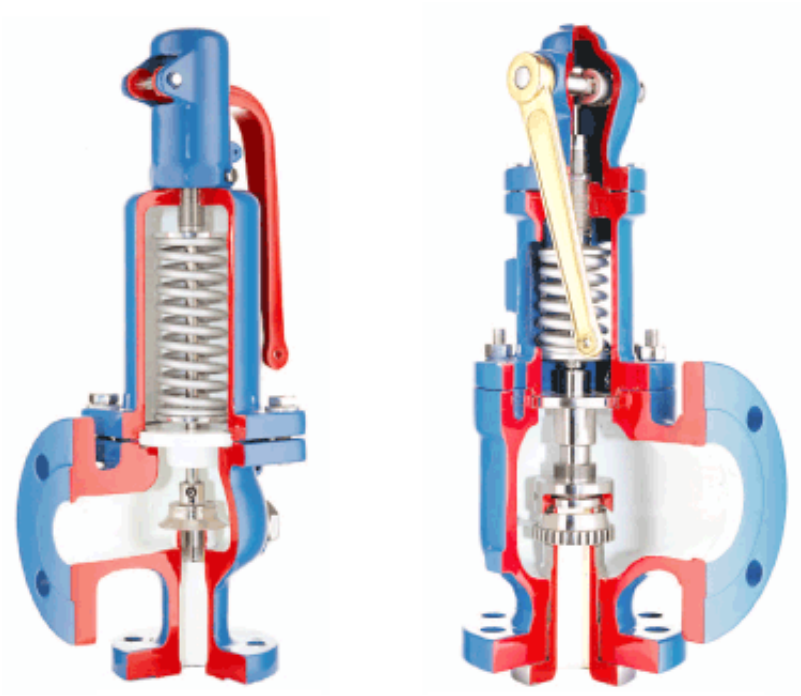

Figure 2.2: Typical Safety valves

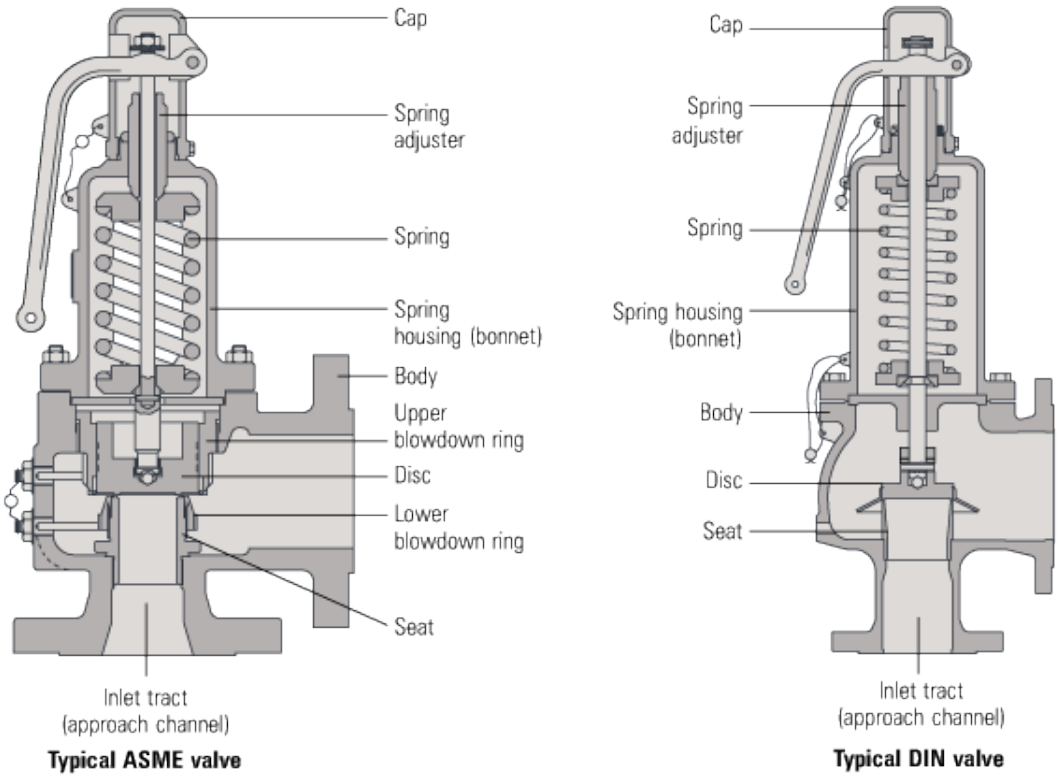

Figure 2.3: Construction of Safety valve

The disc is held against the nozzle seat (under normal operating conditions) by the spring, which is housed in an open or closed spring housing arrangement (or bonnet) mounted on top of the body. Figure 2.3 shows the construction of a safety relief valve according to the ASME and DIN standard. The figure shows the main components of a safety relief valve, i.e. the valve body, the disc (moving element), the valve seat, the spring and the spring adjuster. The standard valve according to the ASME has an additional feature than the standard valve according to the DIN which is the usage of upper and lower blowdown rings for the fine adjustment of the valve operating pressures.

Safety valves should be installed wherever the maximum allowable working pressure (MAWP) of a system or pressure-containing vessel is likely to be exceeded. The valve is adjusted to a pressure called the ***set pressure***. The additional pressure rise required before the safety valve will discharge at its rated capacity is called the ***overpressure***. The allowable overpressure depends on the standards being followed and the particular application. For compressible fluids, this is normally between 3% and 10%, and for liquids between 10% and 25%. Pressure excess could occur because of different reasons such as : supply of external heat to the system, faults in heating systems, chemical reactions, supply of higher pressure gas or liquid, thermal expansion...etc. When the fluid pressure exceeds the maximum allowable pressure, the pressure force pushes the moving element against the spring force and opens the valve. This lift (movement) allows a certain volume of fluid to be discharged out of the system resulting in a pressure reduction. When the normal pressure is restored, the spring force pushes the moving element closed to reseal the system. This pressure called the ***reseat pressure*** and the difference between the set pressure and the reseat pressure is defined as the ***blowdown***. Figure 2.4 shows the valve operation. Figure 2.4 (a) shows the closed (sealing) position when the pressure force exerted on the disc is less than the spring force, i.e the system pressure is less than or equal to the set pressure value. In Figure 2.4 (b) the valve starts to open when the system pressure just exceeds the set pressure and hence a little discharge flow rate comes out from the

system. Therefore, the pressure continues to increase and the disc moves further allowing more fluid to come out (Figure 2.4 (c)). Figure 2.5 presents the lift - pressure characteristics of the safety relief valve at opening and closing conditions and shows the set pressure with a blowdown and the overpressure of 10% of the set pressure.

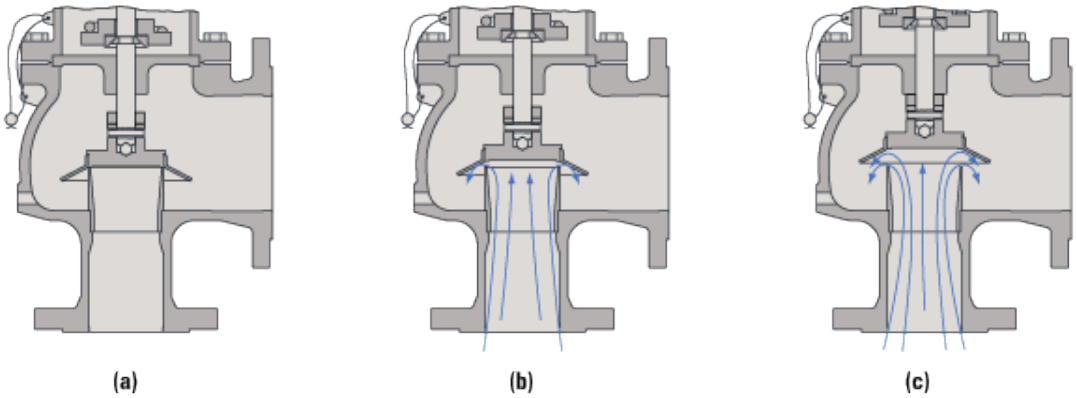

Figure 2.4: Safety valve operation

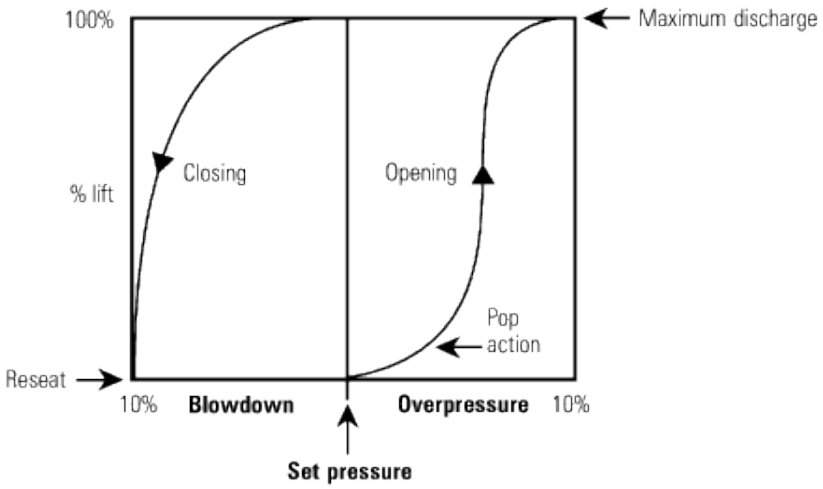

Figure 2.5: Safety valve pressure and lift characteristics

Safety relief valves fall into two types according to the outlet flow direction. The first type is the 90^o angle which describe the right angle between the inlet and outlet flow direction (Figure 2.2). In this type the flow path is separated from the valve components such as the spring, glands...etc. This type is the most convenient for a corrosive or erosive flow to protect the valve components and

reflect an increase in valve lifetime. If the flow is highly corrosive/erosive, a full nozzle could be used to be the only part that is affected by the corrosive/erosive flow and could be replaced apart from the valve body or the valve components. In the second type, the fluids flow through the valve and the flow path is around the valve components (Figure 1.1). The flow path here is much more complicated than the 90^o valve and very sensitive to all of the valve components geometry. In addition, the back pressure in the second type has a more significant effect on the forces and hence the valve opening and closing characteristics. These make the design of the second type more complicated and dependant on more factors than the 90^o one. The safety relief valve shown in Figure 1.1 is investigated in this study and it can be considered a full lift safety relief valve. A detailed description of the valve construction and components is introduced in Section 4.2

Chapter 3

Literature Review

3.1 Safety Relief Valve Design Requirement

The design and operation of safety relief valves are well established in industry and cover a wide range of pressures, temperatures and fluids and require a variety of design solutions which will involve material selection, sealing, spring design , pressure integrity, etc. These issues are important but are not considered here. What is considered in this work are the flow related design issues of flowrate, opening and closing of the valve, i.e. the primary functions of a safety relief valve. It is notable that until recently the design of safety relief valves has relied primarily on experimental design with trial and error solutions to achieve the desired level of performance. National and international standards for safety relief valves have been in existence since the early 1900's and lay down the basic requirements for an acceptable design. A semi-empirical approach is specified for the sizing of the flow areas to ensure that an adequate relief flow is achieved. In addition to the requirements for flowrate the current standards (for example the ISO 4126) also require that the valves open within +10% of the set pressure and close within -15% of the set pressure. In contrast to the flowrate requirements, no guidelines are given on how to achieve these conditions.

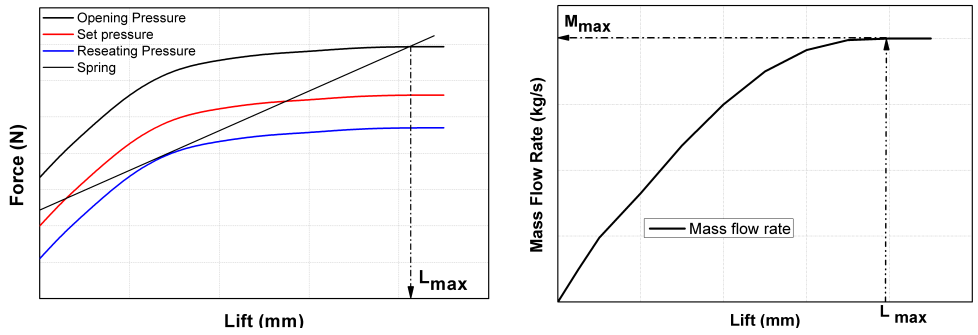

(a) Force-Lift **(b)** Flow-Lift

Figure 3.1: General opening and closing characteristics for a SRV

However, a general methodology based on quasi- steady assumptions can be established from consideration of how the forces and mass flow varies with lift on the valve piston. The piston is the term used in this thesis to describe the main moving element in the valve that responds to the force imbalance due to the

spring and fluid dynamic forces. These vary with the valve opening (valve lift) as shown in Figure 3.1a which shows a typical force-lift characteristic at an opening, set and reseating (closing) pressure. At the opening pressure, the fluid dynamic force will be greater than the opposing spring force and will result in acceleration of the piston and opening of the valve. After the initial piston motion and if the upstream pressure stays steady a balance of the fluid dynamic forces and spring forces will result in a constant opening being achieved at L_{max} (Full lift). From the mass flow lift characteristic, shown in Figure 3.1b the actual value of the mass flow can be determined at L_{max} for an opening pressure corresponding to the set pressure. This should be approximately the value calculated using the International Standards if the flow area has been designed properly. If sized properly the relief valve will lead to a reduction in system pressure which will correspond to lower piston forces and for each pressure a fluid dynamic force-lift curve can be established. Figure 3.1a shows the force-lift curve at the reseating pressure where the fluid dynamic forces are now lower than the spring force. This is the upper pressure limit which will allow the valve to close and can be used to indicate the valve's closure performance and its ability to meet the requirements of the Standards. This approach requires the emphasis to be put on the piston force-lift and mass flow-lift characteristic in addition to the area sizing calculation as suggested in the Standard. The approach is fundamental to valve design and is the approach taken in this thesis. What will be discussed in this and the following chapters is the ability to generate the mass flow and force characteristics using experimental and theoretical methods. It is the prediction of these characteristics that hold the promise of a completely theoretical valve design approach for both single phase and two phase flow conditions. This requires that CFD methods are available to do this and will be found to be the main focus of the thesis. Interestingly this approach has been found not to be widely discussed in the literature, however the published attempts will be reviewed in the following sections which have been specified into two sections for single and two phase flow conditions.

3.2 Single Phase Applications

This chapter will initially discuss the available literature from a single phase flow perspective since the majority of applications and most well established knowledge is with this condition. A thorough understanding of single phase knowledge is also a necessary pre-requisite for understanding two phase applications. The international standards requirements will be discussed and a brief review of sizing methods given. Theoretical methods, beginning with one-dimensional modelling approaches and ending with the use of CFD techniques, will be presented and discussed. A brief review of safety valve operation problems are presented as well.

3.2.1 International Standards Requirements for Safety Relief Valves under Single Phase Flow

The international organisations such as ISO , API and ASME set the specifications and the safety requirements for the sizing and operation of safety relief valves. For example, the international standard ISO 4126- Parts 1 and 7 [3, 4] include guiding arrangements necessary to ensure consistent operation and seat tightness, such as bonnet type, adjusting rings, restricted lift, end connections, spring material, leakage tests...etc. All these issues are very important to follow but it is beyond the scope of this thesis. One of the important tests that should be considered is the so called "Type test" which checks the set pressure, overpressure, reseating pressure, reproducibility of valve performance, lift at overpressure and the mechanical characteristics that could be noticed by sight or hearing such as the ability to reseat satisfactory and absence of chatter, flutter, sticking and harmful vibration. The ISO 4126 -1 standard states that the tolerance accepted in the type test for the operating pressures are

- *Set pressure* $\pm 3\%$ of the set pressure or ± 0.15 bar whichever is greater.
- *Over pressure* $\pm 10\%$ of set pressure or 0.01 bar whichever is greater.
- *Blowdown* minimum 2% and maximum 15% or 0.3 bar whichever is greater.

In general the international standards recommend a calculation method for the discharge area at the operating conditions to ensure the discharged mass flow rate and set limits for the pressure build up and decrease to ensure safe opening and closing. The "Type test" checks that the valve performance meets the standard tolerance and limitations. A detailed review and comparison between international standards for safety relief valves were carried out by Föllmer and Schenttler [28]. The study compares the ISO 4126-1 , ASME VII, ASME I and AD A2[1]/TRD 421[2]. A comparison is presented in Table 3.1 which shows an agreement of the three standards at the maximum opening overpressure limit of 10%, however the ASME *I* gives less tolerance for the max over pressure value and limit it to 3% only. On the other hand the closing pressure tolerance is different in all the standards. The closing tolerance is very high for the ISO 4126-1 which is expected to be changed to a lower value to meet the new strategies of reducing green house gas emmisions. This indicates that there are no common requirements for valve operation worldwide. It is clear that benefits could be gained by imposing consistent conditions.

	ISO 4126-1	ASME VII	ASME I	AD A2/TRD
	Gas/vapour/steam	Gas/vapour/steam	steam	Gas/vapour/steam
Open	manufacturer indication max. 10% or 0.1 bar	max. 10% or 0.2 bar	3%	max.5%- 10% or 0.1 bar
Close	manufacturer indication min. 2% and max. 15% or 0.3 bar	max. 7 % only with adjusting ring or 0.2 bar	max. 4% or 0.28 bar	max. 10% or 0.3 bar

Table 3.1: Comparison of the required function values for safety valves at different standards

[1]Pressure Vessel Equipment safety devices against excess pressure - safety valves (Germany)
[2]Technical Equipment for Steam Boilers Safeguards against excessive pressure - safety valves for boilers of groups I, III & IV (Germany)

3.2.2 Simplified Models for Safety Relief Valve

Due to the complex three dimensional geometry and flows through safety relief valves, common assumptions to simplify the flow conditions or the geometry were used in the literature. One of the most common assumptions is to simplify the three dimensional unsteady flow to a steady one dimensional flow. For example Gringberg and Krichker [32] studied the safety relief valve at full lift at a steady state operation assuming steady one dimensional flow. Maximum flow and working pressure (opening pressure) were used to calculate the fluid force. From the force balance of the fluid force, the spring and the friction force, the setting and the reseating pressure could be estimated and the valve inner diameter could be determined. A similar method was adopted by Sterland [64] but with the aid of experimental measurements. A dimensionless force-lift characteristics was presented. On the other hand, most of the research study simplify the valve geometry into a convergent divergent nozzle. Sharma [61] simplified the valve geometry to an ideal convergent divergent nozzle and used empirical formula to calculate the mass flow rate. A design method for the valve seat, the spindle and the spring based on empirical formulae was presented. Unfortunately the study failed to present a full model. These three publications and many similar ones give the general background knowledge on various aspects of valves, however they fail to provide any insight to the compressible flow conditions that occur within the valve. This is not surprising given the complex flows that exist in the valve and until recently the lack of available experimental and theoretical tools to assess the flows. Because of this, industry has relied on trial and error methods and experience gained from experimental testing.

More successful attempts were made to develop a one dimensional fluid model to predict the flow through the valve. These attempts established a good base to study the compressible flow through safety relief valves and emphasised the importance of the mass flow and force variation with lift as dominant characteristics in valve performance. These models were achieved mainly by simplifying the valve geometry to a convergent divergent nozzle. One of the early attempts

was carried out by Parker [54], who carried out a one dimensional flow analysis through a general safety valve to determine the pressure – lift characteristics. The study considered the spring characteristics to determine the opening and closing of the valve. Predicted results showed reasonable accuracy when compared with experimental test data. With the same assumption of a convergent divergent nozzle, Bett and Francis [6] introduced dimensionless coefficients to present the lift, flow rate and forces in safety relief valves. The study aimed to introduce the safety valve characteristics independent of the operating pressure and the valve geometry. By the same authors, The pressure distribution on the back side of a safety relief valve was determined experimentally [7]. Pressure tappings were inserted under the piston in such a way that every pair is inserted at the same radius but at different circumferential location. This was a good way to check the axisymmetric flow properties. i.e. if the measured pressure at the same radius was equal so that the safety valve could be represented as an axisymmetric geometry. The study showed the choked (critical) area and proved that the two dimensional axisymmetric model is adequate for pressure prediction. Another approach was adopted by Francis J. [29] who divided the flow regions around the disc into different zones to calculate the pressure in each one and hence get the force–lift characteristics. The predicted results were compared with published experimental data. These publications were a good start in studying the compressible flow through safety relief valves and emphasised the importance of the mass flow and force variation with lift as dominant characteristics in valve performance. Although, these above mentioned methods were simple and easy to use, they still have narrow area of application and low accuracy due to the simplification assumptions. However, these methods were the foundation for the international Standards to recommend a sizing method for safety relief valves under single phase flow which is discussed in Section 3.2.3

3.2.3 Sizing of Safety Relief Valves for Single Phase Flow

More attention is given to sizing safety relief valves but not designing safety relief valves in the literature. The sizing procedures depends mainly on calculating the mass flow rate through the safety valve and hence selecting the right valve. Selection and sizing of safety relief valves depend on calculating the effective discharge area using a simple convergent-divergent nozzle approach taking into account a correction factor. This correction factor is called the discharge coefficient and it is determined from experimental testing. The discharge coefficient should be supplied by the valve manufacturer. The international standard ISO 4126-1 [3], the American Petroleum Institute API 520 code and ASME codes use the ideal gas equation for sizing safety relief valves. Although this method gives reasonable accuracy it still depends on experimental work to determine the discharge coefficient and it has some limitations.

At very high pressure or low temperature, gases usually behave in a real manner; intermolecular forces are no longer negligible. Also, friction and heat exchange with walls should be taken into account. Therefore, Luft G. et al [40] checked the accuracy of the international standard ISO 4126-1 and the American Petroleum Institute API 520 [1] method for selecting safety relief valves at high pressures. The study experimentally investigated the discharge coefficient when relieving ethylene at high pressure 150-300 MPa. The study showed that the ISO and API methods overestimated the valve size at high pressure. In a similar manner, Schmidt J. et al [58] derived an equation to calculate the mass flow rate considering the real gas factors. The equation results were compared with the ISO model, CFD simulation and experimental work at high pressure. The comparison showed that the ISO model data is not adequate to calculate the mass flow rate at high pressure. (When the thermodynamic critical point is approached, the ideal gas assumption is not permissible). These studies showed that the sizing models used by the international standards still have limits and are not accurate in some cases. Therefore, more accurate models with a wider area of application are needed which could be found in CFD models.

3.2.4 CFD in Modelling Safety Relief Valve

Using CFD techniques in design and sizing safety relief valves will result in more accuracy and wide area of application. With the development of computational fluid dynamic techniques and increased computing power, the ability to analyse the complex multi-dimensional compressible flow has become possible. Several attempts were carried out to use CFD in valve sizing and design. Sethi and Lai [60] modelled the valve dynamics using a simple force balance to determine the opening and closing of the valve. The dynamic model included force coefficients accounting for the fluid dynamics effect. There was no description of the mathematical model used and the CFD model was limited to determining the force coefficients with the aid of the experimental measurement. It could not be called a CFD model but it was a good start. A more advanced model using CFD was adopted by Berger [5] to investigate the compressible flow behaviour through pneumatic components. A pneumatic ejector and a pipe-nozzle-pipe component with a very simple geometry were simulated. The commercial CFD code TASC-flow was used to solve the mass averaged Navier- Stokes equations with the k-ε turbulence model in a two dimensional axisymmetric model. The predicted results showed good agreement with the experimental results encouraging the use of CFD techniques in such circumstances. Surprisingly there are few published studies of using computational fluid dynamics methods to design or improve safety relief valves. A CFD model of the fluid flow through a pressure relief valve was developed by Sethi and Sabet [59] using the PHOENICS code. Air as an ideal gas was used as the flowing fluid through the relief valve. Steady state Euler equations were used. Predicted results of the disk force and mass flow rate versus lift showed good acceptance; but including the viscosity and transient terms of Navier stokes equations will make the solution more general and realistic. Bilanin and Teske [8] applied the full Navier Stokes equations to flow through a spring loaded safety relief valve to examine and improve the safety valve performance. The predicted results were compared with another calibrated model "COUPLE". No experimental work was carried out to validate the predicted results. Kim et al [35]

studied a liquidised natural gas (LNG) safety valve performance using CFD techniques to improve its performance and develop a design tool. A two-dimensional, axisymmetric, model using the compressible Navier-Stokes equations is carried out to simulate the gas flow only between the nozzle exit and valve disk, the predicted results obtained at different lift to radius ratio (L/R) and operating pressures (P_0/P_a). Predicted CFD results were compared with a one dimensional analytical calculation and gave reasonable agreement. No experimental work was carried out. One of the factors that affect the CFD calculations accuracy is the grid size. Moncalvo et al [47] investigated the effect of the grid size and the turbulence model on the accuracy of predicting the mass flow rate in safety relief valves. ANSYS CFX-Flo. The 441 DN 25/40 and the 459 DN 15/25 standard valves were geometrically presented by a three dimensional grid in three cases of coarse, fine and very fine grid size. Maximum relieving pressure was 4.4 bar. The results showed the same accuracy for the $k-\varepsilon$ and $k-\omega$ turbulence models with slightly more accuracy obtained when using the shear stress transport (SST) turbulence model. The extremely fine grid size gave more accuracy.

Very few studies included the force analysis using CFD in safety relief valves. As mentioned before Sethi [60] only used the CFD as a method of calculating the boundary conditions to assist his dynamic model. Dempster et al [20] developed a two dimensional axisymmetric model of a safety relief valve to predict the flow and force characteristics to develop a design methodology for the safety valves using CFD techniques. The model used Reynolds Average Navier Stokes equations in conjunction with the Energy Equation and the standard k-ε model to account for turbulence effects. The FLUENT software was used for the solution and considered air as an ideal gas. The flow-lift and force-lift curves were obtained. A comparison of predictions with the experimental results gives excellent agreement but showed a significant sensitivity to geometry. This study has found to be the only published work on predicting the flow-lift and force-lift characteristics using CFD to establish CFD in safety relief valve design.

Two CFD studies related to safety relief valves flow prediction were carried

out by D'Alessandro [17] and Muschelknautz and Wellemhofer [49] and involved predicting reaction forces. Although the studies didn't predict any force on the valve components, they provide some information about force predictions using CFD.

3.2.5 Operational Problems of Safety Relief Valve

During operation a safety relief valve may face problems such as the improper sealing after opening, chatter, exceeding a safe level of noise or the rapid wear of the valve seat sealing material. One of the main problems that is related to fluid flow is chatter. Safety relief valves require certain flow rate to maintain the valve seat in the open position. Lower flows result in chattering, caused by rapid opening and closing of the valve closure element. This violent oscillation is due to the dynamic instability of the closure elements at the opening position, so it requires a return to a dynamicly stable position. Hence, chatter basically depends on the valve design parameters, such as the spring stiffness and valve geometry in addition to the operational conditions such as set pressure, back pressure and mass flow rate. Chatter can lead to destruction of the device which is a dangerous situation. Several studies investigate the chatter in safety relief valves. One of the earliest studies to consider the stability of relief valves was carried out by Funk [30]. The study investigated a poppet valve stability derived from the valve design parameters and the system operating conditions. Although the fluid used was an incompressible fluid, the study gave the basic analysis and understanding of the poppet valve stability. MacLeod [41] developed a dynamic model by analysing the dynamic stability of the valve closing to predict the chatter conditions. The ideal gas law were used to assist the dynamic model. Although the method described could be applied to a wide range of applications, it was not in a general form. Experimentally Föllmer [27] carried out an investigation of the oscillation in a safety relief valve generated by the inlet geometry. The study found that the sharp edged valve inlet holds the possibility of flow separation. The study recorded the oscillation frequency and visualised the flow by a high speed

camera. Cremers and Friedel [15] checked the validity of the of the published sizing rules to prevent chatter for the safety valve and the inlet pipe length. The results showed that the sizing rules are still not adequate to predict the safe inlet pipe length. Therefore, a new sizing criterion based on the pressure surge criterion was developed.

3.2.6 Overview

- Understanding the single phase flow through safety valves is a basic step to understanding and analysing two phase flow.
- International standards have recommended methods for sizing safety relief valves and give limits for their safe operation. These limits could be used only as targets for safety relief valve design but do not assist the design process.
- One dimensional models give basic knowledge on compressible flow through safety relief valve but they could not be extended to include more data on valve opening and closing characteristics. i.e. the flow-lift in conjunction with the force lift characteristics.
- All sizing methods for safety relief valves for single phase flow only consider the maximum lift condition, ignoring the valve performance on opening and closing.
- Experimental work could give detailed information of safety relief valves under single phase flow, but it still very expensive and time consuming.
- CFD has shown the ability to model flow through safety relief valves and extend the limits of the experimental work and the one dimensional models. Furthermore CFD can provide the quantitative analysis of many properties through the valve in addition to the flow rate and force characteristics.
- The approach used by Dempster et al [20] is adopted in this study to investigate the safety relief valve design. CFD is used with a two dimensional

model in conjunction with Reynolds Average Navier Stokes and the standard k-ε turbulence model to assist the design of safety relief valves. The force-lift and flow-lift characteristics are obtained with detailed information about flow properties through the valve at different pressures.

3.3 Safety Relief Valve under Two Phase Flow

Designing a safety relief valve for two phase flow is a more complicated process compared to single phase flow. Till present there is no direct general method or equations to design or select safety relief valves for two phase flow. Two phase flow through safety relief valves are very complicated due to the thermal and fluid dynamics phenomena occurring between the two phases. Therefore, modelling or predicting the two phase flow depends on a large number of parameters such as pressure, temperature, relative velocity and phase volume fraction in addition to the mass, momentum and heat transfer parameters. These two phase parameters are associated with the fluid flow, fluid properties, interaction between phases...etc. They also vary with the valve operating conditions which directly affect the flow conditions. Consequently, possible combinations of the two phase parameters result in different types of flow. For example, from the phase change point of view and mass transfer between the two phases, two different types of flow could be recognised; flashing flow, in which phase change occurs and the non flashing "frozen" flow in which there is no phase change. Two phase flow can be classified into many other types of flow, e.g. homogeneous, separated, critical, sub-critical...etc. [16]

To understand, model and analyse two phase flow through pipes, nozzles or safety relief valves three main approaches have been followed in the literature:

Analytically the complexity of two phase flow prevents the formulation of equations representing the exact flow conditions. This has resulted in applying methods which are an extension of single phase formulated methods with suitable assumptions for two phase flow conditions. Hence, algebraic ex-

pressions have been established to describe the two phase flow conditions. In this study, they are referred to as "**Simplified models**" [63].

Computationally two main approaches are used in CFD models to represent two phase flow which are the Eulerian-Eulerian and the Eulerian-Lagrangian approaches and will be discussed in Chapter 5. CFD models have the ability to solve the multi dimensional continuity, momentum and energy equations in addition to the interfacial equations for all phases by using the advanced computational power available nowadays. CFD models make much less assumptions than the simplified models. However, some assumptions are made to reduce the number of equations to be solved to reduce the computational effort. One of the common assumption is to deal with the two fluid flows as one mixture when the flow is a dilute flow. The mixture CFD model is adopted in this study and it is considered a simplified form of the full Eulerian model. The mixture model is presented in Chapter 5.

Experimentally Using practical measurements in the field or in laboratories for the flow properties. Main flow properties measured are the pressure, flow rate, temperature, velocities, and phase volume fraction. These properties provide basic information for identifying general trends and validating the theoretical predictive methods. They also allow empirical or semi-empirical approaches to be deployed and an example of this will be found later in Chapter 5 when scaling parameters are considered.

It is common practice to refer to the international standards as a first step in establishing the safety specifications and limits of a device. In the following subsection the international standards requirements for the use of safety relief valves for two phase flow are reviewed. Since the international standards calculation methods are based on the simplified models, the opportunity is taken to review these at this point. Other related literature for the sizing of safety valves for two phase flow will be discussed thereafter.

3.3.1 International Standards Requirements for SRV under Two Phase Flow

Unlike the case of safety relief valve operation with single phase flow, the international standards for use with two phase flow provide a much more limited set of specifications. For example, the ISO 4126-10 [2] considers only the sizing of safety relief valves under certain conditions with limited simplified models. There are no guidelines on the operation requirements and the opening or closing pressures. The standards recommend calculations for identifying the flow regime and quality at the valve inlet, which are the necessary requirements for sizing the valve under two phase flow. In addition the standards present recommended calculations for determining the mass flow rate to be discharged, depending on the for the reasons of pressure rise in a system. These data helps in understanding the mixture nature and composition. Simplified models and sizing methods are discussed in the following sections.

3.3.2 Simplified Models and Sizing of SRV

Simplified models help in understanding two phase flow behaviour but are limited in accuracy due to the assumptions used to simplify this very complex flow. Simplified models are adopted by the international standards such as ISO, ASME and API to size and select safety relief valve under two phase flow. The two phase flow models that are most used and most suitable for safety relief valves are based on either the Homogeneous Equilibrium Model (HEM) or the Homogeneous Non Equilibrium (HNE) Models. The word “homogeneous” here assumes that the two phases are well mixed so that they behave like a single phase fluid. This modelled fluid has properties that are weight or volume averaged properties of the two fluids. The word “Equilibrium” here assumes that the two phases are in a thermal and mechanical equilibrium implying that there is no temperature or velocity difference between the phases.Three other combinations of these two conditions could cover the remaining possible cases such as the non-

homogeneous equilibrium model , which accounts for the slip velocity between the two phases, the homogeneous non-equilibrium model and the non-homogeneous non-equilibrium model. These models need additional relations for the interfacial mass, momentum and energy transfer rates.

In general, theses models consider the safety relief valve as an ideal convergent-divergent nozzle and an empirically determined discharge coefficient is applied according to the model used. Sizing of the relief valve requires the calculation of the mass flux through the valve nozzle using one of the simplified models according to the flow conditions. The required valve discharge area will be then the required mass flow rate divided by the calculated mass flux and the discharge coefficient K_d (Equation 3.1). Therefore determining the discharge coefficient is one of the challenges in the two phase flow simplified models, as it reflects all of the complexity of the two phase flow in addition to any deficiency in the model. On the contrary the discharge coefficient K_d for the single phase flow will reflect mainly the geometric deviation of the valve from the ideal nozzle.

$$A_d = \frac{\dot{m}}{G_{th}.K_d} \tag{3.1}$$

Lenzing et al. [37] carried out experimental work on commercially available safety relief valves and compared the results with the available models such as the HEM, the model adopted by DIERS[3] (ω method) and the homogeneous frozen model. Lenzing et al defined a simple volume weighted two phase discharge coefficient for the homogeneous equilibrium model (HEM) to improve the model mass flow rate prediction. The discharge coefficient is defined in equation 3.2. Similarly Fauske [24, 25] calculated the two phase mass flux by calculating the gas mass flux and the liquid mass flux separately and then combining them using the mass-weighted average, equation 3.3. These two different methods used by Lenzing et al and Fauske provide a good prediction but in the case of a critical mixture flow they ignore the fact that when calculating the gas phase in critical

[3]Design Institute for Emergency Relief Systems

conditions the liquid phase will be calculated under the non critical conditions which is far from the real case for a critical mixture flow. Therefore, Boccardi et al [10] used equation 3.2 with experimental validation and proved that this equation underestimated the flow rate under the tested conditions. A slight modification of the discharge coefficient using experimental results was presented. On the other hand, Tran [66] showed that using equation 3.3 with the HEM undersized the safety relief valves in many conditions.

$$K_{dm} = \alpha K_{dG} + (1 - \alpha) K_{dL} \tag{3.2}$$

$$G = \left[\frac{1 - x_g}{G_l^2} + \frac{x_g}{G_g^2} \right]^{-1/2} \tag{3.3}$$

An alternative modelling approach is to deal with the safety relief valve as a sharp-edged orifice in the case of compressible two phase flow. This method was adopted by Leung [39] to predict a two phase discharge coefficient in conjunction with the compressibility parameter ω at different flow conditions. In this method the predicted two phase discharge coefficient for a valve not only reflect the complexity of the two phase flow and the geometry deviations but also the area contraction due to the vena contracta associated with orifice flow. The discharge coefficient developed by Leung [39] showed a good agreement with the published experimental work on safety relief valves. However, the method used requires a trial and error steps to get an initial guess for the two phase discharge coefficient and then an iterative steps to obtain a final value. Therefore, simplifying the valve geometry to a nozzle shape is the most representative geometry to consider. Darby [18] showed that for the frozen flow, the two phase discharge coefficient is equal to the liquid discharge coefficient when the two phase flow is not choked, while it is equal to the gas discharge coefficient when the flow is choked.

A special case of the HEM is called the ω method. The ω is named from the ω parameter which was first introduced by Leung [38] in 1986 and then modified in 1995 by the same author. The ω parameter is a compressibility factor defining an

equation of state for the two phase flow . Numerous research studies have been carried out to modify or check the limitation or the working conditions of the ω method and to improve its accuracy. For example, Lenzing et al [36] compared the HEM model with the original and modified ω method for different gases and working conditions to check the model's limits and its deviation for different cases. Boccardi et al [9] investigated experimentally two safety relief valves with the same diameter and two different discharge coefficient and inlet geometries. The results compared well with the ω method and showed the influence of the geometry on the valve sizing. For two phase flow with lower mass qualities the ω method leads to undersized valves. Diener and Schmidt improved the ω method to extend its limits at lower qualities. This model called the HNE-DS (Homogeneous non-equilibrium model Diener-Schmidt) was improved by introducing a boiling delay coefficient, N, based on the mass quality at the critical cross section to account for the thermal non-equilibrium. Another modification was added by the same authors to account for the mechanical non-equilibrium due to friction between phases by introducing correlation for the slip velocity. The same authors applied this method to a standard valve (leser DN 25/40) at different conditions with comparison with the HEM, the ω method and experimental work. The comparison showed better accuracy of the HNE-DS specially at the low quality. The three models achieved the same degree of accuracy at higher quality.

The ω models are easy to use and depend only on the stagnation condition but still need the single phase discharge coefficient of the gas and liquid supplied by the manufacturer or obtained experimentally. The international standards adopted these models as a recommended method for sizing safety relief valves under two phase flow. For example the ISO 4126-10 adopted the HNE- DS model with the mechanical equilibrium assumption only and the API 520 recommend an ω model as well.

Several studies were carried out to discuss the flow rate predictive capability of these models at different flow conditions. Schmidt and Egan [57] compared the mass flux predicted by the ISO and the API adopted models and the ω model

by Leung [38], the HEM and experimental data. The comparison showed that at non-equilibrium conditions (thermal or mechanical) with inlet pressure much less than the thermodynamic critical pressure, the ISO and HNE-DS predict higher flow coefficients which leads to smaller valve sizes compared to the HEM and the API 520 (2009). The study compared the model results with measurements on different valves and for different conditions. The comparison showed that the ISO and the HNE-DS gave acceptable results and more accurate than the other two models. The accuracy of sizing safety relief valves using the ω methods was carried out by Derlin and Friedel [21, 22] at different conditions. The study showed that the ISO model is the most accurate model to size safety relief valves under two phase flow, although it oversized the valves at all working conditions. Moncalvo and Friedel [45] investigated the reproductive accuracy of the models for sizing safety relief valves under two phase flow considering a range of liquid phase viscosities. Different models used in the industry including the ISO model and the ω method model by Leung were compared. The study recommend the ISO model at most of the conditions and showed that the ISO model oversized the selected valve.

All the above studies confirmed that the ISO 4126-10 model is the most accurate model to select safety relief valves under two phase flow in most of the working conditions. But the ISO model still needs the discharge coefficient of the valve for all of phases as single phase. These discharge coefficient should be supplied by the manufacturer or obtained by experimental work. In addition the ISO model oversized the selected valve in all conditions with variable prediction accuracy.

The sizing method and models presented here only calculate the critical mass flow rate through the valve at the maximum lift. These models can not provide more information on the valve force-lift and flow lift characteristics which is essential in determining the opening and closing characteristics of a valve. This is why the simplified models is widely used only for predicting the critical flow rate through the valve and to select the suitable valve with the proper discharge area.

Experimental work could give better information on safety valve characteristics.

3.3.3 Experimental Measurements of SRV

In general, experimental investigations contribute to the understanding of two-phase through safety relief valves. In addition, flow and mass flow characteristics could be obtained by experimental work but no much relevant publications have been found in the literature. Till now the international standards and many models rely on the experimental work to obtain the discharge coefficient and experimental work is essential to validate the theoretical models.

Kendoush et al [34] experimentally investigated steam flow through five different safety relief valves under a pressure range of 4.5-75 bar. A gamma ray densitometer was used to measure the void fraction and a turbine flowmeter was used to measure the water mass flow rate. The results gave basic information of some parameters of the safety relief valve under two phase flow such as the back pressure, void fraction and mass flow rate with time, but without any data on the valve performance. An experimental study on safety relief valves under two phase flow conditions was carried out by Bolle et al [11, 12]. The pressure distribution through the valve with the temperature at the inlet and outlet and the mass flow rate were measured. The study provided good knowledge of the pressure and temperature distribution and the mass and heat transfer of the flashing flow through safety relief valves. Experimental results were used to examine the HEM for the flashing flow conditions and it was found to underestimate the mass flow rate by 20% in most cases. Narabayashi et al [50] evaluated safety relief valve performance by testing scaled model valves. The study showed that the scaling hardly affected the measurements and that the piston force is hardly dependent on the void fraction. The valve opening and closing were checked and found satisfactory. To compare the HEM model with the ω model and make an improved correlation for the discharge coefficient, Boccardi et al [9, 10] developed a test rig to test safety relief valves under two phase flow with very wide testing conditions. The water flow rate was controlled according to the test conditions. The test

pressure range was from 0.5- 1.75 MPa and experimental tests were carried out at different water flow rates and hence various volume fraction but only one fixed lift (full lift). In a similar manner, Moncalvo and Friedel [46] developed a test rig to facilitate the measurement of gas-liquid two phase flow through a safety relief valve. The study aimed to investigate the influence of the liquid phase physical properties on the void fraction at the valve inlet with no data given on mass flow rates or piston forces at different lifts.

All of the mentioned above experimental studies (and many others) provided a very good understanding of the complex two phase flow through safety relief valves. They provide good knowledge on two phase flow behaviour such as heat and mass transfer between phases, pressure drop through the valve and the pressure and volume fraction effect on the valve mass flow rate. Hence, They helped in validating the theoretical models and in proveing them. Although, these experimental studies gave a deeper view of the two phase flow parameters with their operating conditions, they still did not cover the effect of valve characteristics on the opening and closing of the safety relief valve. In addition, experimental work is expensive, time consuming and do not provide local flow details in many conditions. More experimental work concerning the valve performance is still needed. On the other hand CFD could be used to provide both global and local flow details and more visual understanding at a lower cost and faster.

3.3.4 CFD Modelling for Two Phase Flow

As mentioned previously, CFD has been used successfully to predict the flow in safety relief valves under single phase flow. Although there are several examples in the literature of using CFD to predict two phase flow in pipes, ducts, jets...etc., there is no published work for predicting two phase flow through safety relief valves. Some of the published two phase CFD work suggest that it may be possible to use CFD in predicting the flow through safety relief valves. In this respect, the convergent divergent nozzle can be considered the nearest geometry to the safety relief valve. Pougatch [55] developed a two fluid model to predict a

high volume fraction water-air flow in a convergent-divergent nozzle. The water was the continuous incompressible phase while the air was the dispersed compressible phase. A two fluid Eulerian-Eulerian approach was adopted assuming no heat or mass transfer between phases. Two sets of continuity, momentum and energy equations are derived for each phase in addition to the interfacial equations with the standard k-ε turbulence model for the mixture. The two fluid Eulerian-Eulerian model with the standard k-ε turbulence model for the mixture results showed a good agreement with the experimental results. This simple geometry problem with two component frozen two phase flow has given a basic understanding of using CFD for predicting two phase flow. Two CFD studies on two phase flow through pipes were carried out by Ghorai and Nigam [31] and DeSchepper et al [19]. The Studies used a simplified CFD model based on the Eulerian-Eulerian approach called the Volume of Fluid method (VOF). The VOF is a surface-tracking technique applied to a fixed mesh. It is suitable for two or more immiscible fluids. In the VOF model, a single set of momentum equations is shared by the fluids, and the volume fraction of each of the fluids in each computational cell is tracked throughout the domain. Applications of the VOF model include stratified flows and free-surface flows. Ghorai and Nigam [31] modelled the wavy stratified air water flow in a pipe with a satisfactory agreement with the experimental results since the VOF assumption were valid for this case. The VOF is less intensive than a full Eulerian multiphase flow. DeSchepper et al [19] verified the Baker chart for gas-liquid flow through horizontal pipes. The predicted results showed a good agreement with the baker chart. However more accurate CFD results can be obtained if different CFD models were used with the corresponding flow regime. Brennan [14] used the mixture model to investigate a solid-liquid-air flow at a separator cyclone. The mixture model is a simplified form of the full Eulerian model that treats the phases as one mixture. The Reynolds Stress turbulent model was used to count for the swirl and flow reversal that dominate the flow through the cyclone separator. The model prediction for the density profiles showed a qualitatively results, whereas the predicted segregation

was larger compared with the measured one by the gamma ray tomography. One of the main factors that affects the accuracy of the prediction of the segregation of the particles was neglecting the turbulent stress and the fluctuating terms in the slip velocity equation in the model implemented by the Fluent code. In later studies carried out by Narasimha et al [51–53] and Brennan et al [13] the mixture model slip velocity equation has been modified to count for the gravity and the lift near the walls which were important factors affecting the model accuracy. The use of the mixture model showed less computational effort and good prediction for the multiphase flow through the cyclone separator.

Up until now, there are no CFD studies on two phase flow through safety relief valves in the literature. However, the above mentioned studies on two phase flow through pipes, nozzles and cyclones separators suggest using simplified CFD models to predict the two phase flow through safety relief valves. The simplifications depend on the assumptions that have arisen from identifying the flow regimes and determining the flow conditions. In this study the mixture model with the standard k-ε turbulence model are used to predict the air-water flow through safety relief valves. The Mixture model and the standard k-ε turbulence model equations are presented in Chapter 5.

3.3.5 Overview

- International standards provide a recommended method to size the safety relief valve discharge area for gas-liquid flow. There is no information on the recommended working conditions for safe operation. There are no recommendations or guidelines to help in safety valve design for two phase flow conditions.

- Simplified models are easy to use and play an important role in sizing and selecting safety relief valves for two phase flow, but they still have limits and depend on experimental data. Simplified models have not been extended to predict the flow-lift and force-lift characteristics to investigate the opening and closing characteristics.

- Due to the very small scale geometries found in safety relief valves it is only CFD techniques that are likely to provide insight of the distribution of fluid properties (pressure, temperature, velocity etc...) at a low cost and in a fast way.

- Although CFD has not been used in the literature to predict the flow through safety relief valves under two phase flow, It has been shown to provide good information for two phase flow through pipes and nozzles. Hence, this suggest that CFD can be used for predicting the critical flow rate through safety relief valves. The usage of CFD can be extended to predict the basic data required for valve design such as the flow-lift and force-lift characteristics which determine the opening and closing characteristics.

Chapter 4

Single Phase Flow Studies

4.1 Introduction

An essential step to understanding two phase flow through safety relief valves is to firstly understand and model the single phase flow. In this chapter the single phase flow through a safety relief valve is investigated computationally and experimentally. The main objective is to determine the predictive capability of a CFD approach and to establish an experimental methodology for testing. In particular the force and flow lift characteristics will be determined experimentally and used to validate the CFD prediction. Here the commercially available code FLUENT 6.3.26 will be used. In the following sections the valve construction, testing methods computational work and the results will be discussed.

4.2 Valve Construction

The safety relief valve considered in this study is a conventional spring loaded safety relief valve. It has a 1/4" orifice size and intended for use in the refrigeration industry for refrigerant vapours; however it is used here with air. Figure 4.1 shows a cross sectional drawing of the entire valve. Detailed manufacturer's CAD drawings are presented in Appendix A.1 . The safety relief valve is set to open at a pressure safely below the bursting pressure of a pressurised system. The piston (2) is held against the seat by a loaded spring (7) which is fitted between the gland insert (5) and the spring guide (6); excessive pressure forces the piston to open. The valve is designed such that when the valve opens slightly, the pressure builds up to open it fully and to hold the valve open until the pressure drops a predetermined amount. The relieving pressure is set by the initial compression of the spring which can be altered through the adjusting gland (4). Minor modifications have been applied to the valve to facilitate the experimental work; a 4 mm diameter rod 150 mm long has been fitted to the piston rear, the adjusting gland (4) and the adjusting gland insert (5) have been combined and replaced by a single equivalent component and the spring (7) has been cut to a smaller length. The rod diameter is less than the spring inner diameter, so there

is no significant change in the flow area at this region. However, the rod has been chosen to have the minimum diameter that could resist the aerodynamic forces without buckling or failure; however the minimum rod diameter results in 6% less flow area at the valve outlet. Tests on similar valves indicate that these modifications have no significant effect on the measured or the predicted values of the mass flow rate, back pressure or the fluid forces on the piston [20]. To verify this assumption, experimental work has been carried out on the entire assembled valve and the modified valve and will be described later. A modified axisymmetric gland (shown in Figure 4.1) has also been made to decrease the impact of the three dimensional geometry on the force prediction and this will be discussed later.

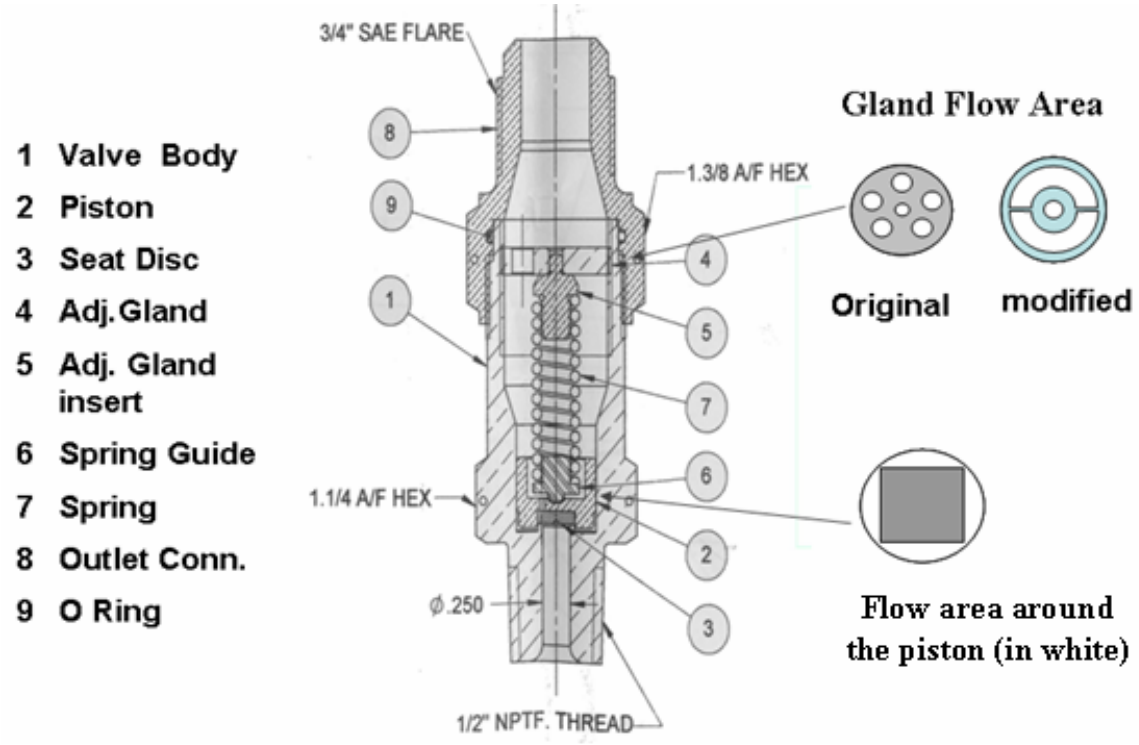

Figure 4.1: Valve construction (Dim. in inches)

4.3 Single Phase Testing

Experimental work has been carried out to obtain the flowrate-lift and force-lift characteristics in order to validate the predicted CFD results. Assuming quasi

steady flow, as mentioned earlier, the flowrate-lift and force-lift characteristics have been obtained at constant test pressure. Hence, each flowrate-lift and force lift curve is associated with a single test pressure value. A test rig was built to facilitate the piston movement (lift), pressure, flow rate and force measurement.

4.3.1 Test Rig Construction

To determine the experimental data for single phase air flow, an existing safety relief valve test facility located in the Department of Mechanical Engineering at the University of Strathclyde has been used. A layout and a schematic drawing of the test rig is shown in Figures 4.2 and 4.3. It has been constructed to measure the net force acting on the piston, the pressure at various locations in the flow and the mass flow through the valve at any piston lift. The tested valve is connected to the end of a 150 mm diameter pipe and supplied with compressed air. The air supply circuit is presented in Figure 4.4. The valve piston is connected via a rod to a load cell which has the range of ±445 N (±100 lbf) (Omega Eng. limited LC203-100). The rod is 4 mm diameter and 150 mm long. The piston back face has been slightly modified to allow the rod to be firmly fixed to it. These slight modifications from the original valve have no significant effect on the flow. A linear cross slide is used to facilitate movement of the piston and the determination of a force-lift characteristic. The mass flow is measured by a Sierra Instruments vortex mass flow meter (Innova-mass series 240) , located in an upstream air supply line of 40 mm diameter (14 in Figure 4.4). The force-lift and mass flow rate-lift characteristics are steady state characteristics and to achieve this the upstream pressure has been maintained constant at any lift value by controlling an upstream throttle valve (7 in Figure 4.4) located in the main air supply line. The valve supply pressure is measured using a bourdon gauge (16 in Figure 4.4) positioned upstream of the valve in the 150 mm diameter pipeline and the piston back pressure is measured by a bourdon gauge connected to a 1 mm diameter pressure tapping on the valve body (Figure 4.3). The piston position (piston lift) is determined by measuring the displacement of the cross slide using a

digital 'dial' gauge which has an accuracy of 0.001 mm; This results in an relative error of the order of 0.01 % to 0.6%. For the force measurements the accuracy is 1 Newton which gives a measurement error range of 0.5% to 2%. The accuracy of the pressure measurement is 3 kPa which gives a relative measurement error of 0.2-2.5%. The mass flow rate is accurate to 1% of the reading.

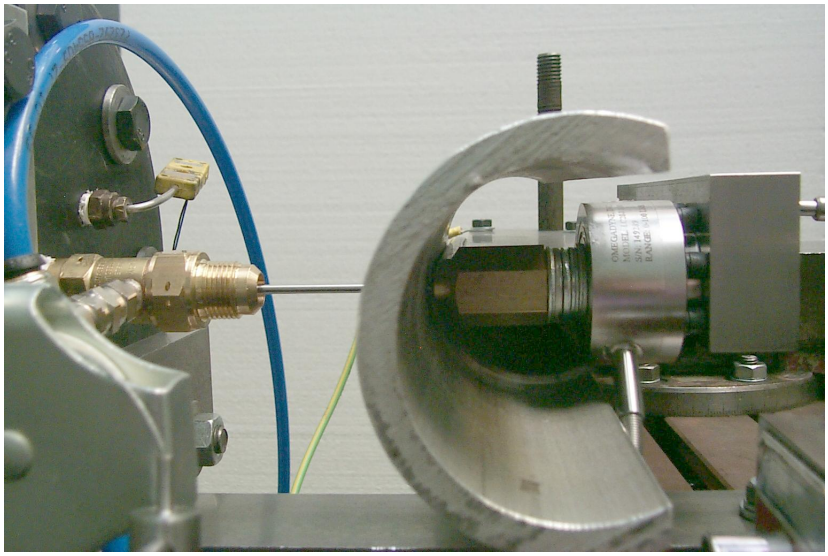

Figure 4.2: Construction of test rig for single phase flow measurement

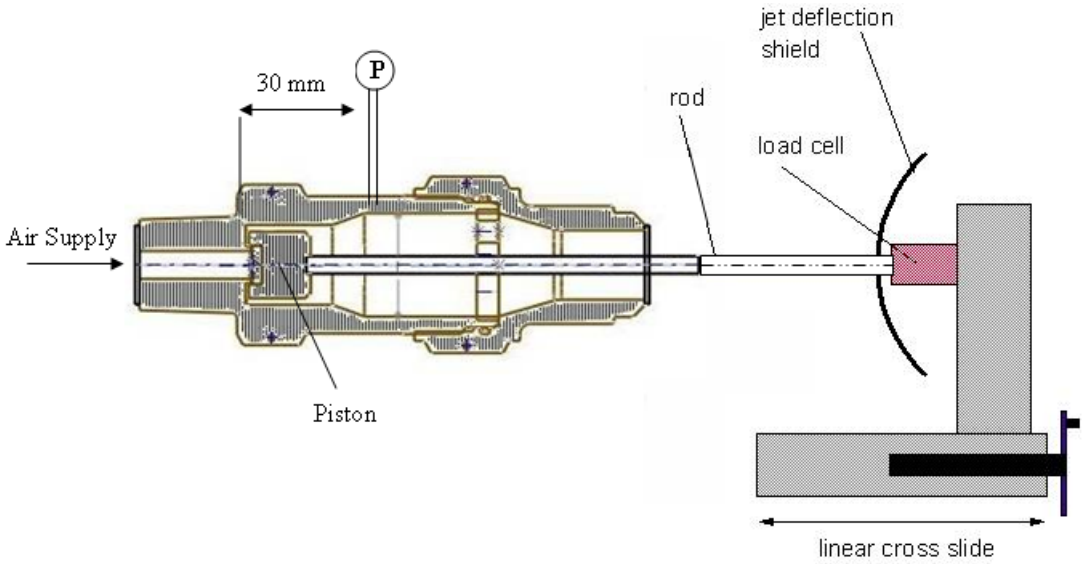

Figure 4.3: Scheme drawing of the test rig for single phase flow

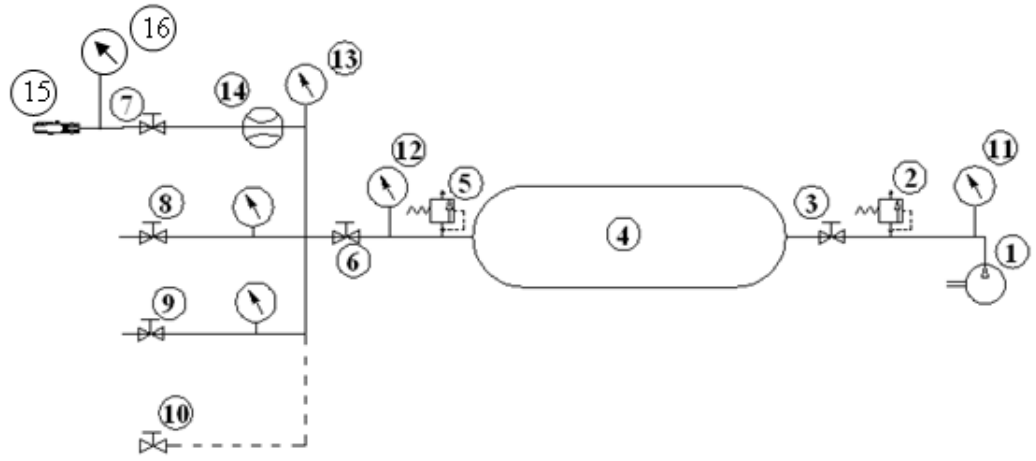

1	Compressor	5	PRV	9	Gate Valve	13	P. Gauge
2	PRV	6	Gate Valve	10	Gate Valve	14	Vortex Flow meter
3	Gate Valve	7	Gate Valve	11	P. Gauge	15	Test Valve
4	Reservoir	8	Gate Valve	12	P. Gauge	16	P. Gauge

Figure 4.4: Air supply circuit diagram

4.3.2 Experimental Procedures

Initially the piston is in a closed position and the air supply gate valve (7 in Figure 4.4) is totally closed. At this state, the piston is pushed against the seat to seal the valve, a reaction force is established due to contact between the seat and the piston face. When the supply system is pressurised and the gate valve (7) is opened, air is supplied to the test valve (15) and an additional force due to the air pressure on the piston front face is noticed. With a further small opening movement of the piston at the same test pressure, the reaction force due to the seat contact will decrease while the pressure force will be constant. The zero lift point is defined as the point where the seat is just untouched by the piston and is believed to correspond with a minimum force measured by the load cell. With further lift, air starts to flow; hence a higher force will be detected by the load cell. So at a constant test pressure a minimum force value is associated with the zero lift position.

Experimental tests start at a suitable sealing position and is taken to be the zero displacement position. The gate valve is slightly opened until the test pressure increases to the desired value. The values of the piston force are recorded

	Test Pressure (barg)				
Characteristics	4.1	5.5	6.9	11.7	13.8
Flow-Lift	√	√	√	√	√
Force-Lift	√	√	√	√	√
Back pressure-Lift	√	√	√	√	√

Table 4.1: Experimental test matrix (Single phase flow)

since the flow rate and the back pressure will be below measurable values. Then the piston is moved in small steps of lift (0.01 mm) till a lift of 5 mm is achieved. Ambient temperature and pressure were measured at the start of each test. At each lift the force, air flow rate and back pressure are recorded. Finally the minimum value of the force is detected and the displacement associated with it, is taken to be the zero lift. These steps are repeated with different test pressure values ranging from 4 - 14 barg ($\sim$ 60 to 200 psig). Table 4.1[1] identifies the experimental conditions for each valve test investigated. Tests in Table 4.1 were carried out for a number of conditions:

1. The standard valve with all the internals (spring and gland) in place.
2. The standard valve with no spring (standard test arrangement).
3. The valve in the standard test arrangement with a modified gland , as shown in figure 4.1
4. The valve in the standard test arrangement with no gland.

The first group of experimental tests were used to verify that removing the spring of the safety relief valve will not affect the mass flow rate, piston back pressure or the piston force. Figure 4.5 shows the comparison of the experimental results obtained when testing the complete valve and the modified valve at 11.7 barg (170 psig) inlet pressure, and shows close correspondence for both conditions. It was concluded that the spring had no effect on either the force or mass flowrate and need not be modelled in the CFD simulation. All subsequent tests were

[1]Full experimental results can be obtained by contacting Wael Elmayyah (elmayyah@yahoo.co.uk) or Dr. William Dempster (william.dempster@strath.ac.uk)

carried out with the spring removed. The second group of experimental tests were carried out on the valve with and without the adjustment gland/insert combination. This allowed back pressure effects to be removed and geometry modelling of the gland to be addressed separately. The effect of the gland on air flow rate and force is presented in Figures 4.6 and 4.7 and is discussed in Section 4.5. A modified gland has been used to examine the three dimensional geometry effect on the force and back pressure prediction. The modified gland was designed to have a larger flow area thus reducing the effect of the back pressure and to have a flow geometry as close as possible to an annulus flow area which is easy to model in two dimensions. A CAD drawing for the modified gland is presented in Appendix A.1.2. In this Chapter the word "gland" refers to the five hole original gland while the modified gland is simply called the "modified gland".

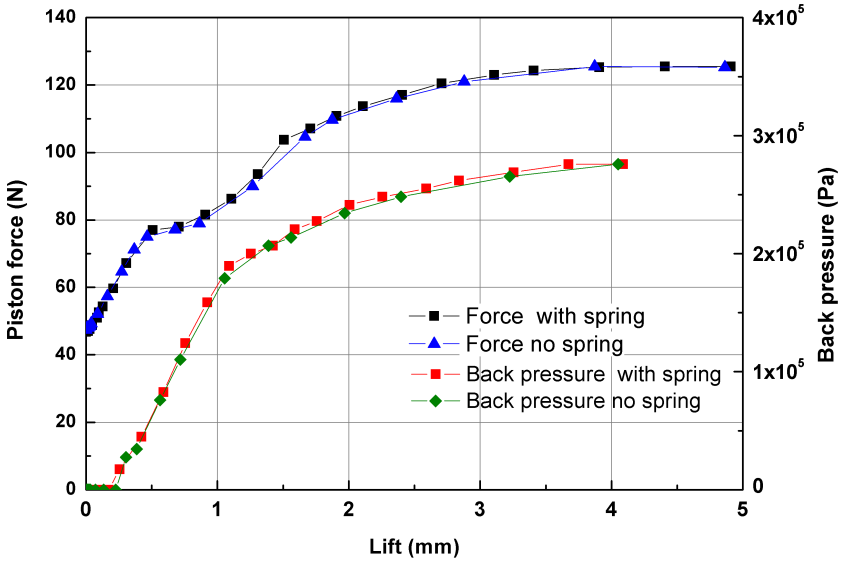

(a) Piston force and back pressure

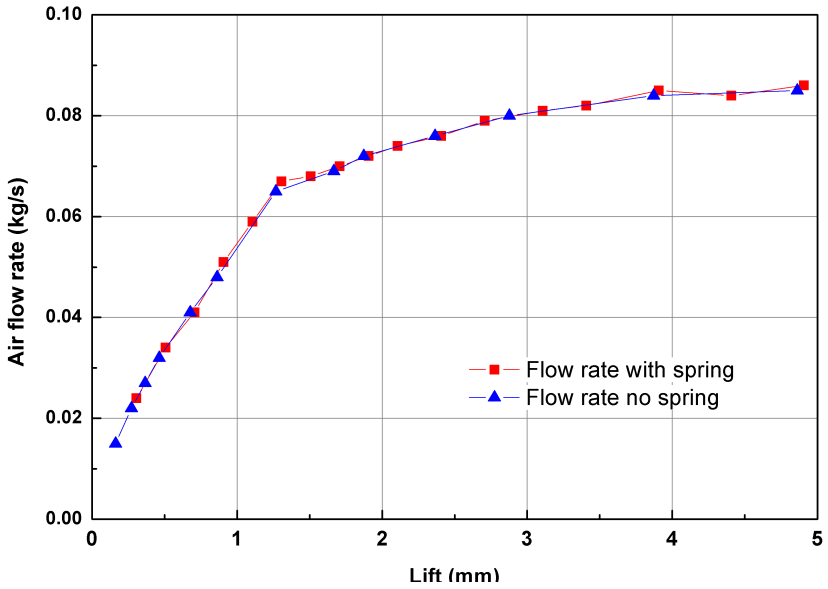

(b) Air flow rate

Figure 4.5: The effect of the spring on the flow rate and piston force

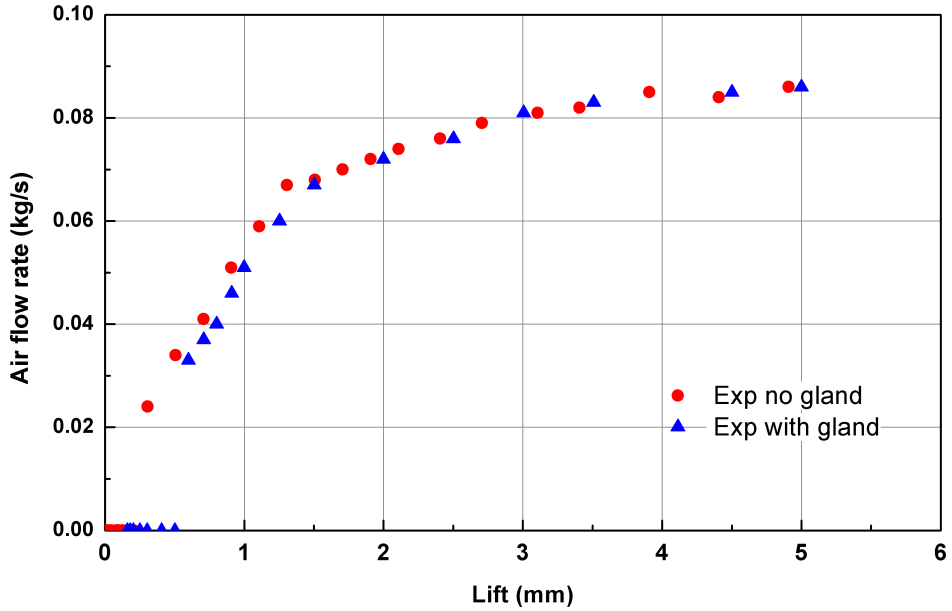

Figure 4.6: The effect of the gland on the air flow rate at 11.7 barg (170 psi)

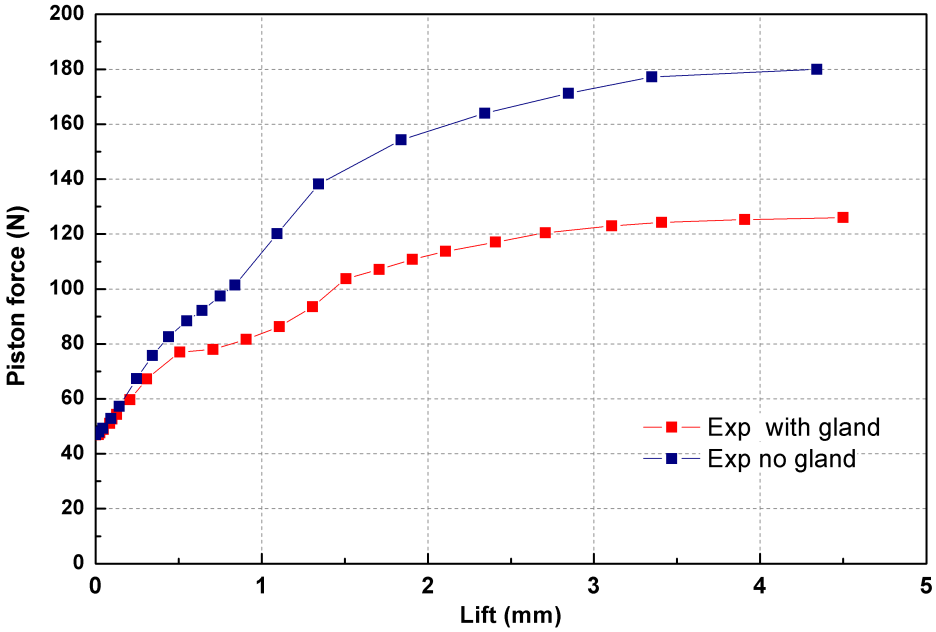

Figure 4.7: The effect of the gland on the piston force at 11.7 barg (170 psi)

4.4 Computational Model

In this section the computational model is discussed by introducing the computational grid details, the mathematical model and the boundary conditions setup.

4.4.1 Model Equations

Although the valve dimensions are very small, the air flow is still a continuum flow and the well known Navier-Stokes equations will be valid. At a very small lift (0.1 mm) the Knudsen number is about 6×10^{-6} which means that the continuum assumption of the flow is still valid. For the flow conditions studied here, the intermolecular forces are negligible since the test pressure is much less than 150 bar where the intermolecular forces can not be neglected. Hence, the ideal gas assumption is valid for air [40,58]. The Navier-Stockes equations have no analytical solution and hence a numerical solution is required. In addition, it is too difficult to solve the exact equations numerically, so the most common approach is to average the Navier-Stokes equations in time. This is based on Reynolds averaging by decomposing the equations into mean (averaged) and fluctuating components and result in the Reynolds Averaged Navier Stokes (RANS) equations. A new term appears in the averaged momentum equation called the Reynolds stress (equation 4.3) and accounts for the turbulence effects on the mean flow. Therefore, an additional equation or sets of equations, referred to as the turbulence model is added to the RANS equations to account for the Reynolds stress. One of the simplest and widely used turbulence models is the two equation standard k-ε model (equations 4.5 and 4.6). The k-ε model shows a very good predictive capability for compressible flow [5,8,20,35,45]. In CFD, RANS equations are used with the Finite Volume Method (FVM). In this method the flow domain is divided into a number of small finite control volumes. Each property of interest is assumed to be in the centroid of each volume. Governing equations are then integrated on each volume individually and interpolation profiles are then assumed to describe the property variation between volume centroids. Many studies have adopted

this technique with the RANS and k-ε model and have shown good prediction for air flow through pipes, small dimensional components and safety relief valves; for example [5, 8, 20, 35, 45]

Here, the CFD code FLUENT 6.3.26 has been used with the Reynolds Averaged Navier-Stokes (RANS) combined with the energy equation and the k-ε turbulent model to predict the highly compressible flow through the valve. Governing equations are presented here:

Continuity equation

$$\frac{\partial \rho}{\partial t} + \frac{\partial}{\partial x_i}(\rho u_i) = 0 \tag{4.1}$$

Momentum Equation

$$\frac{\partial}{\partial t}(\rho u_i) + \frac{\partial}{\partial x_i}(\rho u_i u_j) = -\frac{\partial p}{\partial x_i} + \frac{\partial}{\partial x_i}\left[\mu\left(\frac{\partial u_i}{\partial x_j} + \frac{\partial u_j}{\partial x_i} - \frac{2}{3}\delta_{ij}\frac{\partial u_l}{\partial x_l}\right)\right] + \frac{\partial}{\partial x_j}\left(-\overline{\rho u_i' u_j'}\right) \tag{4.2}$$

Where $\frac{\partial}{\partial x_j}\left(-\overline{\rho u_i' u_j'}\right)$is the Reynolds stress and obtained from the equation

$$\frac{\partial}{\partial x_j}\left(-\overline{\rho u_i' u_j'}\right) = \mu_t\left(\frac{\partial u_i}{\partial x_j} + \frac{\partial u_j}{\partial x_i}\right) - \frac{2}{3}\left(\rho k + \mu_t \frac{\partial u_l}{\partial x_l}\right)\delta_{ij} \tag{4.3}$$

and

$$\mu_t = \rho C_\mu \frac{k^2}{\varepsilon} \tag{4.4}$$

The standard $k - \varepsilon$ model

$$\frac{\partial}{\partial t}(\rho k) + \frac{\partial}{\partial x_i}(\rho k u_i) = \frac{\partial}{\partial x_j}\left[\left(\mu + \frac{\mu_t}{\sigma_k}\right)\frac{\partial k}{\partial x_j}\right] + G_k + G_b - \rho\,\varepsilon - Y_M \tag{4.5}$$

$$\frac{\partial}{\partial t}(\rho \varepsilon) + \frac{\partial}{\partial x_i}(\rho \varepsilon u_i) = \frac{\partial}{\partial x_j}\left[\left(\mu + \frac{\mu_t}{\sigma_\varepsilon}\right)\frac{\partial \varepsilon}{\partial x_j}\right] + C_{1\varepsilon}\frac{\varepsilon}{k}(G_k + C_{3\varepsilon}G_b) - C_{2\varepsilon}\,\rho\frac{\varepsilon^2}{k} \tag{4.6}$$

Where

$$G_k = \mu_t S^2 \tag{4.7}$$

$$S = \sqrt{2S_{ij}S_{ij}} \tag{4.8}$$

$$G_b = -g_i \frac{\mu_t}{\rho Pr_t} \frac{\partial \rho}{\partial x_i} \tag{4.9}$$

$$Y_M = 2\rho\varepsilon M_t^2 \tag{4.10}$$

$$M_t = \sqrt{\frac{k}{a_s^2}} \tag{4.11}$$

And the constants values are as follow

$C_{1\varepsilon} = 1.44$, $C_{2\varepsilon} = 1.92$, $C_{3\varepsilon} = 0.09$, $C_\mu = 0.09$, $\sigma_k = 1$ and $\sigma_\varepsilon = 1.3$,

Energy Equation

$$\frac{\partial}{\partial t}(\rho E) + \frac{\partial}{\partial x_i}\left[u_i(\rho E + p)\right] = \frac{\partial}{\partial x_j}\left(K_{eff}\frac{\partial T}{\partial x_i} + u_i\left(\tau_{ij}\right)_{eff}\right) \tag{4.12}$$

where

$$K_{eff} = K + \frac{C_p \mu_t}{Pr_t} \tag{4.13}$$

$$\left(\tau_{ij}\right)_{eff} = \mu_{eff}\left(\frac{\partial u_j}{\partial x_i} + \frac{\partial u_i}{\partial x_j}\right) - \frac{2}{3}\mu_{eff}\frac{\partial u_k}{\partial x_k}\delta_{ij} \tag{4.14}$$

Ideal gas law

$$\rho = \frac{P_a + P}{(R/M_w)T} \tag{4.15}$$

4.4.2 Computational Grid

To allow computational efficiencies a two dimensional axisymmetric model has been developed to represent the safety valve geometry, Figure 4.8. A two dimensional axisymmetric model has been shown to provide adequate prediction for the mass flow rate and piston force in previous research work [20] for similar safety

valve geometry and flow conditions. In this model the flow areas between the piston and the body and the gland exit holes, shown on Figure 4.8, have been represented as equivalent annulus areas. The flow area around the piston is a very important area for predicting the air flow rate, hence it has been maintained when modelled as an annulus flow area. The piston front face area is also required to be maintained for predicting the piston force. Therefore, the piston seat area has been kept the same (since it is already symmetric), whereas the piston front face outer diameter has been chosen to keep the same piston front face area and hence the flow area around the piston. The gland flow area (5 holes) has been modelled as an annulus area the centre of which is located at a radius of half the valve body radius. The computational mesh has a total of 7000 quadrilateral cells distributed giving an average mesh density of 7 $cells/mm^2$. A more dense mesh of 14000 quadrilateral cells has been used to examine the grid independency, with no significant improvement for the solution. The difference in air flow rate was 0.00001 kg/s , 0.01 N for force and 150 Pa for the back pressure so the cell number was kept about 7000 in all cases.

4.4.3 Boundary Conditions and Solution

The proper setting of the boundary conditions is an essential step to obtain accurate CFD results. The boundary conditions are applied at the valve entrance, valve outlet and valve walls. Valve walls were defined as stationary walls. At the inlet boundary, the stagnation pressure, static pressure and stagnation temperature are applied; in addition an initial value for the turbulence intensity and the hydraulic diameter are introduced. Hence, an initial air mass flow rate is determined at the inlet area then is recalculated from the downstream conditons at the choking plane. At the outlet boundary conditions the static pressure is applied. However, the flow calculation is independent of the outlet boundary condition since the flow is choked for all test pressures in this study. This will be discussed in Section 4.5.3.1. The discretization scheme used for the continuity, momentum, energy, turbulent kinetic and turbulent dissipation energy equations was second

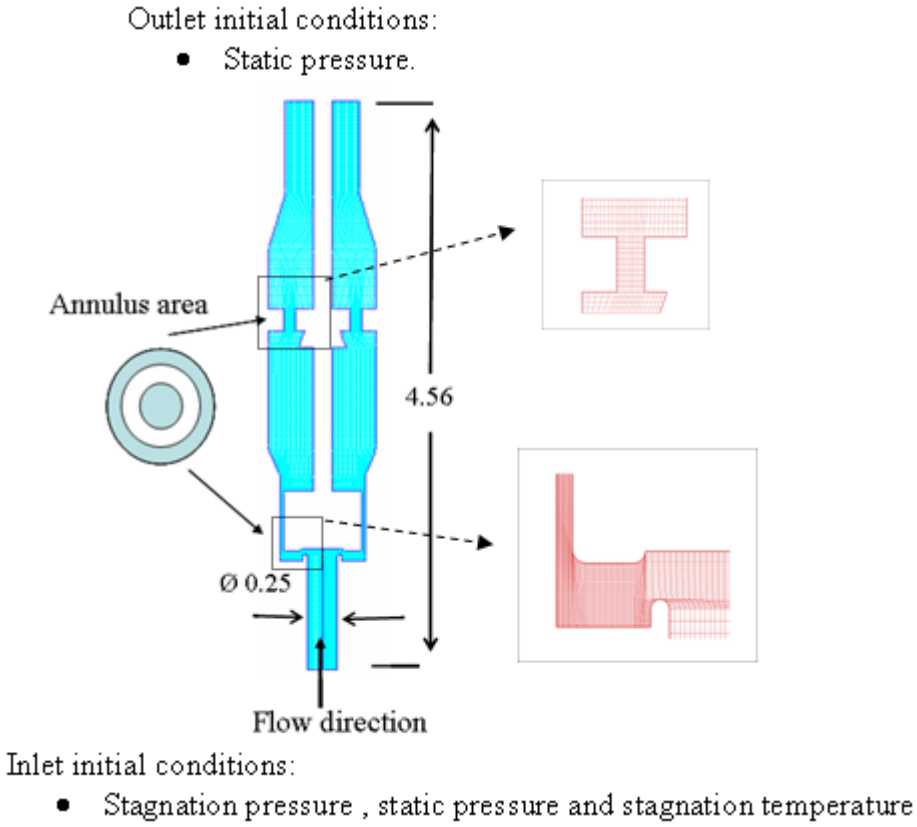

Figure 4.8: Computational grid of the valve (Dim. in inches)

order upwind for the convection terms and second order central difference for the diffusion terms. The convergence criterion was based on the residual values of the calculated variables, i.e., mass, velocity components, energy, turbulent kinetic energy and turbulent dissipation energy. The threshold values were absolute with magnitudes of 1×10^{-3} for all variables, with the exception of the energy equation where it was 1×10^{-6}. All cases have converged in about 20 min on a 2.4 GHz desktop PC . The pressure range used was 4 -14 barg (60 - 200 psig) to allow the model validation by the experimental results which were restricted to maximum pressure of 15.7 barg (230psi).

4.5 Results and Discussion

4.5.1 Experimental Results

The variation with lift of the mass flow rate and net piston force obtained with and without the gland are shown on Figures 4.9 and 4.10. The experimental results of the mass flow rate through the valve with and without the gland proves that the gland has no significant effect on the mass flow rate. For these flow conditions, this suggest that the simplified model of the valve without the gland or other complex exit geometry, could give accurate predictions for the mass flow rate-lift characteristics. Since the flow is choked at all lifts, the mass flow rate is called a "critical flow rate" and it is independent of the flow conditions downstream of the choking position. For these cases the first choking conditions occur at the piston front face or piston side faces which decouples any influence of the downstream gland on the flow rate. Flow-lift characteristics are discussed in Section 4.5.3.1

In Figure 4.10 the force-lift curves indicate that the gland has a noticeable effect on the piston net force. The results with the gland show lower net forces than without the gland and is caused by the effect of the higher pressure on the piston back face (shown in Figure 4.10). Force-lift characteristics are discussed in Section 4.5.3.2

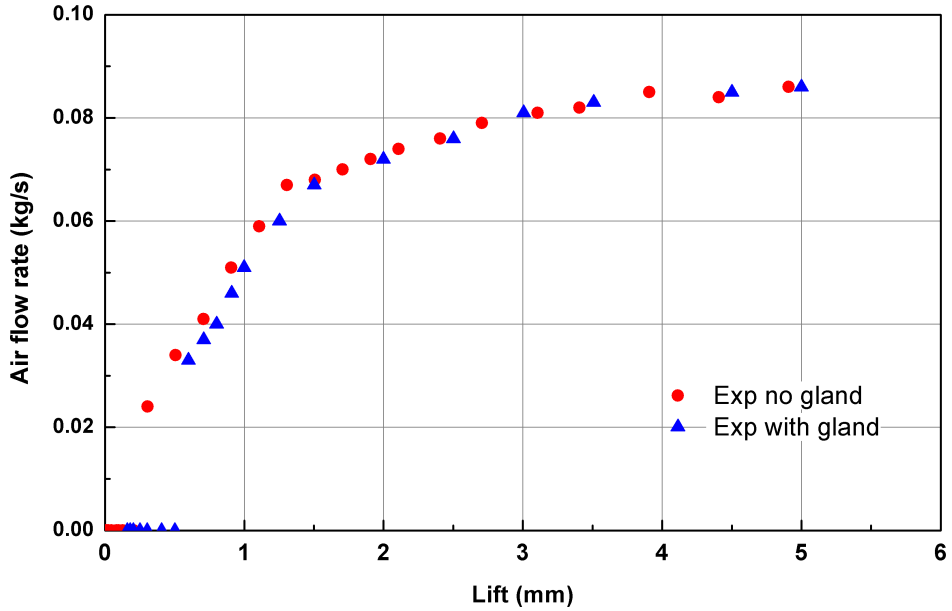

Figure 4.9: The effect of the gland on the air flow rate at 11.7 barg (170 psi)

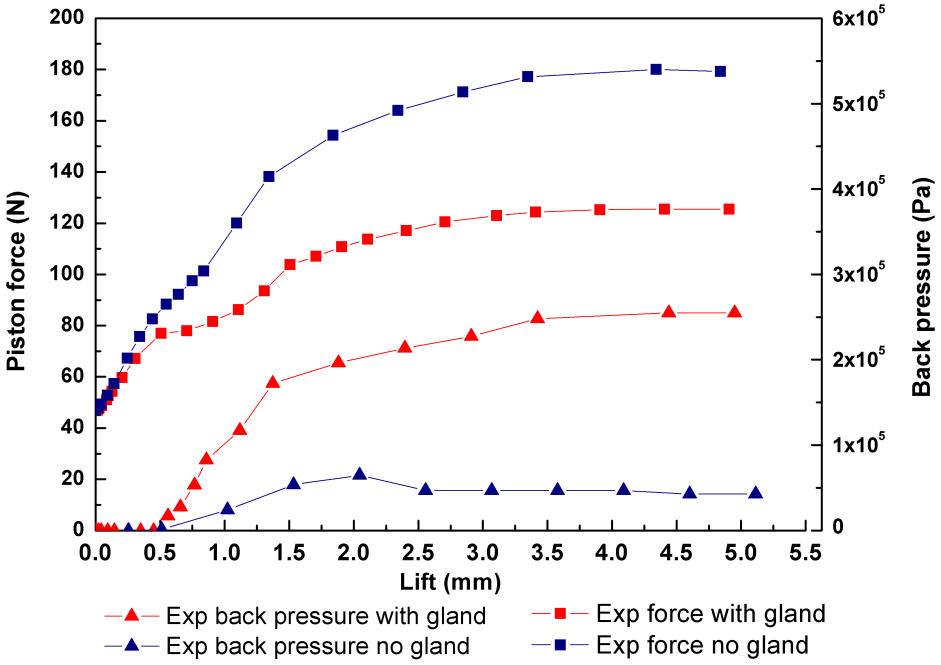

Figure 4.10: The effect of the gland on the piston force and back pressure at 11.7 barg (170 psi)

4.5.2 CFD Results

The results of the CFD model can be used to show the detailed flow and property distributions through the valve. Contours of static pressure, static temperature, velocity and Mach number have been obtained for the flow through the valve at different piston positions. Figures 4.11 and 4.12 shows the pressure, temperature, velocity and Mach number contours at an inlet pressure value of 11.7 barg (170 psig) and a lift of 2.5 mm, which is in the fully open operating range of lifts. The figures show the significant variations of flow properties encountered in the valve. From Mach numbers of 0 to 1.6, temperature variations -60^oC to 20^oC and velocities from 0-400 m/s. A good understanding of the flow behaviour can be achieved by investigating the property distribution throughout the valve. The contours of the velocity at different lifts show the flow acceleration at the valve inlet to reach the sound speed around the piston at different locations according to the lift. The Mach number contours can identify the choking plane (critical plane) at which the Mach number is unity. In Figure 4.12 (a), it can be seen that the critical plane first occurs at the end of the piston. The flow expands downstream of the chocking plane for a short distance before undergoing a compression down stream the piston end due to the existence of the gland. pressure contours are shown in Figure 4.11(b). The change of the static temperature and pressure can be recognised using the contours display tools (Figure 4.11). Air flow is choked again while passing through the gland before performing its final expansion at the valve outlet section.

Predicted flow-lift characteristics along with the experimental results are shown in Figure 4.14 which indicates that the CFD model provides an accurate prediction of the flowrates at all lifts. The predicted forces compare well with the measurements (Figure 4.15). However, when the gland is in place the predictions for both force and back pressure are less accurate and are due to the limitations of modelling the three dimensional flow down stream of the piston and through the gland holes using a two-dimensional model, as is done here. Additional errors arise from the difficulty in accurately representing the geometrical edges of the

gland holes correctly as previously discussed by Dempster et al [20]. To check the three dimensional flow effect on the force prediction, a modified axisymmetric gland has been introduced (Figure 4.1). Figure 4.16 presents CFD predicted results and the experimental results with the modified gland. Force lift characteristics will be discussed in Section 4.5.3.2

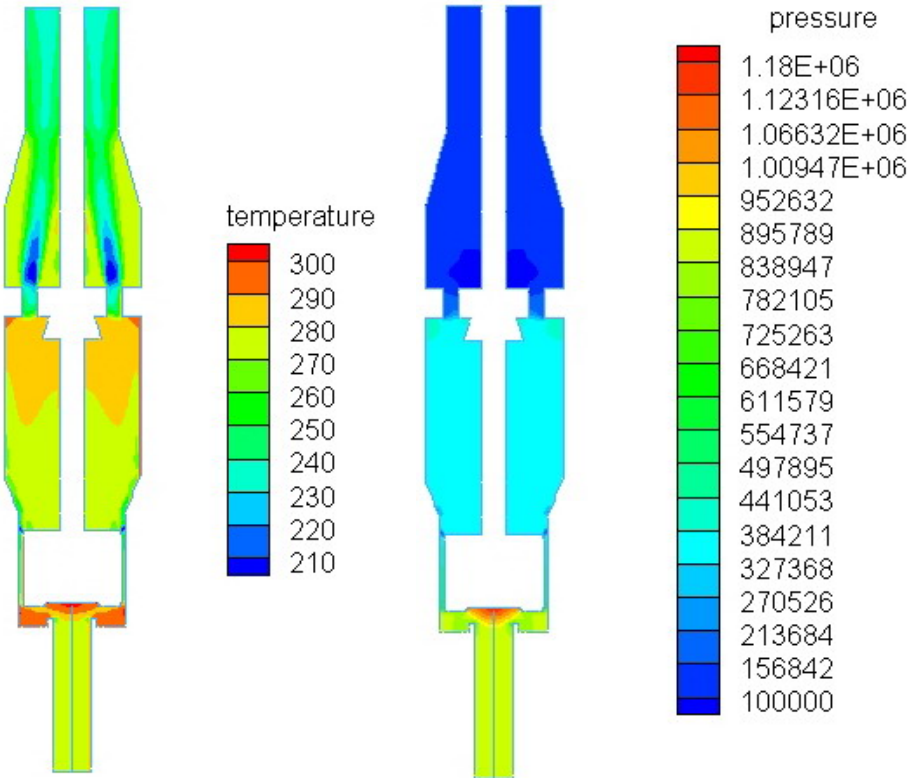

(a) Static Temperature (K) **(b)** Static Pressure (Pa)

Figure 4.11: Contours of static temperature and pressure at 2.5 mm lift and 11.7 barg

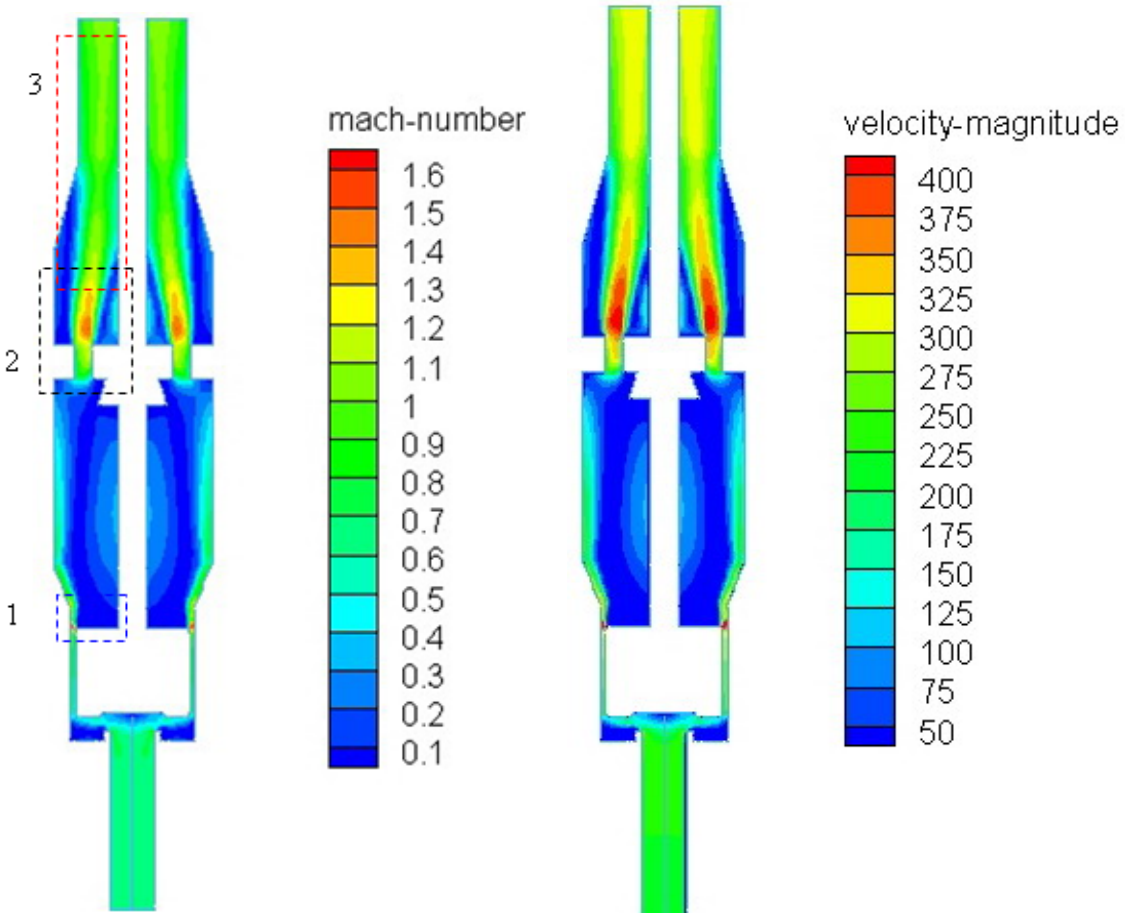

(a) Mach Number (-) **(b)** Air Velocity (m/s)

Figure 4.12: Contours of Mach number and Air velocity at 2.5 mm lift and 11.7 barg. Area 1,2 and 3 are shown in Figure 4.13

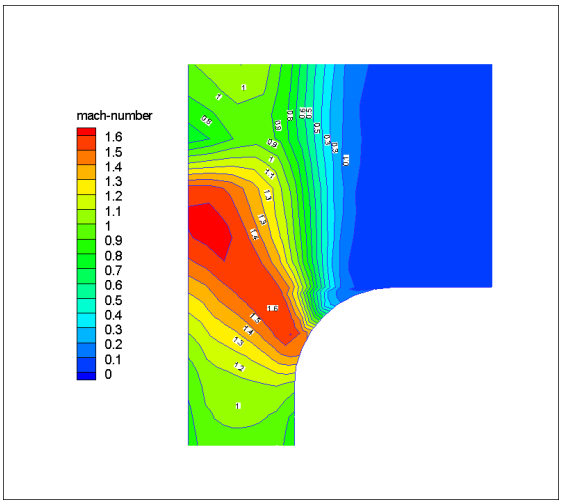

(a) Area 1

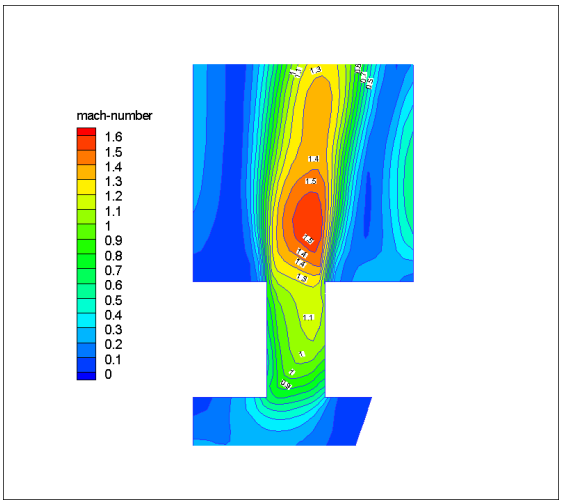

(b) Area 2

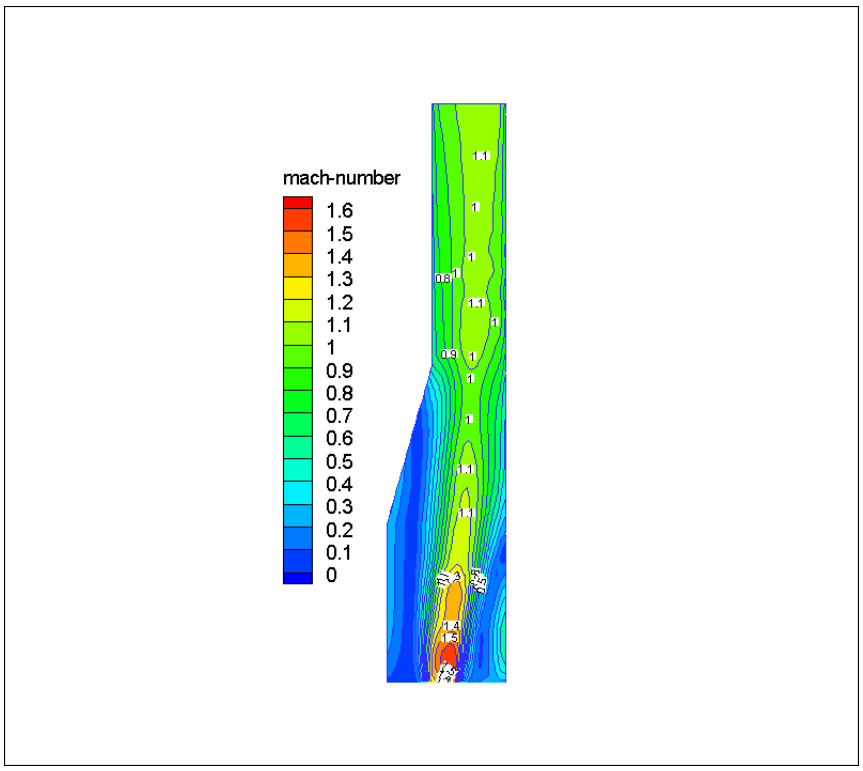

(c) Area 3

Figure 4.13: Contours of Mach number at 2.5 mm lift and 11.7 barg at Area 1,2 and 3 shown in Figure 4.12

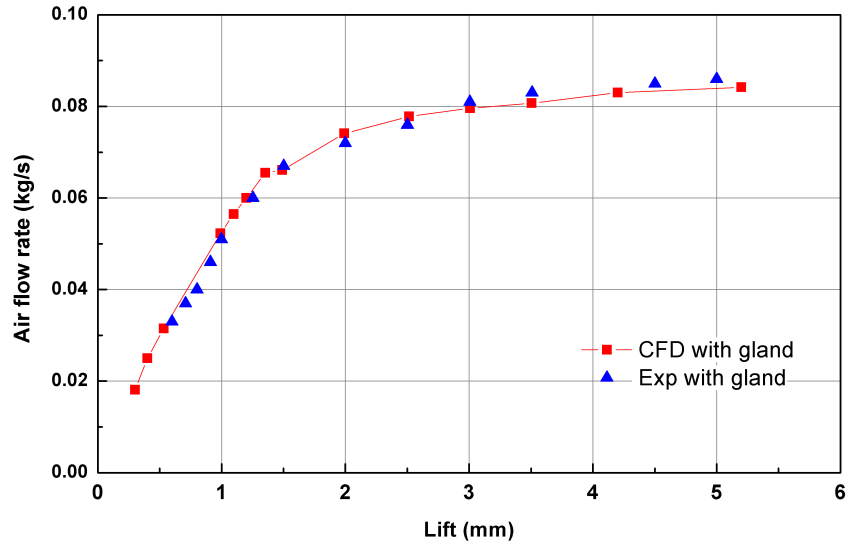

Figure 4.14: CFD and experimental flow-Lift characteristics at 11.7 barg

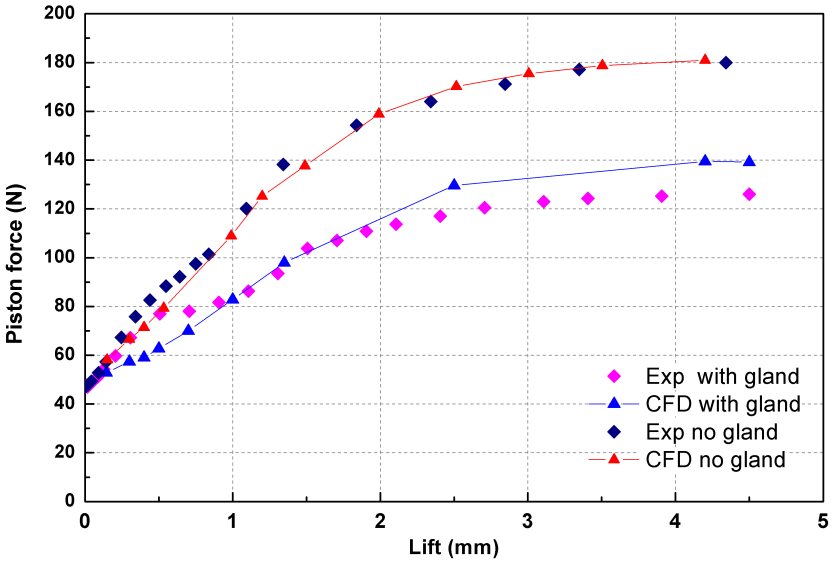

Figure 4.15: CFD and experimental piston force-lift characteristics at 11.7 barg

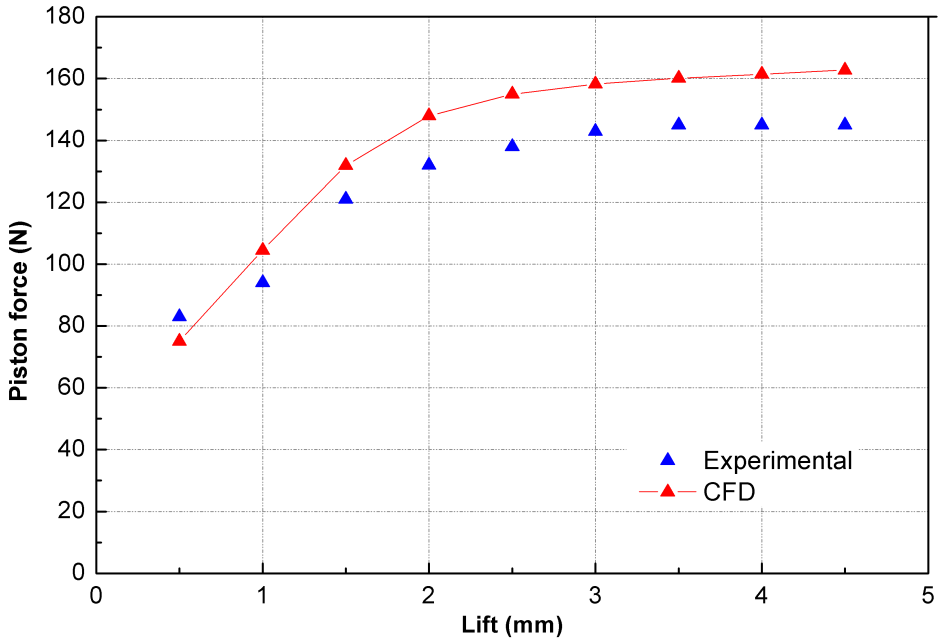

Figure 4.16: Piston force-Lift characteristics at 12 barg with the modified gland

4.5.3 Discussion

4.5.3.1 Flow-Lift Characteristics under Single Phase Flow

The specific form of the flow and force characteristics can be understood by examining the detailed predicted results for a range of lifts. Figure 4.17 shows the mass flowrate for a range of lifts and on this curve regions I and II are identified. In region I, which occurs for lifts between 0 and 1.2 mm, a rapid increase in mass flow rate occurs for a slight change in piston lift. Thereafter, the mass flow changes more slowly to a near constant value.

The reason for these changes can be explained by examination of the Mach number and pressure distributions local to the piston in the valve. Figures 4.18, 4.19 and 4.21 show these parameters for a wide range of lifts. Figure 4.18 shows the Mach number contours in the flow between the valve seat and piston face for lifts for region I, i.e. 0.3 to 1.2 mm. The figure indicates that for these lifts the flow is choked in a plane between the seat and the piston; the dashed lines in Figure 4.18 showing the choking plane for each lift. The mass flow rate is critical

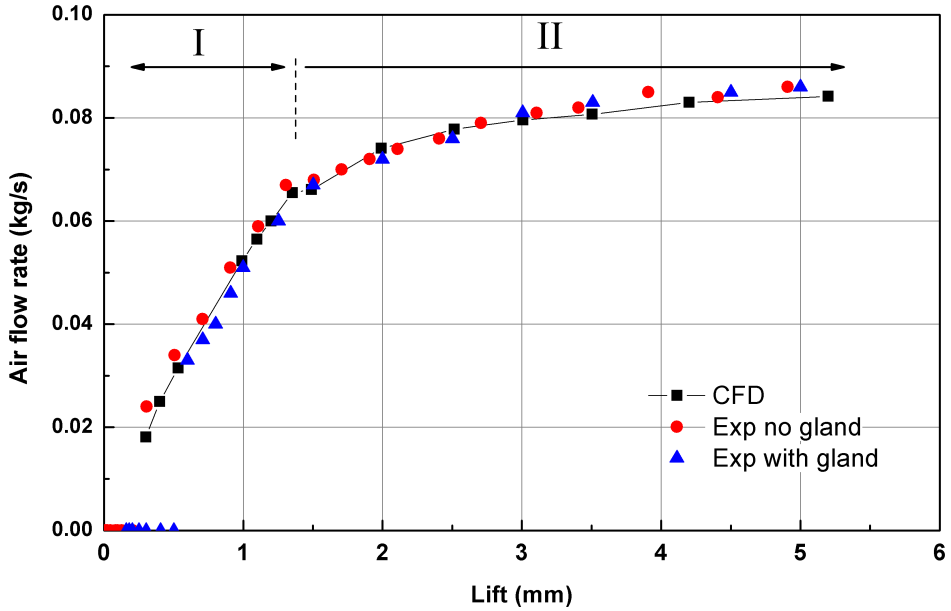

Figure 4.17: Flow-Lift characteristics at 11.7 barg

and controlled by the local geometry.

Since the inlet stagnation pressure and stagnation temperature is fixed for each of the lift positions the mass flowrate is dependent only on area and this a near linear function with lift resulting in the linear change of mass flowrate seen in Figure 4.17 for Region I. When the lift is greater than 1.2 mm the choking plane moves to a position at the exit from the annular passageway between the piston and the valve body, as shown on Figure 4.19, and remains at this position for any further increase in lift. The slower increase in mass flow for higher lifts that can be seen in region II of Figure 4.17 is due to the increase in pressure at the inlet of the annular passageway. This is indicated in Figure 4.20 which shows an increase in static pressure upstream of the piston as the piston lift increases. This will continue to increase as the piston moves away from the seat and will eventually approach a pressure value slightly less than the limiting upstream stagnation pressure due to losses between the valve entrance and the piston side. This also limits any increase in mass flowrate and explains the near constant mass flow found at higher lifts in Figure 4.17.

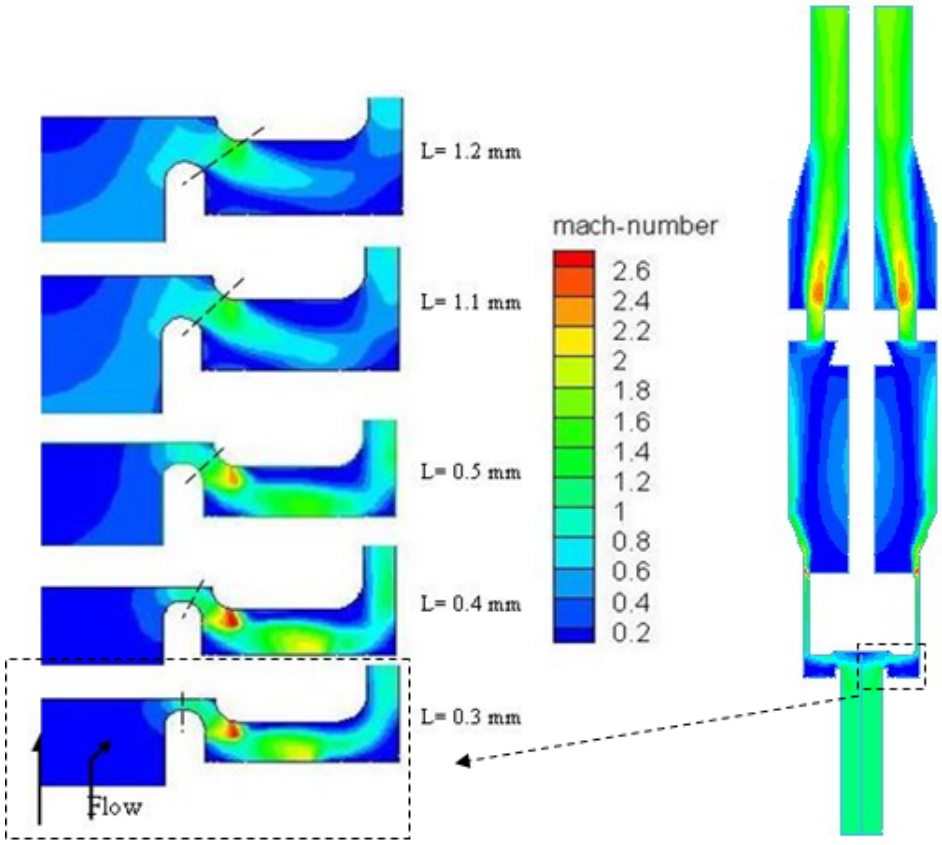

Figure 4.18: The critical plane at piston face at lower lifts

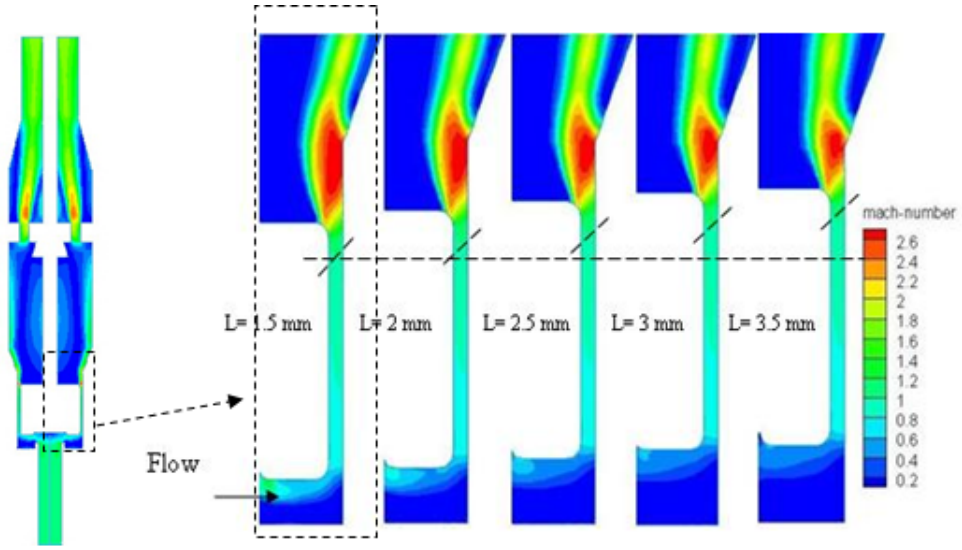

Figure 4.19: Critical plane at piston side at higher lifts (11.7 barg)

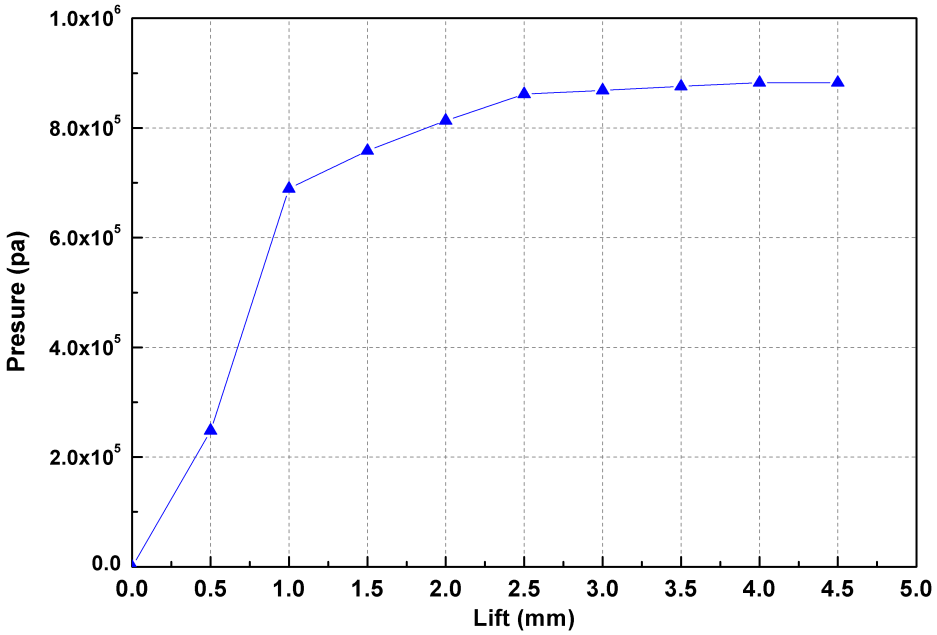

Figure 4.20: Static pressure at the inlet of the passageway around the piston (11.7 barg)

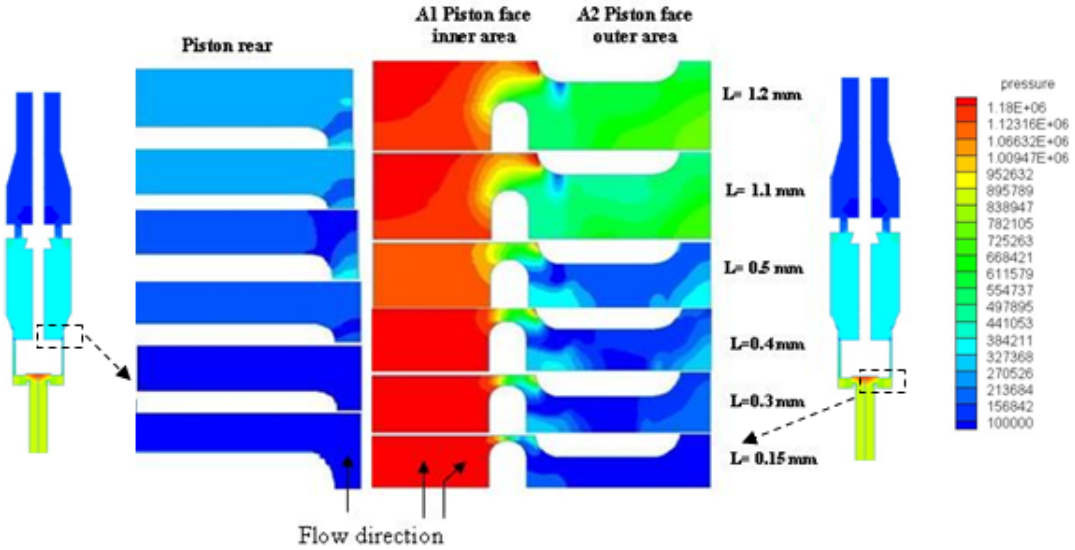

Figure 4.21: Pressure contours on piston front and back face

4.5.3.2 Force-Lift Characteristics under Single Phase Flow

In a similar manner, an understanding of the force-lift characteristics can be obtained by examining the detailed CFD predictions. Figure 4.22 shows three main regions, Region I between 0 and 0.4 mm lift when the net force linearly increases. Region II, which occurs between 0.5 and 1.5 mm and shows an increasing net force, but at a significantly reduced rate compared to Region I. A final region, Region III, can be identified for all lifts above 1.5 mm and shows a steady increase of the net force but finally settles to a steady value. Figure 4.21 shows the pressure distribution at the piston front and back face for a range of lifts. In Region I and at zero lift the net force is dictated by the upstream stagnation pressure acting between the seat sealing locations. As the piston lifts, a choking plane is established that ensures that the stagnation pressure acts across the majority of the piston inner face. However at lifts between 0 and 0.4 mm an increase in force is achieved by the expanding gas close to the valve seat.

The net force in Region I is influenced primarily by increases in pressure over the inner piston area, (Area A1 in figure 4.21) and no significant back pressure. However, as the piston lifts further into Region II, the flow rate increases significantly causing an increase in back pressure as shown in Figure 4.10 and an increase in pressure across the outer periphery of the piston front face, (Area A2 in figure 4.21). The increase in piston back pressure prevents the force from increasing at the same rate as in Region I. As the lift progresses into Region III the flow rate begins to stabilise because the choking position has now relocated to a plane at the back of the piston and stays fixed (see Section 4.5.3.1) and since the back pressure is flowrate dependent it also reaches a steady value. At the higher lifts of Region III both the pressure at the inner and outer regions of the piston front face will increase towards the upstream stagnation pressure. As shown in Figures 4.20 the pressure at face A2 was approximately 7 barg for a 1.2 mm lift, then 8.5 barg for a 2.5 mm lift . Since this is a fixed pressure for all lifts then this combined with a steady back pressure will eventually produce a steady net force. Thus the trends found for both mass flow and force-lift characteristics

can be explained in detail by using the CFD predictions.

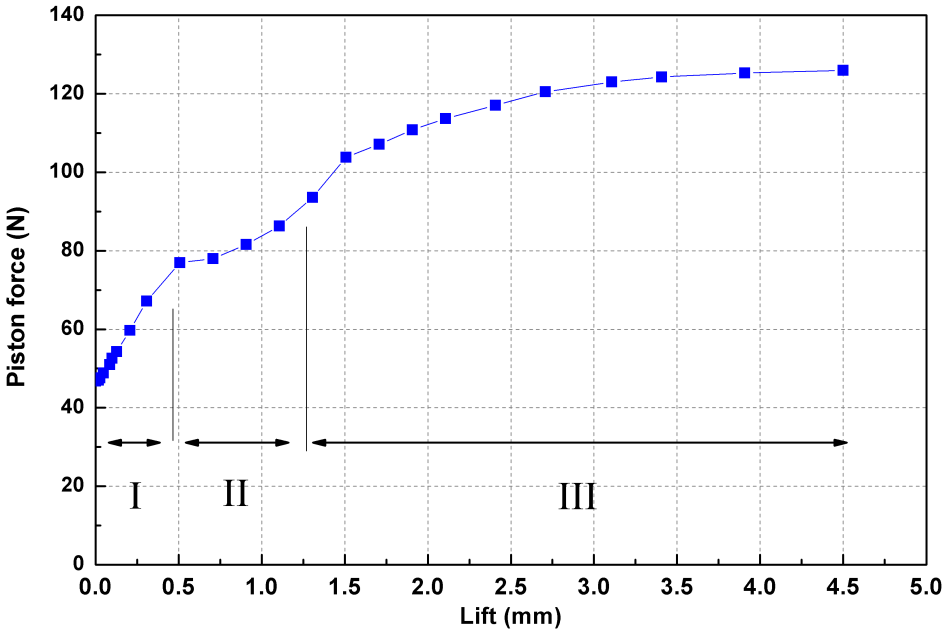

Figure 4.22: Experimental force-lift characteristics with gland at 11.7 barg

Three Dimensional Effects on Piston Force Prediction

To investigate the three dimensional geometry effect on force prediction a modified gland has been used in the experimental testing to produce a geometry consistent with the two-dimensional modelling. The modified gland leads to better CFD predictions for the back pressure than the original gland by 15% (Figures 4.23 and 4.24). However, the CFD prediction for force with the modified gland is poorer when compared to the corresponding experimental results than the CFD predictions with the original gland. This inconsistency required further analysis of the requirements for the piston force prediction with the emphasis given to two/ three dimensional modelling issues. To do this a three dimensional Fluent model was developed and solved with the same conditions as described in Section 4.4. Also the computational results from a parallel three dimensional modelling study by Gronkowski [33] was used. Figures 4.25 and 4.26 show the pressure distribution on the piston front and back face of a three dimensional Fluent model of the valve at 11.7 bar and 4 mm lift. The figures show that the pressure dis-

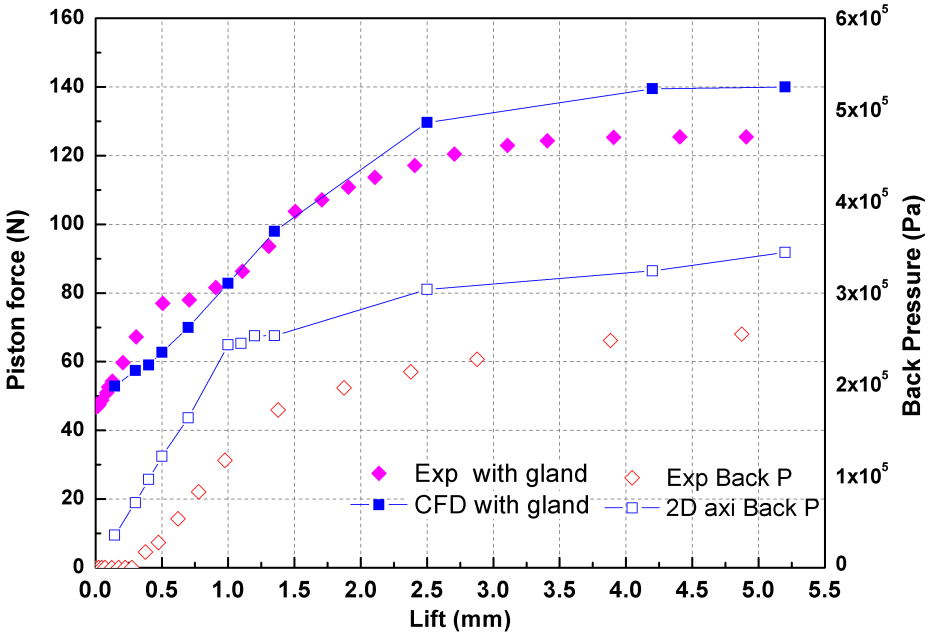

Figure 4.23: Force-lift and back pressure- lift characteristics at 11.7 barg with gland

tribution is non uniform; which suggest a possible error in force prediction when using a two dimensional model.

To investigate this three dimensional effect on the force prediction a comparison between the predicted force by the three dimensional model and the two dimensional axisymmetric model is needed. The three dimensional model used for comparison was made by Gronkowski [33] using the commercial software SolidWorks. Figure 4.27 presents the predicted force and back pressure using the three dimensional model [33] and the two dimensional axisymmetric model. The results of the two dimensional axisymmetric model are shown at Figure 4.27 and show an over predicted back pressure at all lifts, under predicted force from 0.3-0.9 mm lift, over predicted force from 2 to 5 mm and in between these two regions the force is fairly well predicted. A higher predicted back pressure should lead to lower predicted force if the predicted piston front face force is fairly well predicted; which could be noticed at lifts from 0.3 to 0.9 mm in Figure 4.27. For example at 0.5 mm lift, the predicted net force by the three dimensional model is 77 N and the net predicted force with the two dimensional model is 62.7 N. This difference is due to the overpredicted back pressure by the two dimensional

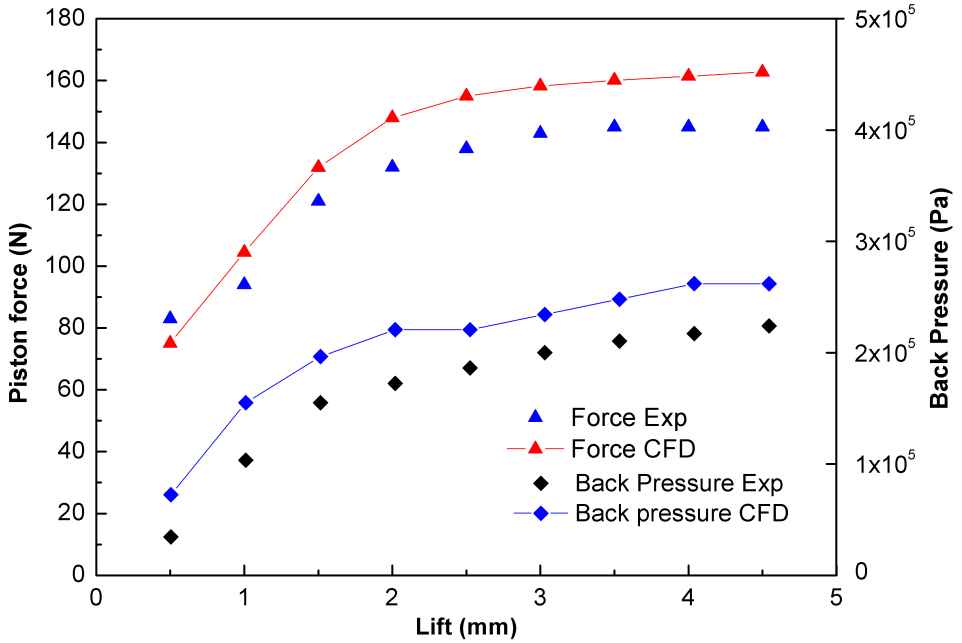

Figure 4.24: Force-lift and back pressure- lift characteristics at 12 barg with the modified gland

model, since the predicted force on the piston front face is similar (88.5 and 90.3 N). Table 4.2 presents the predicted values of forces at 0.5 mm and 4 mm lift at 11.7 bar. The difference in back pressure corresponds to nearly 16 N of difference in net predicted force. Hence, if the predicted force on the piston front face is well predicted the over predicted back pressure will result in a lower net force. With further lift, more of the piston front face area is exposed to the inlet stagnation pressure resulting in a higher force on the piston front face; as discussed in Section 4.5.3.2. Therefore at certain lifts an overpredicted piston front face force will compensate for the over predicted force on the back face; see lifts 0.75-2.0 mm in Figure 4.27. At higher lifts, the net force is overpredicted which results from higher overpredicted force on the piston front face; see lifts from 2.25- 5.2 mm in Figure 4.27. In the case of the two dimensional axisymmetric model the force on the piston front face is 206 N whereas it is 188.8 N for the three dimensional model (table 4.2). Hence, it can be concluded that the predicted forces on the piston front and back faces are affected by the three dimensional effect of the pressure distribution. Although, the pressure value indicated by the two

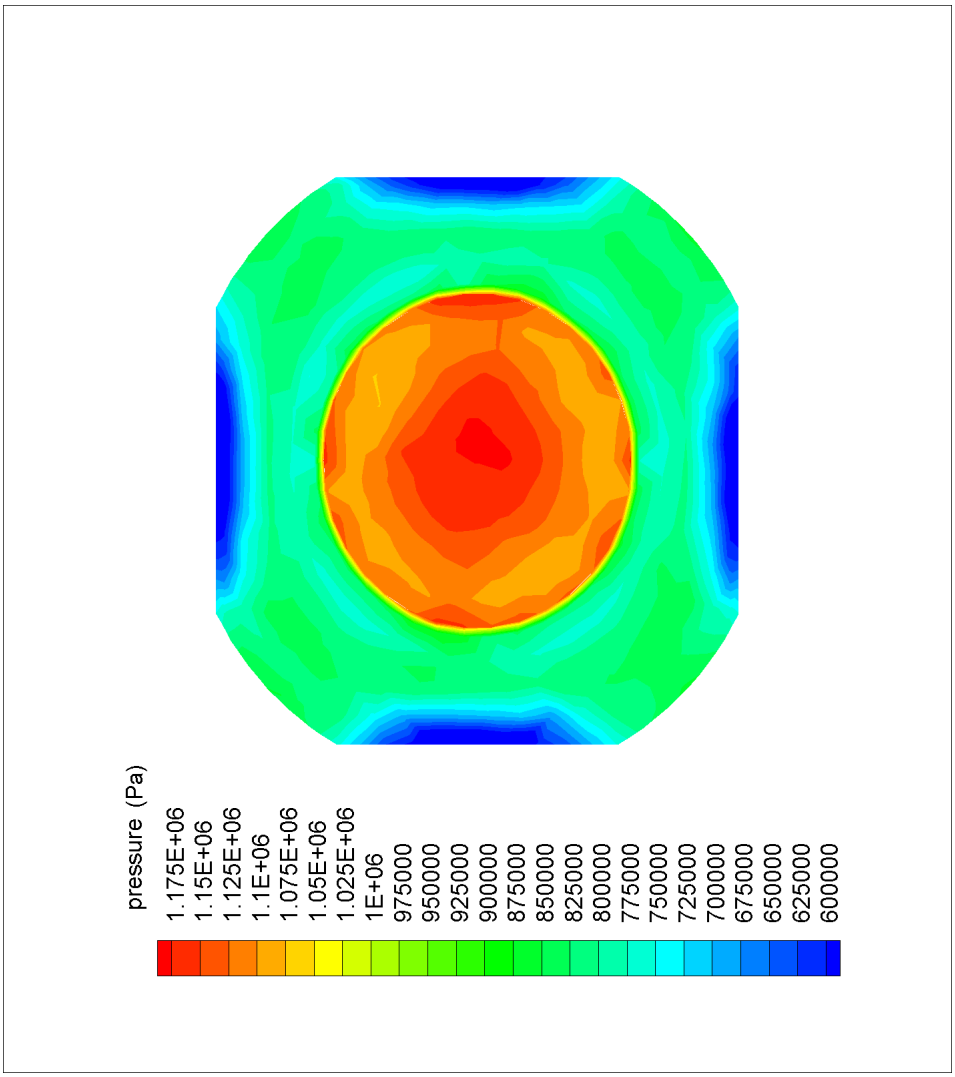

Figure 4.25: Static pressure contours on the piston front face at 11.7 bar (170 psi) and 4 mm lift (Fluent 3D model)

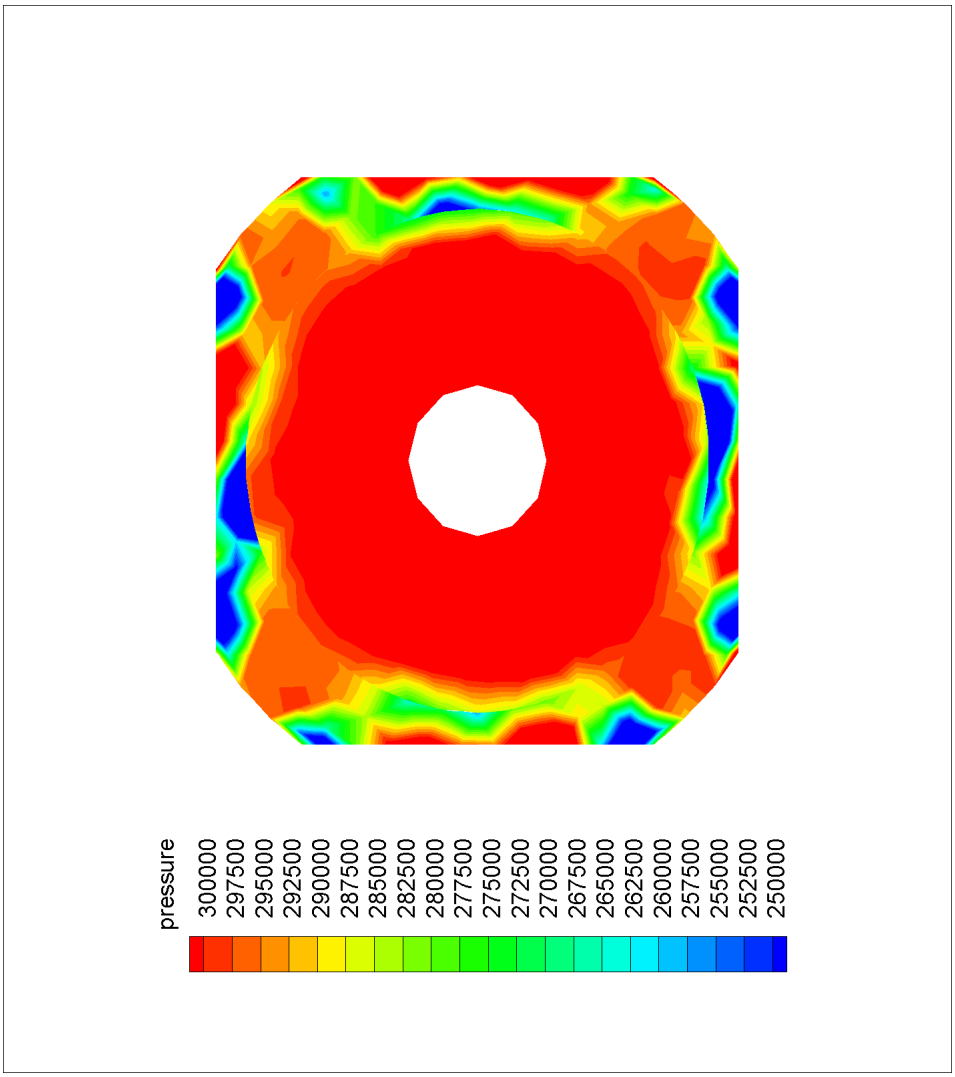

Figure 4.26: Static pressure contours on the piston back face at 11.7 bar (170 psi) and 4 mm lift (Fluent 3D model)

dimensional axisymmetric model on piston front face (or piston back face) is a good indication of the pressure on these faces and the model successfully present the pressure distribution behaviour, there is a deviation in force values due to the non uniformity of the pressure distribution. This non uniformity in pressure distribution can be explained when looking at the piston geometry (shown in Figures 4.25, 4.26 and Appendix A.1.1) and the flow areas around it; as the piston moves in a typical cylindrical part of the valve body. The area around the piston can be divided into eight flow areas. Four of them are very narrow corner flow areas with about 0.5 mm^2, whereas the other four main flow areas are about 10.7 mm^2 . This large difference in adjacent flow area results in a large difference in flow velocity which leads to a large pressure difference between these two areas (shown in Figures 4.25 and 4.26).

These results indicate the limitation in a two dimensional modelling approach are in contrast to the conclusion of Dempster et al [20] who showed accurate predictions in similar valve geometries. As in this study, the commercial CFD code Fluent was used with a similar modelling approach. However, the piston design used by Dempster et al [20] had a circular front face which was more appropriate to a two dimensional modelling approach than the square faced piston used in this study. Valve drawings are shown in Appendix A.1.4. This piston design leads to a uniform distribution of the pressure on the piston face, hence the two dimensional axisymmetric model can well predict the piston force. A three dimensional model for the same valve has been developed to be compared with the two dimensional axisymmetric model. Figure 4.28 shows the uniform static pressure distribution on the piston front face of a three dimensional Fluent model. However, the two dimensional model is much more computationally efficient compared to the three dimensional model.

Forces on Piston			
	Front face	Back Face	Net
0.5mm 3D [33]	88.5	11.5	77
0.5mm 2D	90.3	27.6	62.7
4 mm 3D [33]	188.8	59.8	129
4 mm 2D	206	70.4	135.6

Table 4.2: Predicted force values at 0.5 and 4mm lift at 11.7 bar

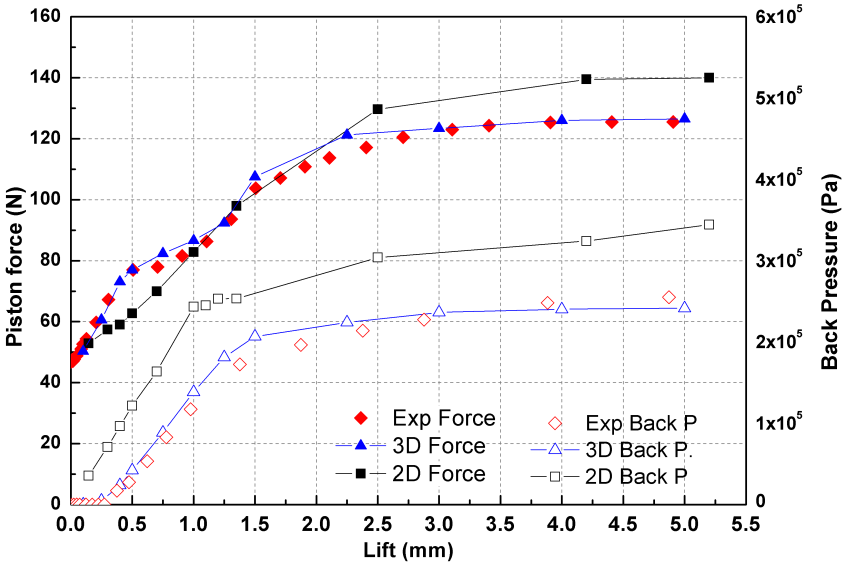

Figure 4.27: Three [33] and two dimensional force-lift characteristics at 11.7 bar (170 psi) with gland

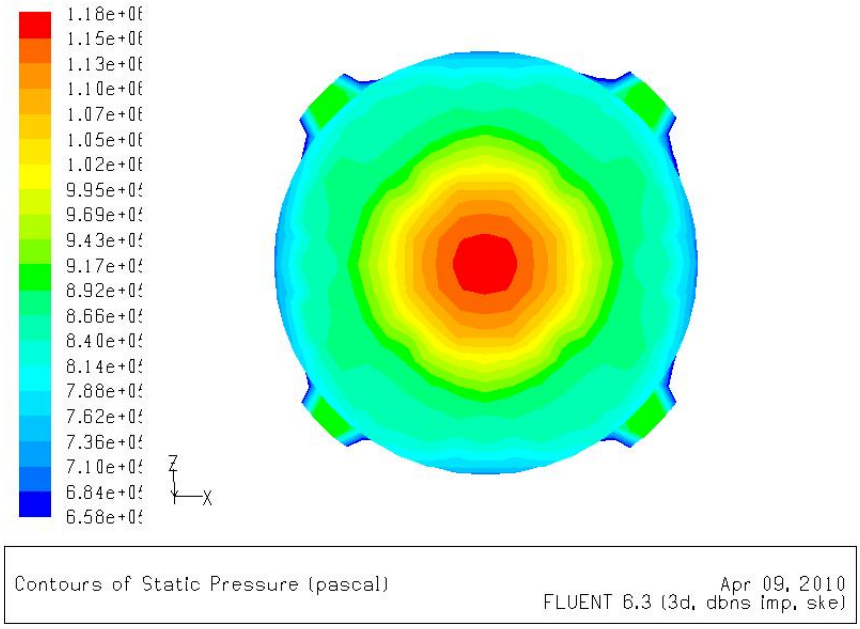

Figure 4.28: Static pressure contours on the piston front face at 11.7 bar (170 psi) (Fluent 3D model [20])

4.6 Valve Design Approach for Single Phase Flow:

To achieve a general approach to the analysis and design of safety relief valves as described in Chapter 3, general force-lift and flow- lift parameters need to be obtained that can be applied to all pressures and flows. This will help to determine the discharge flow rate at the opening pressure and also to determine the closing condition and pressure. The flow-lift and piston force-lift characteristics have been obtained at different pressures. Figures 4.29 and 4.30 present the flow-lift and piston force-lift characteristics at different pressures. A normalised force-lift curve and flow-lift curve for all pressures is necessary to achieve this goal [6, 20, 43, 48]. Figure 4.31 shows how these curves will be used to determine the discharge flow rate at any known pressure. When the forces are normalised, all the force-lift curves at different pressures should collapse onto one curve. If the normalised spring force-lift characteristics are plotted with the normalised piston force-lift characteristics, this will identify the valve working lift. The intersection point will indicate the valve lift and from this point at the normalised flow-lift

curve the valve discharge flow rate could be determined.

For a normalised flow rate when the flow is choked i.e. M=1 [6, 20, 48]

$$\dot{m}_N = \frac{\dot{m}}{P_o\, A_{seat}} \sqrt{T_o} \tag{4.16}$$

For the normalised force the following scaling factor can be used.

$$F_N = \frac{F}{(P_o - P_{atm})\, A_{seat}} \tag{4.17}$$

Using the two scaling parameters, defined in equations 4.16 and 4.17 a single curve for the flow-lift and force-lift characteristics should represent a family of curves at various pressures. Figure 4.32 shows the normalised flow-lift characteristics and Figures 4.33 and 4.34 show the normalised force-lift characteristics with and without the gland. The flow-lift curve show the flow-lift curves at different pressures collapse into one curve with maximum uncertainty of 1.5% since the critical air flow rate at constant lift is only dependant on the stagnation pressure. On the other hand, the net force is the resultant of the force on the piston front face and the opposing force on the piston back face. The piston front face force at fixed lift is only dependant on the stagnation pressure, while the force on the piston back face depends on the back pressure which is a result of the air flow rate and the valve outlet area. The effect of the back pressure results in a slight deviation in the normalised force curve. Back pressure has a more significant effect at higher lifts (higher air flow rate) and when the gland is in place. This deviation can be noticed from a comparison of Figures 4.33 and 4.34. For example the difference between the highest and lowest force value at 4 mm lift without the gland is 0.25, while it is 0.4 at the same lift with the gland due to the effect of the higher back pressure. However, 0.4 deviation results in a force uncertainty of about 23 N at 13.8 bar, so if the mean line of the force curve is used as the force trend line, this will result in a 11.5 N uncertainty. Since at high lift (1.5- 4.5 mm) the flow rate is nearly steady so this will not make a significant difference in the predicted flow rate. At low lift (0- 1.5 mm) a slightly higher deviation in flow rate is expected

due to the steep slope.

This approach can be used to assist in safety relief valves design for single phase air flow. The normalised characteristics can be achieved by obtaining the force-lift and flow-lift characteristics at only one pressure either experimentally (if the valve is already manufactured) or by using CFD if the valve is in the design phase. When safety relief valve characteristics need to be verified, the normalised characteristics for the valve as shown in Figure 4.31 can be used to determine the fully open operation point, the closing pressure and the corresponding lifts at any required discharge flow rate and opening pressure. The force-lift, the spring force-lift and the flow -lift characteristics will be obtained at the opening pressure using the scaling parameters. The spring characteristics can be adjusted to meet the required discharge flow rate at this pressure. Then the closing pressure can be determined by using the scaling parameters to find the pressure that results in a force-lift characteristics lower than the spring force-lift characteristics. General opening and closing characteristics are shown in Figure 4.35 and have been described in Chapter 3. On the other hand, if the system maximum operating pressure is determined, the normalised characteristics can be used to determine the discharge flow rate at the corresponding lift and the closing pressure.

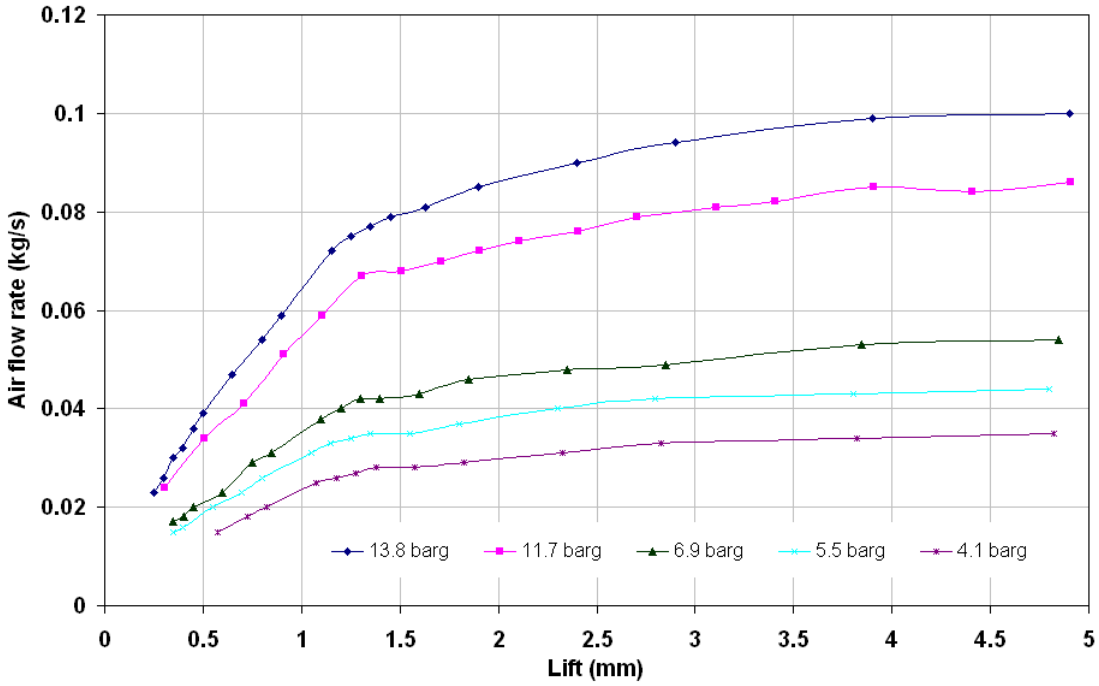

Figure 4.29: Flow-lift characteristics at different pressures with gland

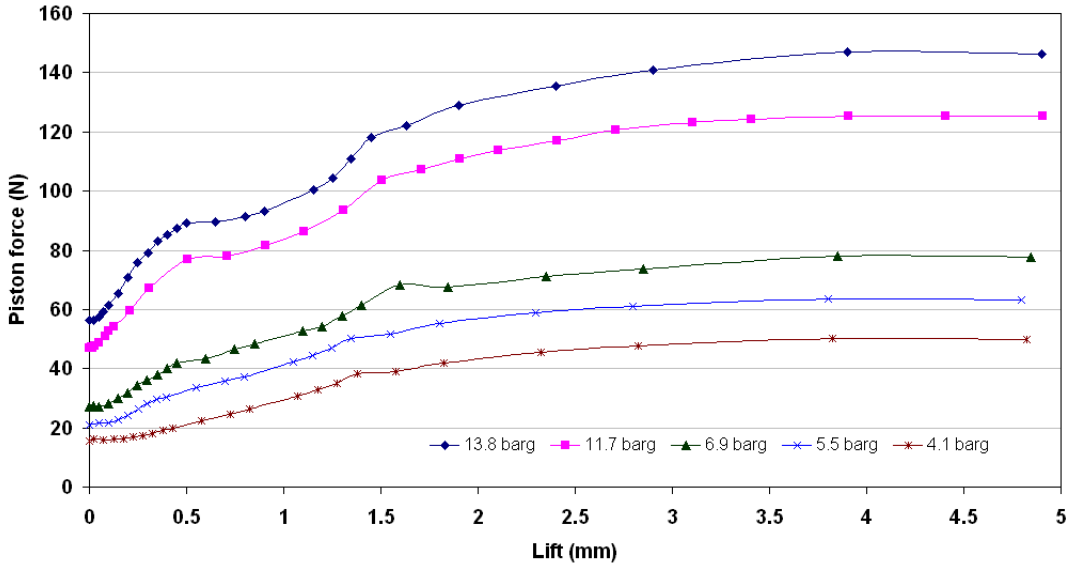

Figure 4.30: Piston force-lift characteristics at different pressures with gland

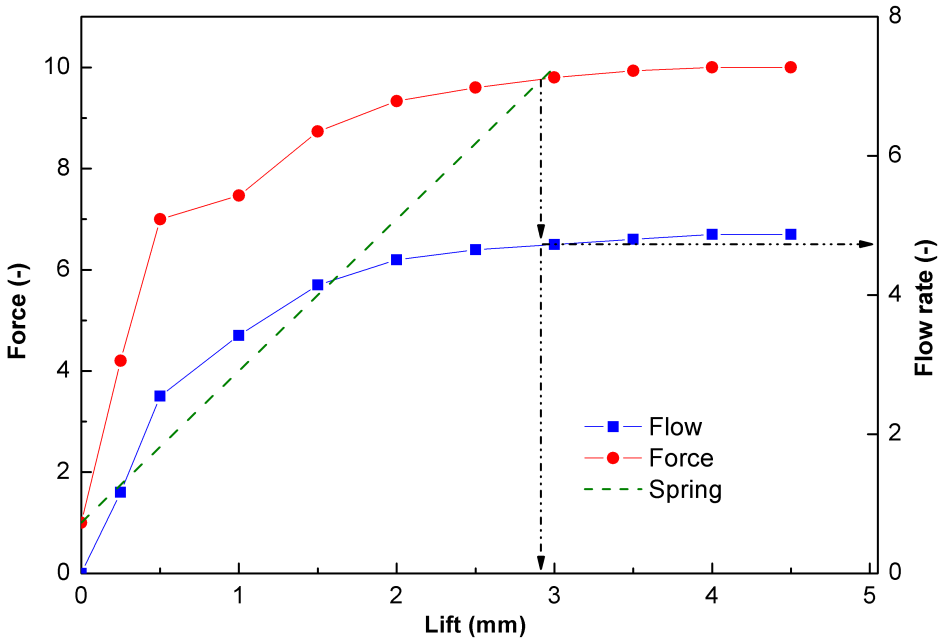

Figure 4.31: Normalised force, flow and spring-lift characteristics

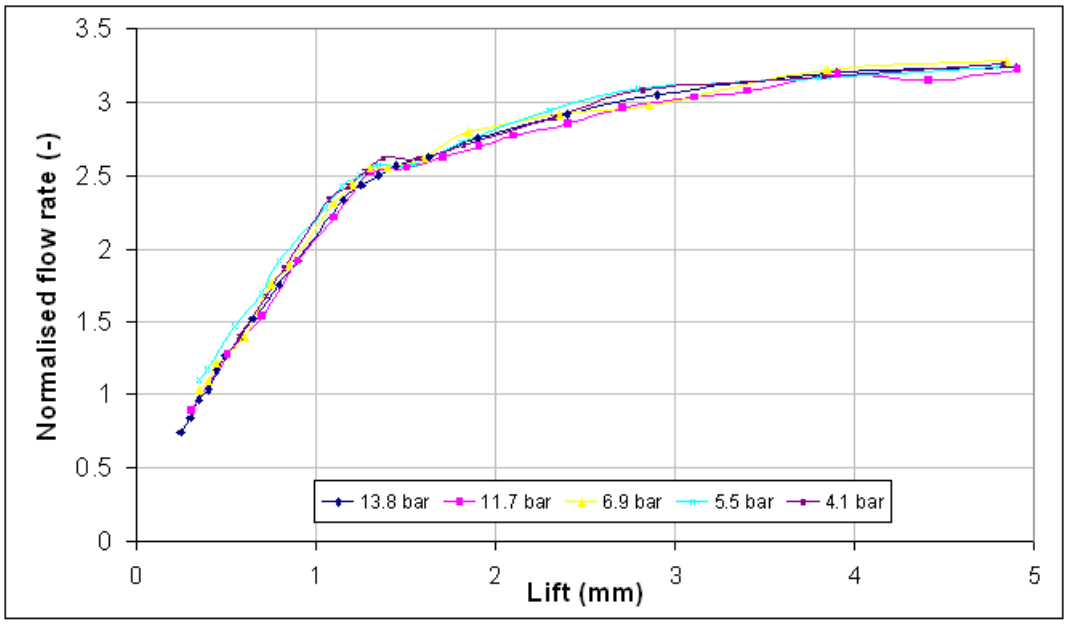

Figure 4.32: Normalised flow rate-lift characteristics

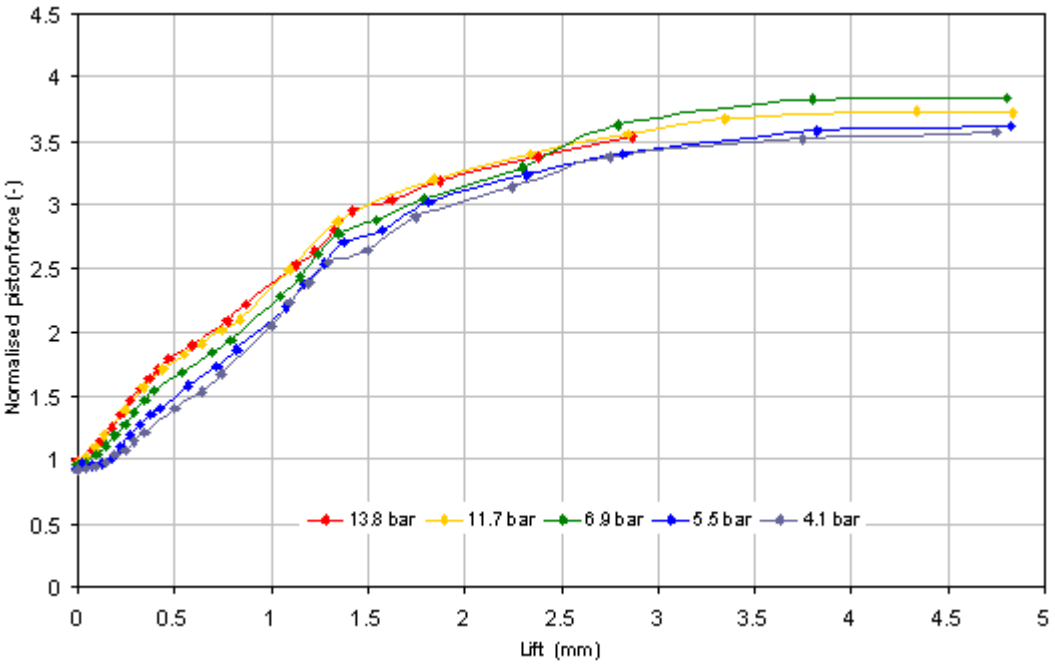

Figure 4.33: Normalised force-lift characteristics (no gland)

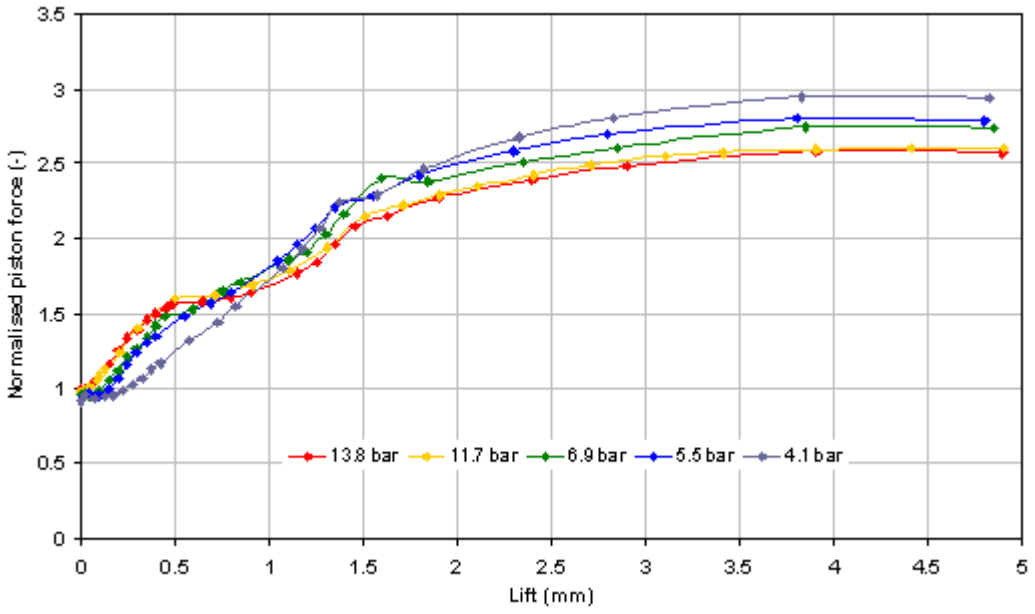

Figure 4.34: Normalised force-lift characteristics (with gland)

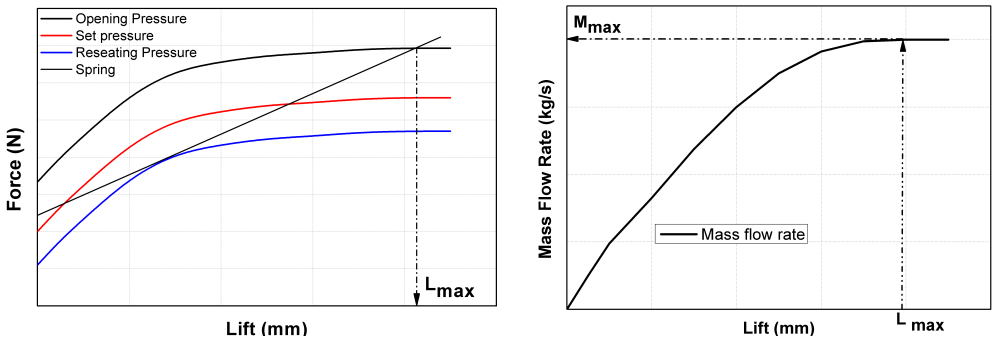

(a) Force-Lift (b) Flow-Lift

Figure 4.35: General opening and closing characteristics for a SRV

Chapter 5

Two Phase Flow Studies

5.1 Introduction

The single phase flow studies have provided good understanding of the compressible flow characteristics through the safety relief valve considered in this study. This has given the basic knowledge and encouragement to move on to the second step which is the two phase flow studies. In this chapter, two phase flow (air-water) through a safety relief valve is investigated computationally and experimentally. The main objective is to determine the predictive capability of a CFD approach for two phase flow and to establish an experimental methodology for testing based on the previous experience with single phase flow. The mixture model with the k-ε turbulence model are used to predict the two phase flow and obtain the flow-lift and force-lift characteristics for the valve at different flow conditions. The test pressure range was from 6.9 to 12.07 barg (100 - 175 psig). The water flow rate was from 0.01 to 0.05 kg/s which gives a range of water mass fraction of 0.1 to 0.71. Water mass fraction is defined as the ratio between the water mass flow rate to the mixture mass flow rate ($x_w = \frac{\dot{m}_w}{\dot{m}_w + \dot{m}_a}$). The commercially available CFD code FLUENT 6.3.26 was used to solve the models equations. CFD modelling details are introduced in Section 5.3. To investigate the predictive capability of the mixture model, experimental tests and CFD calculations has taken place not only at different flow conditions but also at various water injection arrangement with and without the gland. Experimental studies details are introduced in Section 5.2. Experimental and CFD results are presented in Sections 5.4 and 5.5 and discussed in Section 5.7. Well known simplified models are used to compare with the CFD and experimental results for predicting the discharge flow rate at maximum lift. Models used are the Homogeneous equilibrium model (HEM) [18], the Homogeneous non equilibrium model developed by Diener and Schmidt (HNE-DS) [23] and the ISO adopted model [2] which is the HNE-DS but assuming no slip between phases, i.e. the two phases have the same velocity. Simplified model are discussed in Section 5.6. Normalised flow-lift and piston force-lift characteristics are introduced in Section 5.8 to assist in valve design.

5.2 Experimental Studies

The purpose of the experimental work is to obtain the flow-lift and force-lift characteristics at different upstream air pressure and different water flow rates. The air pressure determines the extent of air mass flow with the amount of water being injected. The main idea is to inject water into the flowing air upstream of the valve allowing them to mix prior to entering the valve. A converging nozzle has been used to facilitate the injection and mixing of the fluid. Downstream of the valve, a separator with the necessary connections and adaptors is used to separate the water and the air. The water collected in the separator also acts as a water supply for the water injection pump. In the following subsections a description of the test rig and test procedures are introduced.

5.2.1 Experimental Setup

The test rig, Figures 5.1 and 5.2 , consists of a 100 mm (4 inch) diameter pipe (1) connected to an air compressor to deliver high pressure (1-15 bar) compressed air to the valve. The air supply circuit used for two phase flow is the same circuit used for single phase flow and is described in Section 4.3.1. The tested safety valve (3) is connected to the pipe via a brass converging section (2) with inlet diameter 29 mm and outlet diameter 6.35 mm to adapt to the valve entrance. The dimension of the flow area of the converging section is presented in Appendix A.1.3. An injection nozzle (4) is fitted in the converging section to inject the water. The injection nozzle is a 4 mm tube with a closed end and the exit orifice positioned on the side wall facing downstream and located at the centre of the tube. The orifice allows a well distributed dispersed water flow. To investigate the effect of the water distribution on the flow properties, three different injection nozzles have been developed. The geometry of the nozzle and the effect of the water dispersion is discussed in Section 5.7.3. A PVC tube (5) is threaded to the valve outlet at one end while the other end has a nut to seal it and allow the piston rod to pass through it to the load cell. The PVC piece was designed such that it has

a minimum resistance to the outcoming flow. It has a 50 mm diameter side exit connected to a hose to direct the mixture to the separator, which is maintained close to the atmospheric pressure. A pressure tapping is fitted to the PVC piece to measure the pressure at the valve outlet (Figure 5.1 and 5.2). The piston rod passes through the PVC piece to be attached to the load cell. A clearance of 0.05 mm was allowed between the rod and the sealing nut hole to prevent any friction on the rod that may affect the force measurements. This clearance allow some droplets of water to come out of the PVC piece during the test at high water flow mass fraction. These droplets are collected in a small vessel. The valve piston (6) is attached to a 250 mm long 6 mm diameter rod connected to a load cell (7) which measures the force exerted on the piston. The load cell is connected to a moving traverse table that allows linear piston movements. The load cell (Omega LCMFD-500N) has the range of $\pm 500N$, it has a good water resistance (IP65) and an accuracy of $\pm 0.15\%$ of the range. The piston movement is measured by a digital dial indicator with sensitivity of 0.001 mm. The upstream pressure, back pressure and the outlet pressure are measured by the three Bourdon pressure gauges fitted at (8),(9) and (10) respectively.

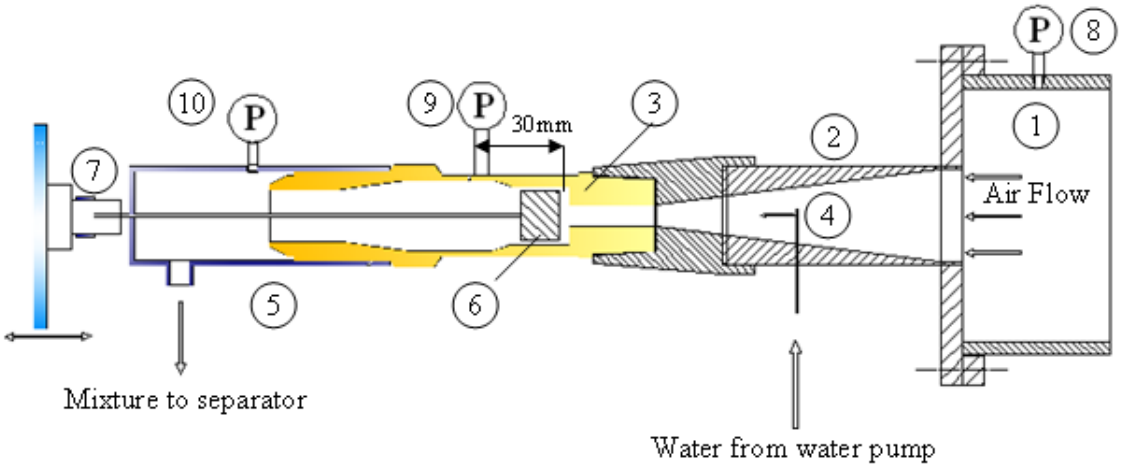

Figure 5.1: Test rig construction scheme

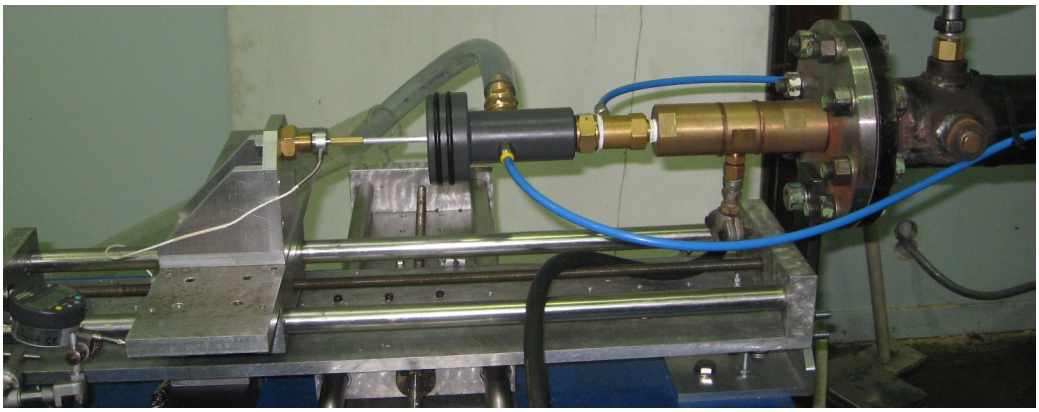

Figure 5.2: Test rig construction

The water injection system (Figure 5.3 and 5.4) consists of a positive displacement diaphragm water pump (Hydra Cell G20) (1) connected to the injection nozzle (5) via a high pressure hose. The water pump has been chosen to work at high pressure to inject water into a high pressure air flow. In addition it has a high volumetric efficiency such that the flow rate decrease with a pressure increase will be minor. High volumetric efficiency will allow a wide range of tests at different air flow pressures. The pump has a maximum flow rate of 3.5 l/min at 100 bar. The pump is driven by an AC motor controlled by a speed controller, which allows fine adjustment for the water flow rate needed. Upstream of the injection nozzle, a flow meter (Platon GMT) (4) is fitted to facilitate measurement of the water flow rate; it has a flow rate range of 0.4 - 4 l/min and has an accuracy of $\pm 2\%$ of the range. A pressure relief valve (2) is attached to the pump outlet to protect the circuit from any unexpected high pressure. A bladder accumulator (FlowGuard DS-20) (3) are connected to the pump outlet to damp the pulsating water flow rate from the pump.

5.2.2 Experimental Procedures

The test starts by clearing the system of any residual water that might have collected in the pipe work. This is done by setting the valve lift at a high value and imposing an upstream pressure of 3 bar to generate an air flow which will carry the water to the separator. For a specific test, the piston is moved to

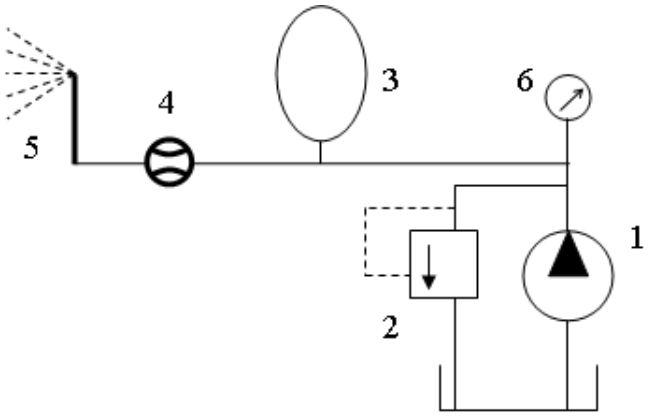

Figure 5.3: Water Injection circuit diagram

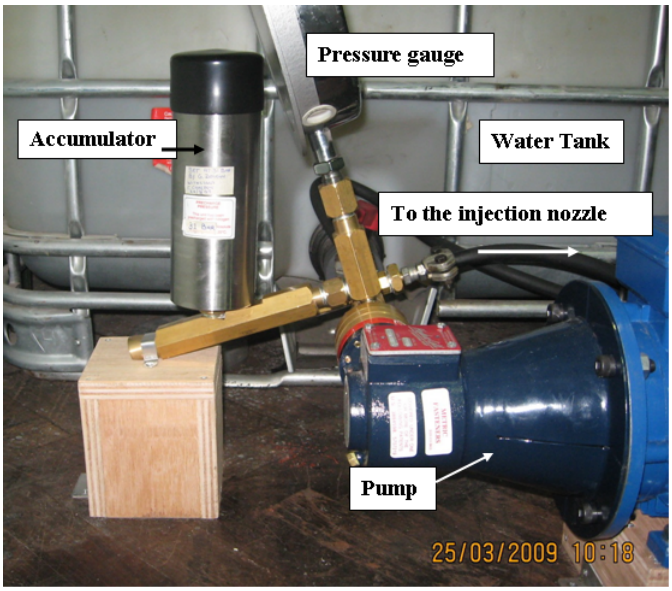

Figure 5.4: Water Injection circuit

the desired starting lift of 4.5 mm. The test pressure is adjusted by controlling the air flow via a throttle valve upstream of the tested safety relief valve. Prior to implementing the air-water test procedures, a single phase air test is carried out at which the zero lift is determined as described in Section 4.3.2. After the single phase air test is completed the two phase (air- water) test is started by maintaining the air flow at the test pressure then switching the water pump motor on. The pump motor speed is increased until the desired water flow rate is achieved. The water flow rate is continuously observed via the water flow meter. After water injection, the test pressure changes due to the water flow, therefore

	Test Pressure (barg)			
Water flow rate (kg/s)	6.9	8.6	10.3	12.07
0.01			√	√
0.02		√	√	√
0.03	√	√	√	√
0.04	√	√	√	√
0.05	√	√	√	√

Table 5.1: Experimental test matrix for two phase flow

the throttle valve needs to be readjusted to maintain the specific test pressure. When the pressure gauge indicates the desired test pressure and the flow meter indicates the correct water flowrate, the air flow rate, force and back pressure are recorded at this lift. The lift is changed to 4 mm then the throttle valve is adjusted again to maintain the test pressure. The air flow rate, force and back pressure are recorded at this lift. The test is repeated at 7, 8.6, 10.3 and 12.07 bar (100, 125, 150 and 175 psi) and water flow rate 0.01, 0.02, 0.03, 0.04 and 0.05 kg/s at lifts from 0.25 to 4.5 mm. However, there were some cases that could not be measured with a reasonable certainty because of the experimental facilities. For example, the minimum air flow that could be measured by the vortex flowmeter is about 0.015 kg/s, hence for a situation with high water flow rate and low lift the flowmeter indicates zero. Another example, at lower test pressures 100, 125 psi with low water flow rate (0.01 and 0.02 kg/s), the mixture pressure is less than the accumulator setting pressure, hence at this point the accumulator does not work correctly and the water flow pulses making the pressures fluctuate. Table 5.1[1]shows the experimental test matrix which has been carried out on the valve with and without the modified gland. These range of pressures and water flow rates give a working air flow rate from 0.015 to 0.86 kg/s and a water mass fraction range from 0.1 to 0.71.

[1]Full experimental results can be obtained by contacting Wael Elmayyah (elmayyah@yahoo.co.uk) or Dr. William Dempster (william.dempster@strath.ac.uk)

5.3 Two Phase Flow Modelling

Two main approaches are used to model two phase flow; the Eulerian-Lagrangian and the fully Eulerian approaches. The Eulerian-Lagrangian approach treats the continuous phase (in this case the air flow) as a continuum; the particles or droplets are tracked by calculating the particles/droplets equation of motion. The Lagrangian approach has been extended to consider the effect of the dispersed phase on the Continuous phase; by calculating the heat, momentum and mass transfer between the continuous and the dispersed phase. However, the Eulerian-Lagrangian approach is limited to dilute flows and assumes that the dispersed phase is well distributed all through the flow path which is not suitable in many cases. The Eulerian approach treats all phases as a continuum and for a two phase flow is often referred to as Eulerian-Eulerian. Each phase has its set of transport equations in addition to the interfacial equations. The full multiphase model that has continuity, momentum and energy equations for each phase with the associated interfacial equations will have many discontinuities associated with the equations and is more complex to develop and numerically solve. A simplified model, called the mixture model, was developed to increase the reliability of the multiphase models for certain conditions. The mixture model will be discussed in the following section. In this study the two phase flow is generated by injecting water into a flow of air. At the point of injection the water jet is a core based flow and not evenly dispersed over the flow area. Although the Eulerian-Lagrangian approach could be used here with the assumption that the water phase are well distributed droplets, the fully Eulerian approach here will be a better representation. The type of flows that exist in the high speed regions of the valve are believed to be dispersed droplets or annular flows with phase distribution and velocity slip modelling being the biggest issues. The mixture model has successfully been applied to these situations [26, 42]. Furthermore, as mentioned in the literature review (Chapter 3), the multi-dimensional two phase flow in a safety relief valve has not been examined in any detail, if at all. Therefore it was thought wise to start with the mixture model which is the simplest CFD model and determine

its effectiveness.

5.3.1 Mixture Model

The mixture model is a simplified model of the full Eulerian-Eulerian multiphase model. This model is considered a good alternative in simulating dilute flows of droplets of liquid in gas, suspension of solid particles in a gas or small bubbles in a liquid. In many cases the flow phenomena are dominated by one phase and the other phase has no effect on the flow. In this case the multiphase flow could be considered a single phase flow and all other phases are neglected but this is not the case in this study in which the secondary phases can not be ignored and has an effect on the flow.

The most significant issue in a multiphase model is the strength of the coupling between the phases, hence we can find the homogeneous flow models, mixture models, multi-fluid models and many combinations between them. In most cases each phase is treated as an interpenetrating continuum with a volume fraction parameter. In the case of strongly coupled phases when their velocities equalise over short spatial length scales, the flow can be considered homogeneous assuming all phases move at the same velocity. A number of models have been developed on the basis of an assumption of local equilibrium. [25, 37, 39]. In other cases gravity and centrifugal forces tend to cause velocity change which could not be ignored.

The mixture model is given in the form of continuity and energy equations for the mixture and one momentum equation, which contains an additional term representing the effect of velocity differences between phases. A model based on a force balance for the dispersed phases is required for computation of the relative velocities. In addition, an equation for the volume fraction for the dispersed phase is introduced. In all multiphase models the main difficulties are due to the interfaces between phases and discontinuities associated with them. Although the full multiphase equations are theoretically more advanced, the uncertainties in the closure relations can make them less reliable than the simpler mixture

model [42]. Another advantage of the mixture model is the considerably smaller number of variables to be solved compared to the full multiphase models and hence it is much more computationally efficient with much smaller solving times.

5.3.1.1 Basic Equations

The mixture model assumes local equilibrium over short spatial length scales, It solves the continuity equation, momentum equation and energy equation for the mixture in addition to the volume fraction equation for the secondary phase as well as algebraic expressions for relative velocities. They are presented below

Continuity equation

$$\frac{\partial}{\partial t}(\rho_m) + \nabla.(\rho_m \overrightarrow{u_m}) = 0 \tag{5.1}$$

where $\overrightarrow{v_m}$ is the mass-averaged velocity:

$$\overrightarrow{u_m} = \frac{\sum_{k=1}^{n} \alpha_k \rho_k \overrightarrow{u_k}}{\rho_m} \tag{5.2}$$

and ρ_m is the mixture density:

$$\rho_m = \sum_{k=1}^{n} \alpha_k \rho_k \tag{5.3}$$

where

$$\sum_{k=1}^{n} \alpha_k = 1 \tag{5.4}$$

Momentum equation

$$\frac{\partial}{\partial t}(\rho_m \overrightarrow{u_m}) + \nabla.(\rho_m \overrightarrow{u_m} \overrightarrow{u_m}) = -\nabla p + \nabla \left[\tau_m + \tau_{Tm}\right] + \rho_m \overrightarrow{g} + \overrightarrow{F} + \nabla.\tau_{Dm} \tag{5.5}$$

Where τ_m is the average viscous stress,

$$\tau_m = \sum_{k=1}^{n} \alpha_k \tau_k \tag{5.6}$$

τ_{Tm} is the turbulent stress,

$$\tau_{Tm} = \sum_{k=1}^{n} \alpha_k \overline{\rho_k u_k u_k} \tag{5.7}$$

τ_{Dm} is the diffusion stress,

$$\tau_{Dm} = \sum_{k=1}^{n} \alpha_k \rho_k \overrightarrow{u_{dr,k}} \overrightarrow{u_{dr,k}} \tag{5.8}$$

Slip velocity and Drift velocity The relative velocity is the velocity of the secondary phase (water (w)) to the velocity of the primary phase (air (a))

$$\overrightarrow{u_{wa}} = \overrightarrow{u_a} - \overrightarrow{u_w} \tag{5.9}$$

The mass fraction for any phase (k) is defined as

$$x_k = \frac{\alpha_k \rho_k}{\rho_m} \tag{5.10}$$

The drift velocity $\overrightarrow{u_{dr}}$ is defined as

$$\overrightarrow{u_{dr,k}} = \overrightarrow{u_k} - \overrightarrow{u_m} \tag{5.11}$$

and can be written in the form

$$\overrightarrow{u_{dr,w}} = \overrightarrow{u_{wa}} - \sum_{k=1}^{n} \alpha_k \overrightarrow{u_{ak}} \tag{5.12}$$

Drag force

The drag force represents the additional forces on a particle due to the velocity relative to the fluid. Drag force for a single rigid spherical particle in air can be written as follows

$$F_D = \frac{1}{2} \rho_a C_D \, A \mid u_{wa} \mid u_{wa} - \frac{1}{2} V_w \rho_a \frac{du_{wa}}{dt} \tag{5.13}$$

The first term on the right hand side is the viscous drag and the second is the virtual mass other sources of drag force such as rotation, concentration gradient, pressure gradient and the effect of past acceleration have been omitted. [16, 42]

The drag coefficient C_D depends on many factors but it could be given by Stokes' law which is valid for low relative Reynolds numbers Re_r

$$C_D = \frac{24}{Re_r} \tag{5.14}$$

Where,

$$Re_r = \frac{d_w \rho_w \mid u_{wa} \mid}{\mu_a} \tag{5.15}$$

The relative velocity expression was obtained by Manninen et al [42] by combining the momentum equation for the mixture (equation 5.5) and the momentum equations of the water droplets (equation 5.16)

$$\alpha_w \rho_w \frac{\partial}{\partial t}(\overrightarrow{u_m}) + \alpha_w \rho_w (\overrightarrow{u_w} \cdot \bigtriangledown)\overrightarrow{u_w} = -\nabla p + \nabla \left[\alpha_w(\tau_w + \tau_{Tw})\right] + \alpha_w \rho_w \overrightarrow{g} + \overrightarrow{F} \tag{5.16}$$

Considering the viscous drag only with the Stokes' flow (equations 5.14 and 5.15)so the relative velocity can be written as

$$\overrightarrow{u_{wa}} = \frac{(\rho_w - \rho_m) d_w^2}{18\mu_a} \overrightarrow{a} \tag{5.17}$$

The acceleration $\overrightarrow{a}$

$$\overrightarrow{a} = \overrightarrow{g} - (\overrightarrow{u_m} . \nabla)\overrightarrow{u_m} - \frac{\partial \overrightarrow{u_m}}{\partial t} \tag{5.18}$$

For higher relative Reynolds number the relative velocity should consider different drag coefficient C_D, so a drag factor was introduced

$$f_{drag} = \frac{C_D Re_r}{24} \tag{5.19}$$

It is clear that when $C_D = \frac{24}{Re_r}$ so $f_{drag} = 1$ and the relative velocity becomes

$$\overrightarrow{u_{wa}} = \frac{(\rho_w - \rho_m) d_w^2}{18 \mu_a f_{drag}} \overrightarrow{a} \tag{5.20}$$

In turbulent flows the relative velocity should contain a diffusion term due to dispersion appearing in the momentum equation for the dispersed phase.

$$\overrightarrow{u_{wa}} = \frac{(\rho_w - \rho_m) d_w^2}{18 \mu_a f_{drag}} \overrightarrow{a} - \frac{\mu_{t,m}}{\alpha_w \sigma_D} \nabla \alpha_a \tag{5.21}$$

Where $\mu_{t,m}$ is the mixture turbulent viscosity and σ_D is a Prandtl dispersion coefficient.

An important term appears in equation 5.20; which is the velocity response time τ_v

$$\tau_v = \frac{\rho_w d_w^2}{18 \mu_a} \tag{5.22}$$

hence equation 5.21 becomes

$$\overrightarrow{u_{wa}} = \frac{\tau_v (\rho_w - \rho_m)}{f_{drag}\, \rho_w} \overrightarrow{a} - \frac{\mu_{t,m}}{\alpha_w \sigma_D} \nabla \alpha_a \tag{5.23}$$

For higher relative Reynolds number the Stokes' law underestimates the drag, so alternative expressions were used to improve Stokes' law. One of the widely used formula was contributed by Schiller and Nauman [16, 42]

$$C_D = \begin{cases} 24(1 + 0.15 Re_r^{0.687})/Re_r & Re_r \leq 1000 \\ 0.4 & Re_r > 1000 \end{cases} \tag{5.24}$$

Volume fraction equation for the secondary phase Assuming there is no mass transfer between phases the mass continuity for the liquid phase is as follow:

$$\frac{\partial}{\partial t} (\alpha_w \rho_w) + \nabla . (\alpha_w \rho_w \overrightarrow{u_m}) = -\nabla . (\alpha_w \rho_w \overrightarrow{u_{dr,w}}) \tag{5.25}$$

Energy equation The energy equation is solved for the mixture and deals with the mixture temperature which is applicable when the temperature difference between the phases are small.

$$\frac{\partial}{\partial t}\sum_{k=1}^{n}(\alpha_k\rho_k E_k) + \nabla.\sum_{k=1}^{n}(\alpha_k\overrightarrow{u_k}(\rho_k E_k + p)) = \nabla.[K_{eff}\nabla T] \tag{5.26}$$

where

$$K_{eff} = \sum_{k=1}^{n}\alpha_k(K_k + K_t) \tag{5.27}$$

$$E_k = h_k - \frac{p}{\rho_k} + \frac{u_k^2}{2} \tag{5.28}$$

K_{eff} is the effective conductivity and K_t is the turbulence conductivity.

Turbulence model The standard k-ε turbulence model is used here for the mixture which is applicable when the density ratios of the phases is near 1 or the volume fraction of the secondary phase is very small as here in this study.

$$\frac{\partial}{\partial t}(\rho_m k) + \nabla.(\rho_m\overrightarrow{u_m}k) = \nabla.\left(\frac{\mu_{t,m}}{\sigma_k}\nabla k\right) + G_{k,m} + G_{b,m} - \rho_m\varepsilon \tag{5.29}$$

$$\frac{\partial}{\partial t}(\rho_m\varepsilon) + \nabla.(\rho_m\overrightarrow{u_m}\varepsilon) = \nabla.\left(\frac{\mu_{t,m}}{\sigma_\varepsilon}\nabla\varepsilon\right) + \frac{\varepsilon}{k}(C_{1\varepsilon}G_{k,m} - C_{2\varepsilon}\rho_m\varepsilon) \tag{5.30}$$

where the turbulent viscosity $\mu_{t,m}$, is computed from

$$\mu_{t,m} = \rho_m C_\mu\frac{k^2}{\varepsilon} \tag{5.31}$$

and the production of the turbulence kinetic energy $G_{k,m}$is computed from

$$G_{k,m} = \mu_{t,m}(\nabla\overrightarrow{u_m} + (\nabla\overrightarrow{u_m})^T) : \nabla\overrightarrow{u_m} \tag{5.32}$$

And the constants values are as follow

$C_{1\varepsilon} = 1.44$, $C_{2\varepsilon} = 1.92$, $C_{\mu} = 0.09$, $\sigma_k = 1$ and $\sigma_{\varepsilon} = 1.3$

5.3.2 Computational Model

A two dimensional axisymmetric model has been shown to provide adequate prediction for the mass flow rate for single phase air flow, as discussed in Chapter 4. The flow and piston force prediction of a safety relief valve under two phase flow using CFD hasn't been investigated in the literature. Therefore, starting with the two dimensional axisymmetric model is considered a reasonable first step in predicting the flow. The detailed investigations of the two dimensional model prediction for the piston force showed that the piston force prediction is dependent on the piston geometry, as shown in Section 4.5. As a result, the three dimensional model shows a better prediction for the piston force compared to the two dimensional axisymmetric model when applied to the valve adopted in this study, as discussed in Chapter 4. However, the two dimensional axisymmetric model is much more computationally efficient than the three dimensional model. A two dimensional axisymmetric model has been developed to represent the safety valve geometry and the converging section, which includes the injection nozzle, Figure 5.5. The flow areas between the piston and the body and the modified gland flow areas, have been shown on Figure 4.8 and have been represented as equivalent annulus areas as described in Chapter 4. The computational mesh has a total of 11350 quadrilateral cells distributed giving an average mesh density of 8 $cells/mm^2$. A more dense mesh of 20000 quadrilateral cells has been used to examine the grid independency, there was no significant improvement for the solution. The difference in air flow rate was 0.00001 kg/s so the cell number was kept about 14000 in all cases. The injection nozzle has been introduced as a water inlet with the same orifice diameter. The boundary conditions used are the pressure inlet, pressure outlet, mass flow inlet and stationary walls.

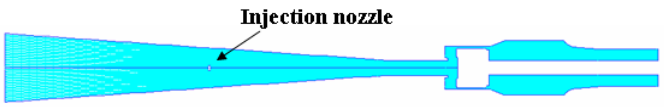

Figure 5.5: Computational grid for the valve and the converging section

5.3.3 Boundary Conditions and Solution

The boundary conditions are applied at the converging section inlet, valve outlet, injecting nozzle inlet and the valve and the converging section walls. Walls of the valve and the converging section were defined as stationary walls. At the inlet boundary, which is an air only inlet, the stagnation pressure, static pressure and stagnation temperature are applied; in addition an initial value for the turbulence intensity and the hydraulic diameter are introduced. At the outlet boundary the static pressure and the stagnation temperature are applied. At the injecting nozzle which is a water only inlet, the stagnation pressure, stagnation temperature and the water mass flow rate is defined; in addition an initial value for the turbulence intensity and the hydraulic diameter are introduced. The discertization scheme used for the continuity, momentum, energy, turbulent kinetic and turbulent dissipation energy equations was second order upwind for the convection terms and second order central difference for the diffusion terms. For the volume fraction equation the discertization scheme was first order upwind for the convection terms and second order central difference for the diffusion terms. The convergence criterion was based on the residual values of the calculated variables, i.e., mass continuity, velocity components, energy, turbulent kinetic energy and turbulent dissipation energy. The threshold values were 1×10^{-3} for all variables except for the energy which was 1×10^{-6} and for the mass continuity, 1×10^{-4} . All cases have converged in about 60 min on a 2.4 GHz desktop PC . The pressures range used was 7 -14 barg (100 - 200 psig) to allow model validation by the experimental results, which have the limits discussed in Section 4.3.2

5.4 Experimental Results

5.4.1 Flow-Lift Characteristics

As discussed in Chapter 3 flow-lift characteristics provide a complete description of the valve discharge with respect to the piston movement. Figures 5.6 and 5.7 show the air mass flow rates and mixture mass flow rates at an inlet pressure of 12.07 barg (175psi) at different water flow rates. Figure 5.6 shows that the air flow rate is decreased with an increase in the water flow rate, while the total mixture flow rate is increased (Figure 5.7). This behaviour indicates that the air flow rate is decreased by an amount less than the water flow rate is increased. The figures also show that the two phase flow- lift characteristics follow the single phase behaviour. i.e. for these range of tests, the critical planes are at the same locations as described in Section 4.5.3.1. Figures 5.8 and 5.9 show the same behaviour at a test pressure of 8.62 barg (125 psi) for various water flow rates. Figures 5.6 and 5.8 show that the two phase air flow rate-lift relation has a lower slope than single phase at high lifts (1.3 - 4.5 mm). This change in the slopes is due to the water flow which results in a lower pressure-lift slope upstream of the inlet of the passageway around the piston as discussed in Section 4.5.3.1. Flow-lift characteristics are discussed in Section 5.7.1.

Two groups of experimental tests have been carried out; one with the modified gland fitted to the valve and the other without the gland. Figure 5.10 shows the effect of the gland on the air flow rate at pressure 12.07 barg (175 psi) and 0.01 kg/s and 0.05 kg/s water flow rate. The figure shows that the modified gland has no significant effect on the air flow rate which agrees with the conclusions discussed in Chapter 4 for single phase flow.

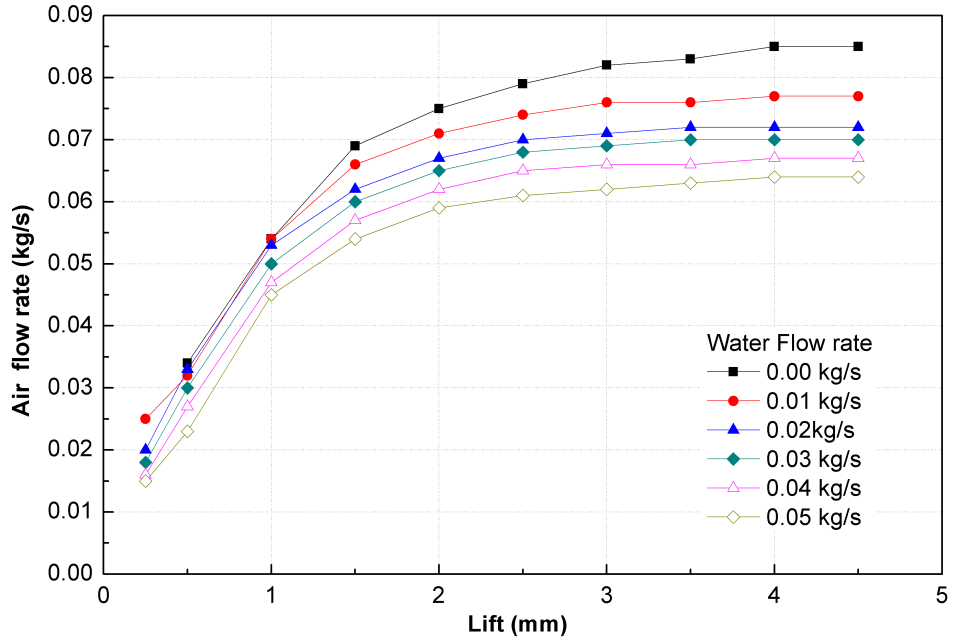

Figure 5.6: Air flow-Lift at 12.07 barg (175psi)

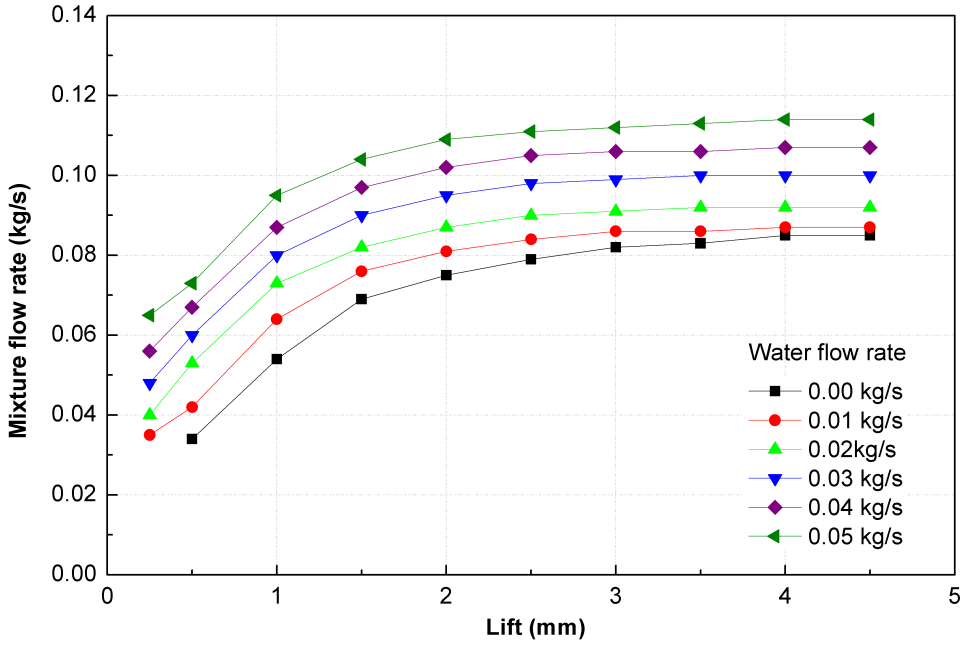

Figure 5.7: Mixture flow-Lift at 12.07 barg (175psi)

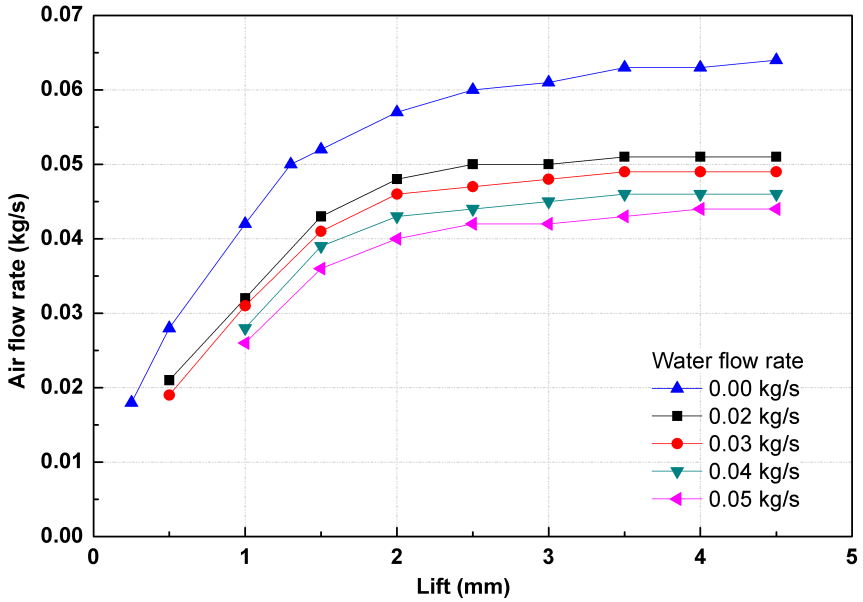

Figure 5.8: Flow-Lift at 8.62 barg (125psi)

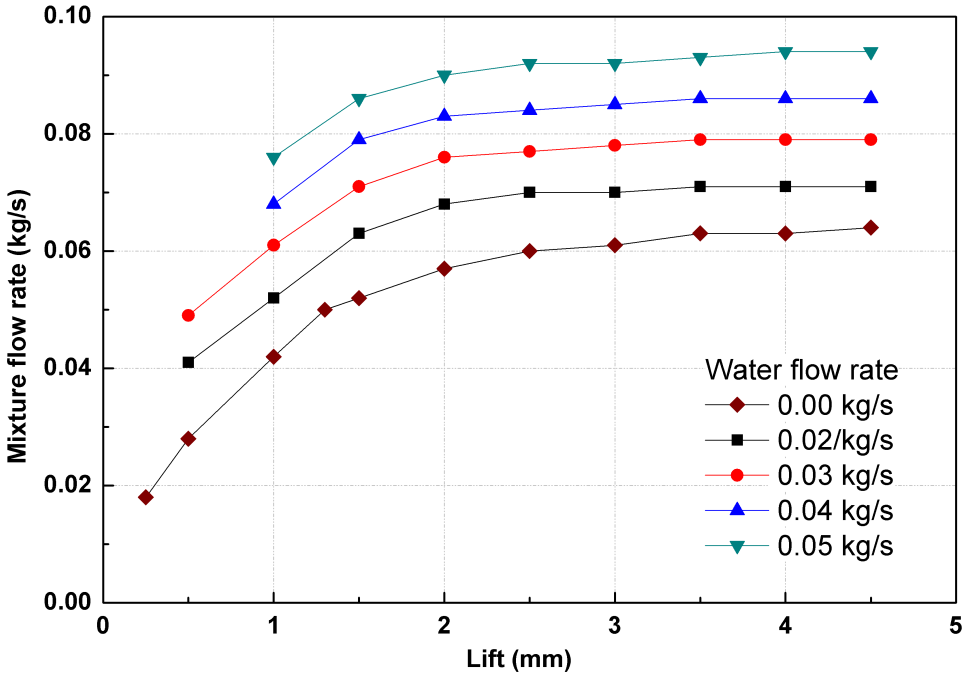

Figure 5.9: Mixture Flow-Lift at 8.62 barg (125psi)

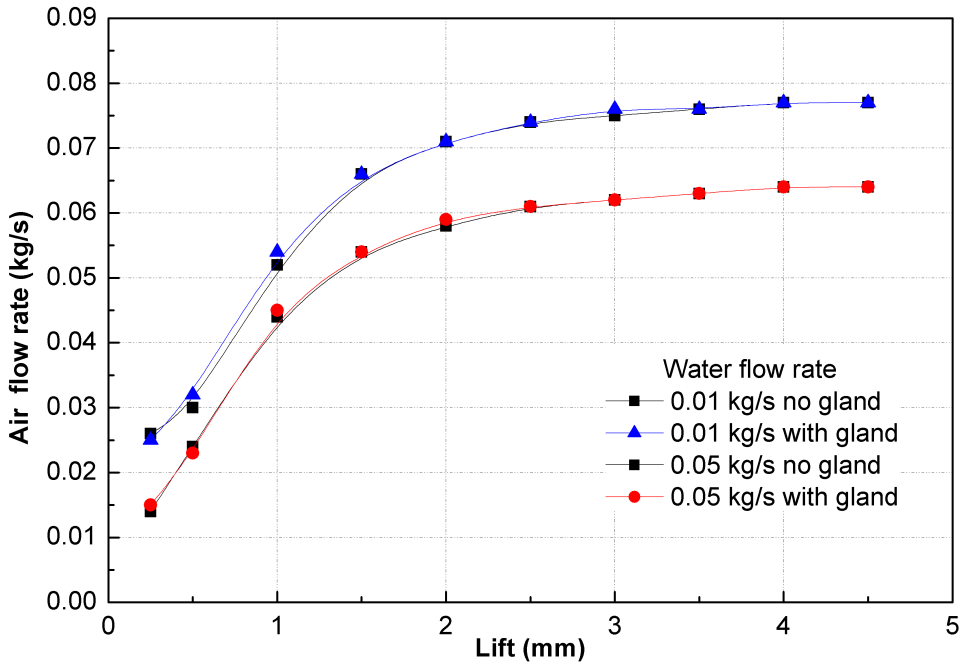

Figure 5.10: The effect of the modified gland on air flow rate

5.4.2 Force- Lift Characteristics

Force-lift characteristics in conjunction with the flow-lift characteristics show at every lift the discharge flow rate and the fluid dynamic force exerted on the piston at this lift. Although the modified gland has no effect on the air flow rate, it has a significant effect on piston force. This is because of the back pressure increase due to the existence of the gland and the reduction in the outlet area. This is similar to the single phase characteristics. Figure 5.11 shows the effect of the gland on piston force at a constant lift of 2 mm with different injected water flow rates.

Figures 5.12 and 5.13 present the force-lift characteristics at pressures of 12.07 and 8.62 barg with the modified gland. The figures show nearly the same curve for the force-lift characteristics at this water flow rate range. It can be stated that the water flow rate has no significant effect on the force-lift characteristics. This indicates that at these range of water flow mass fraction of (0.1 - 0.72) the water flow rate has no significant effect on the force. Also, It is apparent that the two phase force-lift characteristics follow the force-lift characteristics for the

single phase. However, the single phase characteristics have lower force values at lower lifts (0.25 - 1.5 mm) and a higher force values at high lifts (2.5 - 4.5 mm) . This will be discussed in Section 5.7.2

Figures 5.14 and 5.15 show the force-lift characteristics at pressure 12.07 barg and 8.62 barg without the gland. The figures show that the single phase characteristics have lower force values at lower lifts (0.25 - 2 mm) at 12.07 barg and at lifts (0.25 - 2.5 mm) at 8.62 barg. This will be discussed in Section 5.7.2

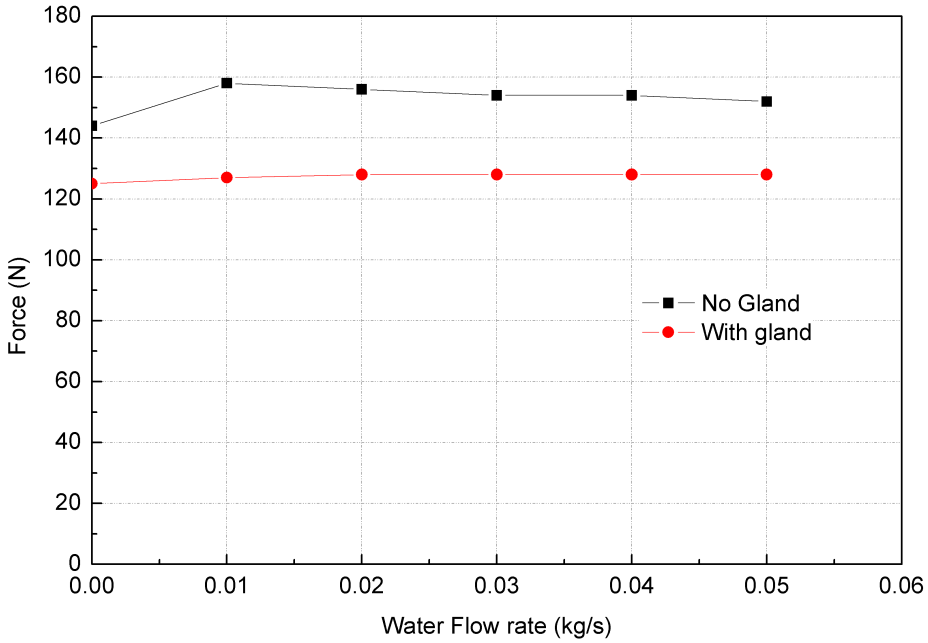

Figure 5.11: Effect of the modified gland on piston force at 2mm lift at 12.07 barg

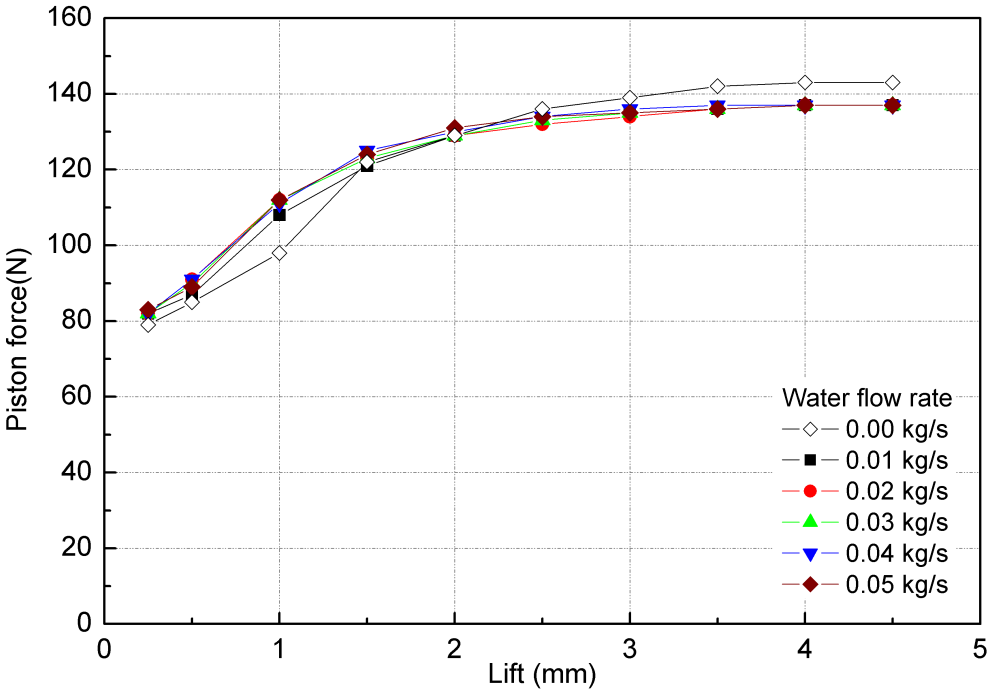

Figure 5.12: Force-Lift at 12.07 barg (175psi) with modified gland

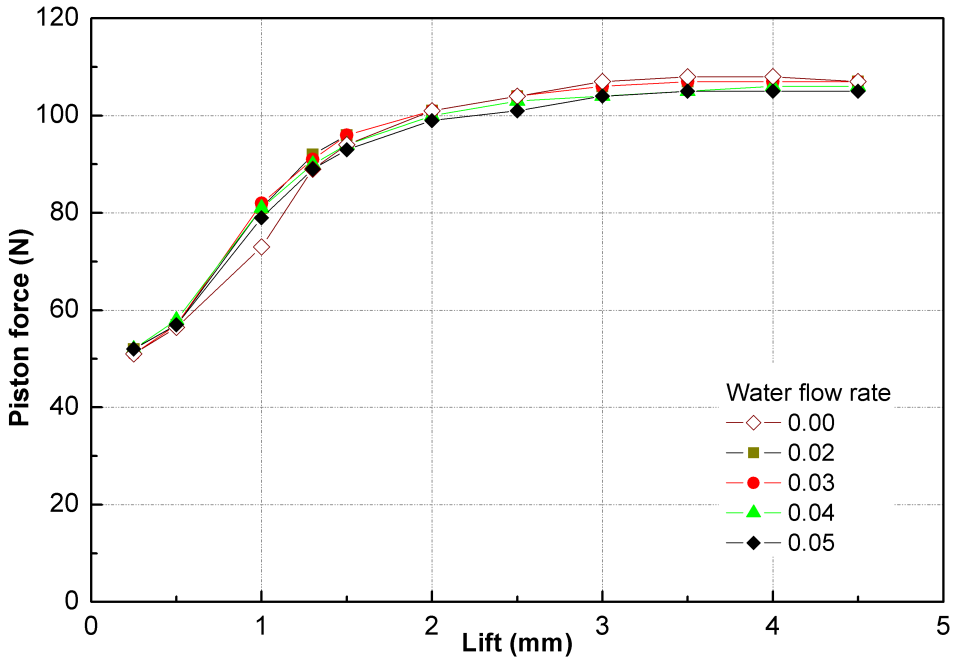

Figure 5.13: Force-Lift at 8.62 barg (125psi) with modified gland

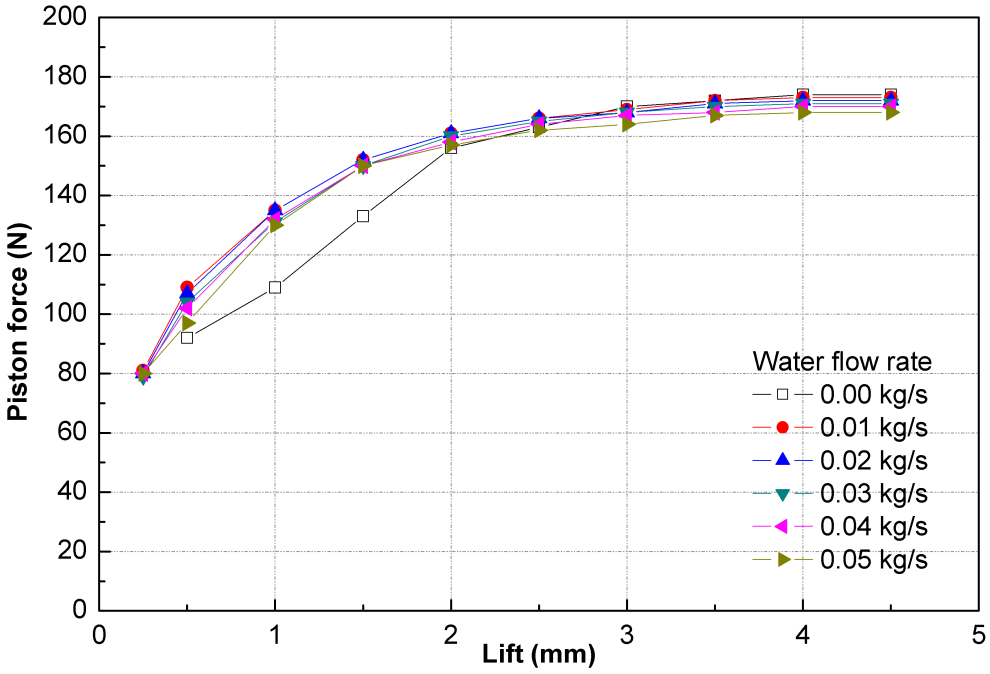

Figure 5.14: Force-Lift at 12.07 barg (175psi) without gland

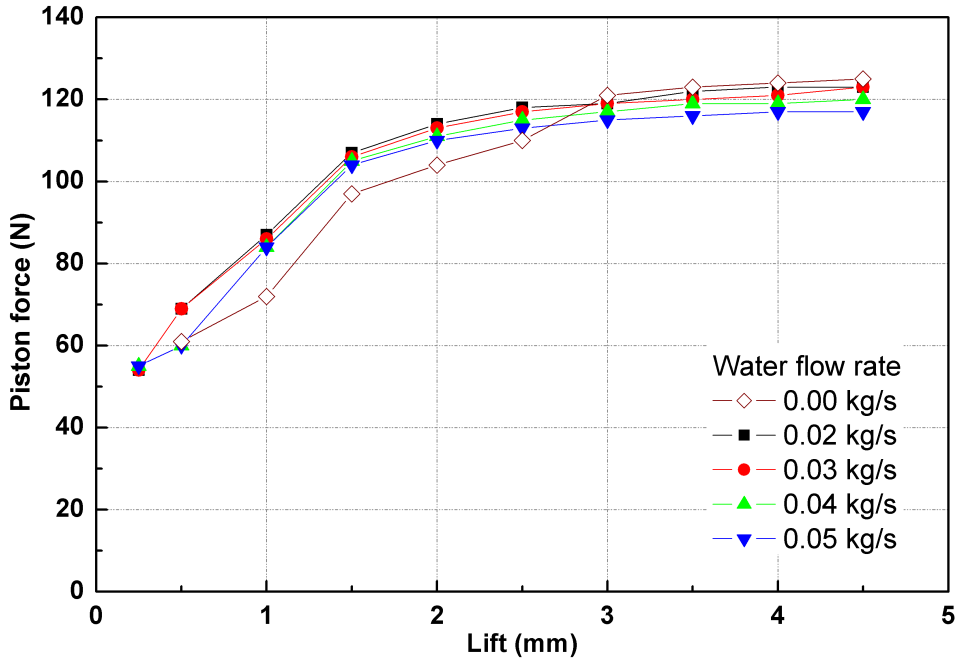

Figure 5.15: Force-Lift at 8.62 barg (125psi) without gland

5.5 Mixture Model CFD Results

Figure 5.16 presents the air and the mixture Mach number contours at 12.07 barg, 3 mm lift and 0.05 kg/s water flow rate. The Fluent code manual did not provide sufficient details on how the Fluent speed of sound for a two phase flow was calculated and this prevented proper interpretation of the results. Thus the definition shown in equation 5.33 based on homogeneous assumptions has been used instead. The Mach number for the mixture is defined as follow

$$M = \frac{u_m}{a_{sm}} \tag{5.33}$$

Where u_m is the mixture velocity, and a_{sm} is the sonic speed in the mixture which is defined for a homogeneous flow with air volume fractions higher than 0.9 as follow [63]

$$a_{sm} = \sqrt{\frac{\gamma p}{\alpha \rho_m}} \tag{5.34}$$

It can be noticed that the critical plane position is similar in the two figures which indicates similar flow-lift characteristics. The figures show that the flow accelerates at the valve entrance until the flow is choked at piston side faces (M=1), then undergoes an expansion downstream of the choking plane for a short distance before undergoing compression due to the existence of the modified gland. The static pressure contours are shown in Figure 5.18 (a). The flow behaviour is similar to the single phase flow in terms of undergoing compression, expansion and the choking plane locations because of the high air volume fraction. Therefore the air Mach number contours is similar to the mixture contours but with different values due to the density difference between the air and the air-water mixture. The air Mach number reaches 1.4, while the mixture mach number reaches 2. Upstream of the modified gland, the flow accelerates to flow through the modified gland, however the flow velocity remains subsonic. Figure 5.18 shows the water volume fraction and static pressure contours at a 4 mm lift with no gland and 0.05 kg/s water flow rate. From the figure it is shown that the

water distribution is characterised by a core based dispersed flow at the valve entrance centre axis then a dispersed flow around the piston but with a higher concentration of water droplets near the piston wall. The water volume fraction ranges from 0 to 0.01.

Figure 5.19 presents the slip contours at 3 mm lift, 12.07 barg, with gland and 0.01 and 0.05 kg/s water flow rate. The figure shows that the slip value is near zero at most of the flow regions. Only at the valve entrance at 0.01 kg/s water flow rate there is a slip value of 200 m/s . At 0.01 kg/s water flow rate, the water flow has a low velocity (6.4 m/s at the injection orifice). Therefore, the high air flow rate results in high slip values between the high velocity air and the low velocity water. However, the slip occurring at 0.01 kg/s has no significant effect on the air flow rate or forces. Figures 5.20 and 5.21 present the predicted flow lift and the force-lift characteristics at 0.01 kg/s with and without slip. It shows that accounting for the slip doesn't make any significant change for the flow rate or the piston force. It can be concluded that as far as the mixture model is concerned a homogeneous assumption can be applied here. Therefore, the flow is considered a homogeneous flow and all further cases were calculated without the slip equation. (equation 5.23). Since the slip will equal zero so the relative Reynolds number and the drag coefficient equal zero and hence equations 5.15 and 5.19 will also not be solved with the model equations. Fluent provides the facility of disabling the drag and slip equations for a homogeneous flow assumption. Figure 5.22 presents a comparison between the air flow-lift predicted by the mixture model and the experimental air flow-lift characteristics at 12.07 barg and water flow rates of 0.01 kg/s and 0.05 kg/s. Figure 5.23 presents a comparison between the mixture flow-lift characteristics predicted by the mixture model and experimental mixture flow-lift characteristics at 12.07 barg and water flow rates 0.01 kg/s and 0.05 kg/s. The figures show in general a good agreement between the predicted and experimental results at high lifts (1.5 - 4.5 mm), while less agreement is noticed at low lifts (0.25 - 1 mm). The figures also show that the mixture model prediction is more close to the experimental results at 0.01 kg/s water flow rate.

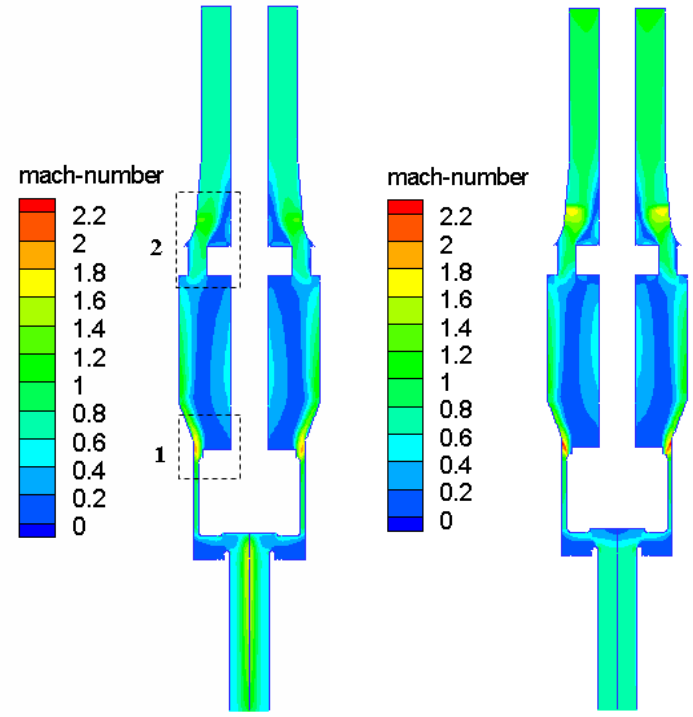

(a) Mixture Mach number **(b)** Single phase air Mach number

Figure 5.16: Contours of Mach number at single phase air and 0.05 kg/s water flow rate, 3mm lift and 12.07 barg (with gland). Area 1 and 2 are shown in Figure 5.17

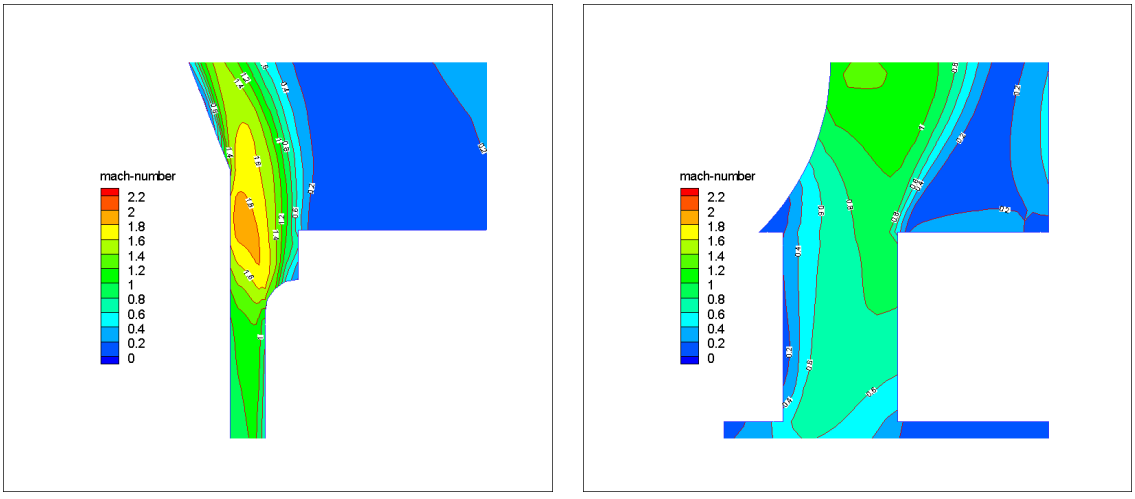

(a) Area 1 **(b)** Area 2

Figure 5.17: Contours of Mach number 0.05 kg/s water flow rate, 3mm lift and 12.07 barg (with gland) at Area 1 and 2(shown in Figure 5.16)

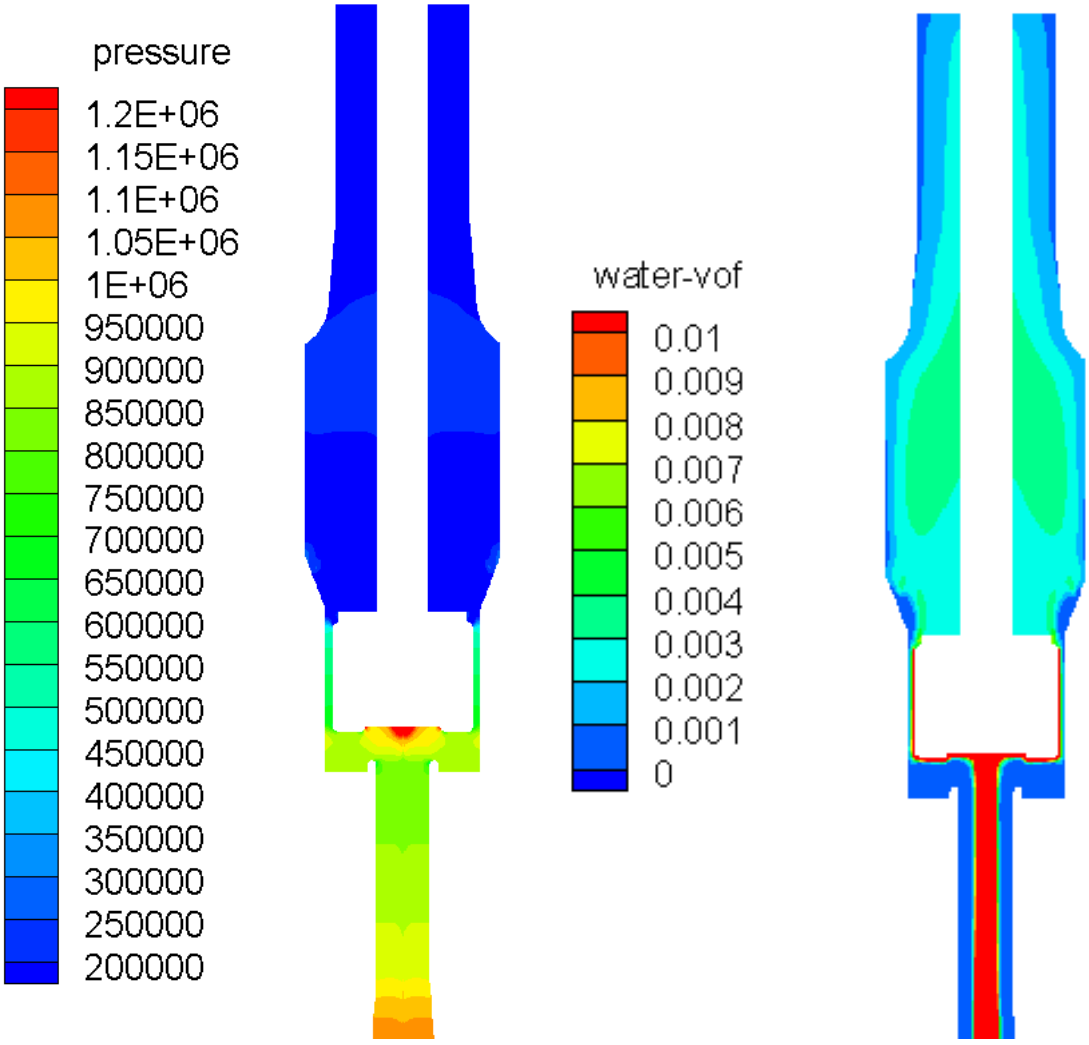

(a) Static pressure **(b)** Water Volume of fraction

Figure 5.18: Contours of Static Pressure and Water volume fraction at 4mm lift and 12.07 barg (no gland)

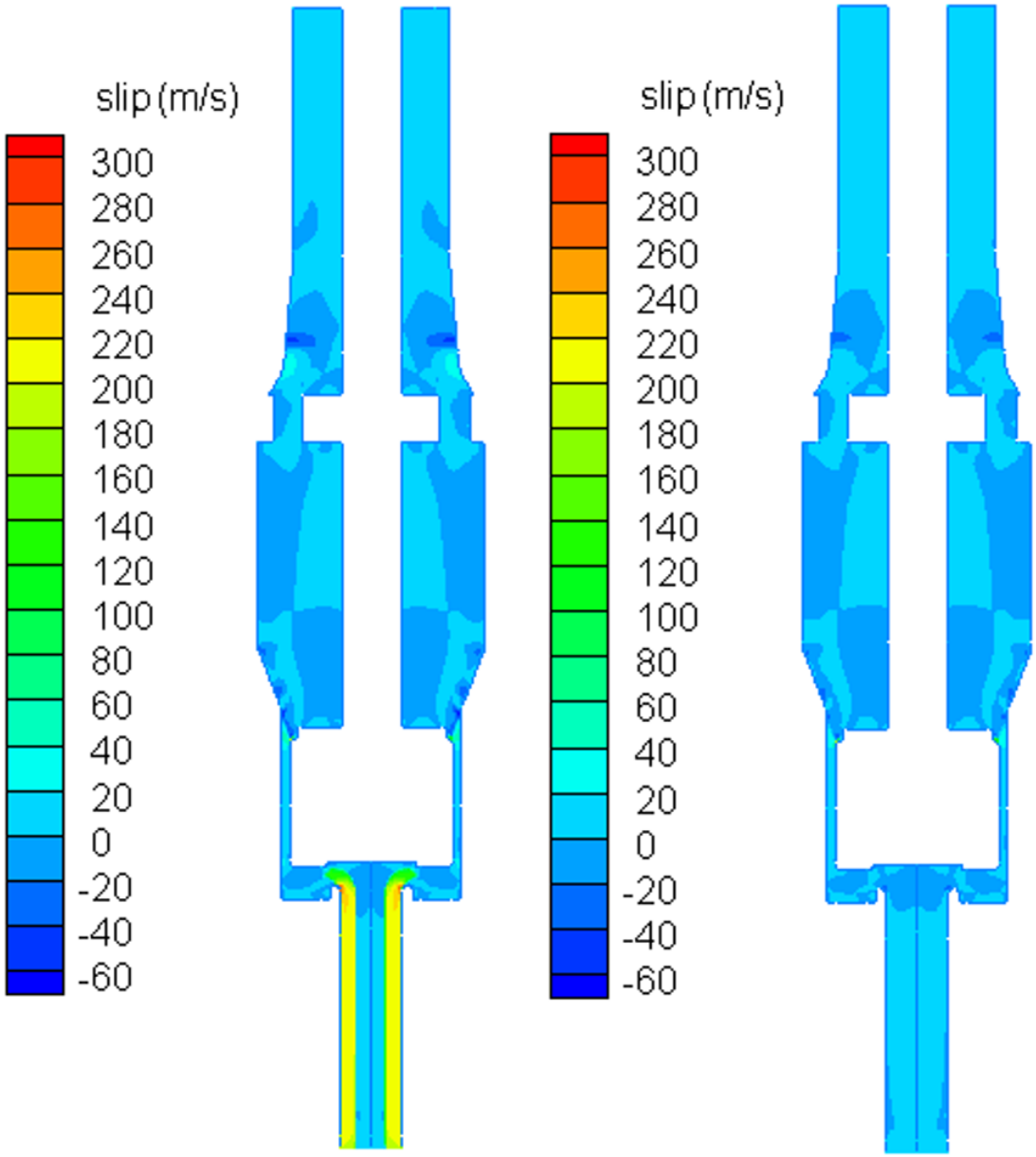

(a) 0.01kg/s **(b)** 0.05 kg/s

Figure 5.19: Contours of slip at 3mm lift and 12.07 barg at 0.01 and 0.05 kg/s (with gland)

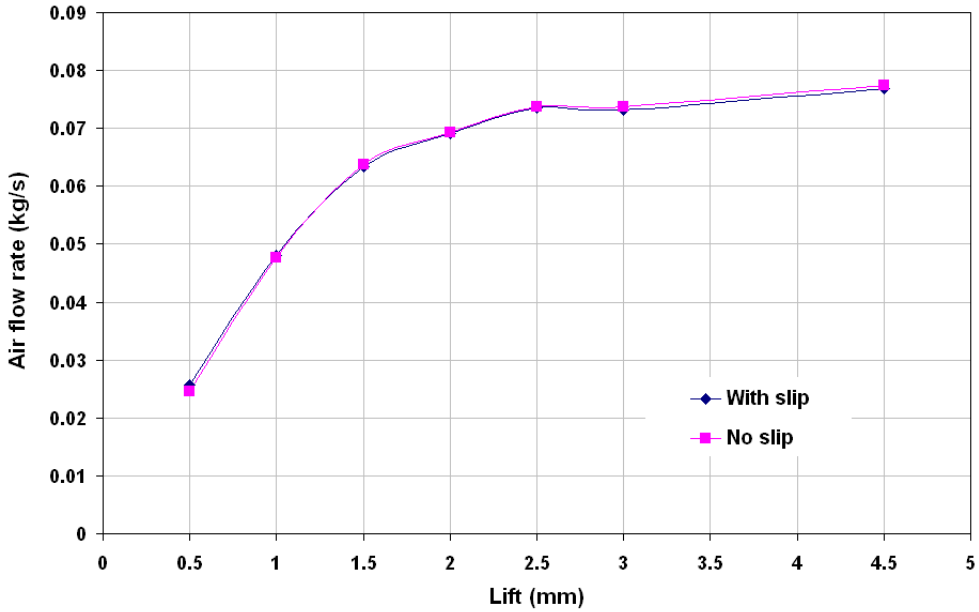

Figure 5.20: Predicted Flow-lift characteristics with and without the slip at 0.01kg/s water flow rate and 12.07 barg pressure.

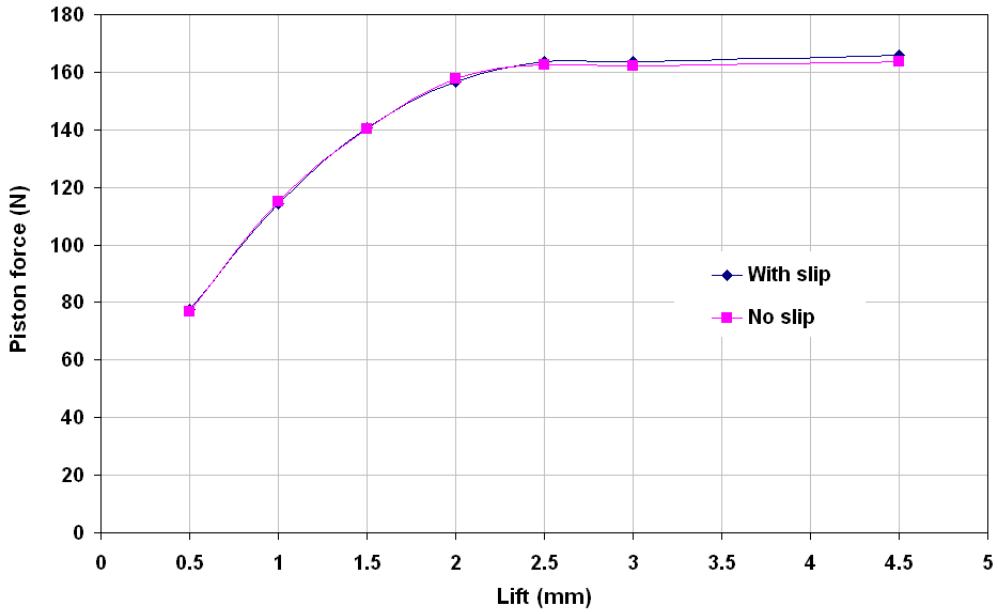

Figure 5.21: Predicted Force-lift characteristics with and without the slip at 0.01kg/s water flow rate and 12.07 barg pressure.

Flow-lift characteristics are discussed in Section 5.7.1

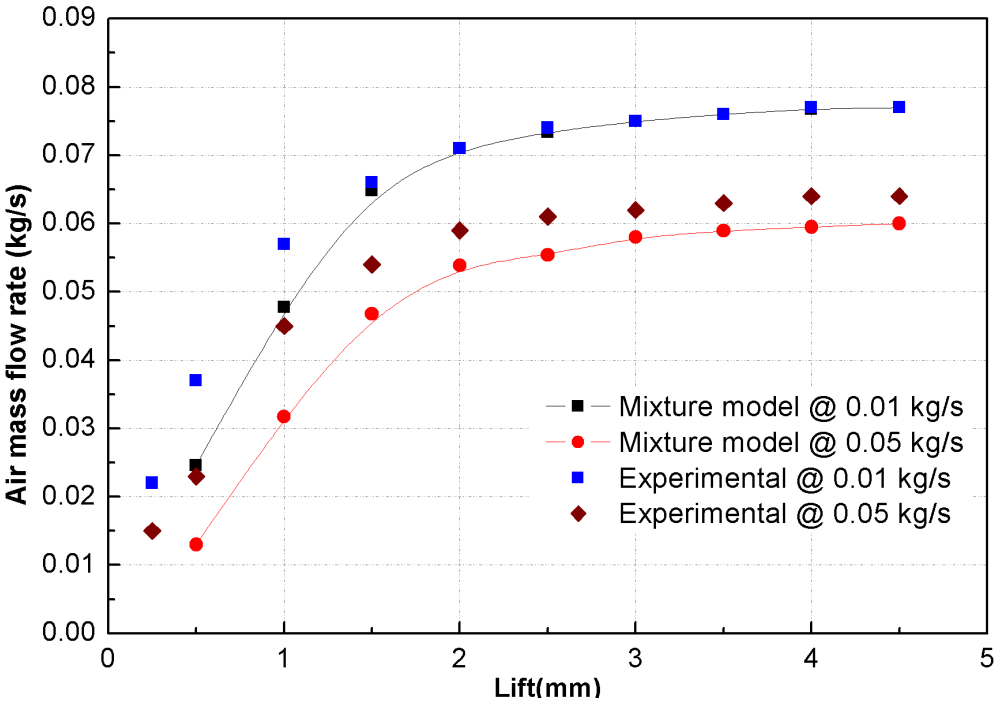

Figure 5.22: Air flow rate- Lift at 12.07 barg (175psi)

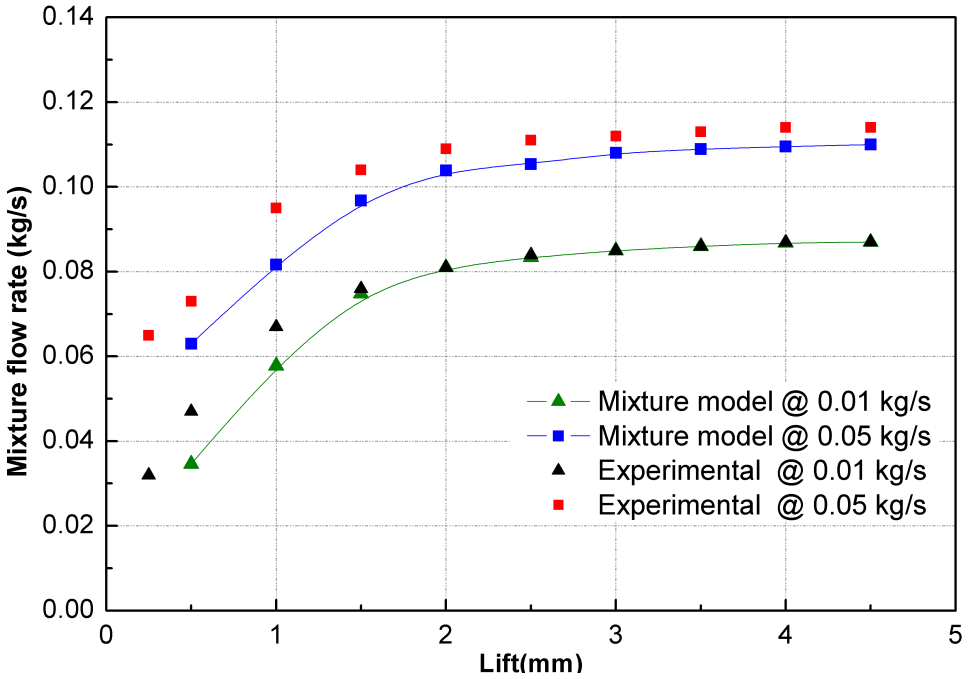

Figure 5.23: Mixture flow rate- Lift at 12.07 barg (175psi)

Figures 5.24 and 5.25 present a comparison between the force-lift characte-

ristics predicted by the mixture model and experimental force-lift characteristics at 12.07 barg and water flow rates 0.01 kg/s and 0.05 kg/s with and without the modified gland respectively. The figures show an overprediction of the piston force at lifts from 1.5-4.5 mm. However, the predicted piston force of the valve without the gland has closer values to the experimental results. Figure 5.26 shows the experimental and the predicted back pressure- lift caracteristics at 0.01 and 0.05 kg/s water flow rate. The figure shows a closer prediction for back pressure at 0.01 kg/s water flow rate due to the closer prediction of the flow rate at this low water mass fraction. On the other hand the pressure on the piston front face is affected by the water flow rate. The piston force is the resultant of the pressure on the piston front face and the piston back face. Force-lift characteristics are discussed in Section 5.7.2.

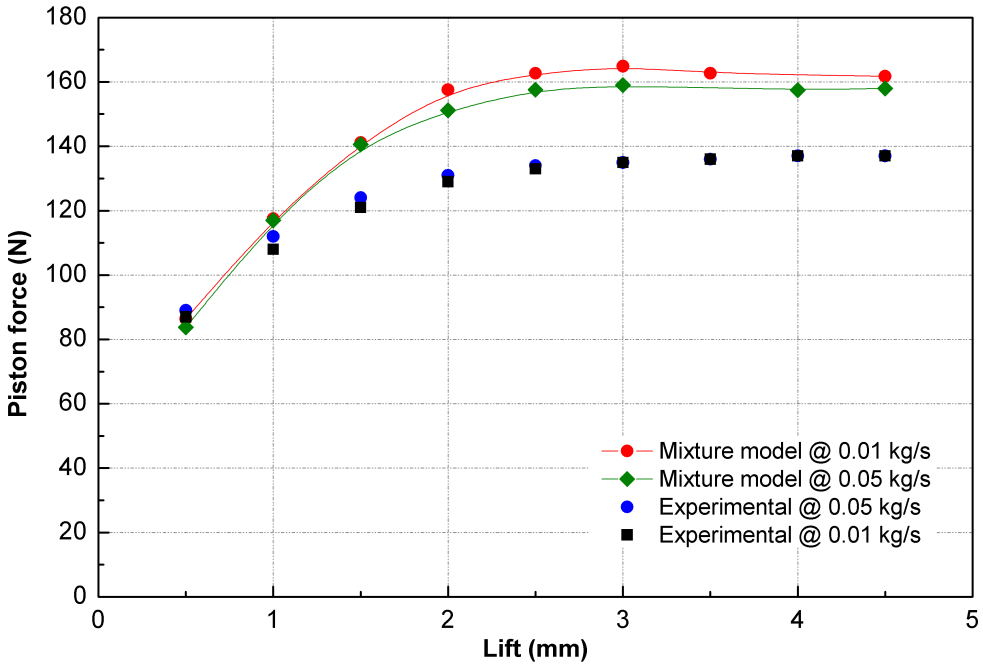

Figure 5.24: Force-Lift at 12.07 barg (175psi) with the modified gland

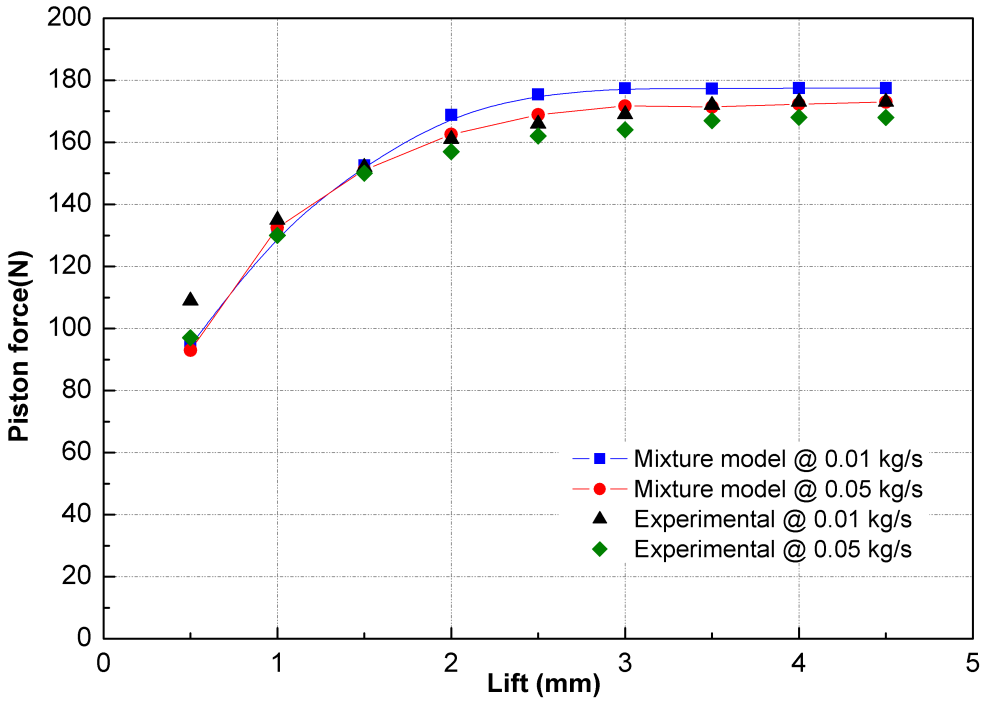

Figure 5.25: Force-Lift at 12.07 barg (175psi) with no gland

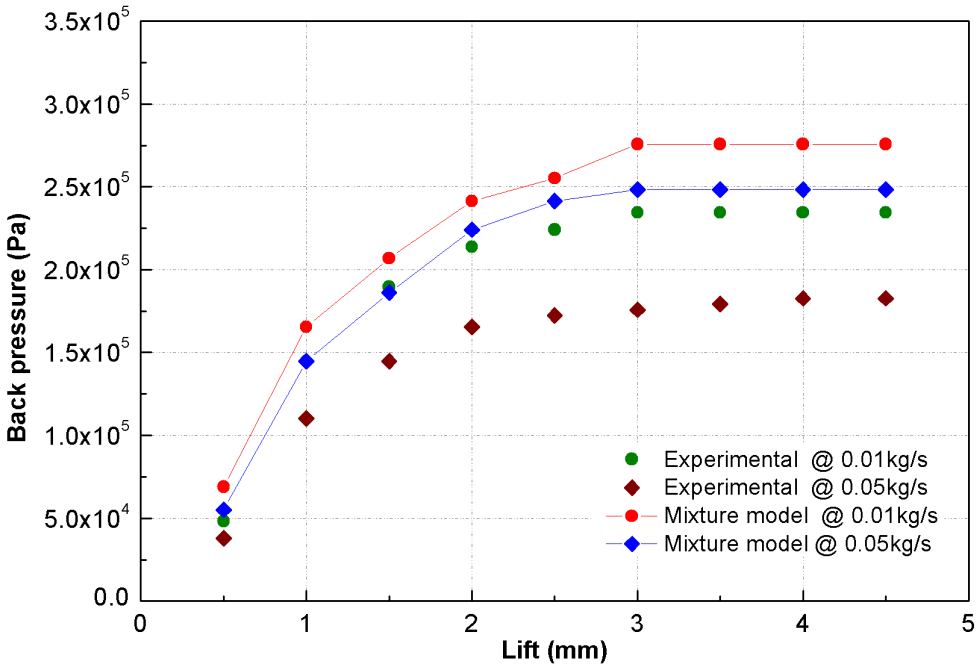

Figure 5.26: Back pressure-Lift at 12.07 barg (175psi) with the modified gland

5.6 Simplified Models

One of the simplest models for determining the flow rate is the homogeneous equilibrium model (HEM). Darby [18] introduced a simple semi empirical model by using the two phase frozen assumption and takes the discharge flow coefficient to be the air discharge coefficient (as the flow is choked). The HEM has been used here to compare with the CFD mixture model results. In this study, the HEM assumptions can be applied to the flow conditions. The flow is considered homogeneous, the water and air are in thermal equilibrium and no mass transfer between phases.

5.6.1 Homogeneous Equilibrium Model Equations

The mass flux is given by the equation

$$G_o = \rho_n \left(-2 \int_{P_o}^{P_n} \frac{dp}{\rho_m} \right)^{1/2} \tag{5.35}$$

Where, ρ_n and P_n are the mixture density and pressure at the valve outlet respectively

$$\rho_n = \alpha \rho_{a,outlet} + (1 - \alpha)\rho_w \tag{5.36}$$

$$\rho_m = \alpha \rho_a + (1 - \alpha)\rho_w \tag{5.37}$$

$$\alpha = \frac{x}{x + (S\,(1 - x)\frac{\rho_a}{\rho_w})} \tag{5.38}$$

Where S represent the slip factor which equals one for the case of a homogeneous flow assumption.

The mixture mass flow rate

$$\dot{m} = k_{da}\, G_o\, A \tag{5.39}$$

Where k_{da} is the gas discharge coefficient that was obtained experimentally. The critical flow rate is achieved at the maximum value of the mass flow rate at the outlet static pressure range. At low liquid volume fraction ($\alpha_w \sim 0.01$), the critical pressure ratio is found to be close to the critical pressure ratio of single phase air flow. Therefore, the critical pressure ratio of the single phase flow could be used as the mixture critical pressure ratio at low water volume fraction ($\alpha_w \sim 0.01$). The homogeneous non equilibrium (HNE-DS) model developed by Diener and Schmidt [23] and the ISO adopted model were used here for comparison. The HNE-DS model accounts for thermal non-equilibrium and slip between phases. The ISO standard ISO-4162-10 adopted the HNE-DS model for selecting safety relief valves for two phase flow, but with no slip defined between the phases. The HNE-DS model and the ISO adopted model equations for non flashing flow are presented in Appendix A.2. Figure 5.27 shows a comparison between the three simplified models, the experimental and the CFD mixture model at 8.6 barg and 7 mm lift. Since the flow here is considered homogeneous the HNE-DS results show an overprediction. On the other hand the ISO adopted model, HEM and the Fluent based mixture model show good prediction of the mixture flow. However the mixture model shows better prediction than the ISO and HEM models for the mixture flow rate in particular at low water mass fraction. Flow-lift characteristics are discussed in Section 5.7.1. It is noticed from Figure 5.27 that the HEM is the most suitable simplified model to predict the mixture flow within the flow condition studied here.

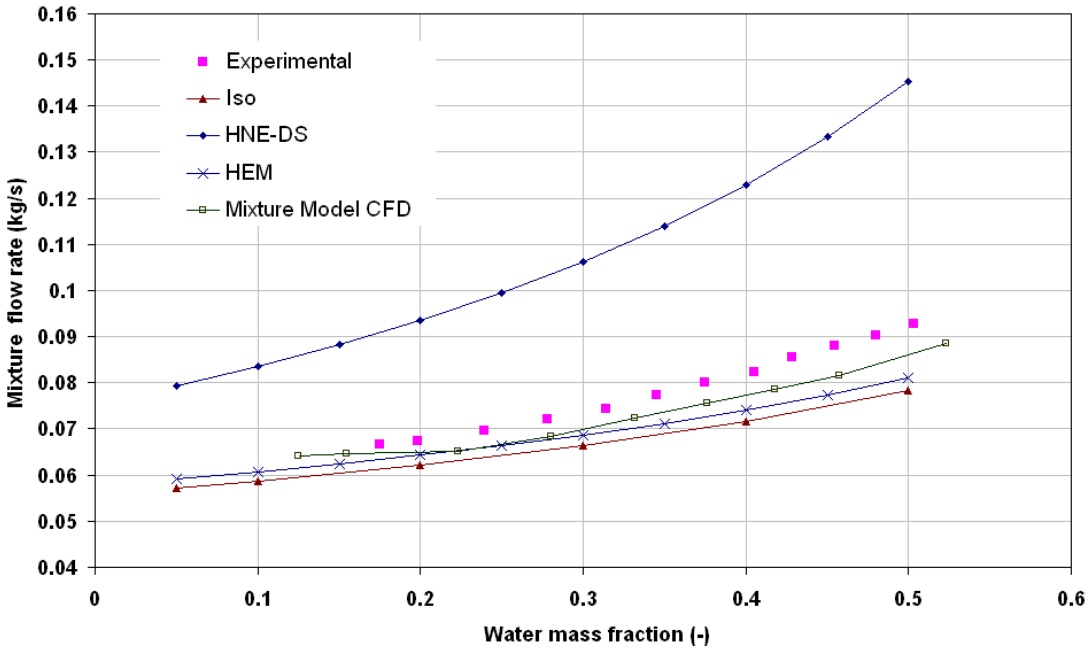

Figure 5.27: HEM, ISO, HNE-DS and the Mixture model at 8.62 barg at valve fully open position (L=7 mm) compared by the experimental results

5.7 Discussion

5.7.1 Flow-Lift Characteristics under Two Phase Flow

Figure 5.28 shows the experimental air flow rate-lift characteristics at single phase and at different water flow rates (0.01-0.05 kg/s). The figure shows that, the air flow-lift characteristics in the two phase flow follow the air flow-lift behaviour for the single phase tests. This suggests that the choking planes for the mixture flow are similar to single phase tests. It is apparent from figure 5.28 that with more water flowing through the valve, the less air flows. This could be explained if the continuity equation is simplified to a one dimensional flow equation at the critical flow plane.

$$\dot{m}_a = \alpha \, \rho \, v \, A \tag{5.40}$$

For the critical air flow rate $M = 1$ which leads to $v = c$ and $A = A_c$ which

is constant for any water flow rate. Hence, at the critical area the air mass flow rate will be a function of the air volume fraction only. i.e. $\dot{m}_a = f(\alpha)$.

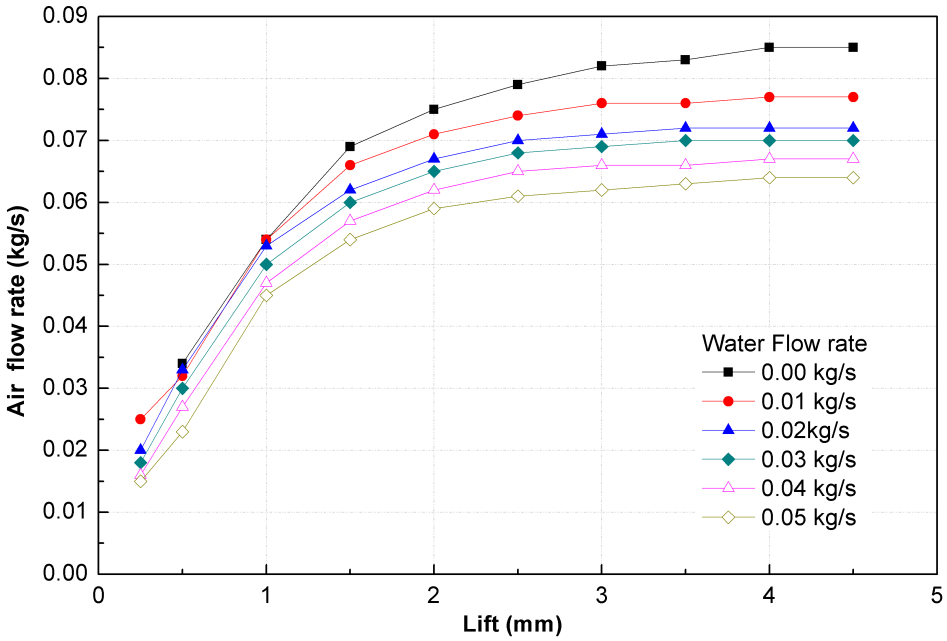

Figure 5.28: Effect of the water flow rate on air flow rate at 12.07 barg

Figure 5.29 shows the water volume fraction at the critical plane at 4 mm lift and inlet pressure 12.07 barg. It is noticeable that at 0.05 kg/s water flow rate, the water droplets decrease the effective area available for the air to flow freely.

The mixture model prediction shows reasonable agreement with the experimental results at higher lifts (choking plane at the piston side face) with low water flow mass fraction (Figure 5.30). The accuracy of predicting the flow is less when the water flow mass fraction increases. Figure 5.30 presents the effect of the water mass fraction on the mixture model prediction accuracy. For example at 10.3 barg (150 psi), the deviation is 2.6 % at 0.13 water flow mass fraction and it is 5.36 % at 0.5. On the other hand, at lower lifts the deviation of the predicted and the experimental results is larger; this is shown in Figure 5.31. The figure shows the mixture flow rate at different water flow qualities. Figure 5.32 presents the percentage deviation of the predicted mixture flow rate with respect to the experimental results at 1 mm and 4 mm lift and shows better accuracy at

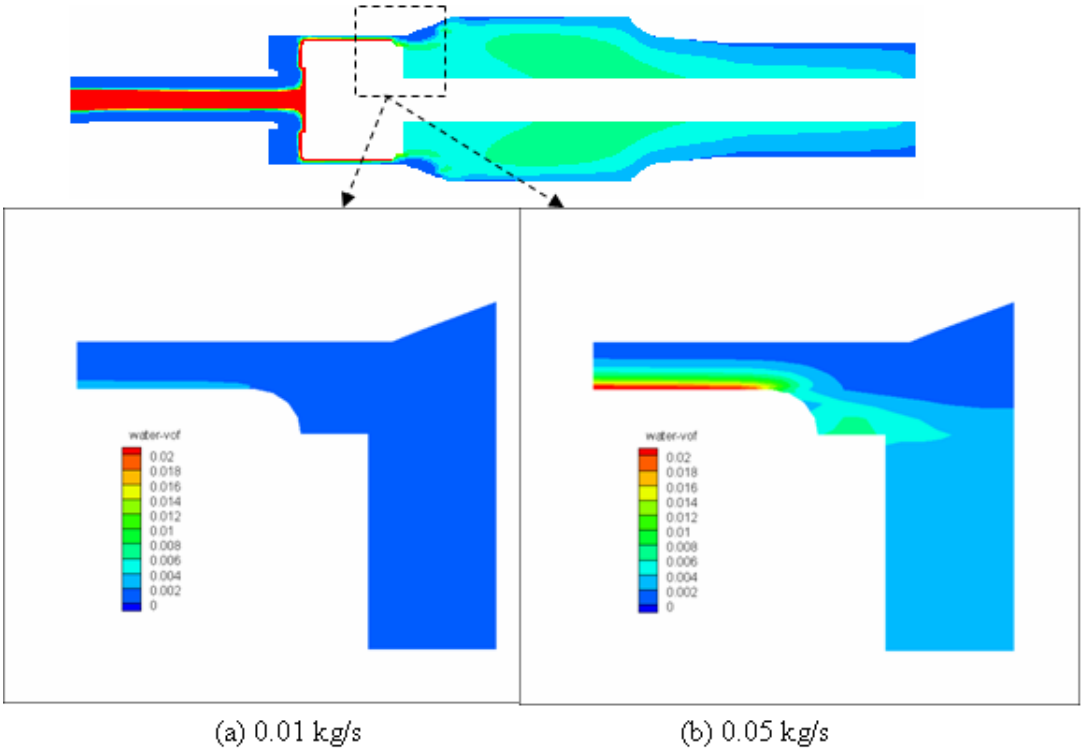

Figure 5.29: Water volume fraction at lift 4mm and 12.07 bar

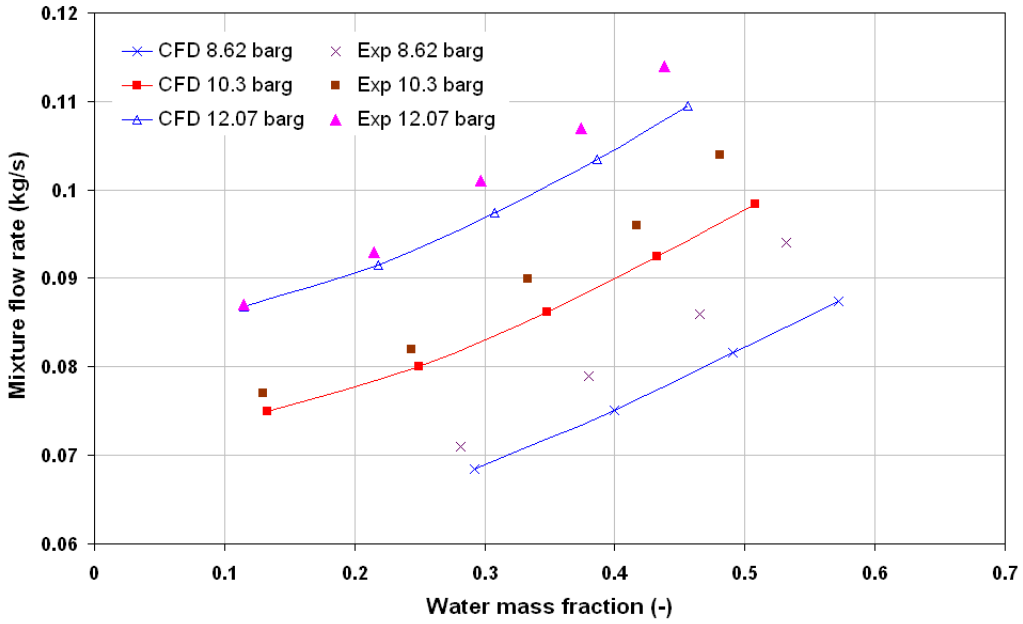

Figure 5.30: Effect of the water mass fraction on mixture flow rate at 4 mm lift

lower water mass fraction. However, the accuracy is less at 1 mm lift at the same water mass fraction. This difference in the mixture model accuracy of predicting the flow rate from low to high lifts can be explained by investigating the two phase inlet flow regime. The inlet flow regime is one of the factors that affect the accuracy of the prediction of the mixture model. The flow regime and the degree of the water dispersion affect the air flow rate. Detailed analysis for the inlet flow regime is presented at Section 5.7.3.

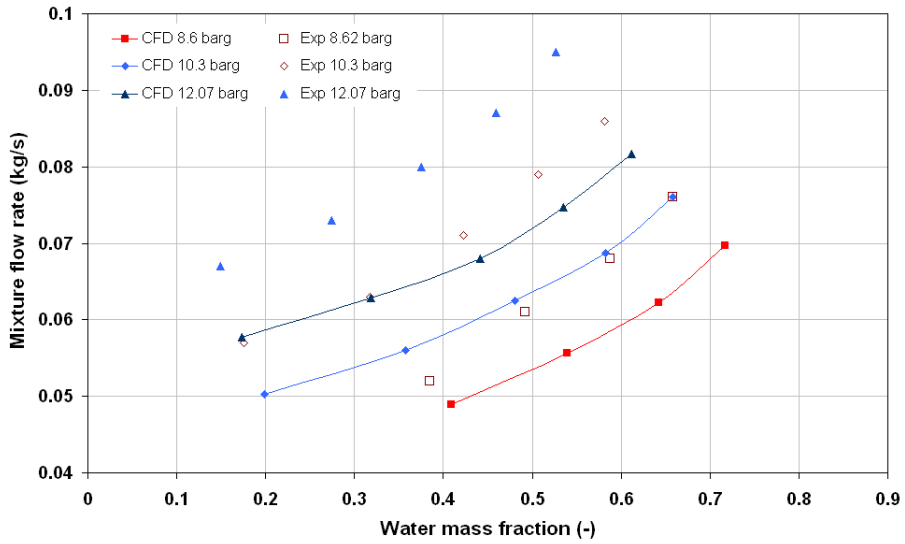

Figure 5.31: Effect of the water mass fraction on mixture flow rate at 1 mm lift

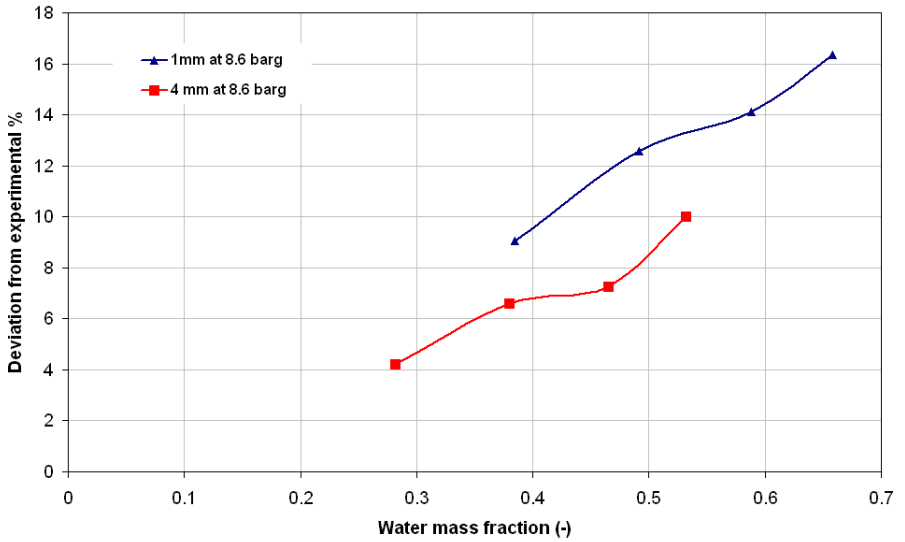

Figure 5.32: Deviation percent of the CFD results from the experimental results at 8.6 barg at 1 mm and 4 mm lift

5.7.2 Force-Lift Characteristics under Two Phase Flow

Figure 5.33 shows the experimental results of the force-lift characteristics at single phase, 0.01 kg/s water flow rate and 0.05 kg/s water flow rate. The figure shows that the single phase force is higher than the two phase flow force at higher lifts (Interval II) and it is less than the two phase flow at lower lifts (Interval I). The net piston force is mainly affected by the pressure magnitude and distribution on the piston front face. In single phase flow the pressure value and distribution on the front face is affected only by the air flow rate at a fixed test pressure. In two phase flow the water flow increases the pressure and changes the pressure distribution on the piston front face which leads to a higher net force. On the other hand, the water flow results in an air flow rate decrease, as discussed in Section 5.7.1, and results in a force decrease. Hence, it can be concluded that when water flows, two factors affect the piston net force, the pressure increase due to the water flow and the pressure decrease due to the air flow decrease. Figure 5.34 shows that the air flow decrease for single phase flow conditions increases with the lift. Hence, a small decrease in air flow rate due to the water flow at low lifts results in a net piston force increase (Interval I in Figure 5.33). Figure 5.35 shows the predicted pressure distribution on the piston front face at 0.5 mm lift and 12.07 barg for the case of single phase air flow and air-water flow with 0.01 kg/s water flow rate. The figure shows that the pressure distribution in both cases are similar but with higher values for the air-water flow case. The pressure distribution on the centre and the edges of the valve front face has a larger value which results in higher net force at this lift. On the other hand, at larger air flow decrease (Interval II in Figure 5.33) the net force will decrease. Figure 5.36 presents the predicted pressure distribution on the piston front face at 4 mm lift and 12.07 barg for the case of single phase air flow and air-water flow with 0.01 kg/s water flow rate. The figure shows a lower pressure level for the two phase flow case due to the air flow rate decrease. Therefore, depending on the lift, the change in the piston force is the result of an increase due to the liquid flow or a decrease due to the reduction in airflow.

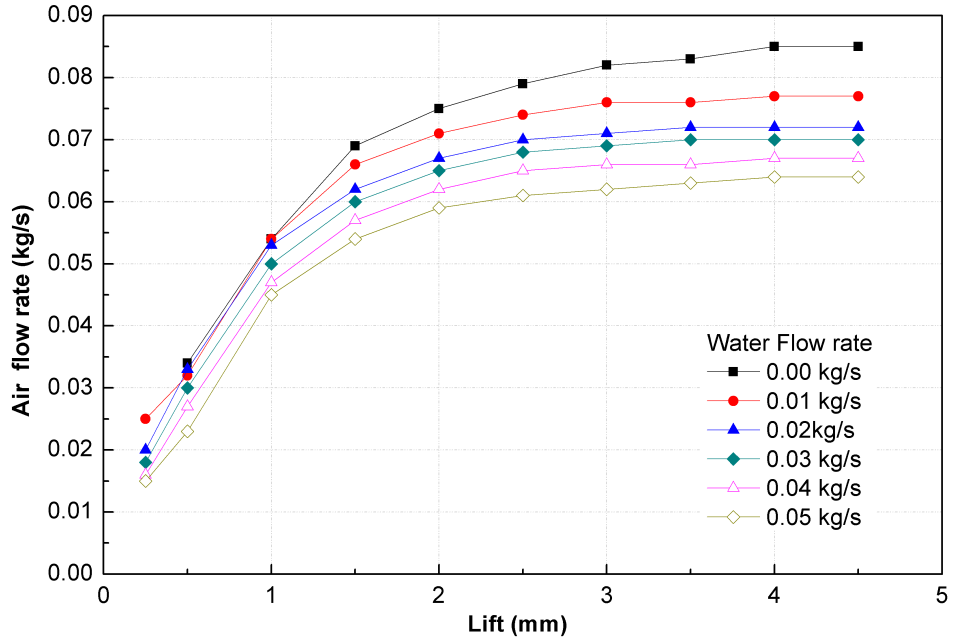

Figure 5.34: Air flow-lift at 12.07 barg (175psi)

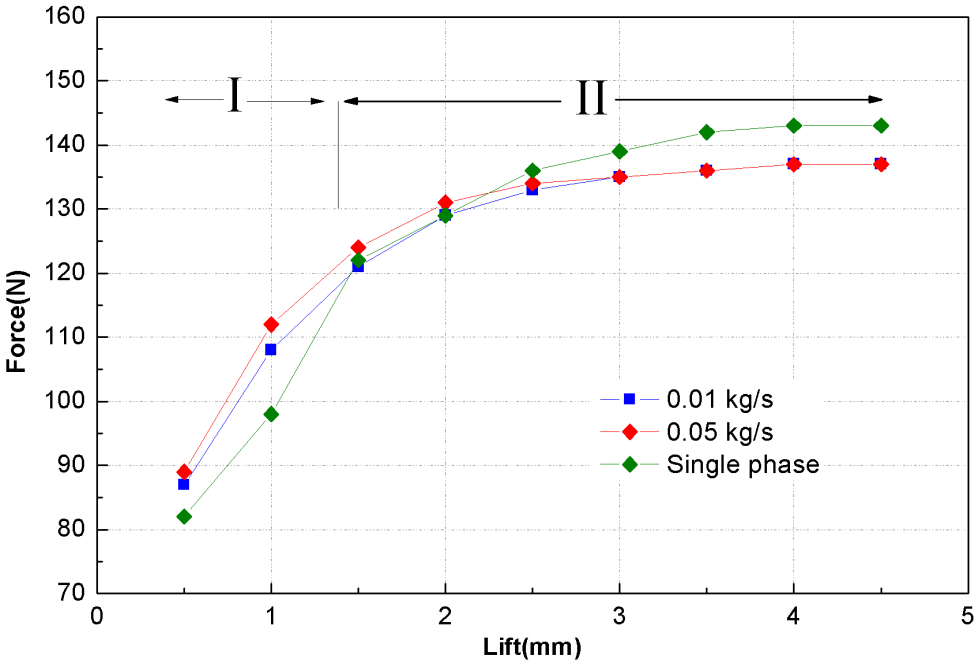

Figure 5.33: Force-lift Characteristics at 12.07 barg

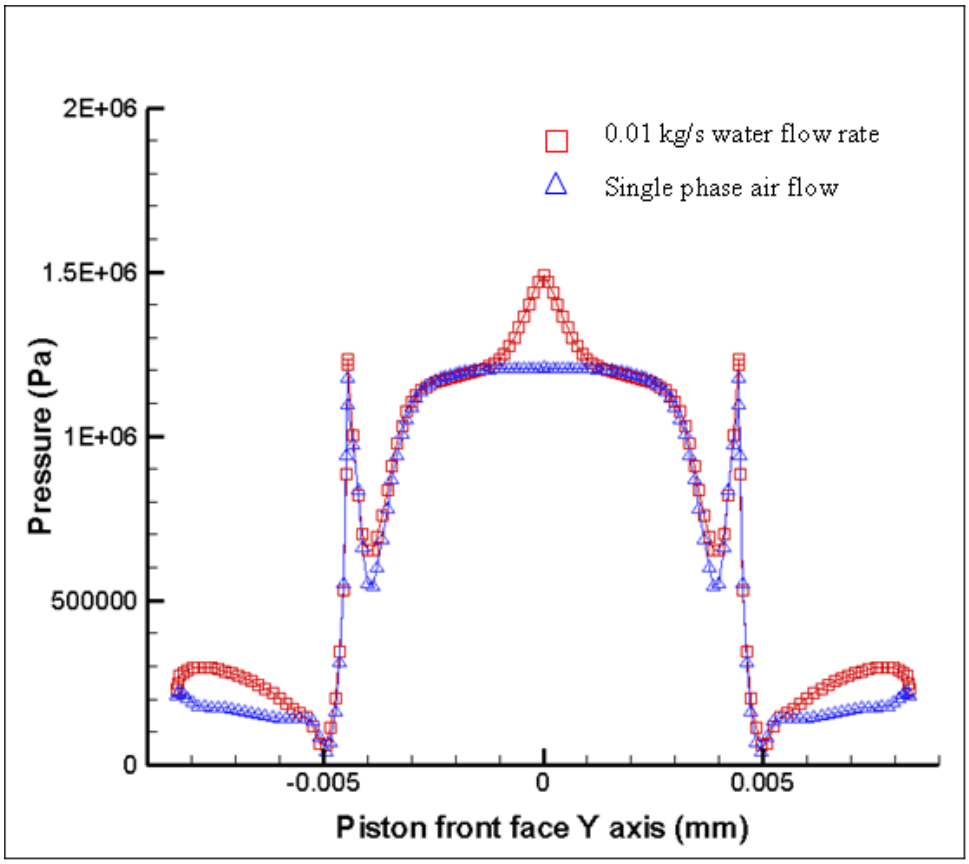

Figure 5.35: Pressure distribution on piston face at 0.5 mm lift, 12.07 bar

Comparison between the force-lift experimental results with the CFD predictions is shown in Figure 5.24. The Figure shows a maximum deviation of about 20 N which nearly gives 14% over prediction of the force. The net force exerted on the piston is the resultant force due to pressure on the piston front face, pressure on piston back face and the viscous force. The net viscous force is very small (around 1 N) and is neglected. In general, the pressure on the piston front face is over predicted due to the non uniform pressure distribution on the piston front face as discussed in Chapter 4. When the modified gland is in place the predicted back pressure agrees with the experimental values; this leads to higher predicted net force (Figure 5.24). When the modified gland is removed the back pressure is overpredicted due to the uncertainty caused by the occurrence of a shock wave downstream of the piston, which will be discussed in Section 5.7.2.1. The over predicted back pressure will compensate for the effect of the overpredicted pressure on the piston front face resulting in a better agreement of the

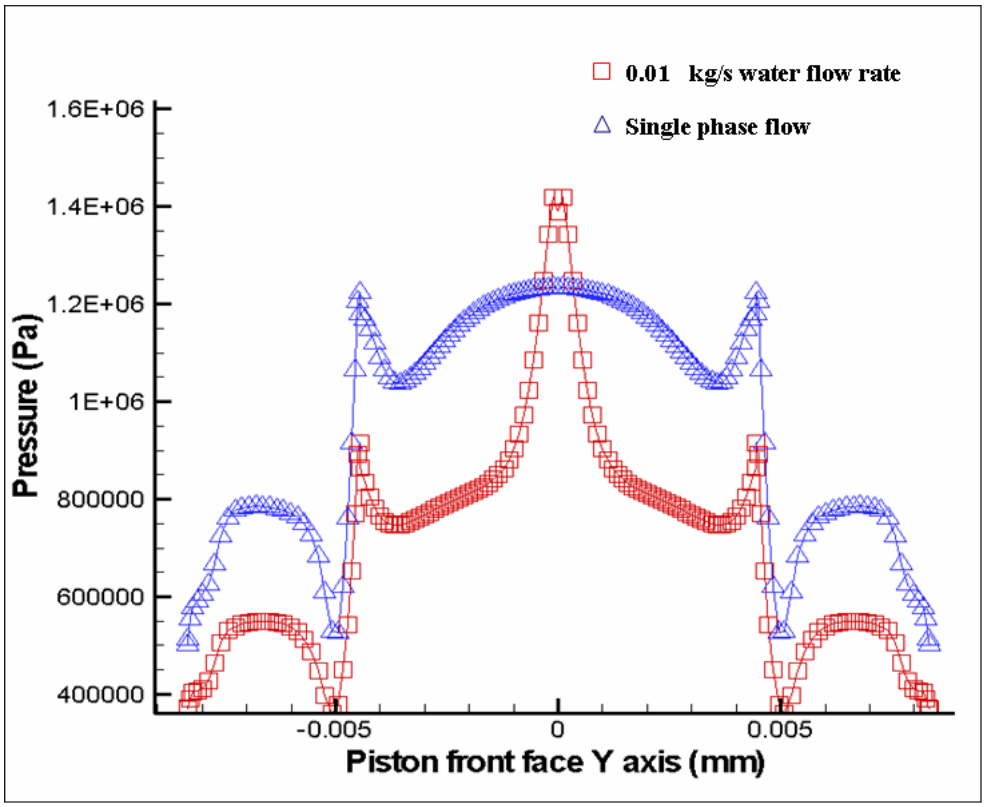

Figure 5.36: Pressure distribution on piston face at 2 mm lift, 12.07 bar

predicted force with the experimental values as indicated in Figure 5.25. Air flow rate has a significant effect on the pressure on the piston face at all lifts, while it has a less effect on the back pressure at low lifts. Therefore, when the mass flow rate is underpredicted at low lifts, the predicted piston force will tend to have a good agreement with the experimental values.

5.7.2.1 Effect of the gland on the flow

Figure 5.11 shows a change in the behaviour of the force for valve tests with the gland compared to without the gland. To look closer at these effects the back pressure should be taken into consideration. To check why the force is increased suddenly at 0.01 kg/s for the case of the valve without the gland, a more detailed set of experimental tests has taken place. Figure 5.37 presents the measured back pressure and piston force at 15.5, 13.8 and 12.07 barg (225, 200 and 175 psi) with water flow rate from 0 to 0.035 kg/s at a lift of 2 mm without the gland. These test

pressures have been chosen to produce low water flow mass fraction, which allow fine increments in water flow rate to capture this phenomena. The figure shows that with an increase in water flowrate the back pressure increases until a sudden drop occurs at a certain flow rate which varies with the test pressure value. The pressure reduction results in a piston force increase. A further increase in water flow rate (beyond 0.03 kg/s) results in less air flow rate and hence a pressure decrease which leads to a force decrease (Figure 5.11)

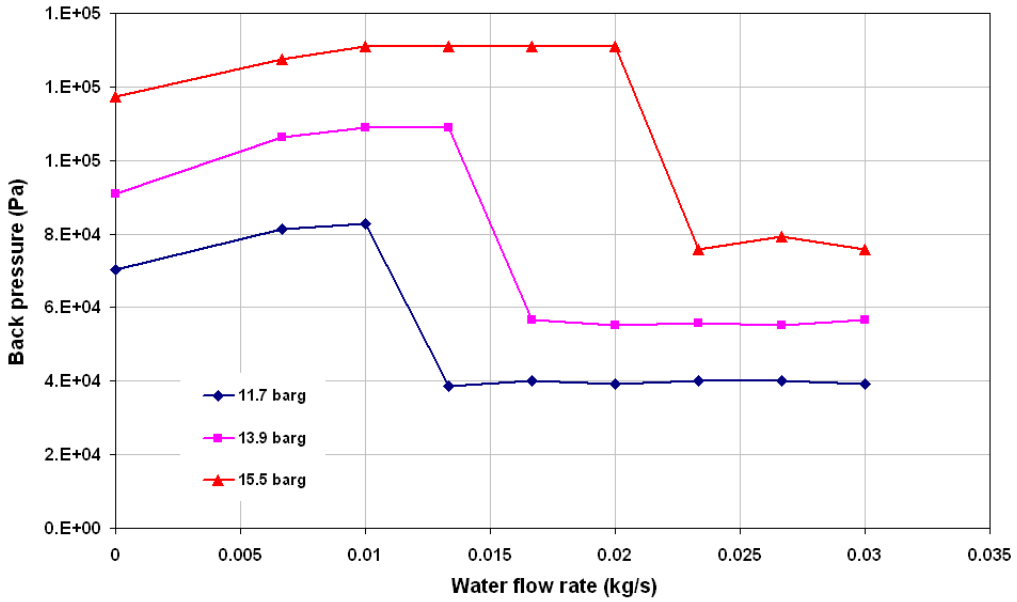

(a) Back pressure-water flow rate

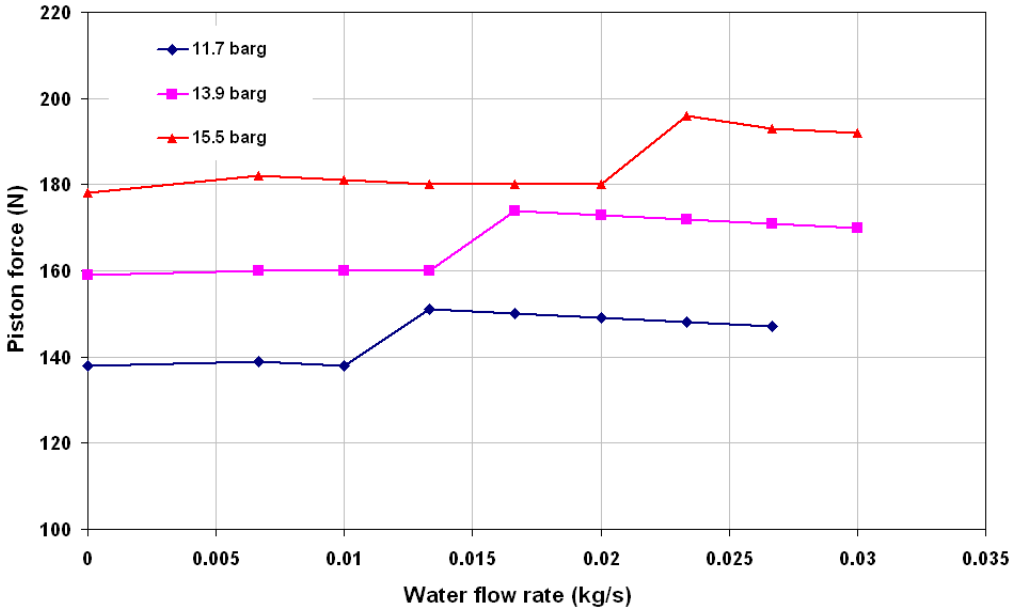

(b) Force-water flow rate

Figure 5.37: Force and back pressure at different water flow rate at 2 mm lift with no gland

To find the reason for the pressure reduction, the predicted flow field pressure contours downstream of the piston have been investigated. Looking at the piston back pressure contours on Figure 5.38 with the modified gland (case 1) and figure 5.39 without the gland (case 2), it can be seen that not only are the pressure

values different but also the pressure distributions on the piston back face and piston side face in the two cases. Both cases are at 0.05 kg/s water flow rate, 12.07 barg test pressure and 4 mm lift. In both cases the choked flow undergoes an expansion just down stream of the choking plane. The black dashed arrow in Figures 5.38 and 5.39 shows the flow direction down stream of the choking plane. In case 2 in Figure 5.39, the flow starts to accelerate and the pressure decreases locally. Under the influence of the geometry, the expansion wave near the upper wall follows the boundary and propagates parallel to the inclined wall of the valve (the blue arrow). On the other hand, the expansion wave near the corner edge of the piston back face undergoes a compression before expanding again down stream. The compression wave is marked by the red dotted circle. Unlike case 2, the presence of the modified gland results in higher pressure levels in case 1, as shown in Figure 5.38. Therefore the flow undergoes an expansion for a short distance then undergoes a compression wave which propagates parallel to the inclined wall of the valve (the blue arrow). The compression wave near the corner edge of the piston is much stronger in case 2 than in case 1.

In case 2, the flow is supersonic and the pressure gradient in the expanding wave near the walls are very high and takes a small distance to collide with the compression wave at supersonic velocity. This distance is indicated by the length of the blue arrow in Figure 5.39. The collision here identifies a standing shock wave which results in these discrepancies in the experimental and predicted results. The shock wave plane is noted by the dotted black line. The plot of the static pressure and the mach number values along the valve walls will indicate the shock wave establishment. Figures 5.40 and 5.41 show the presence of the shock wave at nearly 0.075 m from the valve inlet centre. At this point the pressure suddenly rises and the mach number drops from supersonic flow at 2.8 to subsonic flow at 0.2. Thus one can declare that, the presence of the shock wave at the inclined wall of the valve and the propagation of an expanding wave with a compression wave at the piston back face can introduce an uncertainty in measuring the back pressure or predicting it. This will directly affect the net force

exerted on the piston. Although the removal of the gland is not a practical case, this should draw the attention of the designers that the flow is very sensitive to the flow path geometry and CFD is very helpful in describing the flow behaviour.

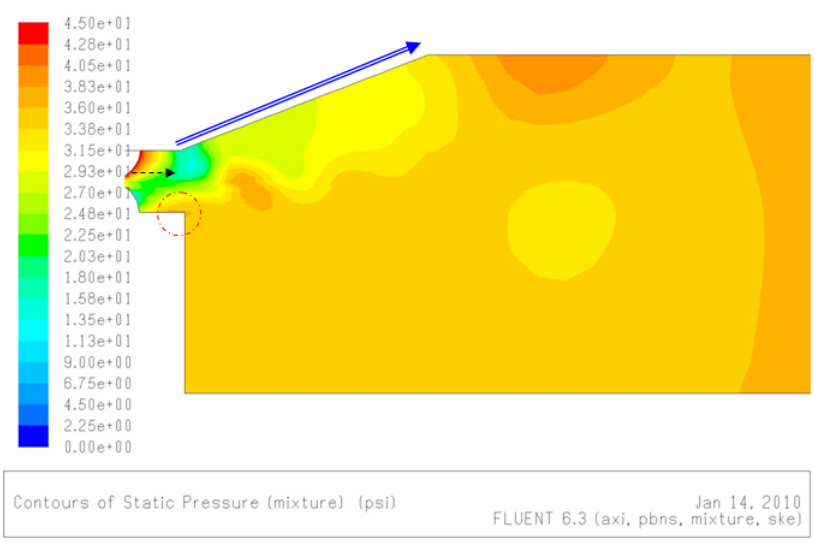

Figure 5.38: Static pressure contours at 4 mm lift ,12.07 bar with the modified gland (case 1)

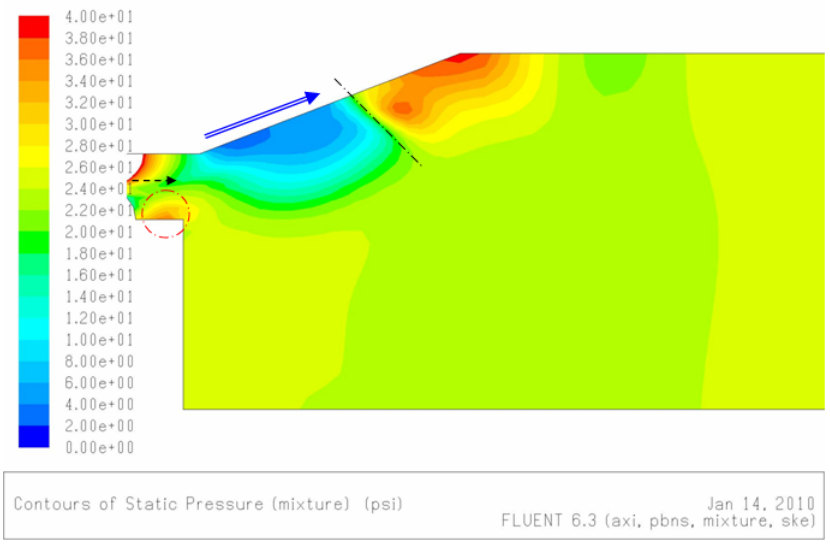

Figure 5.39: Static pressure contours at 4 mm lift ,12.07 bar without the gland (case 2)

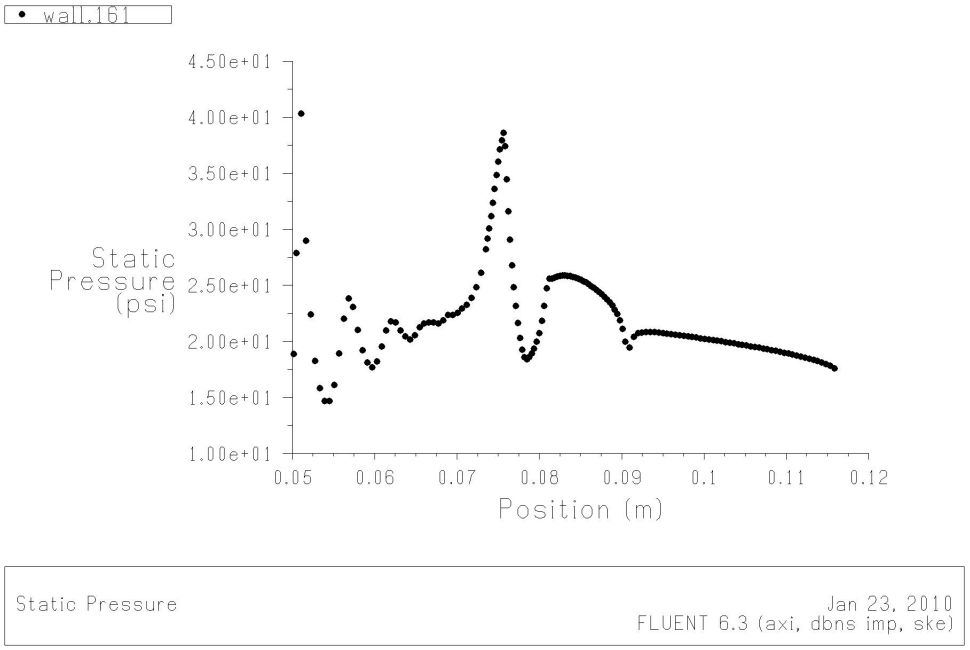

Figure 5.40: Static pressure at the piston walls ,4 mm lift ,12.07 bar without the gland (case2)

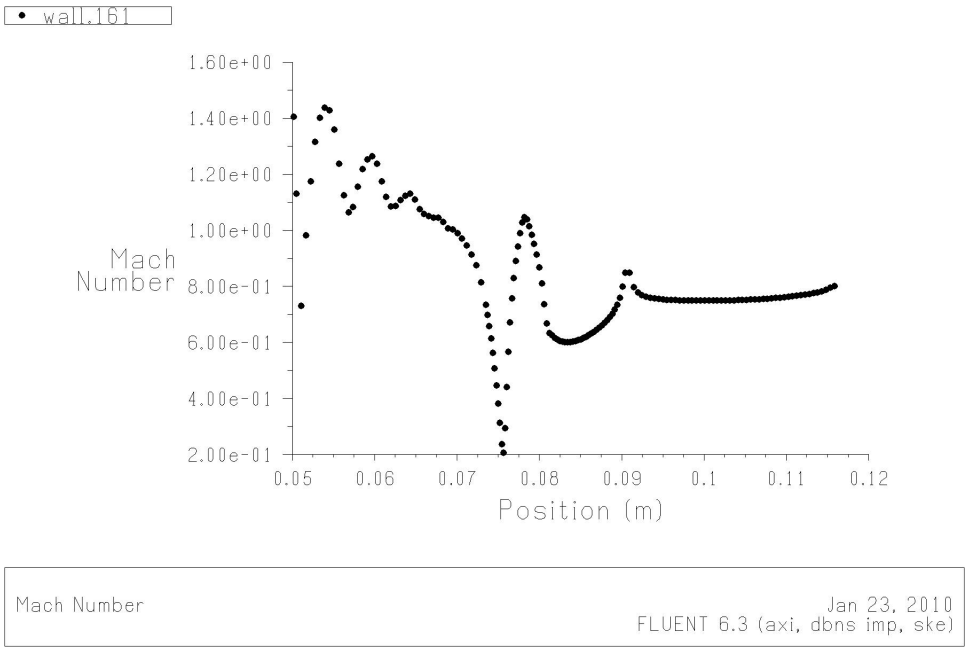

Figure 5.41: Static pressure contours at 4 mm lift ,12.07 bar without the gland (Case 2)

A closer look at the single phase flow behaviour without the gland should give a better understanding. Figure 5.42 shows the experimental measured back pressure at different lifts (Note the pressure tapping position in Figure 5.1). It can be noticed that at certain lifts the back pressure reduces significantly. Figures

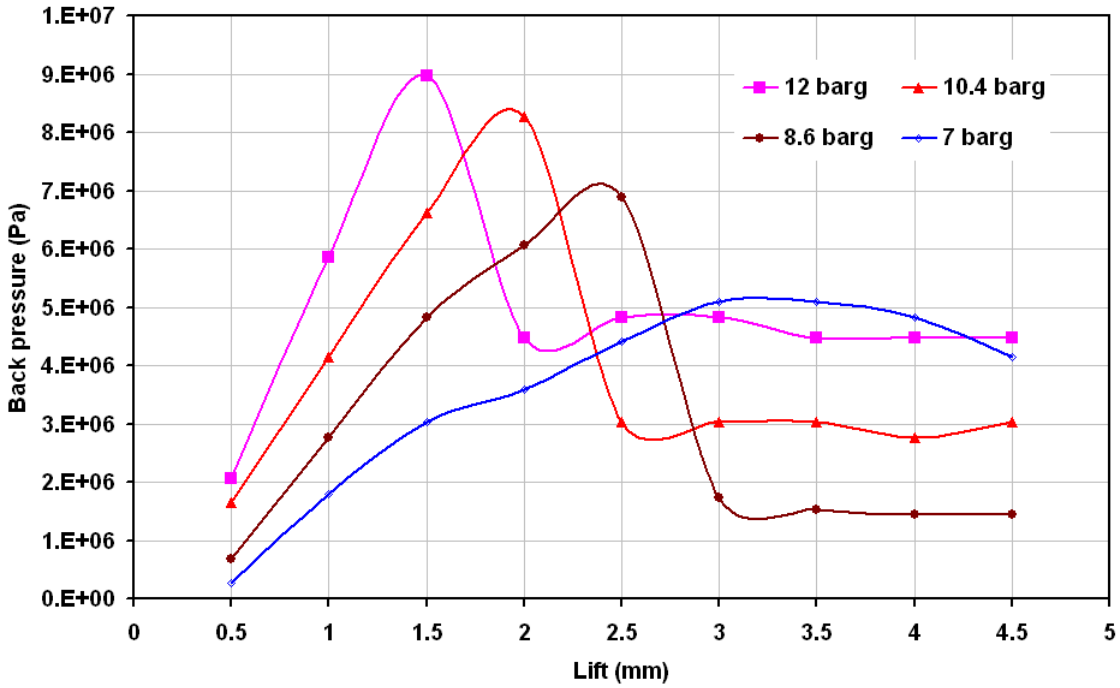

Figure 5.42: Back pressure at single phase flow at different pressures

5.43, 5.44 and 5.45 show the difference in the pressure distribution and the shock wave location at the valve for no gland. For three different test pressures, the three figures are for single phase flow and a 2.5 mm lift. At 8.6 barg (shown in Figure 5.43) the pressure gradient is very small and only a weak nuclei for the shock wave is apparent; the compression wave is still very weak at the piston back face. At 12.07 and 13.8 barg (shown in Figures 5.44 and 5.45) the shock wave is clear at the valve wall (noted by the dotted black line) and the compression wave at the piston back face can be noticed easily.

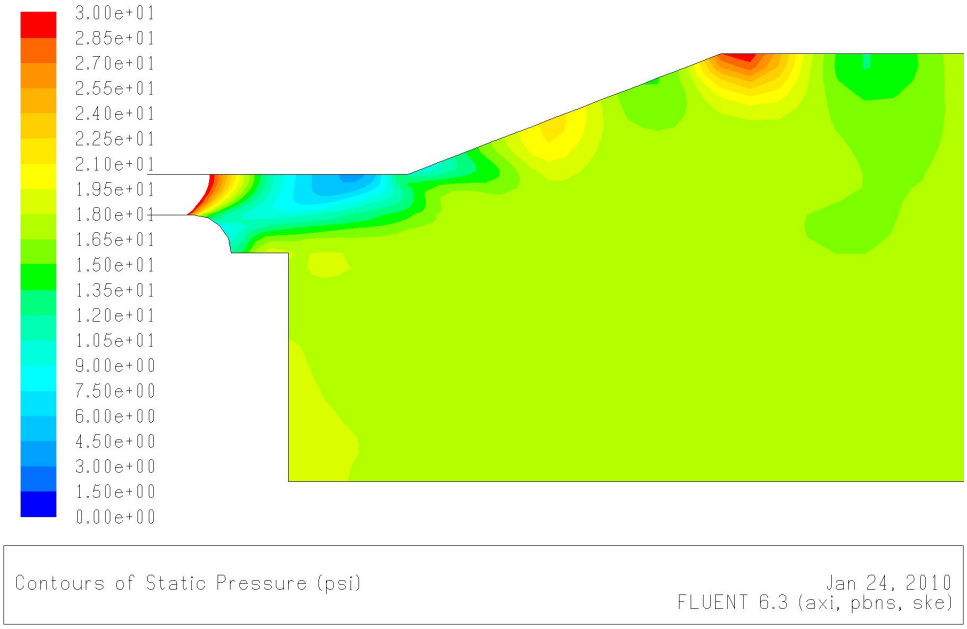

Figure 5.43: Static pressure contours single phase at 2.5 mm lift , 8.6 bar with no gland

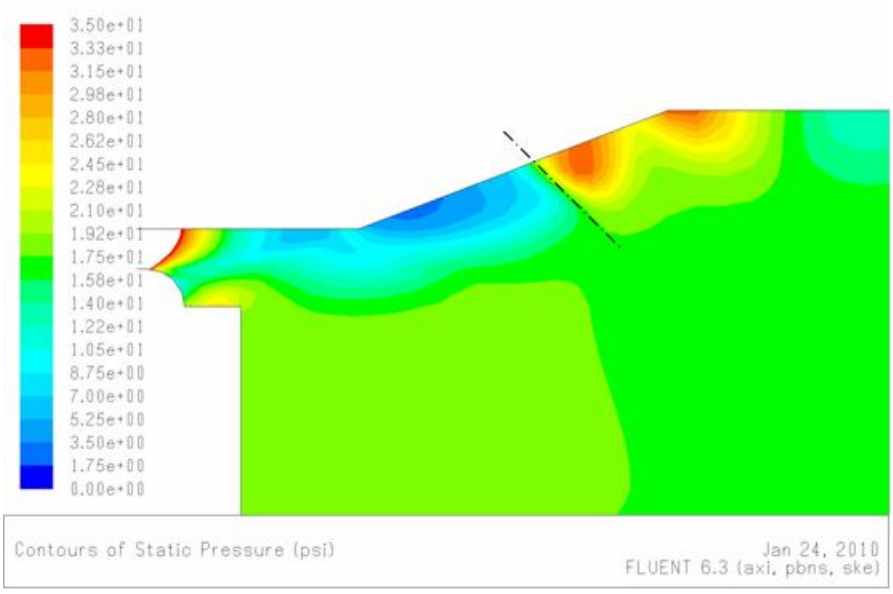

Figure 5.44: Static pressure contours single phase at 2.5 mm lift ,12.07 bar with no gland

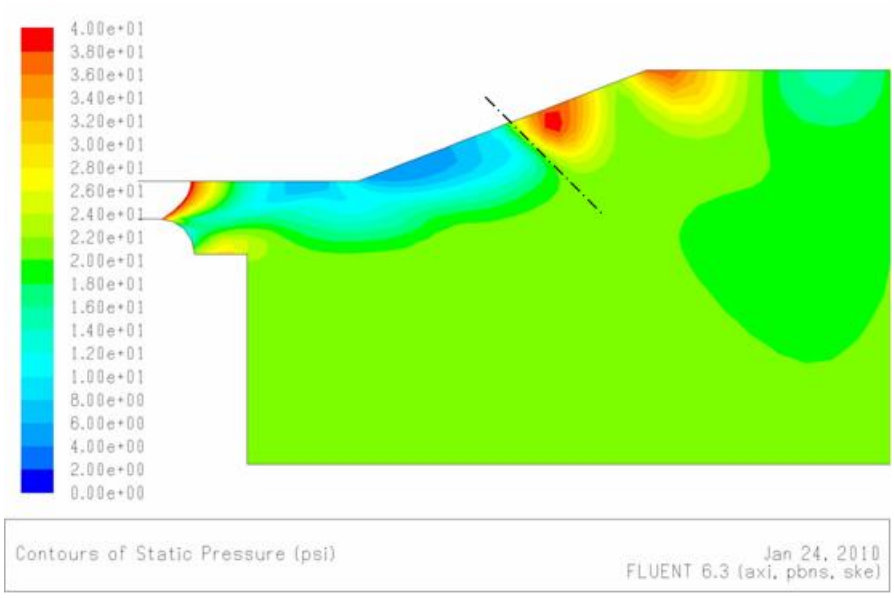

Figure 5.45: Static pressure contours at 2.5 mm lift ,13.8 bar with no gland

5.7.3 Effect of Water Dispersion on Flow Properties

One of the factors that affect the safety relief valve performance is the water distribution in the mixture through the valve. Changing the injection nozzle geometry and orientation leads to different water inlet distributions. Three different injection nozzles have been used to investigate the effect of the water dispersion on valve discharge flow rate and piston force. The three injection nozzles are as follows:

- Nozzle 1: Orifice outlet diameter 1 mm and oriented such that the water flows downstream and parallel to the pipe axis.
- Nozzle 2: Orifice outlet diameter 2 mm and oriented such that the water flows downstream and parallel to the pipe axis.
- Nozzle 3: The nozzle has 2 outlets, each 1 mm in diameter. The two orifices are oriented such that the water flows radially, normal to the pipe axis and in opposite directions.

To compare the effect of the three distributions; only one lift (2 mm) was chosen and tested at several different water flow rates. Figure 5.46 shows the effect of

injection nozzle diameter and orientation on air flow rate. It is apparent that:

- Increasing the injection area by 400% from Nozzle 1 to Nozzle 2 doesn't have any significant effect on air mass flow rate at the same lift and water flow rate.
- A very small decrease in air flow rate occurs for the case of Nozzle 3. The difference ranging from 1.4% to 5 % and increases with an increase in the water mass flow rate.

Therefore, It can be considered that there is no significant difference between these three types of injection arrangement on the air flow rate, although a different injection arrangement with a significant water dispersion may have a greater effect on the flow rate.

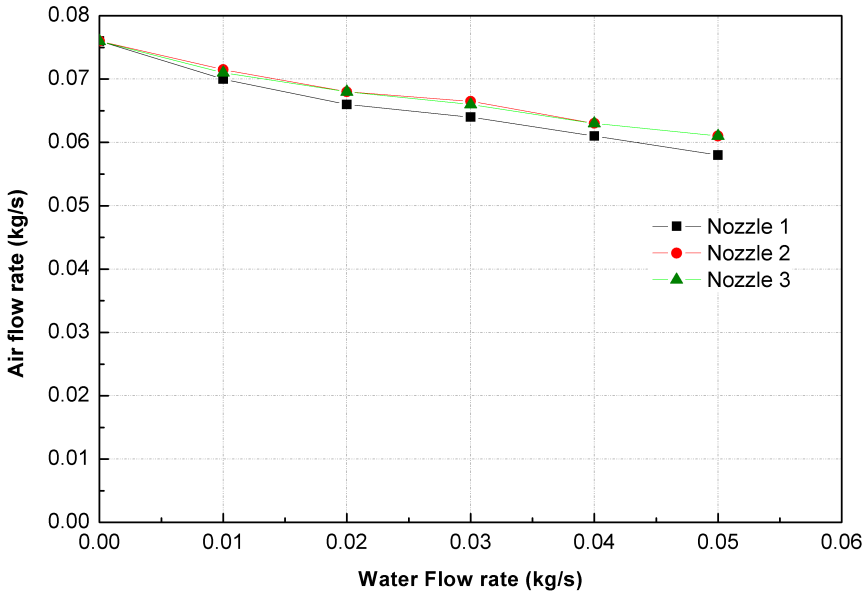

Figure 5.46: Effect of injection nozzle geometry on air flow rate

The effect of the 3 nozzle arrangement on force is presented in Figure 5.47. The figure shows the force to be similar for the three injection cases at a constant lift of 2 mm.

To investigate this more using CFD, three different computational grids have been developed to present different water injection distribution schemes. Nozzle 1

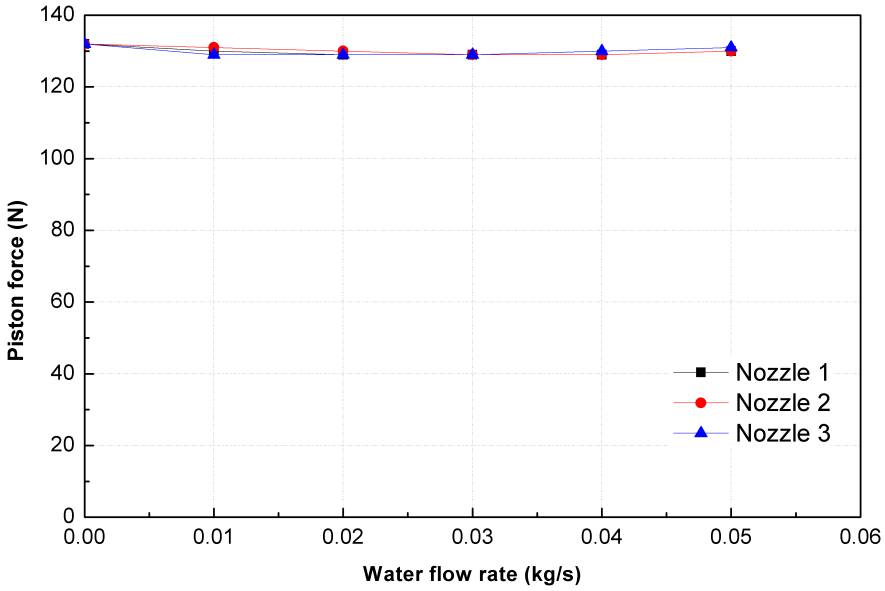

Figure 5.47: Effect of injection nozzle geometry on force

and Nozzle 3 have been modelled along with a multi-inlets annulus area injection, called Nozzle 4, Figure 5.48) and a homogeneous uniform water distribution over the valve entrance area, definied by a volume fraction at the inlet, called Nozzle 5. These five injection arrangements have been used to investigate the effect of water dispersion on the air flow rate using the mixture model. Figures 5.49 and 5.51 show the experimental results for air flow- water flow rate and air flow- water mass fraction for Nozzle 1 and Nozzle 3 in addition to the CFD results for Nozzles 1,3,4 and 5. The figures show these cases at 2 mm lift, which is considered a high lift. A lower lift of 1 mm is shown in Figures 5.50 and 5.52. From the figures it can be noticed that:

- The experimental tests show that the inlet injection variations for Nozzle 1 to 3 are not large, they have a maximum of 7% at 0.05 kg/s water flow rate.

- The mixture model results for Nozzle 1 to 3 show a greater deviation which reaches 15% at 0.05 kg/s water flow rate and it is much more at lower lifts (Figure 5.50)

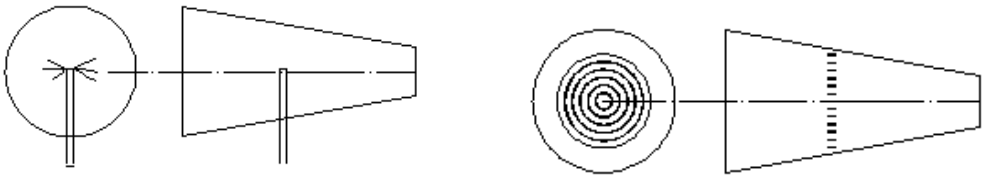

(a) Nozzle 3 **(b)** Nozzle 4

Figure 5.48: Injection Nozzle geometry

- The mixture model shows low sensitivity to inlet liquid distributions when the liquid is modelled with fully dispersed type inlet distributions, i.e. Nozzle 3, 4 and 5.

Therefore, it can be stated that

- The air flow rate is affected by the inlet flow regime and the water dispersion. The more the water is dispersed the less air flows.
- The Fluent mixture model overpredicts the dispersion for Nozzle 3 which results in a lower air flow rate prediction.
- The Fluent mixture model shows a sensitivity to inlet flow distributions greater than that indicated by the experimental data, particularly at the higher range of liquid mass qualities investigated here. A more in depth study is required to investigate this further.

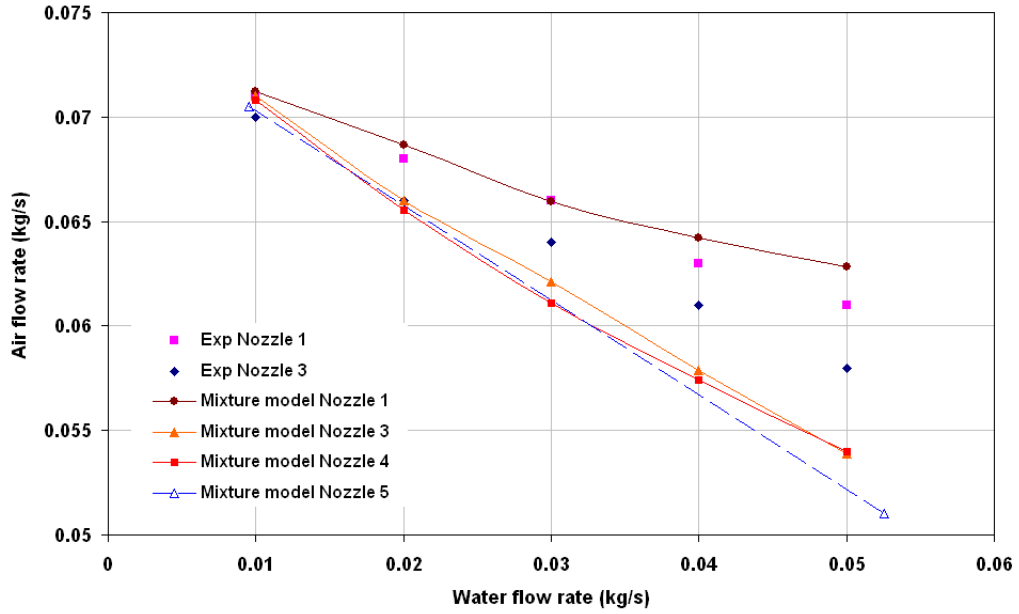

Figure 5.49: Air flow rate at 2 mm lift at different water flow rate, pressure 12.07 barg (175psi)

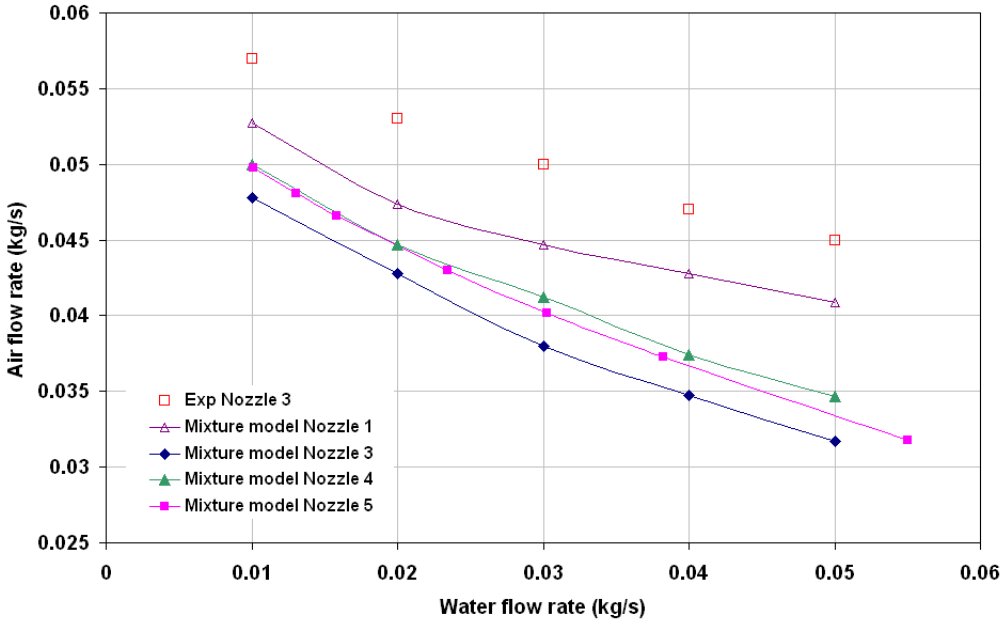

Figure 5.50: Air flow rate at 1 mm lift at different water flow rate, Pressure 12.07 barg (175psi)

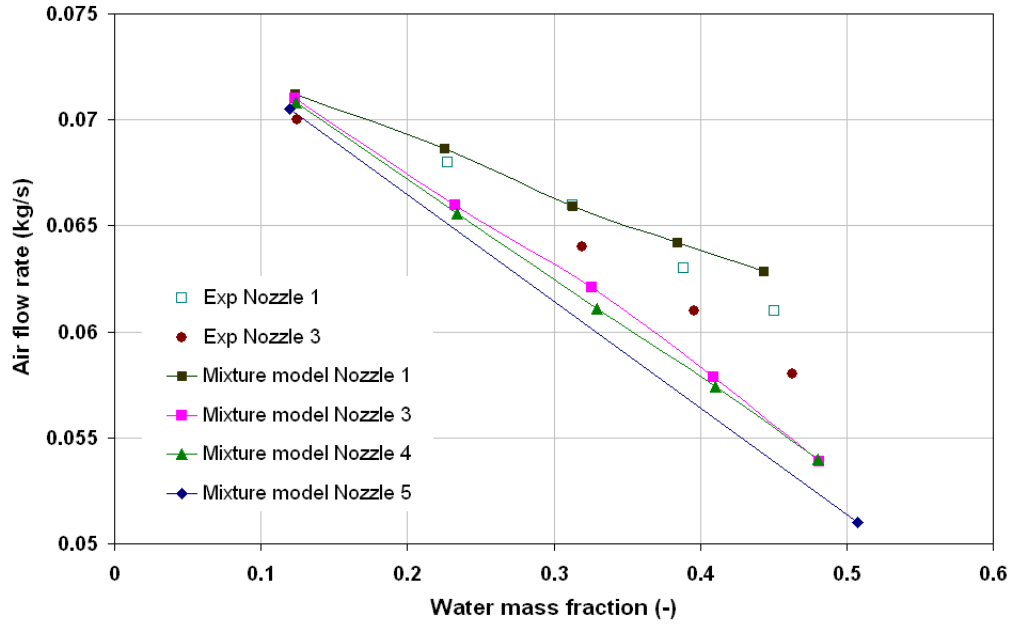

Figure 5.51: Air flow rate at 2 mm lift at different water mass fraction, Pressure 12.07 barg (175psi)

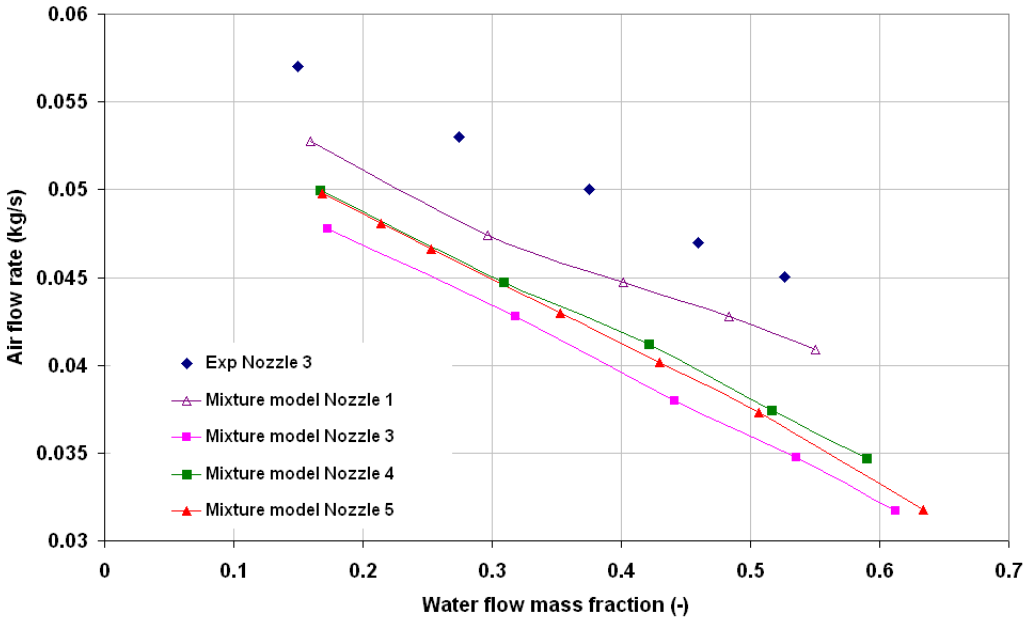

Figure 5.52: Air flow rate at 1 mm lift at different water mass fraction, Pressure 12.07 barg (175psi)

Experimental results for Nozzle 1 is closer to the CFD predictions using Nozzle 3, which indicates that the predicted water dispersion in Nozzle 3 is closer to the experimental water dispersion of Nozzle 1. i.e. the mixture model represent the

water in a more dispersed flow than the experimental tests. This agrees with Brennan's [14] conclusion of the overprediction of the particles segregation by the mixture model implemented by Fluent discussed in Chapter 3. Thus, if the water flows as a full film flow near the piston wall (local water volume fraction $\alpha_w = 1$) in the experimental test, it will be presented as droplets with high concentration near the piston walls ($\alpha_w < 1$) by the mixture model. which can be shown in Figure 5.29 where the $\alpha_w = 0.02$ near the piston walls. This difference in water dispersion in the mixture model results in this deviation in air flow rate prediction (Figure 5.49). This deviation is more clear at lower lifts (L $\leq$ 1.2 mm, Figure 5.50) where the critical plane is at the piston front face. This can explain the underprediction of the air flow rate by the mixture model at low lifts.

5.8 Valve Design Approach for Two Phase Flow

It was shown in Chapter 4 how the single phase flow results could be extended to other operating conditions by normalising the force-lift and the flow-lift curves. This method accounts for the changes in operating pressure and temperature. However, for two phase flow the additional effect of the water content needs to be accounted for. The following sections will discuss the requirements for two phase flow and propose a scaling method to account for pressure and water flow rate.

5.8.1 Normalised Air Flow Rate

The normalised flow rate parameter uses the pressure and the valve seat area to describe the flow-lift characteristics at all pressures (equation 5.41) for single phase flow conditions, i.e.

$$\dot{m}_N = \frac{\dot{m}}{P_o \, A_{seat}} \sqrt{T_o} \tag{5.41}$$

The effect of the water flow mass fraction on the flow-lift curves has been shown in Sections 5.4.1 and 5.7, to have a significant effect. Therefore, to normalise the air flow-lift characteristics for two phase flow, a term accounting for the water

content should be introduced into the equation. The water flow mass fraction is a suitable term to represent the water content for the two phase flow condition. The air mass flow-water mass fraction relation is a power relation

$$x = \frac{\dot{m}_w}{\dot{m}_w + \dot{m}_a} \tag{5.42}$$

Rearranging for $\dot{m}_a$

$$\dot{m}_a = \dot{m}_w(x^{-1} - 1) \tag{5.43}$$

For a constant water flow rate the air mass flow - water mass fraction relation will have a power characteristic regardless of the lift or the pressure value. Figure 5.53 shows the air mass flow- water mass fraction at all pressures and lifts. A curve fitting has been applied to the data at each water flow rate to extract a direct relation between the air mass flow and the water flow mass fraction. In Figure 5.53 (a) the power fitting is used and in (b) the exponential fitting is used.

In Figure 5.53 (b), the best fit for the data is the exponential one for the water flow rate of 0.02 - 0.05 kg/s . Whereas the best curve to fit the 0.01 kg/s data is found to be the power curve in Figure 5.53 (a). Hence, the exponential approximation should give an acceptable representation for the air mass flow-water mass fraction relation. Thus, equation 5.43 can be written as follows:

$$\dot{m}_a = \dot{m}_w(x^{-1} - 1) \backsimeq C\, e^{n x_w} \tag{5.44}$$

Therefore, equations 5.41 and 5.44 can be combined together to represent the normalised air mass flow rate as follows:

$$\dot{m}_N = \frac{\dot{m}}{P_o\, A_{seat}} \sqrt{T_o}\, e^{n x_w} \tag{5.45}$$

An appropriate selected value for the exponential index n can minimise the difference between the data and make all the curves fall into one. To find the optimum value of the exponential index n the difference between several points from different flow-lift relations have been selected to optimise the index n. The

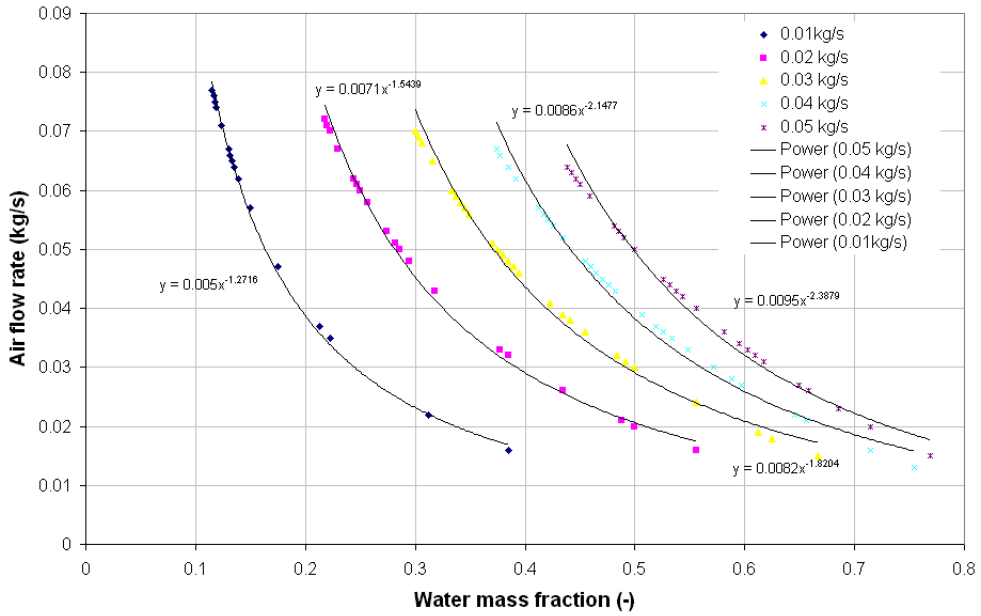

(a) Power approximation

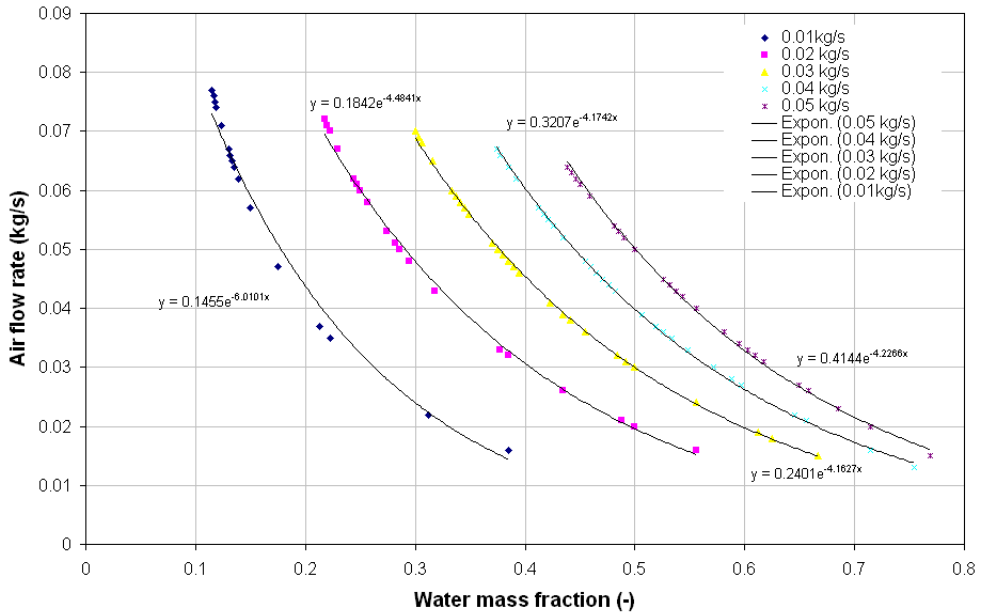

(b) Exponential approximation

Figure 5.53: Air flow rate - water mass fraction at all lifts and pressure

optimum value was found to be 0.7 which makes the normalised air mass flow-lift (equation 5.46) become

$$\dot{m}_N = \frac{\dot{m}}{P_o\, A_{seat}} \sqrt{T_o}\, e^{0.7 x_w} \tag{5.46}$$

Figure 5.54 shows the normalised flow- lift characteristics. The curves nearly collaps to one curve with a maximum deviation of 0.25 unit. If the middle curve is used to represent the curves, the maximum uncertainty of the predicted mass flow rate at any lift will be about 5%.

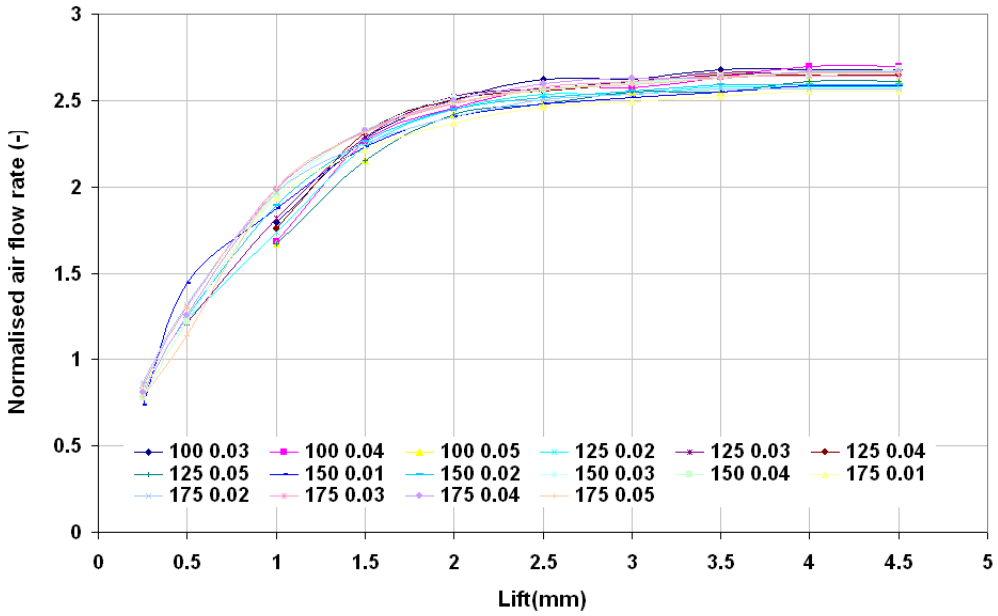

Figure 5.54: Normalised flow -lift characteristics

5.8.2 Normalised Force

For single phase flow conditions, the normalised force has been achieved by using equation 5.47 in which the pressure and the valve seat area have been used to represent the force-lift characteristics at all pressures, i.e.

$$F_N = \frac{F}{(P_o - P_{atm})\, A_{seat}} \tag{5.47}$$

In Sections 5.4.2 and 5.7 it was shown that the water flow rate has no si-

gnificant effect on force-lift characteristics; unlike the air flow-lift characteristics. Thus, equation 5.47 should be satisfactory for presenting the normalised force-lift characteristics for two phase flow as well as for single phase flow. Figure 5.55 shows the normalised force-lift characteristics. The curves nearly collaps to one with a maximum deviation of 0.20 unit. If the middle curve is used to represent the curves, the maximum uncertainty of the predicted mass flow rate at any lift will be about 3%.

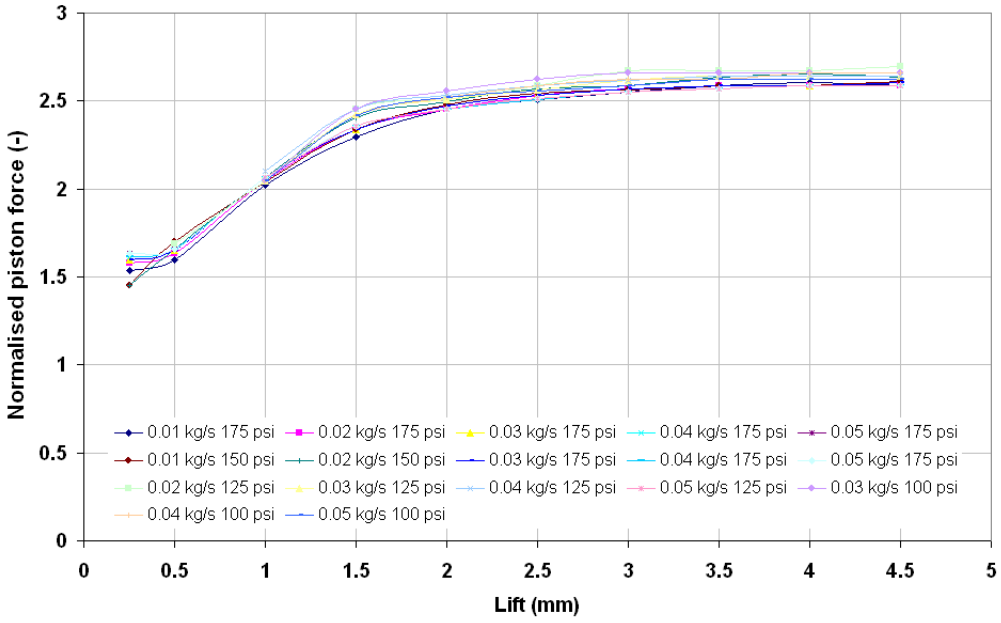

Figure 5.55: Normalised force- lift characteristics

Chapter 6

Conclusions and Future Work

6.1 Summary

A computational fluid dynamics and experimental approachs have been used to investigate safety relief valves for single phase air flow conditions and air-water two phase flow conditions. The CFD approach used a two dimensional axisymmetric model which has been discussed and has shown good predictive capability. An experimental methodology has been established for testing safety relief valves under single and two phase flow conditions. Flow-lift and force-lift characteristics have been obtained experimentally and by using CFD. Scaling parameters for the flow-lift and force-lift characteristics have been introduced to help in safety relief valve design under single and two phase flow conditions. All the following conclusions are limited to the flow conditions investigated in this study, i.e. pressure from 4.3 to 13 barg for single phase flow and from 7 to 12 barg for two phase flow and from 0.1 to 0.71 water mass fraction.

6.2 Single Phase Studies Conclusions

- A detailed understanding of the compressible flow through a safety relief valve has been presented.

- An experimental approach used by Dempster et al [20] has been adopted and found satisfactory for the safety relief valve used in this study. Various tests have been carried out to verify this approach.

- There is no effect of the spring or the gland on the mass flow rate, while the gland has a significant effect on the back pressure and hence the piston force. In addition, removing the gland allows the flow to undergo an expansion wave downstream of the choking plane with a high possibility of the establishment of a standing shock wave which depends on the test pressure and piston lift. This introduces undesirable characteristics and a valve designe for single phase flow should avoid such situations in the valve operation range.

- The air flow rate at low lifts (0 - 1.2 mm) at fixed test pressure depends on the flow area between the piston front face and the valve seat, as the choking plane occurs in this area at low lifts.

- At high lifts (lift $>$ 1.2 mm) the choking plane is moved to the piston side and is fixed for any higher lift. Therefore, the air flow rate at a fixed test pressure depends only on the pressure value at the inlet of the passageway around the piston.

- A two dimensional axisymmetric computational model based on a RANS and k-ε turbulence model has been found satisfactory in predicting the flow rate.

- The CFD tools have been used to analyse the flow and identify the choking planes and the effective flow area. These significantly affect the air flow rate.

- Simplification of the valve model can be achieved by neglecting the valve spring and the valve gland if only mass flow prediction is desired. This will lead to a significant reduction in computational effort

- Presenting the three dimensional flow areas by an equivalent annulus flow areas have been found to be satisfactory in predicting the flow rate with a maximum deviation of 2% from the experimental results. On the other hand, presenting the three dimensional geometry of the piston and the original five holed gland has shown an overprediction of piston forces by a maximum of 13% .

- The accuracy of predicting the force by using a two dimensional axisymmetric model depends on the geometry of the piston and the gland. A good prediction of the piston force of a safety relief valve has been obtained by Dempster et al [20] using a two dimensional axisymmetric model. A comparison between the piston used by Dempster et al and the piston used in this study has been presented. The three dimensional effects of

the piston geometry on pressure prediction was discussed. The comparison showed that the closer the piston geometry is to a two dimensional axisymmetric geometry the more accurate the force prediction obtained. A modified gland with geometry closer to axisymmetric geometry improved back pressure prediction by 15%.

- The three dimensional computational model developed by Gronkowski [33] has shown a better prediction for the piston forces and pressures than the two dimensional axisymmetric model adopted here. However, The two dimensional axisymmetric model is much more computationally effective than the three dimensional model.

- Flow-lift and force lift characteristics have been obtained at different test pressures experimentally and by using the CFD model.

- Importantly the CFD predictions allowed a detailed understanding between valve geometry and the trends observed in the valve flow and force characteristics. Since these characteristics are fundamental for valve operation, an understanding of the interaction between the flow and valve geometry and the effects on the characteristics is necessary for the development of more effective designs.

- A design approach for safety relief valves used by Betts and Francies [6] and Dempster et al [20] has been verified for the valve studied here. Scaling parameters to normalise the flow-lift and force-lift characteristics have been introduced to assist in this safety relief valve design approach. Using the flow scaling parameter has shown a good representation for the flow-lift curves at all pressures with maximum uncertainty of 1.5% whereas the force scaling parameter has shown less accuracy with uncertainty of 7% due to the effect of the back pressure on the net piston force.

6.3 Two Phase Studies Conclusions

- An experimental approach has been developed for testing safety relief valves under two phase flow. A test rig has been developed to facilitate the implementation and measurement of air-water flow through safety relief valves. The experimental approach, with the measurement of the air and water flow rate, pressures, temperature and lift, has been found satisfactory for obtaining the valve flow-lift and force lift characteristics at different test pressures and water mass fractions. The experimentally measured flow-lift and force lift characteristics have helped in understanding the two phase flow behaviour and validated the mixture model.

- Various groups of experimental tests have been carried out to investigate the gland and flow regime effect on the flow characteristics. Tests have been carried out with and without the modified gland and with three different geometry injection nozzles.

- In general, the two phase flow-lift characteristics have a similar behaviour to the single phase flow characteristics. However, at high lifts (lift $>$ 1.2 mm) the two phase flow has a lower slope.

- At any fixed test pressure and lift, with a water flow increase the air flow decreases due to the decrease in air volume fraction.

- There is no effect of the modified gland on the mass flow rate, but it has a significant effect on the back pressure and hence the piston force. In addition, removing the gland allows the flow to undergo an expansion wave downstream of the choking plane with a high possibility of the establishment of a standing shock wave which depends on the test pressure, piston lift and water mass fraction. This introduces undesirable characteristics and a valve designer for two phase flow should avoid such situations along the valve operation range.

- The water flow rate has no significant effect on the piston force. The two

phase force-lift characteristics have a similar behaviour to the single phase flow characteristics with close values but slightly different slopes.

- The CFD mixture model has shown to give good predictions for flow and piston forces. However, the deviation in force and pressure prediction due to the three dimensional effects are as valid in two phase flow as well as in single phase flow. The model has also shown the capability to give good details on the flow regime and flow properties distributions with identifying the critical planes and the shock waves.

- Accounting for the slip doesn't have a significant effect on the flow. On the other hand the assumption of a single temperature to represent the mixture temperature is accepted here as the model has shown good prediction for the flow rate. Hence, the flow has been considered homogeneous and in thermal equilibrium.

- The mixture model prediction for the mixture flow rate shows a very good agreement with the experimental results at high lifts (choking plane at the piston side face) with low water mass fraction. The deviation from the experimental results is only 0.5% at 0.11 water mass fraction. However, the accuracy of predicting the flow rate is less when the water mass fraction increases. The deviation from the experimental results is 9% at 0.55 water mass fraction. At lower lifts the deviation of the predicted results from the experimental are larger and reach 15%. This shows the limitation of the CFD mixture model at high water mass fraction and the deficiency to predict the flow regimes at low lifts. An improved model will result in better prediction.

- The inlet flow regime affects the air flow rate. The more the water is dispersed the less air flows. The mixture model and the standard k-ε turbulence model overpredict the dispersion of the water which results in less accurate predicting of the flow regime.

- The mixture model has shown a better agreement with the experimental results than the HEM, HNE-DS model and the ISO adopted model for predicting the mixture flow rate at a high lift.

- A design approach for safety relief valves used for single phase flow has been modified for two phase flow. A scaling parameter accounting for the water mass fraction has been introduced to normalise the flow-lift characteristics. The normalised flow characteristics have shown nearly one curve with an uncertainty of 5%.

- As the water flow rate has no significant effect on the force-lift characteristics, the same scaling parameter used for single phase flow is valid for two phase flow as well. The normalised piston force characteristics have shown nearly one curve with an uncertainty of 3%.

6.4 Future Work

- A computational three dimensional model should be developed. This may give more accurate predictions for piston forces under single and two phase flow conditions.
- The mixture model predictability should be examined at wider range of operating conditions, i.e. higher and lower pressures and higher and lower water flow rates. Hence, experimental work for a wider range of operating pressure is needed to validate/develop the mixture model
- The effect of the turbulence models on the mixture model prediction needs to be investigated.
- The study to should be expanded to include a non homogeneous flow and a non thermal equilibrium flow to check the limits of the mixture model in predicting a non-homogeneous non-thermal equilibrium flow.
- More inlet flow regimes should be investigated experimentally and by using the mixture CFD model.
- Investigation of the transient operation of the valve at different flow conditions should be undertaken.
- Further studies to be made for a more general design methodology for wider range of operating condition and with application on different safety relief valves.

Bibliography

[1] Api std 520 sizing 2005, selection, and installation of pressure-relieving devices in refineries: Part i - sizing and selection. american petroleum institute (api). Technical report.

[2] Iso 4126-10 safety devices for protection against excessive pressure – part 10: Sizing of safety valves and connected inlet and outlet lines for gas/liquid two-phase flow. international organization for standardization (iso). Technical report, 2004.

[3] Iso 4126-1:2004 safety devices for protection against excessive pressure. safety valves. international organization for standardization (iso). Technical report, 2004.

[4] Iso 4126-7:2004 safety devices for protection against excessive pressure. safety valves.international organization for standardization (iso). Technical report, 2004.

[5] Harald Berger. Numerical simulation of gas flow in pneumatic components. *Forschung im Ingenieurwesen*, 58(3):67–74, March 1992.

[6] P. L. Betts and J. Francis. Design of high-lift pressure relief valves with non-adjustable blowdown for gas/steam. *Journal of Process Mechanical Engineering*, 209(Part E), 1995.

[7] P. L. Betts and J. Francis. Pressures beneath the disc of a compensated pressure relief valve for gas/vapour service pressure relief valve for gas/vapour service. *Journal of Process Mechanical Engineering*, 211:285–289, 1997.

[8] A. J. Bilanin and M. E. Teske. Modeling flow through spring loaded safety valves. volume 190, pages 29–36. ASME PVP conference, ASME, 1990.

[9] Gino Boccardi, Roberto Bubbico, Piero, and Fausto Di Tosto. Geometry influence on safety valves sizing in two-phase flow. *Journal of Loss Prevention in the Process Industries*, 21(1):66–73, January 2008.

[10] Gino Boccardi, Roberto Bubbico, Piero, and Barbara Mazzarotta. Two-phase flow through pressure safety valves. experimental investigation and model prediction. *Chemical Engineering Science*, 60(19):5284–5293, September 2005.

[11] L. Bolle. Experimental and theoretical analysis of flashing water flow through a safety value. *Journal of Hazardous Materials*, 46(2-3):105–116, April 1996.

[12] L. Bolle, P. Downar-Zapolski, J. Franco, and J. M. Seynhaeve. Flashing water flow through a safety valve. *Journal of Loss Prevention in the Process Industries*, 8(2):111–126, 1995.

[13] M. Brennan, M. Narasimha, and P. Holtham. Multiphase modelling of hydrocyclones prediction of cut size. *Minerals Engineering*, 20(4):395–406, April 2007.

[14] M. S. Brennan. Multiphase cfd simulations of dense medium and classifying hydrocyclones. pages 59–63. Third International Conference on CFD in the Minerals and Process Industries CSIRO, Melbourne, Australia, December 2003.

[15] J. Cremers and L. Friedel. Design of spring loaded safety valves with inlet and discharge pipe against chatter in the case of gas flow. *Chemical Engineering & Technology*, 26(5):573–576, 2003.

[16] Clayton Crowe, Martin Sommerfeld, and Yutaka Tsuji. *Multiphase Flows with droplets and particles*. CRC Press, 1998.

[17] Robert D'Alessandro. Thrust force calculations for pressure safety valves. *Process Safety Progress*, 25(3):203–213, 2006.

[18] Ron Darby. On two-phase frozen and flashing flows in safety relief values: Recommended calculation method and the proper use of the discharge coefficient. *Journal of Loss Prevention in the Process Industries*, 17(4):255–259, July 2004.

[19] Sandra C. K. De Schepper, Geraldine J. Heynderickx, and Guy B. Marin. Cfd modeling of all gas liquid and vapor liquid flow regimes predicted by the baker chart. *Chemical Engineering Journal*, 138(1-3):349–357, May 2008.

[20] W. Dempster, C. K. Lee, and J. Deans. Prediction of the flow and force characteristics of safety relief valves. *Proceedings of PVP2006-ICPVT-11 2006 ASME Pressure Vessels and Piping Division Conference*, July 2006.

[21] H. Derlien and L. Friedel. Accuracy of safety valve two-phase mass flow capacity sizing. *Chemical Engineering & Technology*, 29(1):87–96, 2006.

[22] H. Derlien and L. Friedel. Reproductive accuracy of generic omega parameter safety valve two phase critical mass flow models based on water and refrigerant r-134a data. *Chemical Engineering & Technology*, 30(9):1181–1192, 2007.

[23] R. Diener and J. Schmidt. Extended omega-method applicable for low inlet mass flow qualities. Ludwigshafen, Germany, June 1998. 13th Mtg. ISO/TC185/WG1.

[24] Hans K. Fauske. Sizing rupture disks (rds) for two phase flow. Technical report, 1988.

[25] Hans K. Fauske. A practical approach to certifying the capacity of pressure relief valves in two phase flow service. Technical report, October 2002.

[26] *Fluent 6.3 User Guide*, 2006.

[27] B. Follmer. Oscilliating functioning of safety valves generated by their inlet geometry. International Symposium of Flow Visualisation, September 1980.

[28] Bernhard Follmer and Armin Schnettler. Safety relief valves according new requirments of en(ped) versus ad/trd or asme. Technical report, 2004.

[29] J. Francis. Zone modeling of high lift safety relief valves subject to choked compressible flow. pages 795–806. Proceeding Of The 3rd International Seminar on Fire and Explosion Hazards, 2001.

[30] James E. Funk. Poppet valve stability. *Journal of Basic Engineering*, pages 207–212, June 1964.

[31] S. Ghorai and K. Nigam. Cfd modeling of flow profiles and interfacial phenomena in two-phase flow in pipes. *Chemical Engineering and Processing*, 45(1):55–65, January 2006.

[32] I. S. Grinberg and I. R. Krichker. Design method for safety valves with pressure applied above the seat. *Chemical and Petroleum Engineering*, 9(8):696–698, 1973.

[33] Jordan Gronkowski. Integration of computational fluid dynamics and transient analysis methods into relief valve design. Master's thesis, University of Strathclyde, Glasgow, UK, 2010.

[34] A. Kendoush. Thermohydraulic effects of safety relief valves. *Experimental Thermal and Fluid Science*, 19(3):131–139, July 1999.

[35] Heuy-Dong Kim, Jun-Hee Lee, Kyung-Am Park, Toshiaki Setoguchi, and Shigeru Matsuo. A study of the gas flow through a lng safety valve. *Journal of Thermal Science*, 15(4):355–360, December 2006.

[36] T. Lenzing, L. Friedel, and M. Alhusein. Critical mass flow rate in accordance with the omega-method of diers and the homogeneous equilibrium model. *Journal of Loss Prevention in the Process Industries*, 11(6):391–395, November 1998.

[37] T. Lenzing, L. Friedel, J. Cremers, and M. Alhusein. Prediction of the maximum full lift safety valve two-phase flow capacity. *Journal of Loss Prevention in the Process Industries*, 11(5):307–321, September 1998.

[38] J. C. Leung. A generalized correlation for one-component homogeneous equilibrium flashing choked flow. *AIChE Journal*, 32(10):1743–1746, 1986.

[39] Joseph C. Leung. A theory on the discharge coefficient for safety relief valve. *Journal of Loss Prevention in the Process Industries*, 17(4):301–313, July 2004.

[40] G. Luft, J. Broedermann, and T. Scheele. Pressure relief of high pressure devices. *Chemical Engineering & Technology*, 30(6):695–701, 2007.

[41] G. MacLeod. Safety valve dynamic instability:an analysis of chatter. *Journal of Pressure Vessel Technology*, 107:172–177, May 1985.

[42] Mikko Manninen, Veikko Taivassalo, and Sirpa Kallio. On the mixture model for multiphase flow. Technical report, Technical research center of Finland, 1996.

[43] Genick B. Meir. *Fundamentals of Compressible Fluid Mechanics (e-book)*. Free Software Foundation, Inc., USA, October 2007.

[44] Lester Millard. Safety relief valves protect life and property. Technical report, June 2002.

[45] D. Moncalvo and L. Friedel. Reproductive accuracy of safety valve two-phase mass flow capacity models in case of air/water, resp., viscous liquid flow duty. *Forschung im Ingenieurwesen*, 70(2):133–138, May 2005.

[46] D. Moncalvo and L. Friedel. Influence of the liquid phase physical properties on the void fraction at the inlet of a full-lift safety valve. *Chemical Engineering & Technology*, 32(2):273–282, 2009.

[47] D. Moncalvo and L. Friedel. A simple, explicit formula for the critical pressure of homogenous two-phase nozzle flows. *Journal of Loss Prevention in the Process Industries*, July 2009.

[48] Bruce R. Munson, Donald F. Young, and Theodore H. Okiishi. *Fundamentals of Fluid Mechanics*. John Wiley & Sons, Inc., 5th edition, 2004.

[49] S. Muschelknautz and A. Wellenhofer. Flow reaction forces upon blowdown of safety valves. *Chemical Engineering & Technology*, 26(7):797–803, 2003.

[50] Tadashi Narabayashi, Hideo Nagasaka, Masao Niwano, and Yoshiteru Ohtsuki. Safety relief valve performance for two-phase flow. *Journal of Nuclear Science and Technology*, 1986.

[51] M. Narasimha, M. Brennan, and P. Holtham. Numerical simulation of magnetite segregation in a dense medium cyclone. *Minerals Engineering*, 19(10):1034–1047, August 2006.

[52] M. Narasimha, M. Brennan, P. Holtham, and T. Napiermunn. A comprehensive cfd model of dense medium cyclone performance. *Minerals Engineering*, 20(4):414–426, April 2007.

[53] M. Narasimhaa, M. S. Brennanb, P. N. Holthamb, and T. J. Napier-Munn. Sciencedirect - minerals engineering : A comprehensive cfd model of dense medium cyclone performance. *Minerals Engineering*, 20:414–426, 2007.

[54] G. J. Parker. 'pop' safety valves: a compressible flow analysis. *International Journal of Heat and Fluid Flow*, 6(4):279–283, December 1985.

[55] K. Pougatch, M. Salcudean, E. Chan, and B. Knapper. Modelling of compressible gas-liquid flow in a convergent-divergent nozzle. *Chemical Engineering Science*, 63(16):4176–4188, August 2008.

[56] Spirax Sarco. *http://www.spiraxsarco.com/uk/*. 2009.

[57] J. Schmidt and S. Egan. Case studies of sizing pressure relief valves for two-phase flow. *Chemical Engineering & Technology*, 32(2):263–272, 2009.

[58] J. Schmidt, W. Peschel, and A. Beune. Experimental and theoretical studies on high pressure safety valves: sizing and design supported by numerical calculations (cfd). *Chemical Engineering & Technology*, 32(2):252–262, 2009.

[59] S. Sethi and A. Sabit. Predicting the fluid flow through a pressure relief valve using the cfd code phonics. volume 26, pages 229–235. Proceeding of the 11th Annual Simulators Conference, 1994.

[60] Samir Sethi and Ying S. Lai. A simulation model to predict the performance characteristics of safety relief valves,http://www.acslsim.com.

[61] D. K. Sharma. State-of-the-art design of spring loaded safety valves. Joint conference of the Pressure Vessels and Piping, Materials, Nuclear Engineering and Solar Division., 1981.

[62] Peter Smith and R. W. Zappe. *Valve Selection Handbook*. 5th edition, 2004.

[63] Herbert Staedtke. *Gasdynamic Aspects of Two-Phase Flow: Hyperbolicity, Wave Propagation Phenomena, and Related Numerical Methods*. WILLY-VCH Verlag GmbH & Co. KGaA, Weinheim, September 2006.

[64] P. R. Sterland. Understanding the behaviour of relief valve. *IMechE*, C373/84:57–62, 1984.

[65] Yu Taras'ev and V. A. Kuzin. Classification of safety valve designs. *Chemical and Petroleum Engineering*, 4(10):851–854, October 1968.

[66] Q. K. Tran and M. Reynolds. Sizing of relief valves for two phase flow in bayer process. Technical report, 2002.

Appendix A

A.1 CAD Drawings

A.1.1 Valve CAD Drawings

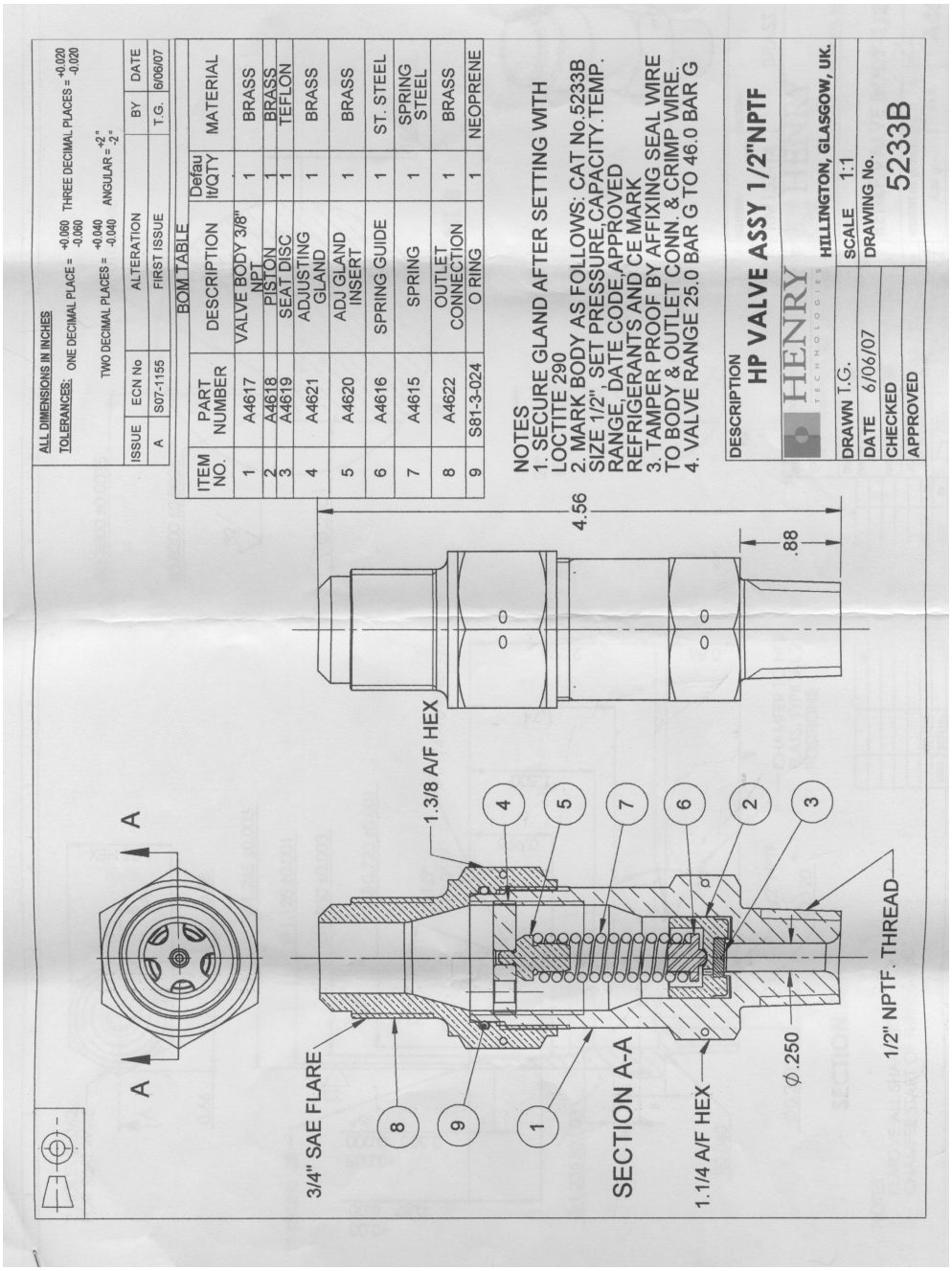

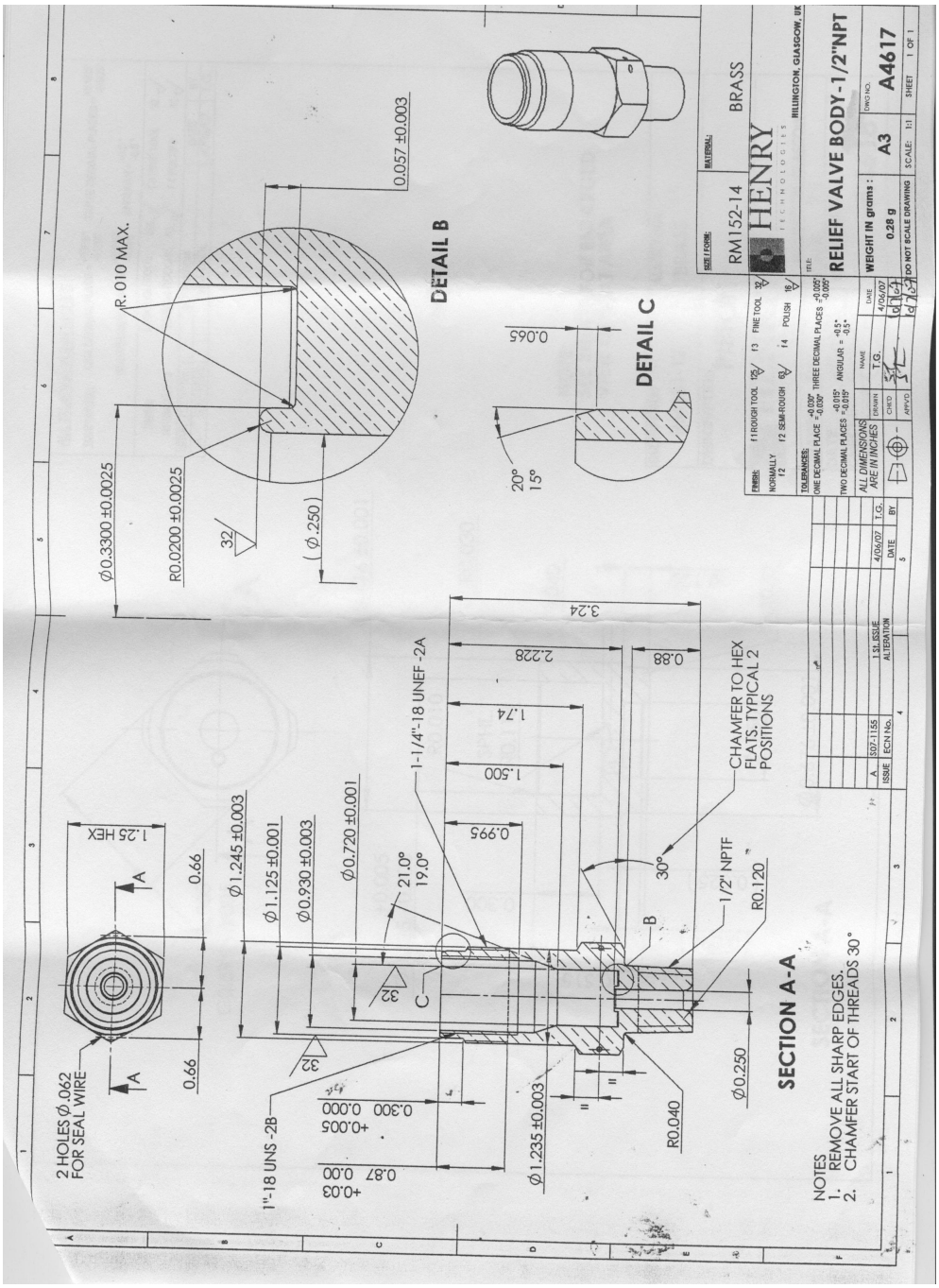
RELIEF VALVE BODY-1/2"NPT
HENRY
TECHNOLOGIES
HILLINGTON, GLASGOW, UK
RM152-14
BRASS
A4617
A3
0.28 g
DO NOT SCALE DRAWING
SECTION A-A
DETAIL B
DETAIL C
NOTES
1. REMOVE ALL SHARP EDGES.
2. CHAMFER START OF THREADS 30°
2 HOLES Ø.062 FOR SEAL WIRE
1"-18 UNS -2B
1-1/4"-18 UNEF -2A
CHAMFER TO HEX FLATS, TYPICAL 2 POSITIONS
1/2" NPTF
R0.120
R0.040
Ø0.250
1.25 HEX
0.66
3.24
2.228
1.74
1.500
0.995
0.88
0.057 ±0.003
R. 010 MAX.
Ø0.3300 ±0.0025
R0.0200 ±0.0025
(Ø.250)
0.065
20°
15°
21.0°
19.0°
30°
Ø1.245 ±0.003
Ø1.125 ±0.001
Ø0.930 ±0.003
Ø0.720 ±0.001
Ø1.235 ±0.003
0.87 +0.03 0.00
0.300 +0.005 0.000
ISSUE
ECN No.
ALTERATION
DATE
BY
1ST. ISSUE
4/06/07
T.G.
DRAWN
CHK'D
APP'D
TOLERANCES:
ONE DECIMAL PLACE ±0.030"
TWO DECIMAL PLACES ±0.015"
THREE DECIMAL PLACES ±0.005"
ANGULAR = ±0.5°
ALL DIMENSIONS ARE IN INCHES
FINISH:
NORMALLY
f1 ROUGH TOOL
f2 SEMI-ROUGH
f3 FINE TOOL
f4 POLISH
SIZE / FORM:
MATERIAL:
WEIGHT IN grams :
DWG NO.
SCALE:
SHEET
1 OF 1

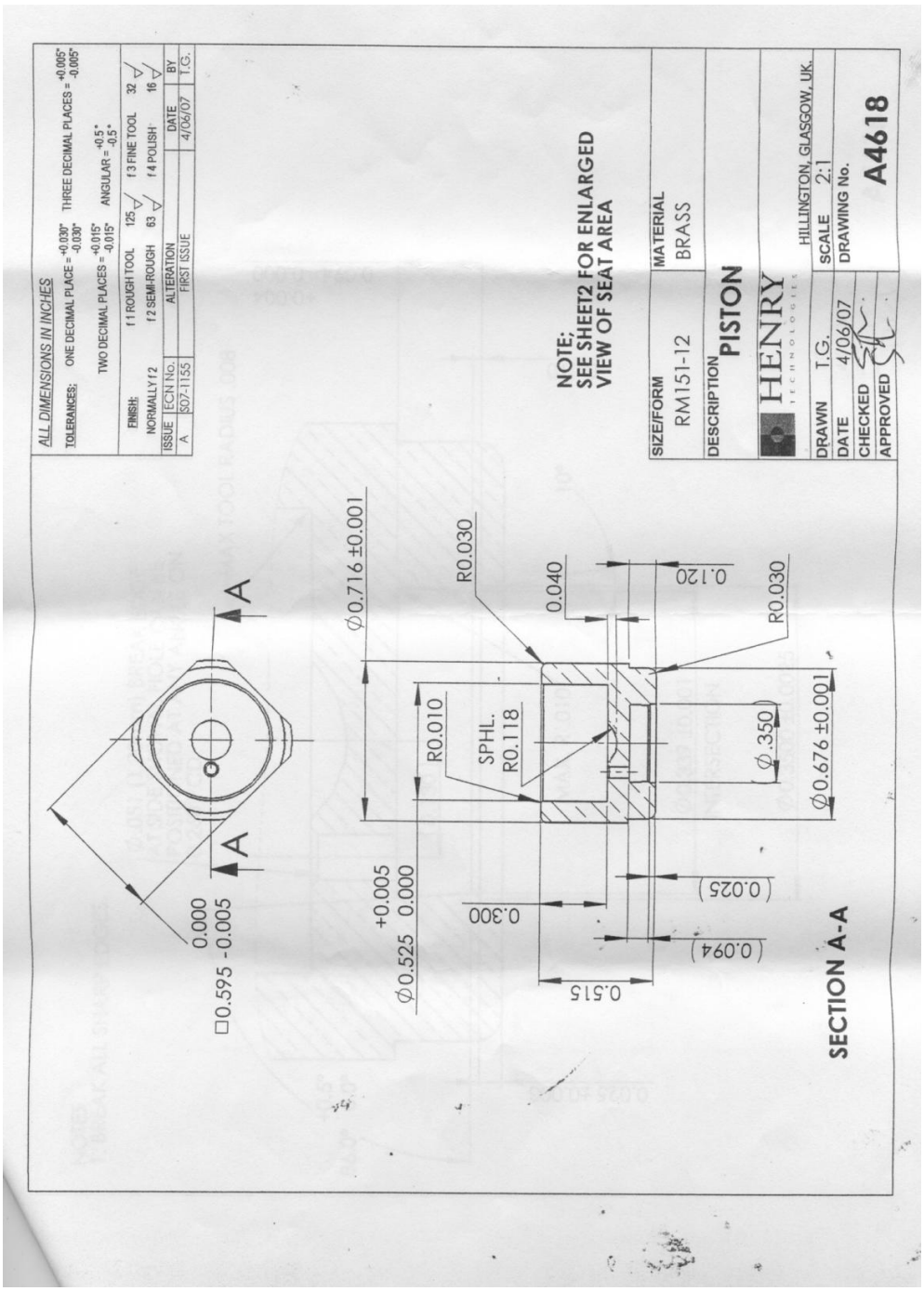
ALL DIMENSIONS IN INCHES
TOLERANCES: ONE DECIMAL PLACE = +0.030" -0.030" THREE DECIMAL PLACES = +0.005" -0.005"
TWO DECIMAL PLACES = +0.015" -0.015" ANGULAR = +0.5° -0.5°
FINISH: f1 ROUGH TOOL 125 f3 FINE TOOL 32
NORMALLY f2 f2 SEMI-ROUGH 63 f4 POLISH 16
ISSUE ECN No. ALTERATION DATE BY
A S07-1155 FIRST ISSUE 4/06/07 T.G.
NOTE; SEE SHEET2 FOR ENLARGED VIEW OF SEAT AREA
SIZE/FORM RM151-12
MATERIAL BRASS
DESCRIPTION PISTON
HENRY TECHNOLOGIES
HILLINGTON, GLASGOW, UK.
DRAWN T.G.
DATE 4/06/07
CHECKED
APPROVED
SCALE 2:1
DRAWING No. A4618
SECTION A-A
A
A
0.000 -0.005
□0.595
+0.005 0.000
Ø0.525
Ø0.716 ±0.001
R0.030
R0.010
SPHL. R0.118
0.040
0.120
R0.030
0.300
0.515
(0.025)
(0.094)
Ø.350
Ø0.676 ±0.001

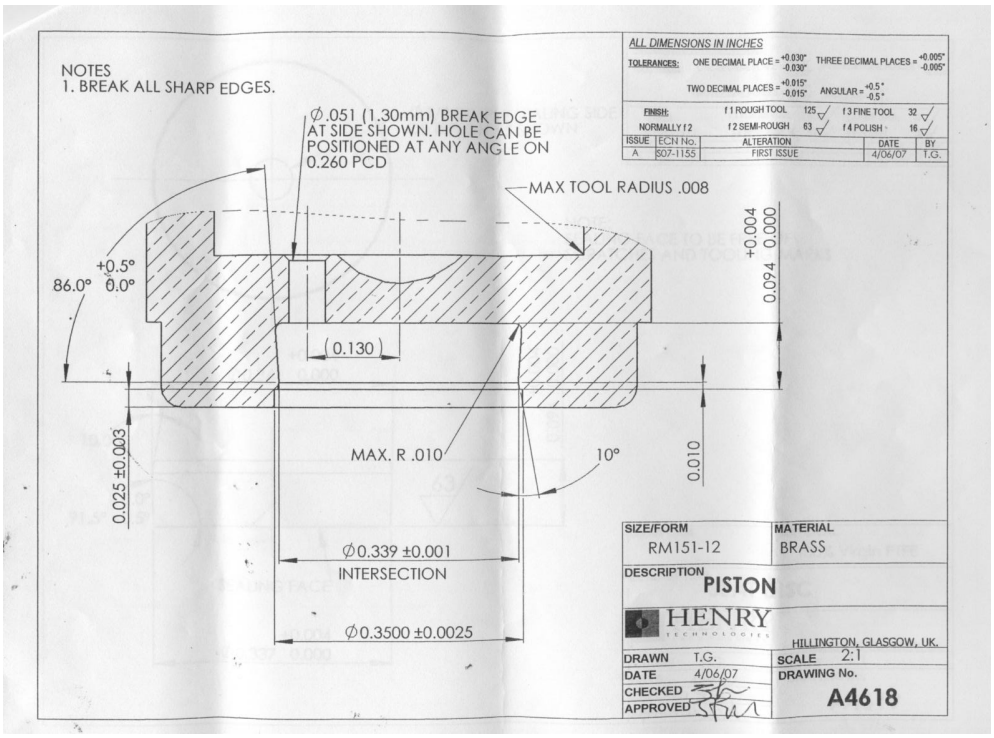
NOTES
1. BREAK ALL SHARP EDGES.
Ø.051 (1.30mm) BREAK EDGE AT SIDE SHOWN. HOLE CAN BE POSITIONED AT ANY ANGLE ON 0.260 PCD
MAX TOOL RADIUS .008
+0.5° 0.0°
86.0°
+0.004 0.000
0.094
0.130
0.025 ±0.003
MAX. R .010
10°
0.010
Ø0.339 ±0.001
INTERSECTION
Ø0.3500 ±0.0025
ALL DIMENSIONS IN INCHES
TOLERANCES: ONE DECIMAL PLACE = +0.030 -0.030 THREE DECIMAL PLACES = +0.005 -0.005
TWO DECIMAL PLACES = +0.015 -0.015 ANGULAR = +0.5 -0.5
FINISH: NORMALLY f2 f1 ROUGH TOOL 125 f2 SEMI-ROUGH 63 f3 FINE TOOL 32 f4 POLISH 16
ISSUE ECN No. ALTERATION DATE BY
A S07-1155 FIRST ISSUE 4/06/07 T.G.
SIZE/FORM RM151-12
MATERIAL BRASS
DESCRIPTION PISTON
HENRY TECHNOLOGIES
HILLINGTON, GLASGOW, UK.
DRAWN T.G.
DATE 4/06/07
CHECKED
APPROVED
SCALE 2:1
DRAWING No. A4618

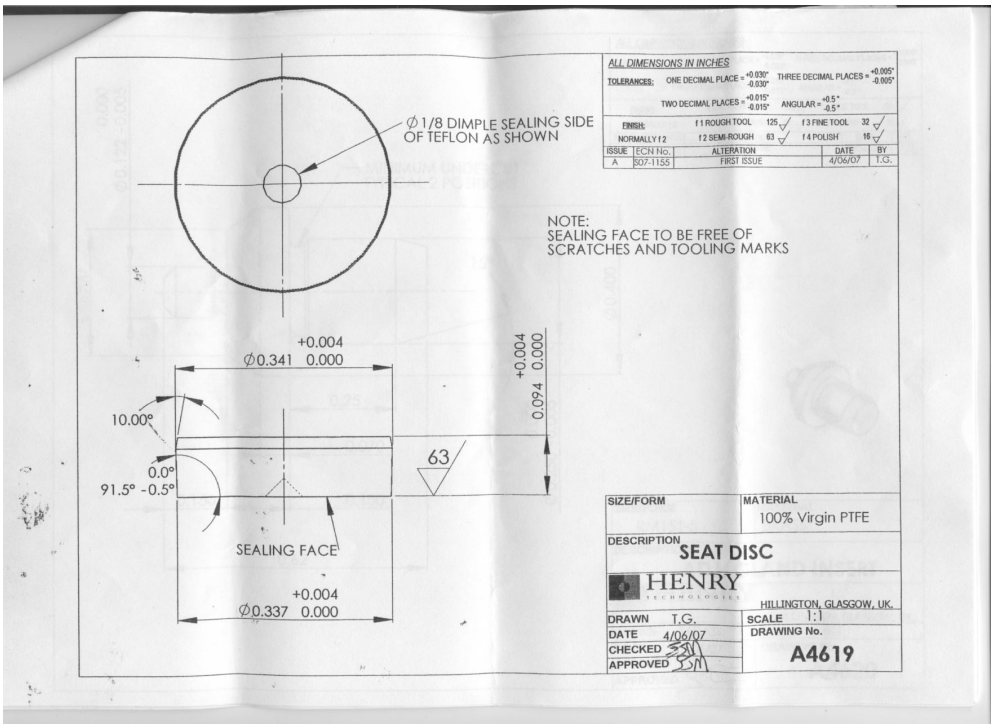
Ø1/8 DIMPLE SEALING SIDE OF TEFLON AS SHOWN
NOTE:
SEALING FACE TO BE FREE OF SCRATCHES AND TOOLING MARKS
+0.004
Ø0.341 0.000
+0.004 0.000
0.094
10.00°
0.0°
91.5° -0.5°
63
SEALING FACE
+0.004
Ø0.337 0.000
ALL DIMENSIONS IN INCHES
TOLERANCES: ONE DECIMAL PLACE = +0.030 -0.030 THREE DECIMAL PLACES = +0.005 -0.005
TWO DECIMAL PLACES = +0.015 -0.015 ANGULAR = +0.5 -0.5
FINISH: NORMALLY f2 f1 ROUGH TOOL 125 f2 SEMI-ROUGH 63 f3 FINE TOOL 32 f4 POLISH 16
ISSUE ECN No. ALTERATION DATE BY
A S07-1155 FIRST ISSUE 4/06/07 T.G.
SIZE/FORM
MATERIAL 100% Virgin PTFE
DESCRIPTION SEAT DISC
HENRY TECHNOLOGIES
HILLINGTON, GLASGOW, UK.
DRAWN T.G.
DATE 4/06/07
CHECKED
APPROVED
SCALE 1:1
DRAWING No. A4619

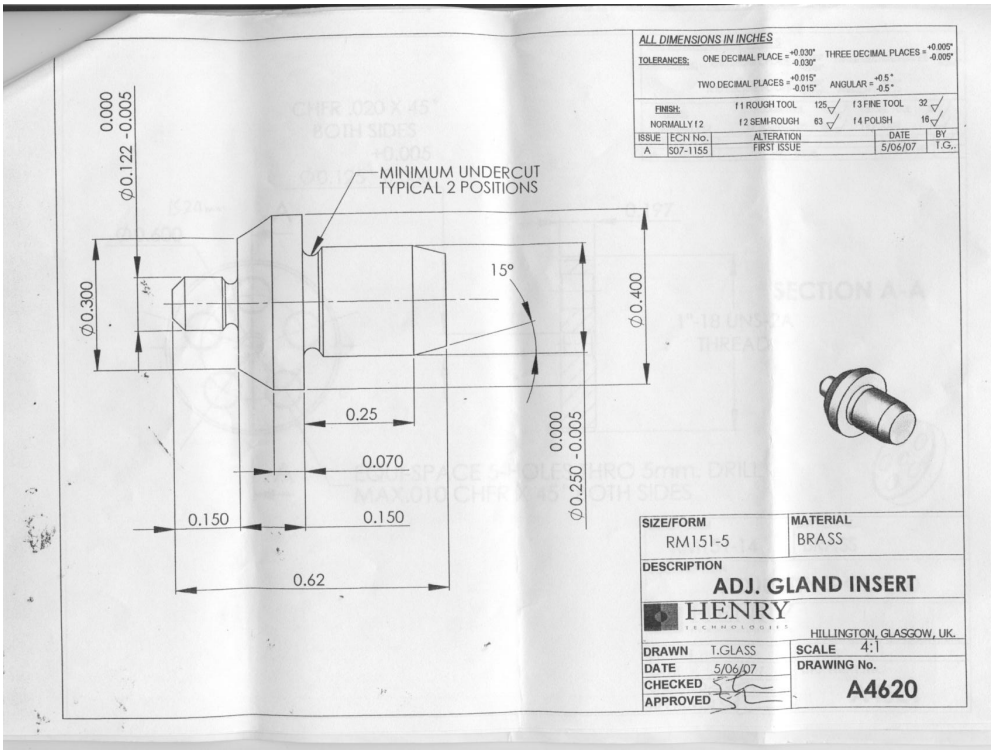
ALL DIMENSIONS IN INCHES
TOLERANCES: ONE DECIMAL PLACE = +0.030 -0.030 THREE DECIMAL PLACES = +0.005 -0.005
TWO DECIMAL PLACES = +0.015 -0.015 ANGULAR = +0.5° -0.5°
FINISH: NORMALLY f2 f1 ROUGH TOOL 125 f2 SEMI-ROUGH 63 f3 FINE TOOL 32 f4 POLISH 16
ISSUE ECN No. ALTERATION DATE BY
A S07-1155 FIRST ISSUE 5/06/07 T.G.
0.000 -0.005
Ø0.122
MINIMUM UNDERCUT
TYPICAL 2 POSITIONS
15°
Ø0.300
Ø0.400
0.25
0.070
0.150
0.150
0.62
0.000 -0.005
Ø0.250
SIZE/FORM RM151-5
MATERIAL BRASS
DESCRIPTION ADJ. GLAND INSERT
HENRY TECHNOLOGIES
HILLINGTON, GLASGOW, UK.
DRAWN T.GLASS
DATE 5/06/07
CHECKED
APPROVED
SCALE 4:1
DRAWING No. A4620

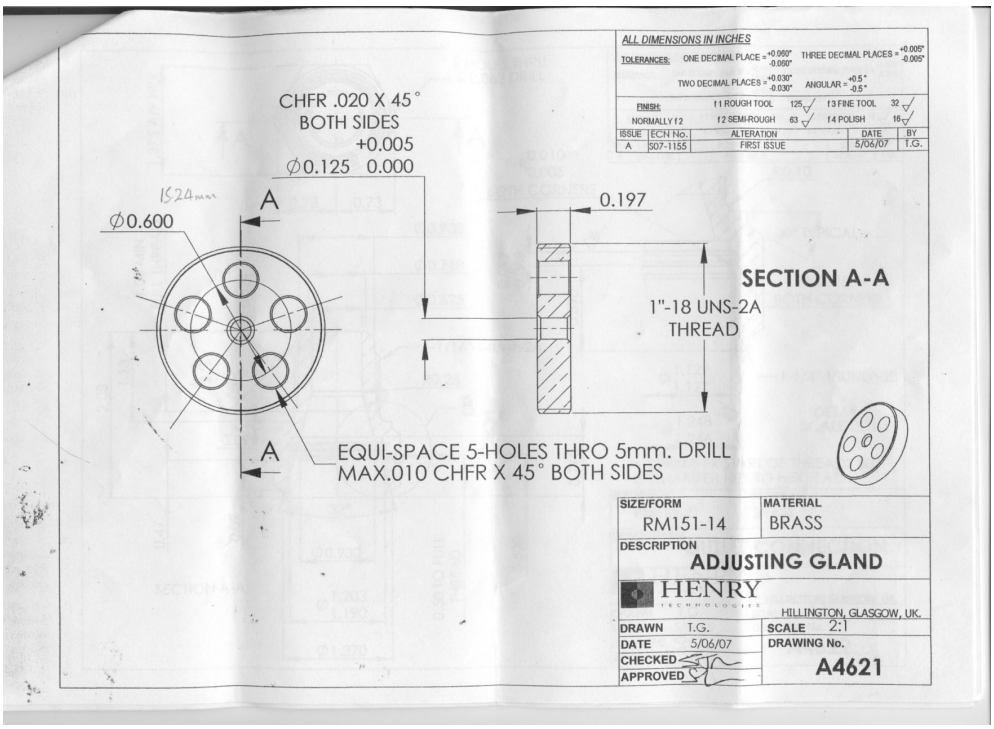
ALL DIMENSIONS IN INCHES
TOLERANCES: ONE DECIMAL PLACE = +0.060 -0.060 THREE DECIMAL PLACES = +0.005 -0.005
TWO DECIMAL PLACES = +0.030 -0.030 ANGULAR = +0.5° -0.5°
FINISH: NORMALLY f2 f1 ROUGH TOOL 125 f2 SEMI-ROUGH 63 f3 FINE TOOL 32 f4 POLISH 16
ISSUE ECN No. ALTERATION DATE BY
A S07-1155 FIRST ISSUE 5/06/07 T.G.
CHFR .020 X 45°
BOTH SIDES
+0.005
Ø0.125 0.000
1524mm
A
Ø0.600
0.197
SECTION A-A
1"-18 UNS-2A
THREAD
A
EQUI-SPACE 5-HOLES THRO 5mm. DRILL
MAX.010 CHFR X 45° BOTH SIDES
SIZE/FORM RM151-14
MATERIAL BRASS
DESCRIPTION ADJUSTING GLAND
HENRY TECHNOLOGIES
HILLINGTON, GLASGOW, UK.
DRAWN T.G.
DATE 5/06/07
CHECKED
APPROVED
SCALE 2:1
DRAWING No. A4621

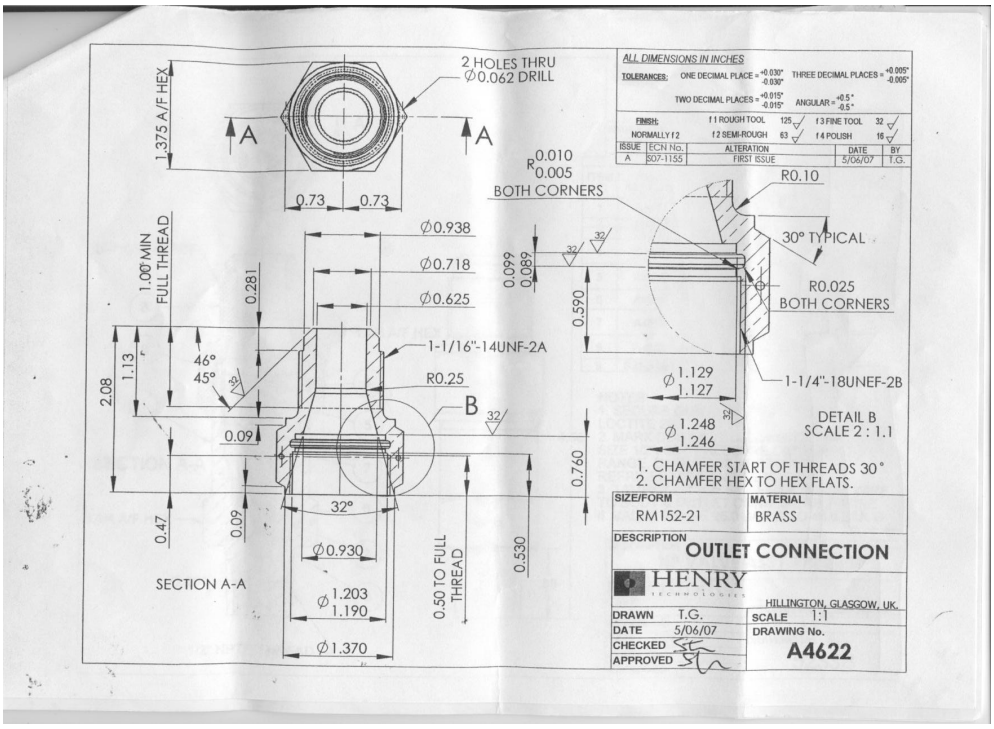
2 HOLES THRU
Ø0.062 DRILL
1.375 A/F HEX
A
A
0.73
0.73
R 0.010 0.005
BOTH CORNERS
R0.10
30° TYPICAL
R0.025
BOTH CORNERS
Ø0.938
Ø0.718
Ø0.625
1.00 MIN
FULL THREAD
0.281
0.099
0.089
0.590
1-1/16"-14UNF-2A
46°
45°
R0.25
B
2.08
1.13
0.09
0.47
0.09
32°
Ø0.930
Ø 1.203
1.190
Ø1.370
0.50 TO FULL
THREAD
0.530
0.760
SECTION A-A
Ø 1.129
1.127
1-1/4"-18UNEF-2B
Ø 1.248
1.246
DETAIL B
SCALE 2 : 1.1
1. CHAMFER START OF THREADS 30°
2. CHAMFER HEX TO HEX FLATS.
ALL DIMENSIONS IN INCHES
TOLERANCES: ONE DECIMAL PLACE ±0.030 -0.030 THREE DECIMAL PLACES ±0.005 -0.005
TWO DECIMAL PLACES ±0.015 -0.015 ANGULAR ±0.5° -0.5°
FINISH: NORMALLY f2
f1 ROUGH TOOL 125
f2 SEMI-ROUGH 63
f3 FINE TOOL 32
f4 POLISH 16
ISSUE | ECN No. | ALTERATION | DATE | BY
A | 607-1155 | FIRST ISSUE | 5/06/07 | T.G.
SIZE/FORM
RM152-21
MATERIAL
BRASS
DESCRIPTION
OUTLET CONNECTION
HENRY
TECHNOLOGIES
HILLINGTON, GLASGOW, UK.
DRAWN T.G.
DATE 5/06/07
CHECKED
APPROVED
SCALE 1:1
DRAWING No.
A4622

A.1.2 The Modified Gland

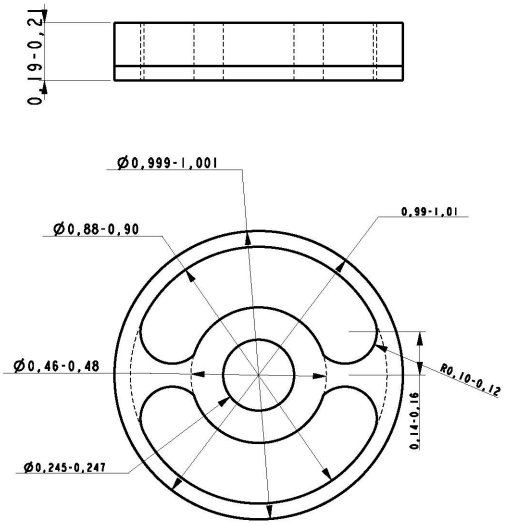

A.1.3 The Converging Section Dimensions

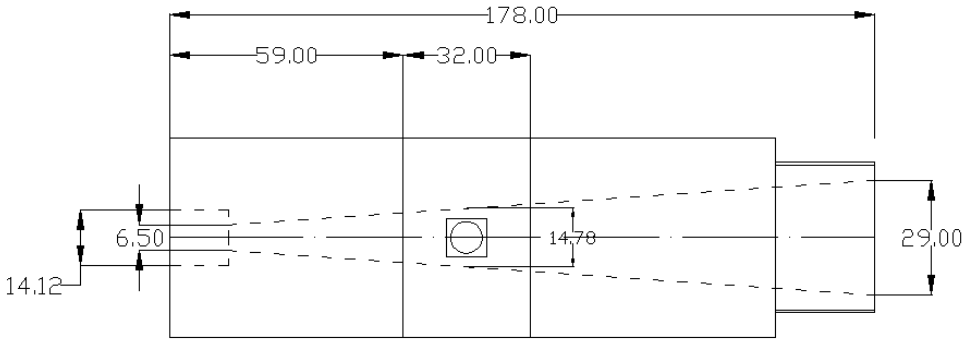

A.1.4 Dempster et al [20] Valve drawing

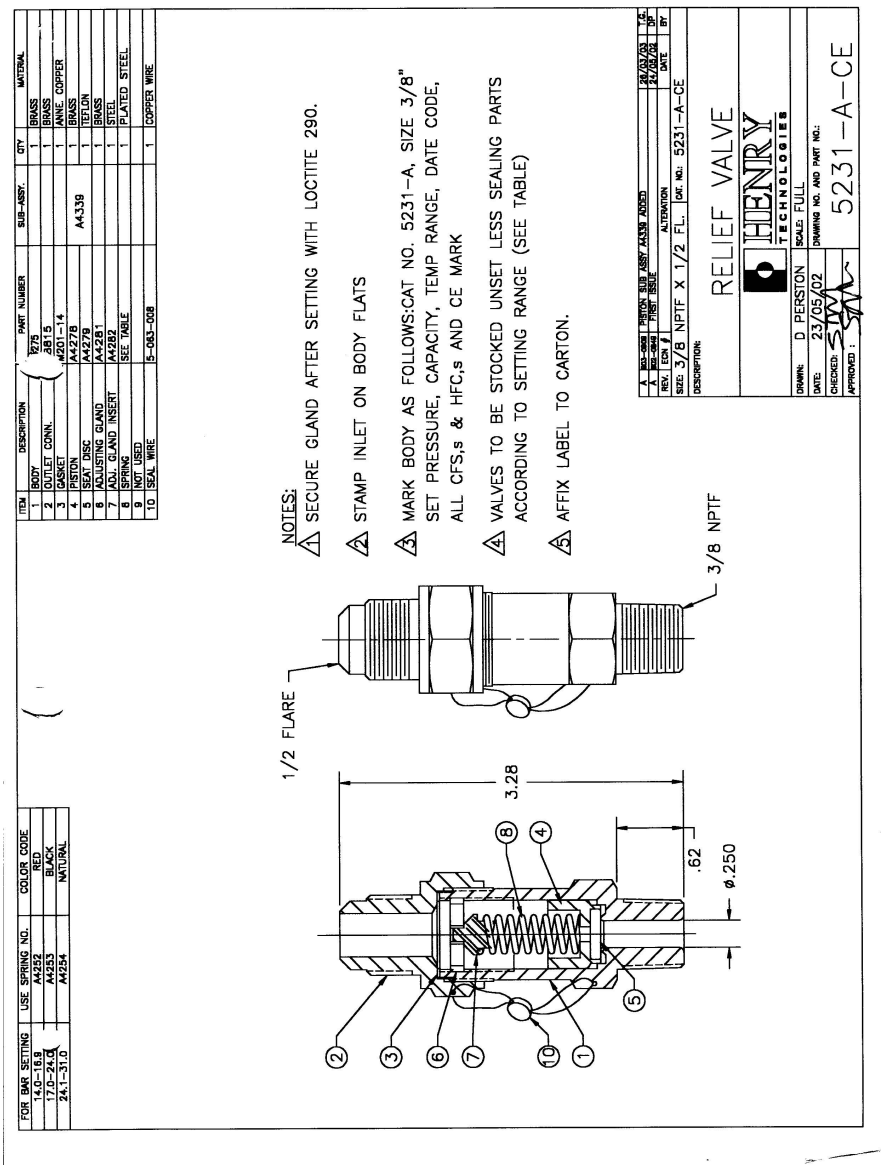

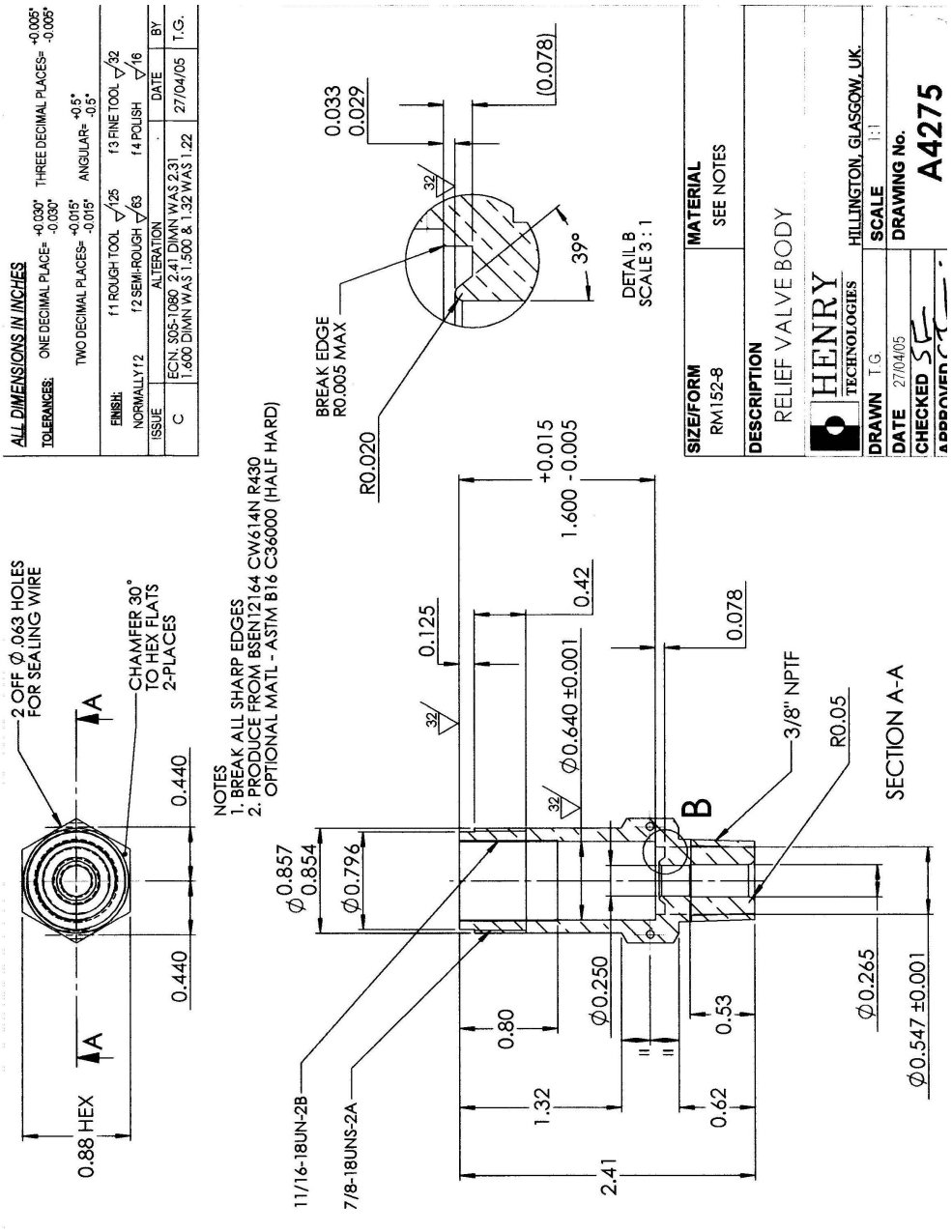
ALL DIMENSIONS IN INCHES
TOLERANCES: ONE DECIMAL PLACE= +0.030" -0.030" THREE DECIMAL PLACES= +0.005" -0.005"
TWO DECIMAL PLACES= +0.015" -0.015" ANGULAR= +0.5° -0.5°
FINISH: f1 ROUGH TOOL 125 f3 FINE TOOL 32
NORMALLY f2 SEMI-ROUGH 63 f4 POLISH 16
ISSUE | ALTERATION | DATE | BY
C | ECN. S05-1080. 2.41 DIMN WAS 2.31 1.600 DIMN WAS 1.500 & 1.32 WAS 1.22 | 27/04/05 | T.G.
NOTES
1. BREAK ALL SHARP EDGES
2. PRODUCE FROM BSEN12164 CW614N R430
OPTIONAL MATL - ASTM B16 C36000 (HALF HARD)
2 OFF Ø .063 HOLES FOR SEALING WIRE
CHAMFER 30° TO HEX FLATS 2-PLACES
0.440
0.440
0.88 HEX
A
A
BREAK EDGE R0.005 MAX
R0.020
0.033
0.029
(0.078)
39°
DETAIL B SCALE 3 : 1
1.600 +0.015 -0.005
0.125
0.42
Ø0.640 ±0.001
0.078
3/8" NPTF
R0.05
Ø0.857
0.854
Ø0.796
Ø0.250
0.80
1.32
2.41
0.53
0.62
Ø0.265
Ø0.547 ±0.001
11/16-18UN-2B
7/8-18UNS-2A
B
SECTION A-A
SIZE/FORM RM152-8
MATERIAL SEE NOTES
DESCRIPTION RELIEF VALVE BODY
HENRY TECHNOLOGIES
HILLINGTON, GLASGOW, UK.
DRAWN T.G.
DATE 27/04/05
CHECKED
SCALE 1:1
DRAWING No. A4275

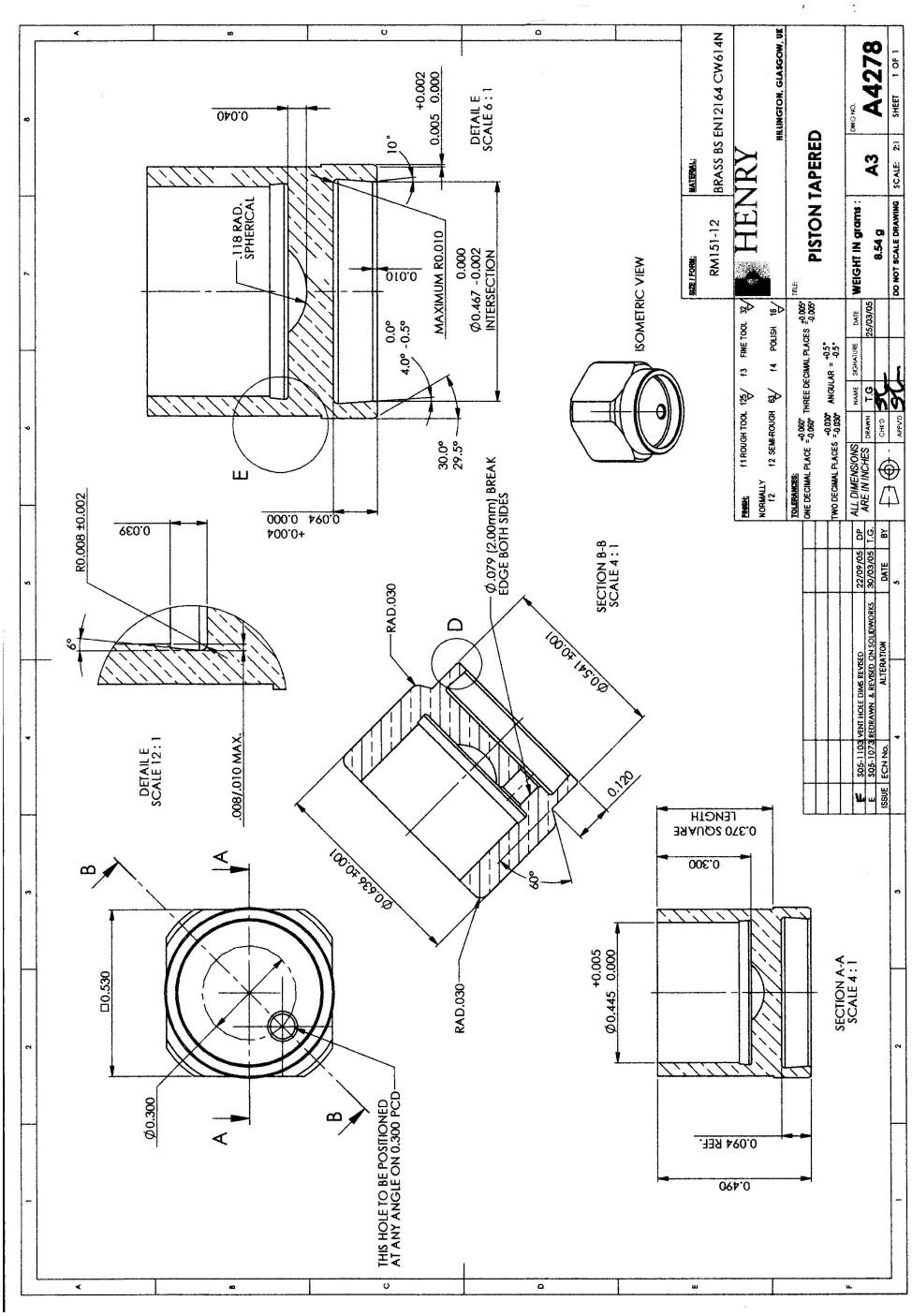
HENRY
HILLINGTON, GLASGOW, UK
PISTON TAPERED
MATERIAL: BRASS BS EN12164 CW614N
RM151-12
A3
A4278
WEIGHT IN grams : 8.54 g
DO NOT SCALE DRAWING
SCALE: 2:1
SHEET 1 OF 1
ISOMETRIC VIEW
SECTION B-B SCALE 4 : 1
SECTION A-A SCALE 4 : 1
DETAIL E SCALE 6 : 1
DETAIL F SCALE 12 : 1
.118 RAD. SPHERICAL
MAXIMUM R0.010
INTERSECTION
RAD.030
Ø0.079 (2.00mm) BREAK EDGE BOTH SIDES
0.120
60°
0.370 SQUARE LENGTH
0.490
0.094 REF.
THIS HOLE TO BE POSITIONED AT ANY ANGLE ON 0.300 PCD
ALL DIMENSIONS ARE IN INCHES
ISSUE ECN No. ALTERATION DATE BY
E 305-1103 VENT HOLE DIMS REVISED 22/09/05 DP
E 305-1078 REDRAWN & REVISED ON SOLIDWORKS 30/05/05 T.G.

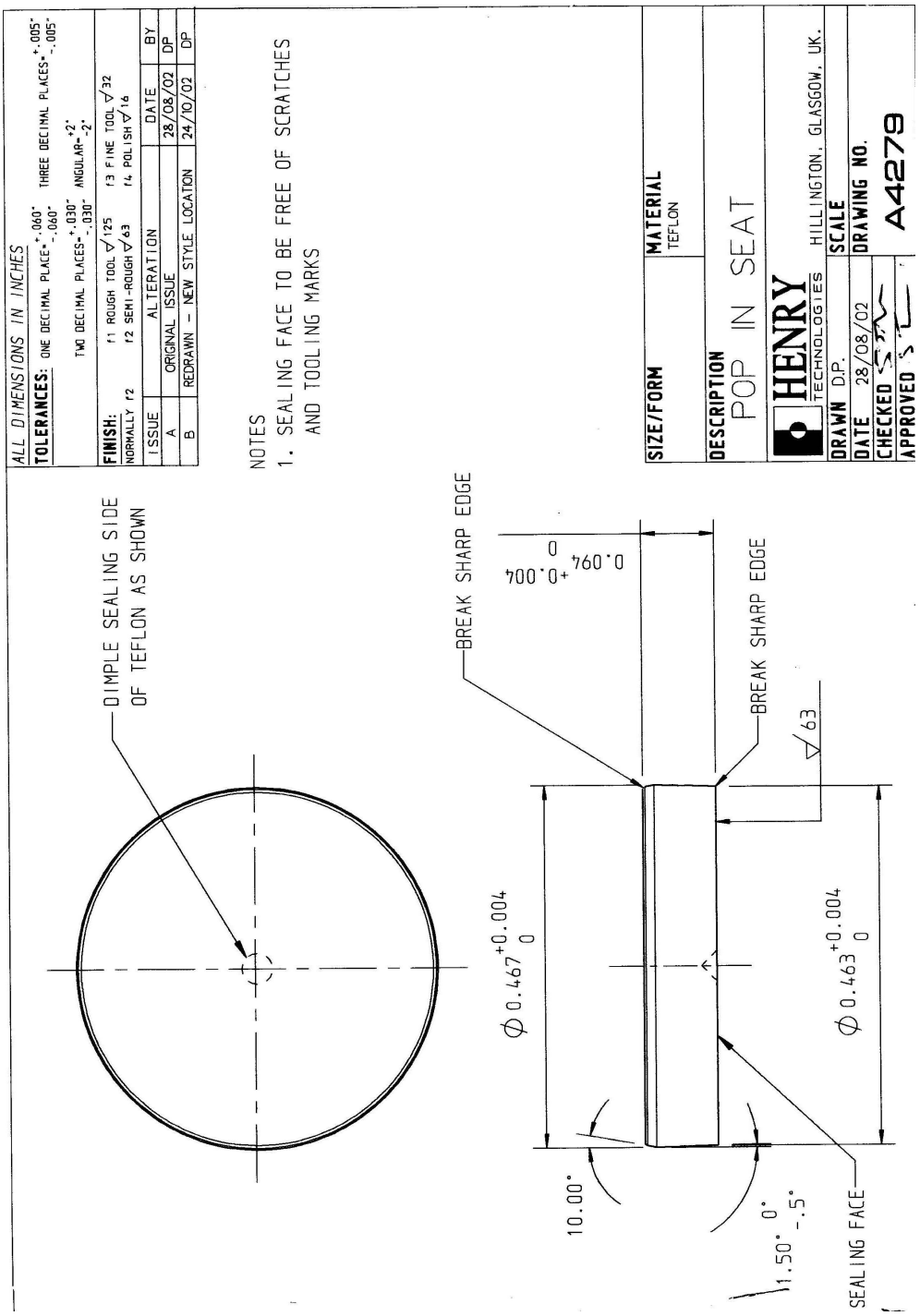
ALL DIMENSIONS IN INCHES
TOLERANCES: ONE DECIMAL PLACE ±.060" THREE DECIMAL PLACES ±.005"
TWO DECIMAL PLACES ±.030" ANGULAR ±2°
FINISH: NORMALLY r2
f1 ROUGH TOOL √125 f3 FINE TOOL √32
f2 SEMI-ROUGH √63 f4 POLISH √16
ISSUE | ALTERATION | DATE | BY
A | ORIGINAL ISSUE | 28/08/02 | DP
B | REDRAWN – NEW STYLE LOCATION | 24/10/02 | DP
NOTES
1. SEALING FACE TO BE FREE OF SCRATCHES AND TOOLING MARKS
SIZE/FORM
MATERIAL TEFLON
DESCRIPTION POP IN SEAT
HENRY TECHNOLOGIES HILLINGTON, GLASGOW, UK.
DRAWN D.P.
DATE 28/08/02
CHECKED
APPROVED
SCALE
DRAWING NO. A4279
DIMPLE SEALING SIDE OF TEFLON AS SHOWN
BREAK SHARP EDGE
BREAK SHARP EDGE
0.094 +0.004 0
√63
Ø 0.467 +0.004 0
Ø 0.463 +0.004 0
10.00°
1.50° 0° -.5°
SEALING FACE

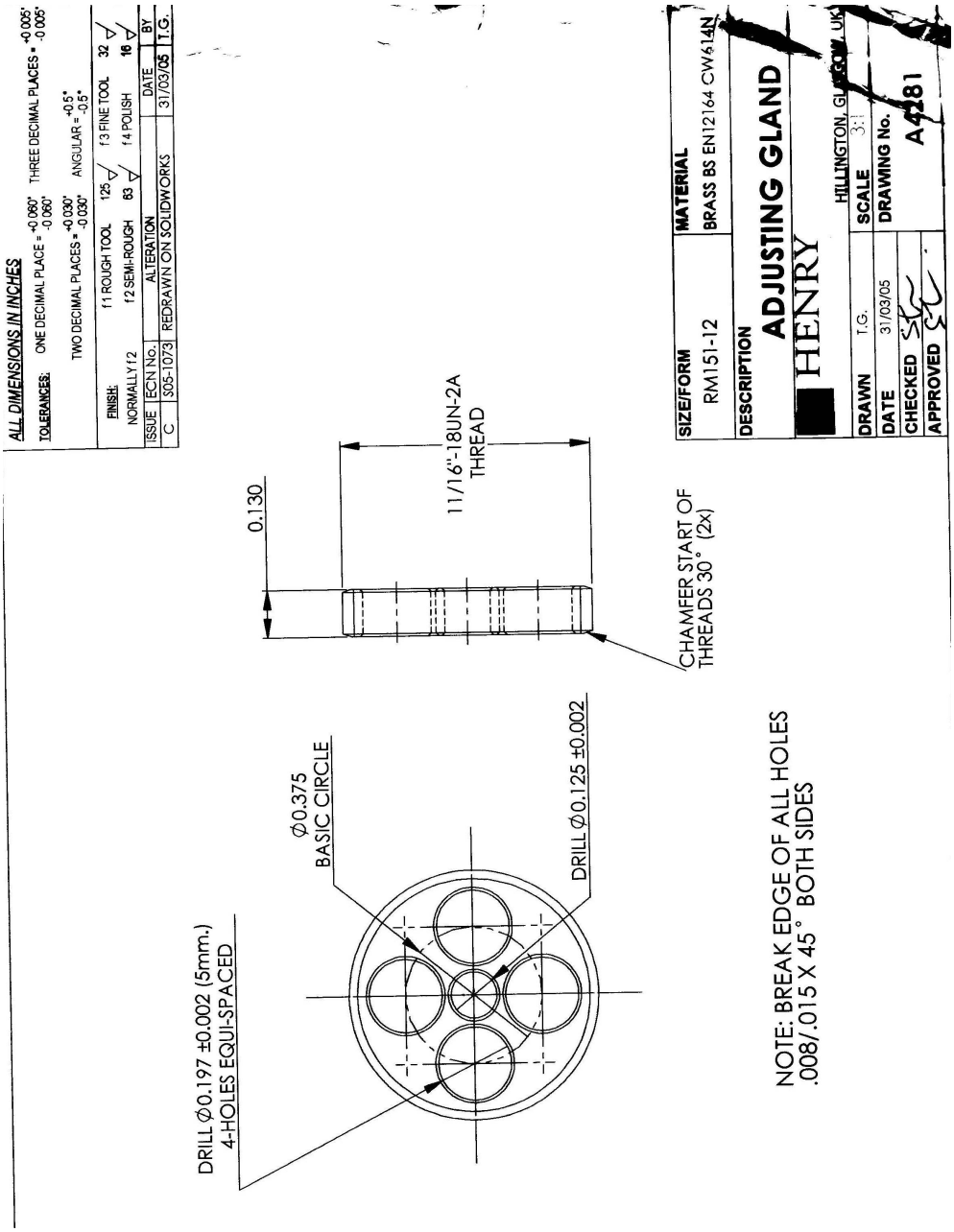
ALL DIMENSIONS IN INCHES
TOLERANCES: ONE DECIMAL PLACE = +0.060° -0.060° THREE DECIMAL PLACES = +0.005° -0.005°
TWO DECIMAL PLACES = +0.030° -0.030° ANGULAR = +0.5° -0.5°
FINISH: NORMALLY f1 ROUGH TOOL 125 f2 SEMI-ROUGH 63 f3 FINE TOOL 32 f4 POLISH 16
ISSUE | ECN No. | ALTERATION | DATE | BY
C | 305-1073 | REDRAWN ON SOLIDWORKS | 31/03/05 | T.G.
SIZE/FORM RM151-12
MATERIAL BRASS BS EN12164 CW614N
DESCRIPTION ADJUSTING GLAND
HENRY
HILLINGTON GLASGOW UK
DRAWN T.G. SCALE 3:1
DATE 31/03/05 DRAWING No. A4281
CHECKED
APPROVED
0.130
11/16"-18UN-2A THREAD
CHAMFER START OF THREADS 30° (2x)
DRILL Ø0.197 ±0.002 (5mm.) 4-HOLES EQUI-SPACED
Ø0.375 BASIC CIRCLE
DRILL Ø0.125 ±0.002
NOTE: BREAK EDGE OF ALL HOLES .008/.015 X 45° BOTH SIDES

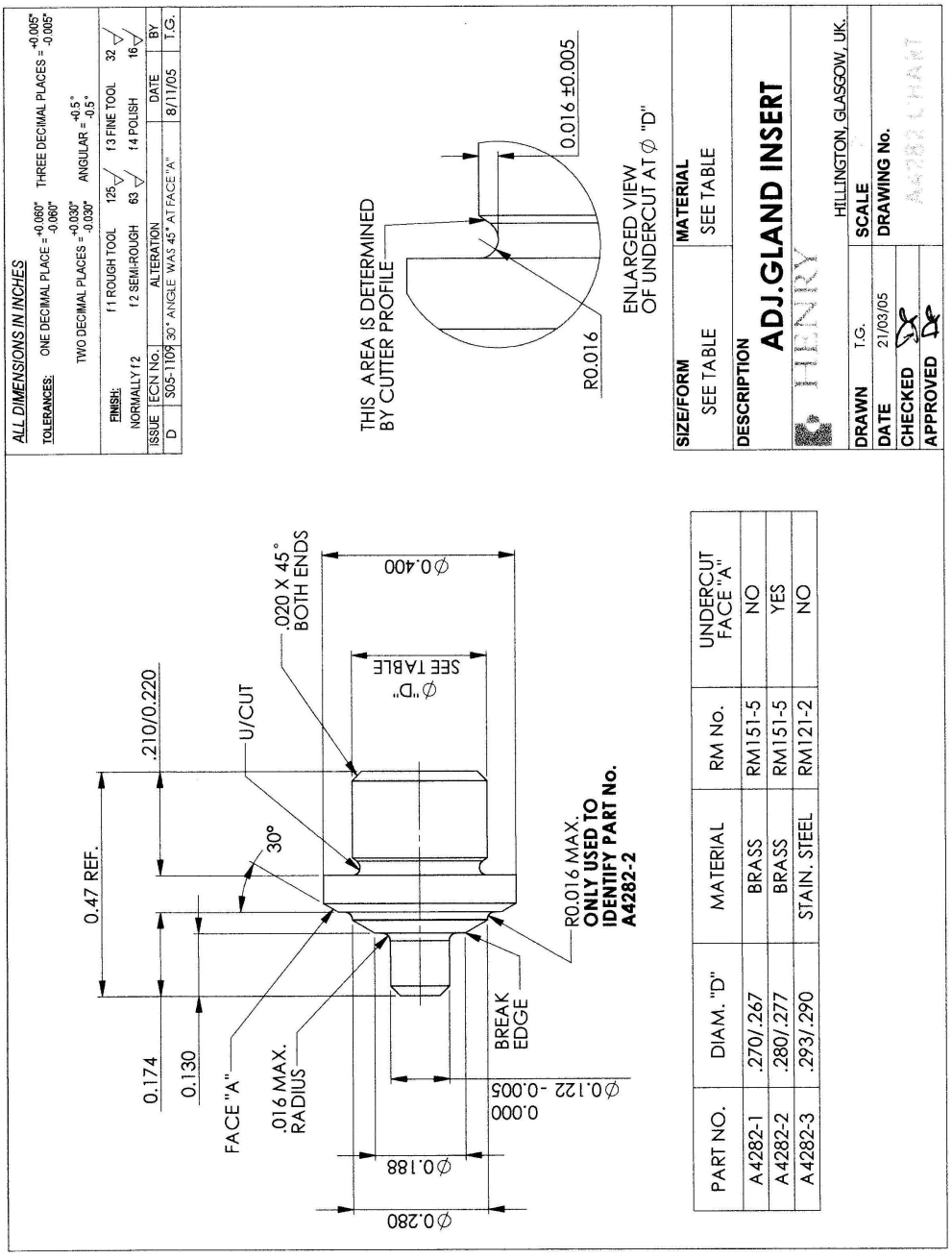

PART NO.	DIAM. "D"	MATERIAL	RM No.	UNDERCUT FACE "A"
A4282-1	.270/.267	BRASS	RM151-5	NO
A4282-2	.280/.277	BRASS	RM151-5	YES
A4282-3	.293/.290	STAIN. STEEL	RM121-2	NO

A.2 HNE-DS model equations

Ideal mass flux

$$G = K_d\, C \sqrt{2\frac{P_o}{v_o}} \tag{A.2.1}$$

Discharge coefficient

$$K_d = \alpha_{seat}\, K_{dg} + (1 - \alpha_{seat})\, K_{dw} \tag{A.2.2}$$

$$\alpha_{seat} = 1 - \frac{v_l}{v_o \left[\omega\,(\frac{1}{\eta} - 1) + 1\right]} \tag{A.2.3}$$

Compressibility factor for non flashing flow

$$\omega = \frac{1}{\gamma}\,\frac{x.v_{go}}{v_o} \tag{A.2.4}$$

Critical pressure ratio η

$$0 = \eta_{crit}^2 + (\omega^2 - 2\omega)(1 - \eta_{crit})^2 + 2\omega^2 ln(\eta_{crit}) + 2\omega^2(1 - \eta_{crit}) \tag{A.2.5}$$

flow coefficient C

$$C = \frac{\sqrt{\omega\, ln(\frac{1}{\eta}) - (\omega - 1)(1 - \eta)}}{\omega\,(\frac{1}{\eta} - 1) + 1} \tag{A.2.6}$$

Where for critical flow,

$$\eta = \eta_{crit} \tag{A.2.7}$$

The mixture specific volume

$$v_o = x_o\, v_{go} + (1 - x_o) v_{lo} \tag{A.2.8}$$

Mass flow quality

$$x_o = \frac{\alpha_o \, v_{lo}}{(1-\alpha_o) \, v_{go} + \alpha \, v_{lo}} \tag{A.2.9}$$

Slip factor

$$\phi = \sqrt{\frac{v_o}{v_l}} \left\{ 1 + x_o \left[(\frac{v_{go}}{v_l})^{\frac{1}{6}} - 1 \right] \left[1 + x_o \left[(\frac{v_{go}}{v_l})^{\frac{5}{6}} - 1 \right] \right] \right\}^{-\frac{1}{2}} \tag{A.2.10}$$